1997

Single-angle compression members welded by one leg to gusset plates.

Sherief Sharl Shukry. Sakla
University of Windsor

INFORMATION TO USERS

This manuscript has been reproduced from the microfilm master. UMI films the text directly from the original or copy submitted. Thus, some thesis and dissertation copies are in typewriter face, while others may be from any type of computer printer.

The quality of this reproduction is dependent upon the quality of the copy submitted. Broken or indistinct print, colored or poor quality illustrations and photographs, print bleedthrough, substandard margins, and improper alignment can adversely affect reproduction.

In the unlikely event that the author did not send UMI a complete manuscript and there are missing pages, these will be noted. Also, if unauthorized copyright material had to be removed, a note will indicate the deletion.

Oversize materials (e.g., maps, drawings, charts) are reproduced by sectioning the original, beginning at the upper left-hand corner and continuing from left to right in equal sections with small overlaps. Each original is also photographed in one exposure and is included in reduced form at the back of the book.

Photographs included in the original manuscript have been reproduced xerographically in this copy. Higher quality 6" x 9" black and white photographic prints are available for any photographs or illustrations appearing in this copy for an additional charge. Contact UMI directly to order.

UMI

A Bell & Howell Information Company
300 North Zeeb Road, Ann Arbor MI 48106-1346 USA
313/761-4700 800/521-0600

SINGLE-ANGLE COMPRESSION MEMBERS

WELDED BY ONE LEG TO GUSSET PLATES

by

Sherief Sharl Shukry Sakla,
M.A.Sc., P.Eng.

A Dissertation

Submitted to the Faculty of Graduate Studies and Research

through the Department of Civil and Environmental Engineering

in Partial Fulfilment of the Requirements for

the Degree of Doctor of Philosophy at the

University of Windsor

Windsor, Ontario, Canada

1997

I hereby declare that I am the sole author of this document.

I authorize the University of Windsor to lend this document to other institutions or individuals for the purpose of scholarly research.

Sherief Sharl Shukry Sakla

I further authorize the University of Windsor to reproduce the document by photocopying or by other means, in total or in part, at the request of other institutions or individuals for the purpose of scholarly research.

Sherief Sharl Shukry Sakla

This Dissertation has been examined and approved by:

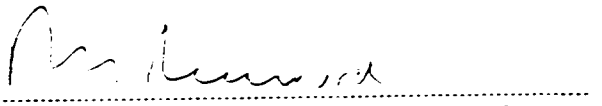

Dr. R. G. Redwood, External Examiner
Civil Engineering, McGill University

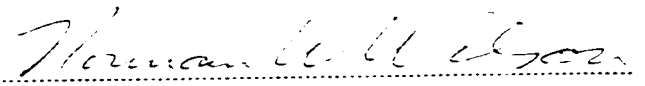

Dr. N. W. Wilson
Mechanical and Materials Engineering,
University of Windsor

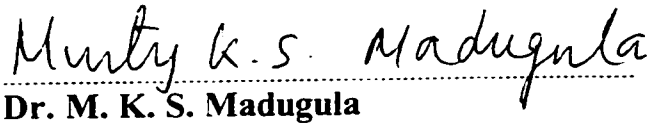

Dr. M. K. S. Madugula
Civil Engineering, University of Windsor

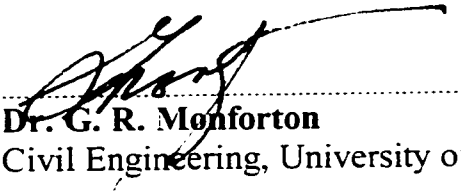

Dr. G. R. Monforton
Civil Engineering, University of Windsor

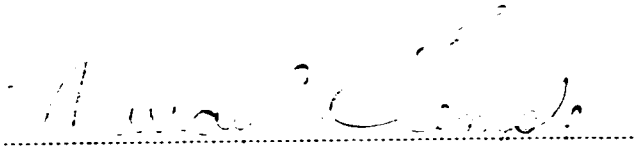

Dr. M. C. Temple, Advisor
Civil Engineering, University of Windsor

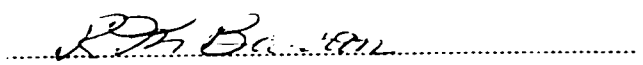

Dr. R. M. Barron, Chair
Interim Associate Dean,
Faculty of Graduate Studies and Research

ABSTRACT

Single-angle compression members are simple structural elements that are very difficult to analyse and design. These members are usually attached to other members by one leg only. Thus the load is applied eccentrically. To further complicate the problem, the principal axes of the angle do not coincide with the axes of the frame or truss of which the angle is a part. Although it is known that the end conditions affect the ultimate load carrying capacity of these members, procedures have not been developed to do this as it is difficult to evaluate the end restraint in many practical cases.

Different design practices were presented and evaluated using experimental test results obtained from previous research. The two generally accepted design procedures, the simple-column and the beam-column approaches, in general, underestimate the load carrying capacity of single-angle compression members attached by one leg to a gusset plate. There is a great variation between different design practices in the prediction of the compressive resistance of single-angle members. With that great variation it is difficult to determine the most appropriate design procedure to follow.

The major objective of this research is to obtain a better understanding of the behaviour and load carrying capacity of single-angle compression members attached by one leg to a gusset plate. An experimental investigation was carried out and verified through the use of the finite element analysis. The effect of the gusset plate width, thickness and the unconnected length were studied. The effect of the weld length and pattern used in

connecting the angle to the gusset plate was studied as well. It was found that the thickness and width of the gusset plate significantly affect the load carrying capacity, but the unconnected length has only a minor effect. The effect of the length of weld and the weld pattern used in the connection on the ultimate load carrying capacity can be neglected.

It was found that the finite element method can be used, with a reasonable degree of accuracy, to predict the behaviour and load carrying capacity of these members. The finite element method was used to study some 1800 different combination of parameters. It was found that out-of-straightness, residual stresses, Young's modulus of elasticity, and the unconnected gusset plate length do not have a great effect on the load carrying capacity. The most significant parameter is gusset plate thickness with the gusset plate width being the second most important parameter. An empirical design equation is proposed and illustrated by two design examples.

To My Parents and My Sisters

for their love, support and encouragement.

ACKNOWLEDGEMENTS

I wish to begin with expressing my sincere gratitude to my supervisor, Dr. M. C. Temple, for the excellent guidance, effort, inspiration, and continuous encouragement which he so enthusiastically provided throughout the course of my research studies.

My thanks are also extended to Dr. G. Abdel-Sayed for his open door policy regarding any questions or concerns pertaining to this study and for his encouragement and assistance throughout my doctoral program.

I would like to thank the faculty and staff of the Department of Civil and Environmental Engineering as well as the computer consultants of the Computing Services at the University of Windsor for their assistance during this research. Special thanks are also due to Mr. Richard Clark, the laboratory technician, Mr. Dieter Liebsch and the members of the Technical Support Centre for their assistance in the preparation and testing of the specimens during the experimental part of this study.

I would also like to acknowledge the financial support provided by the Natural Sciences and Engineering Research Council of Canada.

Last, but not least, the author wishes to thank his family for their great support and encouragement throughout the course of this study.

Finally, to all the staff and faculty in the Civil and Environmental Engineering Department at the University of Windsor, I wish you continued success.

TABLE OF CONTENTS

LIST OF TABLES

LIST OF FIGURES

LIST OF SYMBOLS

A_g	gross cross-sectional area of an angle member
a_1 ,a_2 ,a_3	constants in an empirical equation that depends on the ratio of the gusset plate width to the angle leg width
B_g	gusset plate width
b	leg width of an equal-leg angle
b_x, b_y	width of angle leg parallel to the x and y axes, respectively
b_1 ,b_2, b_3	constants in an empirical equation that depends on the ratio of the gusset plate thickness to the angle leg width
C_m	equivalent moment factor for beam-columns
C_r	compressive resistance
C_w	angle warping constant
C_1, C_2	constants for determining the minimum gusset plate thickness required to prevent local buckling of the gusset plate prior to the failure of the angle
c_y	the distance from the centroid to contact face of gusset plate
c_1 ,c_2, c_3	constants in an empirical equation that depends on the slenderness ratio, L/r_y
E	Young's modulus of elasticity
e_w, e_z	eccentricity of load point as measured from principal axes
e_y	eccentricity of load point as measured from the y axis
F_a	applied compressive stress due to axial load and bending

F_{CRC}	Column Research Council basic column strength formula
F_y	actual yield stress
I_x, I_y	the moment of inertia about the x and y axes, respectively
J	torsional constant
K	effective length factor
K_a	constant in empirical equation
K_{a1}	constant in empirical equation that depends on the gusset plate width
K_{a2}	constant in empirical equation that depends on the gusset plate thickness
K_{a3}	constant in empirical equation that depends on the slenderness ratio, L r
KL r	slenderness ratio
L	length of angle
L_g	unconnected length of gusset plate
L_w	weld length on each side of angle leg
M_{nx}, M_{ny}	nominal flexural strength about the x and y axes, respectively
M_{ux}, M_{uy}	required flexural strength about the x and y axes, respectively
M_y	moment about the y axis required to produce compressive yielding in the extreme fibre when axial load is zero
M_1, M_2	bending moments acting at the ends of the member taking into account the end restraint caused by the truss chords. M_1 is numerically greater than M_2
P	axial compressive load
P_{cr}	elastic buckling load
P_E	Euler's load about the y axis
P_n	nominal compressive strength for concentric axial compression

P_o axial load carrying capacity in the absence of bending

P_u required compressive strength

P_y yield load

R_e vector of external applied loads

R_i vector of internal resisting loads

R_u vector of unbalanced loads

r radius of gyration

r_x radius of gyration about the geometric axis perpendicular to the gusset plate, the x axis

r_y radius of gyration about the geometric axis parallel to the gusset plate, the y axis

r_z radius of gyration about the minor principal axis, the z axis

t thickness of angle leg

t_p thickness of the gusset plate

u vector of nodal displacements

w major principal axis

w_o the coordinate of the shear centre with respect to the w axis

x,y geometric axes

y_c the distance from the centroid of the angle to its compressive edge measured along the x axis

z minor principal axis

z_o the coordinate of the shear centre with respect to the z axis

α	angle between the axis parallel to the gusset plate, the y axis, and the failure axis
ϵ_y	yield strain
θ	angle of cross-sectional rotation
λ	slenderness parameter
Π_p	potential energy of the finite element system
ϕ	resistance factor
ϕ_b	resistance factor for flexure
ϕ_c	resistance factor for compression
[K]	global stiffness matrix
$[K_e]$	global elastic stiffness matrix
$[K_G]$	global geometric stiffness matrix
$[K_T]$	tangent stiffness matrix
$\{P\}$	global load vector
$\{U\}$	global displacement vector

CHAPTER I

INTRODUCTION

1.1 General

Single angles are the most basic shape of hot rolled steel sections. They are being used extensively in many structural applications, as web members in trusses or steel joists, as bracing members, and as main members in communication towers. Because of the simplicity of their cross-section and their relative ease of construction, steel angles are widely available and designers like to use them. Steel angles can be very conveniently joined at their ends to gusset plates, webs of tees, or other structural elements as shown in Figures 1-1 and 1-2. Currently, these joints are usually either shop welded or field bolted or welded. Welded gusset plate connections are widely used in braced steel frames in commercial and industrial buildings.

Welds are probably used more often than bolts in making connections between angles and other members. Welding has become more popular in recent years because it is faster, often cheaper, requires less fabrication, and results in a better connection than any other method of making joints. Welded design and construction offer the opportunity to achieve more efficient use of materials. The speed of fabrication and erection can help compress production schedules. Welds offer the best method of making rigid connections resulting in reduced member size and weight.

In spite of the apparent simplicity of single-angle compression members, they are among the most complex structural members to analyze and design. When attached by one leg the problem gets more complicated as the load is applied eccentrically to the angle. An example of a typical gusset plate connection to a single-angle bracing member is shown in Figure 1-2. To further complicate the problem, the principal axes of the angle cross-section do not coincide with the axis of the frame or truss of which the angle is a part. Since angles are connected to gusset plates or other structural members, the problem is further complicated by the fixity that exists at the ends of the angle. This fixity, in most practical cases, is hard to account for since the magnitude of the end restraint is not known. The magnitude of this restraining end moment for a given angle size is a function of the gusset plate thickness, width, and length. All these factors make the analysis and design of these compression members perhaps the most difficult of all structural members.

1.2 Design Practices

In Canada and the United States there are several design practices for the design of single-angle compression members. The CISC Handbook of Steel Construction (1995) provides no explicit guidance as to a preferred design procedure for these compression members. The past practice in Canada seems to be to neglect the load eccentricity about the principal axes and to design such members as concentrically loaded pin-ended columns that buckle about the minor principal axis of the cross-section, the z-axis as shown in Figure 1-3. The effective length factor is commonly taken as 1.0 but values as low as 0.9 have been used.

The AISC Manual of Steel Construction, Load and Resistance Factor Design (1986, 1994), more explicitly recommends that such members be designed as beam-columns. A

numerical example is given in the Manual to outline this procedure. The load is assumed to act at the centre of the gusset plate and the moments about the principal axes are calculated, as shown in Figure 1-4.

Although the AISC-LRFD beam-column approach seems to reflect the expected behavior of single angles as beam-columns, it can underestimate the load carrying capacity resulting in a very conservative design. This seems to be due, in part, to neglecting the end fixity. This end fixity could be of the type shown in Figure 1-2 where the angle is welded to a gusset plate.

It can be seen that the simple-column approach is not a rational approach. The assumptions used in this approach do not reflect the behavior of single angles observed in experimental testing. The assumptions that the angle is pin-ended and loaded at the centroid are not true. The angle does not buckle about the weak axis as it is connected by one leg.

With the great variation between different design practices in the prediction of the compressive resistance of single-angle compression members it is difficult to determine the most appropriate design procedure to follow.

To further complicate the design of single angles attached by one leg to a gusset plate, the load carrying capacity of these single-angle compression members vary significantly when the gusset plate dimensions are changed. The ultimate load carrying capacity increases considerably if, for example, the gusset plate thickness or width is increased. Changing the gusset plate dimensions changes the restraining moments provided by the gusset plates to the ends of the angle. This changes the apparent location of the load in such a way that it is much closer to the centroid. That is why the simple-column approach yields results that are in much better agreement, in many cases, than those predicted using the AISC beam-column approach.

1.3 Weld Patterns

In many cases, angles are connected at their ends by welds which are not balanced about the projection of the centroid on the connected leg. This type of weld may be used when there is not enough room to place a balanced weld.

A balanced weld on an angle member is one in which the forces at the connection of the angle are balanced about the projection of the centroid on the connected leg through the distribution of fillet welds (Figure 1-5). If a load is applied, the sum of the moments at the connection about the projection of the centroidal axis on the welded leg is equal to zero. An equal weld is a weld balanced about the centre of the welded leg. An unbalanced weld or an equal weld therefore are distributed in such a manner that they cause a moment about the centroidal axis.

Both the Canadian Standard CAN/CSA-S16.1-94 (1994) and the American Specification, AISC, Load and Resistance Factor Design Specification for Structural Steel Buildings (1994) do not require the welds to be balanced about the centroid of the angle members under static loads. This is based on a study carried out by Gibson and Wake (1942). In this study a few angles were tested in tension under different weld patterns. It was found that there was no need to balance the end fillet welds about the projection of centroidal axis on the attached leg. Based on this research, it was assumed that the same conclusion applies to compression members.

Sakla (1992) carried out eighteen ultimate strength compression tests to study the effects of balanced, equal, and unbalanced welds on the load carrying capacity of single-angle compression members connected to torsionally stiff members. The angles were welded to HSS's at their ends. It was concluded in that research that the effect of unbalanced welds

seemed to be beneficial for slender angles but had a detrimental effect on the load carrying capacity of angles of intermediate length. The effect of different weld patterns on angles connected at their ends to more flexible elements such as gusset plates or webs of tees has not been studied.

1.4 Research Objective

The main objective of this research is to obtain a better understanding of the behavior of single-angle compression members welded to gusset plates by one leg so a more efficient design approach can be obtained. As can be noted from the discussion above, none of the current design procedures accurately predict the ultimate load carrying capacity of single-angle compression members welded by one leg to a gusset plate. There is no published research that relates the gusset plate dimensions to the ultimate load carrying capacity of single-angle compression members. Such a study is crucial to define the most influential design parameters that affect the ultimate load carrying capacity.

To achieve this goal, an experimental investigation was carried out and verified through the use of a finite element analysis. Once good agreement between the experimental tests results and finite element analysis is confirmed, the latter is used to carry out a parametric study. In this research the effects of the following variables on the behavior and ultimate load carrying capacity of single-angle compression members welded to gusset plates by one leg only were studied:

1. The effects of changing the unconnected length, width and thickness of the gusset plate. The unconnected length of the gusset plate is defined as the distance from the end of the angle to the section at which a plastic hinge

forms.

2. The effect of the length of weld used in the connection.
3. The effect of using different weld patterns (balanced, equal, and unbalanced) used to connect angles to gusset plates.

Using a finite element analysis allows the study of the effect of some parameters, such as initial out-of-straightness and residual stresses, that cannot be studied economically by experimental testing. Finite element analysis was also used to generate a wide range of numerical models in order to obtain enough data for use in the development of design curves or equations. This empirical equation will help the CISC and AISC to produce load tables for single-angle compression members that are welded by one leg to a gusset plate.

1.5 Research Program

An experimental program was carried out to obtain data that was used to verify the theoretical results obtained from the finite element model. It consisted of 51 ultimate strength tests of single-angle members connected to tee sections. Three different column lengths were used in this investigation. Twenty-one slender specimens were tested. Thirty specimens of intermediate length were tested with nine of the specimens being longer than the other twenty-one.

A commercial finite element analysis package ABAQUS (Hibbit et al. 1994) was used to predict the load carrying capacity and behavior of these compression members. It was used subsequently to conduct a parametric study so that a design procedure could be obtained.

CHAPTER II

LITERATURE REVIEW

2.1 Previous Research

A lot of research has been conducted on structural steel angles. The following literature review is not complete, but contains only those studies that provide information related to the behaviour and design of single-angle compression members attached by one leg. Studies that are of significant importance to this research are highlighted.

2.1.1 Stability of Axially Loaded Single Angles

The end connection of single-angle compression members causes load eccentricity and both torsional and flexural rotational restraint. The elastic stability of axially loaded single-angle compression members can be treated as a special case of the stability of thin-walled members as shown in many references (e.g., Timoshenko and Gere, 1961; Bleich, 1952). The warping constant can be reasonably assumed to be zero as the shear centre is located at the intersection of the two legs.

The elastic buckling load of an unequal-leg column which is loaded through the centroidal axis is the lowest root of the following cubic equation (Galambos, 1968).

$$(P_{cr} - P_z)(P_{cr} - P_w)(P_{cr} - P_\phi) - P_{cr}^2 (P_{cr} - P_z)\frac{w_0^2}{r_0^2} - (P_{cr} - P_w)\frac{z_0^2}{r_0^2} = 0 \qquad (2\text{-}1a)$$

where P_{cr} is the buckling load, w_o and z_o are the coordinates of the shear centre with respect to the w and z axis, respectively,

$$P_z = \frac{\pi^2 E I_z}{(K_z L)^2} \qquad P_w = \frac{\pi^2 E I_w}{(K_w L)^2} \qquad P_\phi = \frac{G J + \pi^2 E C_w / L^2}{r_o^2} \qquad (2\text{-}1b)$$

$$r_o^2 = z_o^2 + w_o^2 + \frac{I_z + I_w}{A_g} \qquad (2\text{-}1c)$$

and the z, w refer to the principal axes of the angle as shown in Figure 1-3. The warping constant C_w can be conservatively taken as zero.

2.1.2 Eccentrically Loaded Single Angles

When an angle is attached by one leg, the load is applied with eccentricities e_z and e_w with respect to the principal axes of the angle, as shown in Figure 1-4. In addition, the gusset plate provides end restraints against rotation. Thus, the problem is not a bifurcation buckling problem but a beam-column problem where lateral deformations occur at any level of loading.

Trahair (1969) studied the elastic problem of eccentrically loaded and end-restrained single-angle struts, for the special case of end restraint provided by tee stubs which represent the chords of a truss. This was done for the elastic case where the maximum stresses were limited to the yield stress. Usami and Galambos (1971) studied the inelastic case. Good

agreement was achieved between test results and the numerical predictions in both cases.

2.1.2.1 Leigh and Galambos (1972)

Leigh and Galambos (1972) carried out tests on compression webs of long span steel joists. It was observed that the dominant deflection of the angle was perpendicular to the connected leg. They proposed two design procedures. The first design procedure was based on a simplified ultimate strength interaction equation. The authors suggested that the problem should be treated as a uniaxial bending beam-column problem and that the slenderness ratio should be based on r_y, where y is the geometric axis parallel to the connected leg (see Figure 1-4). The AISC beam-column interaction expression would be used to evaluate the axial capacity as follows.

$$\frac{P}{P_o} + \frac{C_m M_1}{M_y [1 - \frac{P}{P_E}]} = 1 \qquad (2\text{-}2)$$

where P is the axial compressive load; P_o is the axial load carrying capacity in the absence of bending; M_y is the moment about the y axis required to produce compressive yielding in the extreme fibre when the axial load is zero; M_1 is the largest bending moment acting at the end of the member taking into account the end restraint caused by the truss chords; $C_m = 0.6 - 0.4(M_2/M_1)$ where M_1 and M_2 are the member end moments and M_1 is numerically greater than M_2, the ratio (M_2/M_1) is positive for double curvature and negative for single curvature; and P_E is the Euler load about the y axis.

It was found that this equation gave satisfactory, if somewhat conservative, predictions of the actual load carrying capacity provided that the end eccentricities were

reduced to account for the end restraint. The problem is that it is difficult to account for this reduction in end eccentricity since the end restraints are not easy to evaluate. This procedure has not been accepted by practising engineers since it involves the use of the beam-column equation, a fairly lengthy procedure for what appears to be a simple structural element.

The other empirical design equation proposed by Leigh and Galambos (1972) is a simplified form of the uniaxial bending beam-column approach. This procedure sets the applied compressive stress equal to the Column Research Council (1966) stress from the equation in effect at that time. The applied compressive stress is the sum of the stress due to the axial load and due to the flexural stress caused by the eccentricity of the applied load. The flexural stress, as mentioned before, is based on bending about the geometric axis parallel to the attached leg, the y axis. This equation is written as

$$F_a = \frac{P}{A_g} - \frac{C_m M_1 y_c}{I_y} \qquad (2\text{-}3)$$

and

$$F_{CRC} = F_y \left[1 - \frac{F_y (KL\, r_y)^2}{4 \pi^2 E} \right] \qquad (2\text{-}4)$$

where F_a is the applied compressive stress due to the axial load and bending; A_g is the cross-sectional area of the angle; y_c is the distance from the centroid of the angle to its compressive edge; I_y is the moment of inertia about the y axis; F_{CRC} is the Column Research Council basic column strength formula; F_y is the yield stress; K is the effective length factor; L is the length of the angle; and E is Young's modulus of elasticity.

2.1.2.2 Woolcock and Kitipornchai (1986)

Woolcock and Kitipornchai (1986) suggested a design procedure that uses the uniaxial beam-column interaction equation for designing of web compression members in trusses. They further suggested use of a specific eccentricity e_y ($e_y = c_y - \frac{1}{2}t$) for the case when all the angles are placed on the same side of the steel joist or truss where c_y is the perpendicular distance from centroid to contact face of gusset and t is the thickness of the angle leg. They indicated that this procedure cannot be used for unequal single angles if the long leg is the welded leg.

2.1.2.3 Elgaaly et al. (1991, 1992)

Elgaaly et al. (1991, 1992) tested 50 stocky single-angle struts as part of a truss. The testing program included testing members with single- and double-bolted connections. Results were compared with AISC-LRFD and ASCE Manual 52, Guide for design of steel transmission towers (1988). The test results indicated that ASCE Manual No 52 can yield an unsafe design while the AISC specification resulted in a conservative design.

2.1.2.4 Adluri and Madugula (1992)

Adluri and Madugula (1992) compared the results of experimental data on eccentrically loaded steel single-angle struts with the AISC-LRFD (1986) and AISC-ASD (1989) specifications. The current design practice interaction equations were derived for doubly symmetric sections used in frames. These interaction equations when applied to eccentrically loaded single-angle struts yield very conservative results and thus need reevaluation. The following modification for the current interaction equations was proposed.

The moment interaction factors could be changed to 2/3 from the present value of 8/9 for the range of $P_u / \phi P_n$ between 0.5 and 1.0 as shown below:

$$For \quad \frac{P_u}{\phi_c P_n} \geq 0.5, \qquad \frac{P_u}{\phi_c P_n} + \frac{2}{3}\left(\frac{M_{uz}}{\phi_b M_{nz}} + \frac{M_{uw}}{\phi_b M_{nw}}\right) \leq 1.0 \tag{2-5a}$$

$$For \quad \frac{P_u}{\phi_c P_n} < 0.5, \qquad \frac{P_u}{2\,\phi_c P_n} + \left(\frac{M_{uz}}{\phi_b M_{nz}} + \frac{M_{uw}}{\phi_b M_{nw}}\right) \leq 1.0 \tag{2-5b}$$

where P_u is the required compressive strength; P_n is the nominal compressive strength for a concentric axial load; M_{nz} and M_{nw} are the nominal flexural strengths about the z and w axes, respectively; M_{uz} and M_{uw} are the required flexural strengths about the z and w axes, respectively; and ϕ_b and ϕ_c are the resistance factors for flexure and compression, respectively.

2.2 Design Practices

There are several design practices used in Canada and the United States. These practices will be reviewed.

2.2.1 Simple-Column Design Practice

In Canada and the United States there are two approaches to the design of single-angle compression members attached by one leg. One approach is to treat the angle as a concentrically loaded column, which will be referred to as the "simple-column" design approach.

In Canada, the CISC Handbook of Steel Construction (1995) provides no guidance as to a preferred design approach for these members. Past practice seems to be to ignore the eccentricity of the load about the principal axes. The angle is designed as if it is a concentrically loaded member that buckles about the z axis, the minor principal axis of the cross section (Figure 1-3). The effective length factor is usually taken as 1.0 but some engineers use an effective length factor as low as 0.9. This approach, although not widely used in the United States, is gaining acceptance in that country.

2.2.2 Beam-Column Design Practice

The AISC Manuals of Steel Construction (1986, 1994) have consistently recommended that bending about both axes be accounted for in the design of single-angle struts. Design examples for single-angle struts have been presented illustrating the application of the biaxial bending-axial load interaction expression shown below.

$$For \quad \frac{P_u}{\phi_c P_n} \geq 0.2, \qquad \frac{P_u}{\phi_c P_n} + \frac{8}{9}\left(\frac{M_{uz}}{\phi_b M_{nz}} + \frac{M_{uw}}{\phi_b M_{nw}}\right) \leq 1.0 \tag{2-6a}$$

$$For \quad \frac{P_u}{\phi_c P_n} < 0.2, \qquad \frac{P_u}{2\,\phi_c P_n} + \left(\frac{M_{uz}}{\phi_b M_{nz}} + \frac{M_{uw}}{\phi_b M_{nw}}\right) \leq 1.0 \tag{2-6b}$$

In addition to the numeric effort involved, the difficulty with the biaxial bending approach is in determining where the load acts. It is common to assume that the load transferred to a web strut in a truss acts at the mid-plane of the gusset or at the mid-plane of

the Tee chord (Figure 1-4). The location of the load in the plane of the chord is less well defined, but is often assumed to act either at the centre of the bolts or at the centre of resistance of the welds or at the centre of the attached leg.

The design examples use a specific effective length KL, but do not suggest that an effective length factor of less than one should be used. There is considerable restraint about the x axis (Figure 1-4) due to the bending stiffness of the chord and undoubtedly also some restraint about the y axis due to the torsional stiffness of the chord. It is very difficult to evaluate this end restraint numerically in order to obtain an appropriate effective length. This is further complicated by the fact that the principal axes of the angle do not coincide with the x and y axes.

In addition to the above noted difficulties in evaluating the location of the load and the effective length factor, there is the problem related to application of the interaction expressions which were developed for doubly-symmetric sections. For a doubly-symmetric section the sum of the terms of the interaction expression represents a stress condition occurring at one of the four corners of the section, whereas for single angles, summation of the absolute value of the terms will only reflect the critical stress condition when the moments are applied in a particular direction. Thus, simply adding the flexural terms to the axial term in the interaction expression for a section which is singly-symmetric or non-symmetric can lead to extremely conservative solutions.

The AISC Manual of Steel Construction, Load and Resistance Factor Design (1986), includes a numerical example in which a single angle, attached by one leg, is treated like a beam-column. The load is assumed to act at the centre of the gusset plate and approximately at the centre of the attached leg. The LRFD beam-column interaction equation is used to

determine the axial capacity of the angle.

The AISC Manual of Steel Construction, Allowable Stress Design (1989) has a similar example that illustrates the use of the ASD beam-column interaction expression.

The AISC Manual of Steel Construction, Load and Resistance Factor Design (1994), once again included a numerical example in which the eccentricity of the load about the principal axes was considered. There were some changes, however, from the procedure used in the 1986 Manual of Steel Construction. These changes are

(a) the upper limit of the single-angle flexural strength is taken as 1.25 the yield moment when the width-to-thickness ratio is less than some specified values,

(b) the resistance factor for compression has increased from 0.85 to 0.9,

(c) torsional-flexural buckling is not considered,

(d) the sense of the flexural stresses in the combined force interaction equation may be taken into account although this has not been done in the example in the Manual, and

(e) C_m, the coefficient applied to the bending term in the interaction formula to account for the fact that not all members will be subjected to uniform moment throughout the length, was taken as 0.85. This, in fact, is an error and C_m should be taken as 1.0.

These changes result in a slight increase in the compressive resistance as will be discussed later.

2.2.3 The ASCE Standard, Design of Latticed Steel Transmission Structures (1991)

The ASCE Standard, Design of Latticed Steel Transmission Structures (1991), uses a different approach for the design of single-angle compression members connected by one

leg. The design approach is to consider the angles as "simple columns", but to use a modified slenderness ratio when calculating the compressive resistance. The slenderness ratio is modified, empirically, to account for both the end eccentricity and end restraints. For angles with a low slenderness ratio, the eccentricity of the end connections is considered to be the predominant factor. For slender angles, the rotational restraint is considered to be more important.

This standard specifies that for members with normal framing eccentricities at both ends of the unsupported panel

$$\frac{KL}{r} = 60 + 0.5\,\frac{L}{r} \qquad 0 \le \frac{L}{r} \le 120 \tag{2-7}$$

A normal framing eccentricity is defined as when the bolts lie in between the centre of the leg and the projection of the angle centroid on the connected leg.

For members unrestrained against rotation at both ends of the unsupported panel, i.e. attached using a single bolt at each end:

$$\frac{KL}{r} = \frac{L}{r} \qquad 120 \le \frac{L}{r} \le 200 \tag{2-8}$$

For members partially restrained against rotation at both ends of the supported panel, i.e. attached by welding or by two or more bolts that are close to the centroid of the angle:

$$\frac{KL}{r} = 46.2 + 0.615\,\frac{L}{r} \qquad 120 \le \frac{L}{r} \le 250 \tag{2-9}$$

The CSA Standard S37-94, Antennas, Towers, Antenna-Supporting Structures (1994) uses the same design approach, considering the angles as "simple columns", and uses the same equations for modifying the slenderness ratio of the single-angle member. This modified

slenderness ratio is then used to find the load carrying capacity using the same equations given in Clause 13.3.1 in CAN/CSA-S16.1-94.

2.2.4 Evaluation of Design Practices in Light of Trahair et al. (1969) Test Results

The experimental study carried out by Trahair et al. (1969) was used to evaluate current design practices and design procedures proposed in previous research. It also provided a means to measure how good the agreement is between the finite element modelling of the specimens and the experimental results. This would give confidence in using the finite element method to predict the behaviour and ultimate load carrying capacity of single-angle compression members. The study included testing 45 eccentrically loaded equal and unequal single-angle struts. The angles were welded to tee sections thus representing a truss chord or gusset plates in a braced frame. The loads were applied to the tees and hence eccentrically to the angles. A detailed description of the test specimens used in Trahair et al. (1969) study is given in the section below. Discussion and comparison of the results of different design approaches is given in Chapter VI. A comprehensive comparison with Trahair et al. (1969) test results is also provided in Chapter VI.

2.2.5 Trahair et al. Test Program

Trahair et al. (1969) tested 45 eccentrically loaded single-angle struts. The specimens covered a wide range of slenderness ratios, three different steel types, and three different end conditions. This wide range of these three variables made these test results very suitable for the assessment of current design practices and previous research findings.

A typical test specimen consisted of a 51 x 51 x 6.4 mm (2 x 2 x ¼ in.) angle welded to structural tee sections representing the chords of a truss or a gusset plate in a braced frame. The loads were applied through the tees and hence eccentrically to the angles. A typical test specimen is shown in Figure 2-1.

Three end conditions were used in these tests. Only two of these end conditions were considered in this study as the third one has no practical application. The first end condition, as shown in Figure 2-2, was fixed-ended where the displacements and rotations at the ends of the specimen were prevented. The second was a hinged condition where the angle could deflect in the direction of the outstanding leg, an out-of-plane deflection. An example for the first end condition would be the case where the gusset plate is firmly attached to a beam and column. Another example for the fixed end condition would be the case if the chord of a truss is embedded in, or firmly attached to, a concrete floor or where the chord of the truss is torsionally stiff like a heavy HSS. The pin-ended condition is similar to the case where the chord of a truss is a very light and torsionally weak, hence provides small bending restraint to the angle.

The test specimens were divided into three different groups of which only the results of two of these are discussed in this study. For Series A, the 51 x 51 x 6.4 mm (2 x 2 x ¼ in.) angles were made of ASTM A242 steel. Series B were identical to Series A but the angles were made of A36 steel. Series A consisted of nineteen tests of which eleven were fixed-ended and eight were hinged such that out-of-plane buckling was allowed. Series B included six tests of which three were fixed ended and three were hinged.

In all the specimens, the ends of the angle were welded to a 203.2 mm (8 in.) length of ASTM A36 ST 6I 17.5 structural tee section. Two 114.3 mm (4.5 in.) lines of 6.4 mm (¼

in.) fillet welds were used along the toe and heel of the angle.

2.3 Balanced and Unbalanced Weld Patterns

2.3.1 Previous Work

There is little published research on the effect of balanced and unbalanced welds for angle compression members. Gibson and Wake (1942) published the first paper found in the literature related to this subject. They carried out fifty-four ultimate strength tension tests with angles welded to flat plates. Fifteen different weld patterns were used in that investigation. The tests included eccentric single-angle as well as double-angle tests. The specimens were designed to fail in the welds themselves. It was concluded in that research that the arrangement of the welds in the connection has very little effect on the behaviour of single-angle tension members at working loads. The conventional practice of balancing the welds about the projection of the centroid of the angle on the connected leg is not essential to maintain a good design. Little difference (3%) was noted between the strength of the angles when connected with balanced or unbalanced welds.

Sakla (1992) carried out eighteen ultimate strength compression tests to study the effects of balanced, equal, and unbalanced welds on the load carrying capacity of single-angle compression members connected to torsionally stiff members. The tests included two different column lengths which could be classified as slender and of intermediate length, respectively. The angles were welded to HSS's that were fixed at their ends.

It was concluded in that research that the effect of unbalanced welds seemed to be beneficial for slender angles but had a detrimental effect on the load carrying capacity of intermediate length columns. Using unbalanced welds reduced the load carrying capacity of

intermediate length columns by about 10% when compared to the load carrying capacity of the same specimen with balanced welds. The flexibility of the angles increased as the weld pattern was changed from a balanced to an unbalanced weld.

2.3.2 Standards and Specifications

Before the Gibson and Wake research, the designing and detailing of welded connections of angle members was often complicated by the conventional practice of using welds that are balanced about the projection of the centroid on the connected leg in the connection.

The Canadian Standard CAN/CSA-S16.1-94, Clause 21.7 states that "Except for members subject to repeated loads, disposition of fillet welds to balance the forces about the neutral axis or axes for end connections of single-angle, double-angle, or similar types of axially loaded members is not required."

The American Specification, AISC LRFD (1986, 1994) and the British Standard "Structural use of steel work in building. Part 1: Code of practice for design in simple and continuous construction; hot rolled sections" (BSI 1985) have basically the same requirement.

2.3.3 Comparison

In the Gibson and Wake study (1942) the specimens were designed to break in the weld under tension. In the research carried out by Sakla (1992) the angle compression members were attached to torsionally stiff members fixed at their ends. In the experimental portion of this dissertation the single-angle members were attached to tee section fixed at their ends. The stem of the tee section provided less bending restraint than HSS's.

CHAPTER III

EXPERIMENTAL PROCEDURE

3.1 General

An experimental program was carried out to obtain data that was used to verify the theoretical results obtained from the finite element model. The experimental program was designed to study the effects of gusset plate dimensions, balanced and unbalanced welds, and the amount of weld used to attach the angle to the gusset plate on the ultimate load carrying capacity and behaviour of single-angle compression members attached with welds to a gusset plate by one leg. These variables were not included in Trahair et al. (1969) experimental study. The experimental program consisted of 51 ultimate strength tests of single-angle members connected to tee sections. The webs of the tee sections were used to simulate gusset plates. A typical test specimen is shown in Figure 3-1. The angles were designed according to CAN CSA-S16.1-M89, "Limit States Design of Steel Structures" (1989). In order to reduce the number of variables in this research the same size angle was used for all tests. Three different lengths of angles were used. This resulted in slenderness ratios that fell in the slender and intermediate length ranges. Twenty-one slender specimens were tested. Thirty specimens of intermediate length were tested with nine of the specimens being longer than the other twenty-one.

For the slender specimens and for the shorter intermediate length specimens five different variables were investigated. The variables were:

(i) the unconnected length of the gusset plate, L_g,

(ii) the gusset plate width, B_g,

(iii) the gusset plate thickness t_g,

(iv) the length of weld used in the connection L_w, and

(iv) a weld balanced about the projection of the centroid on the connected leg, a weld balanced about the centre of the leg, which will be referred to as an equal weld, and a weld that is unbalanced about the projection of the centroid of the angle on the connected leg.

For the longer intermediate length specimens, only the effects of the gusset plate width and thickness were investigated.

3.2 Test Specimens

Three different lengths of angle members, 2100, 1550, and 990 mm, were used in this study. The specimens had slenderness ratios, L/r_z, of 170, 125, and 80 which means that the three types could be classified as slender, and as of intermediate length. Typical specimens, as shown in Figures 3-1 and 3-2, consisted of a single-angle member welded to a tee section at each end. The compression members were made from 64 x 64 x 7.9 mm (2½ x 2½ x 5/16 in.) angles and the tee sections were cut from either a W530 x 82 (a W21 x 55 in Imperial units) or a W530 x 123 (W21 x 83) depending on the required gusset thickness. Tables 3-1 gives a full description of the dimensions of all the specimens tested in this study. The centroidal x axis of the angles coincided with the centre of the tee sections.

A 6 mm fillet weld was used to weld the angles to the tee sections. Weld lengths used in different specimens are listed in Table 3-1. An effective length factor of 1.0 was used to

predict the compressive resistance of the angle member according to CAN/CSA-S16.1-M89 (1989) except for the specimens used to study the effect of weld length, specimens L-D and S-D, where an effective length factor of 0.8 was used to design the welds. Using an effective length factor of 1.0 to predict the compressive resistance means that welds were designed as if the angles were concentrically-loaded and pin-ended. This is a common design practice to assume an effective length factor and calculate the ultimate load carrying capacity of the compression member. The weld length is then designed to transfer the predicted ultimate load carrying capacity to the gusset plate. As explained later, the minimum length of fillet welds, as given by CAN/CSA-W59-M89 (1989), was not used. Different weld patterns were used in this study to determine their effects on the ultimate load carrying capacity. The weld patterns used for the slender and shorter intermediate length specimens are show in Figures 3-3 and 3-4, respectively. Equal welds placed on the angle sides only were used for all the nine longer intermediate length specimens.

3.3 Comparison Between Trahair et al. (1969) Test Specimens and the Specimens Used in This Study

Trahair et al. (1969) used the same size structural tee section for all their test specimens. In other words, the same gusset plate was used throughout the entire study. As gusset plate dimensions have a significant effect on the load carrying capacity, the current study included a wide range of different gusset plate dimensions to relate the ultimate load carrying capacity of single-angle compression members to the dimensions of the gusset plate.

The Trahair et al. test specimens had the same weld length and pattern in spite of different angle length used. The weld length of the specimens in this study was different for

each angle length. The effect of the assumed effective length factor used for designing the weld was studied as well as different weld patterns used for connecting the angle to the tee section.

3.4 Preparation of Test Specimens

The angle members were cut to proper length from 6.1 m (20 ft.) lengths of angles. The tee sections were prepared by splitting the W sections longitudinally into two equal sections using a plasma arc cutter. The obtained tee sections were then cut to the proper length. The tee sections were machined at both ends to ensure that they were the same length and that the ends were perpendicular to the longitudinal axis of the tee section. The final length after machining was either 150 or 225 mm depending on the specimen type. Four guiding holes of 12.7 mm ($\frac{1}{2}$ in.) in diameter and 114.3 mm (4.5 in.) apart, were drilled in the flanges of the tee sections to accommodate countersunk bolts as shown in Figures 3-2 and 3-5. These holes were located as precisely as possible since they were used for the alignment of the specimens.

The tee sections, in all specimens, were attached to the upper and lower platens of the testing frame and held firmly in position by the countersunk bolts. The angle was then welded to the tee sections. This procedure follows, as close as possible, the procedure used to fabricate trusses or to erect bracing members in frames. The welding was done by an experienced certified welder using E480XX electrodes. Flux and slag were removed from all welds after welding. After welding the specimen was removed from the test frame to measure the out-of-straightness and to apply the whitewash.

3.5 Test Setup and End Fixtures

All the tests were carried out in the Civil Engineering Structural laboratory at the University of Windsor. The Gilmore Load Fatigue Frame was used for testing as it could be adjusted to accommodate the different lengths of test specimens. The test setup is shown in Figures 3-6 and 3-7 for a shorter intermediate length specimen and slender specimen, respectively.

Fixed end conditions were created at the ends of the specimen. This was achieved by bolting the tee sections directly to the base and top platens of the Gilmore Load Fatigue Frame. These end fixtures were designed to eliminate lateral displacements and rotations about each of the three global axes at the ends of the specimen. Only displacement in the vertical direction at the lower end of the specimen was allowed to apply the load. Details of the setup at the bottom are shown in Figures 3-6 and 3-7. This end condition corresponds to the case where an angle is used as a bracing member and is welded to a gusset plate which in turn is welded to the intersection of a column and a beam. It is also about the same as an angle welded to a tee section embedded in a concrete floor.

Each of the upper and lower plates had four holes 12.7 mm in diameter. The countersunk bolts were used to firmly fix the specimen to the end plates. This achieved three main purposes. First, they were used to guide the specimen into the upper and lower plates which were fixed to the upper and lower platens of the Gilmore Load Fatigue Frame to ensure that the centroid of the specimen coincided, as closely as possible, with the load applied to the specimen by the hydraulic jack. Second, tightening these bolts ensured the elimination of any gap that might exist between the specimen and the loading plates . Third, this procedure ensured fixed end conditions at the ends of the specimen as there were four points which were

prevented from any displacement during the application of the load to the specimen. In addition to these main purposes, the countersunk bolts also prevented the ends of the specimens from slipping or kicking out during testing.

3.5.1 Loading Jack

At the base, the load was applied to the specimens through a computer-controlled hydraulic jack with a capacity of 448 kN (100 kips). A steel plate was fabricated with four 12.7 mm diameter guiding screwed holes. The plate was attached directly to the piston of the loading jack by means of a steel collar to prevent rotation of the plate about the axes perpendicular to the direction of loading.

3.5.2 The Load Cell

A Strainsert flat load cell with a 448 kN (100 kips) capacity was used to determine the applied load and was attached to the top platen of the Gilmore Load Fatigue Frame. The load cell was connected to a data acquisition system that converted the voltage readings to a load at any instant during the application of the load.

A steel plate similar to the one attached to the loading jack was fabricated and attached to the underside of the load cell with guiding holes to provide a connection to the top of the test specimen. The specimen to be tested was placed in between the upper and lower platens of the Gilmore Load Fatigue Frame. The upper crosshead was used as the upper support for the specimen. The lower plate resting on the loading jack was used as the lower support. Figures 3-6 and 3-7 show the complete setup of mechanical jack, lower plate, specimen, upper plate, load cell and the top bracket. This setup was used for all the

specimens.

3.5.3 Instrumentation

The most critical aspect of the experiment was to acquire sufficient data so that the behaviour of the single-angle compression member using different gusset plate properties, and balanced and unbalanced weld conditions could be accurately studied and then compared to the results from a finite element analysis.

Due to the simple buckled shape of the single-angle specimens, obtaining data for lateral displacements was not complicated. Three dial gauges were placed at the mid-height of the specimen, as shown in Figure 3-8, to measure displacements and rotations. Two other dial gauges were placed on the web of the tee section at the upper end of the angle. The purpose of these dial gauges was to measure the lateral deflection and rotation of each angle to determine the effect of each gusset plate or weld variable on both the magnitude of the deflection and the position of the failure axis.

In order to test the precision of the finite element model in predicting the behaviour and ultimate load carrying capacity of single-angle compression members, one slender specimen, L-A-3, and one shorter intermediate length specimen, S-A-3, were strain gauged as shown in Figure 3-9. The strain gauges were located so that the behaviour of the ends of the gusset plate and the angle cross section at mid-height could be studied and checked with the finite element model results.

3.6 Test Procedure

First, the specimens were measured to determine their out-of-straightness prior to the

application of the load. Two steel blocks, of known thickness, a thin wire and a digital calliper were used. The steel blocks were clamped at the ends of the same side of an angle leg and a wire was tightly stretched over the steel blocks as shown in Figure 3-10. The blocks and the wire were clamped to the angle leg. The digital calliper was then used, at mid-height and at the two quarter points of the angle, to measure the distance between the leg of the angle and the wire. This procedure was repeated for each leg of each angle in each specimen. The thickness of the steel blocks was then subtracted from the distance measured between the wire and the leg of the angle to give the initial out-of-straightness of the angles in both x and y directions.

All the specimens were coated with a thin layer of whitewash before testing in order to detect the yield pattern as the load was increased. Coating the surface of the angles with a thin whitewash coating, which was allowed to dry before testing, resulted in a brittle coating that flaked off when yielding occurred. This provided an economical way of detecting the yield pattern.

The specimen was now ready to be placed in the test frame. A small load of approximately 8 kN was applied to the specimen at the beginning to ensure that the top and lower plates were in complete contact with the ends of the specimen. The countersunk bolts were inserted and tightened. The preload was then released to almost zero. Dial gauges were positioned and set to zero before loading started.

The load on the specimens was applied slowly in increments of 5 kN for slender specimens and 10 kN for intermediate length specimens. This load increment was then reduced to 2 kN for slender specimens and 3 kN for intermediate length specimens after reaching 70% of the expected failure load.

In all cases, the system was allowed to reach equilibrium, the point at which the lateral displacements stopped increasing, within acceptable limits, at a given load, prior to reading the dial gauges. In all tests, the failure load was taken as the load at which a small increment of applied load caused large displacements. A typical test took an average of two hours to complete both the setup and testing.

3.7 Data Reduction

3.7.1 Load

The hydraulic jack of the Gilmore Load Fatigue Frame was controlled by a computer. The required jack displacement was input to the computer which in turn controlled the hydraulic jack to displace a specified amount. A data acquisition system retrieved the strain readings of the calibrated load cell and converted them into loads that were displayed on a computer screen. The load cell was calibrated only once as the variation in the calibration factor, within a short period of time, was found, from previous experience, to be extremely small.

3.7.2 Displacement

The lateral displacements of each angle in both the x and y directions and rotation of the cross section were recorded and analysed. The lateral displacement and rotation of the gusset plate were recorded as well. An aluminum strip, attached to the angle by C-clamps, was used to determine the displacement at two points so that the rotation could be determined.

The major displacement occurred in the x direction, perpendicular to the plane of the

welded leg. The ratio between the displacements in both the x and y directions was used to determine the axis about which the angle buckled so that the effect of the weld pattern on the position of this axis could be determined. The displacements versus the corresponding load were plotted for all the tested specimens.

3.7.3 Strain

In order to verify the accuracy of the finite element model used throughout this study to predict the ultimate load carrying capacity and behaviour of single-angle compression members, foil strain gauges were used. Strains were measured at ten points at the mid-height of the angle and at the ends of the gusset plates. Due to the time and cost associated with using strain gauges, two specimens only were strain-gauged to verify the finite element results.

3.7.4 Locations of Yield Points

All the specimens were coated with a thin layer of plaster coating before testing in order to detect the yield pattern while loading. The surface of the steel members was covered by a thin whitewash coating and allowed to dry completely before testing. This brittle coating flaked off at the point of yielding exposing the steel surface below and this provided a very economical solution for detecting zones in which yielding has occurred.

3.7.5 Out-of-Straightness

The measured out-of-straightness was used to describe the geometry of the test specimens in the iterative-incremental procedure to predict the theoretical load-deflection

curves. The out-of-straightness of an angle was prescribed at mid-height and the two quarter points.

3.8 Ancillary Tests

3.8.1 Tension Test

Three tension tests were conducted on specimens taken from the same stock as that of the test specimens in order to determine the yield stress and Young's modulus of elasticity. Three tension test specimens were prepared, each one cut from a different length of angle. The specimens were prepared according to the CAN/CSA-G40.20-M92 Standard (1992), but their dimensions were adapted to suit the dimensions of the angles and the grips of the testing machine. The thickness of the specimen was that of the angle. The dimensions of these specimens are shown in Figure 3-11.

In order to determine Young's modulus of elasticity, two electric resistance strain gauges were used to determine the strain in the specimen, one on each side at the centre of the reduced cross section.

The tension tests were carried out in the universal testing machine. The strain was measured by a strain indicator which was connected to a switch and a balance unit. Average values of yield stress were used in the computations.

3.8.2 Calibration Test

A calibration test was carried out for the 448 kN load cell used in the compression tests. This test was also carried out in the universal testing machine. The calibration test results were then fed to the computer that controlled the loading process.

CHAPTER IV

THEORETICAL ANALYSIS

4.1 General

It is always desirable to predict the behaviour of various structures and structural members under different applied loads by using a numerical model. Thus, the experimental and theoretical results can be compared and, if in good agreement, the numerical model can be used extensively to conduct an comprehensive parametric study. Numerical modelling is a faster and cheaper means of collecting data about a certain problem than depending entirely on an extensive, and expensive, experimental investigation.

The recent rapid development in digital computers made the application of the finite element method a common practice in structural engineering research. The finite element method can handle structural engineering problems that cannot be effectively solved using classical methods or for which a closed form solution is inconceivable to obtain. The finite element method is the most powerful and flexible method capable of providing a complete description of the structural behaviour within the elastic and post-elastic loading stages.

Although a single-angle member might be looked at as a very simple member, the complexity of determining its strength by either experimental investigation or finite element method should not be underestimated especially if the angle is subjected to compressive loads and attached by one leg. Angle members are sensitive to the load position and end conditions.

A commercial finite element package, ABAQUS (Hibbitt et al. 1994), was used to perform a nonlinear static analysis. Both material and geometric nonlinearity were considered in the analysis of the specimens. Residual stresses due to the manufacturing process of the angles were considered to determine their effects, but residual stresses due to the welding of the specimen were excluded from the analysis due to the difficulty of determining such stresses. The steel was modelled as a linear elastic, perfectly plastic material. Different weld patterns were modelled by changing the boundary conditions.

4.2 Finite Element Program

ABAQUS is designed as a flexible tool for the numerical modelling of the structural response in both linear and nonlinear analyses and is run as a batch application. In order to use ABAQUS to analyse a structural problem, a data deck describing the problem has to be prepared. The data deck consists of two parts : the model data and the history data. The model data describes the nodes, elements, nodal constraints, elements properties, material description and the data required to define the model itself. ABAQUS also has a large library of elements from which plate elements were used in the analysis process. Two different nodal constraints were used (i) boundary constraints: in which a specific boundary condition is defined for a node, and (ii) equations: which are linear relationships between certain degrees of freedom of certain nodes.

The history data defines what happens to the model. In other words, the history data describes the order of loading for which the model's response is sought. The history data also includes the control parameters for the nonlinear solution procedures, and the output requests. This history is divided into a sequence of steps within which, in addition to the

imposed loading, adding or removing of model elements is permitted.

In the nonlinear analysis the load is applied in increments. The nonlinear procedures in ABAQUS offer two approaches to obtain a convergent solution at minimum cost. The first option is a direct user control of increment size. The user specifies the increment scheme. This is useful in repetitive analysis where the user has a very good feel for the problem. This option was used throughout the course of this study. The second option is automatic control in which the user defines a period of history and at the same time specifies certain tolerances or error measures. ABAQUS then automatically selects the increments to model the step.

In this study, static loads were applied and the nonlinear static response was computed. The applied loads were assigned up to fifty increments, as an upper bound, to reach the ultimate load. Each increment was assigned up to 15 iterations to converge or the increment was automatically reduced.

4.3 Finite Element Procedure

In the next two sections, a brief discussion of the finite element analysis of structures and the incremental-iterative procedure is described. This method gives the theoretical load-deflection curves which in turn can be used to determine the ultimate load carrying capacity.

4.3.1 Basics of Finite Element Analysis

A three-dimensional nonlinear finite element analysis was used to study the behaviour and ultimate load carrying capacity of the test specimens using eight-node plate elements.

The first step in a finite element analysis is to discretize the problem into sets of structural components. Each finite element is interconnected with the adjacent elements by

the nodal points. Nodal forces act at each nodal point which, in turn, is subjected to displacements and rotations. A standard set of simultaneous equations can be written to relate these physical quantities. Assembling these elements to form the whole structure is equivalent physically to superimposing these element equations mathematically. The result is a huge set of simultaneous equations that can be solved using computers.

From the potential energy formulation, the following equation in a matrix form is obtained:

$$\Pi_p = \frac{1}{2}\{U\}^T [K_e] \{U\} + \frac{1}{2}\{U\}^T [K_G] \{U\} - \{U\}^T \{P\} \quad (4\text{-}1)$$

where Π_p is the potential energy of the system; {U} is the global displacement vector; {P} is the global load vector; $[K_e]$ is the global elastic stiffness matrix; and $[K_G]$ is the global geometric stiffness matrix. The geometric stiffness matrix is included in the analysis to account for the deformed geometry of the elements in the equilibrium equations since the problem of angle members under a compressive load is a large deflection problem.

Differentiating with respect to the displacement and equating the result to zero to determine the minimum potential energy of the system results in the following:

$$[K_e] \{U\} + [K_G] \{U\} = \{P\} \quad (4\text{-}2)$$

Which can be simplified to the following basic finite element equation relating the global displacements and the global loads

$$[K] \{U\} = \{P\} \quad (4\text{-}3)$$

where $[K] = [K_e] + [K_G]$.

4.3.2 Nonlinear Iterative-Incremental Analysis

Nonlinearity of structural members may arise from large displacement effects, material nonlinearity and boundary nonlinearity.

In a linear problem, loads are applied to a model and the response can be obtained directly. In a nonlinear finite element analysis several linear steps are taken to solve the problem. This is done because the stiffness matrix itself is a function of displacements and the displacements are unknown which makes the one step solution of the nonlinear structure impossible.

Geometric nonlinearity is caused by the difference between the stiffness matrix of the reference structure and that of the deformed structure under a load increment. Many solution procedures have been proposed to solve nonlinear problems. ABAQUS uses the well known Newton's method as a numerical technique for solving the nonlinear equilibrium equations.

The nonlinear solution of the problem is obtained iteratively by solving a series of linear problems. For any displaced state of the structure, let u be the vector of nodal displacements; R_i the vector of internal resisting loads (i.e. the vector of loads in equilibrium with the internal forces of the structure); R_e the vector of external applied loads; and K_T the current tangent stiffness matrix of the structure. The vector of unbalanced loads, R_u, is given by

$$R_u = R_e - R_i \tag{4-4}$$

and provides a measure of the solution error.

The iterative sequence for Newton-Raphson iteration is as follows :

$$R_u^j = R_e - R_i^j \tag{4-5}$$

$$\Delta u^j = (k_T^j)^{-1} R_u^j \tag{4-6}$$

$$u^{(j-1)} = u^j + \Delta u^j \tag{4-7}$$

$$R_i^{(j-1)} = function\ (u^{(j-1)}) \tag{4-8}$$

in which j is the iteration number

The loading is divided into several increments and at each load increment the nonlinear equations are solved using either Newton's method or variations of it which are referred to as quasi-Newtonian techniques.

Using an estimated load, as an upper load limit, automatic load increments were applied. The automatic scheme for the procedure is based on the convergence of the iteration process of each increment, until the specified load tolerance in R_u^j was achieved.

If the number of iterations exceeded the maximum allowed, the increment size was reduced by a factor of four. If this resulted in a smaller increment than was specified as a minimum in the input, the run was terminated.

4.4 The Finite Element Model

In the following sections, the steps and assumptions considered in the modelling are reviewed. The review includes considerations in choosing the mesh, the verification of the model, material modelling, modelling of the initial out-of-straightness, modelling of residual stresses, and the modelling which is the boundary conditions.

4.4.1 Choice of Mesh

A convergence study was carried out in order to choose the proper finite element mesh. The choice of the three-dimensional finite element mesh is conventionally based on

pilot runs and is a compromise between economy and accuracy. Several element types were tested in the pilot runs. The number of elements used in the angle and gusset plate meshes was varied as well. Models of a whole specimen were compared with similar models considering only half the specimen with appropriate boundary conditions to reflect symmetry. In order to save time, it was also decided to model only half the specimen as no significant difference in the results was noted.

As the load transfers to the angle member, first through the gusset plate, through the welds to the connected leg and then to the entire cross section, it was crucial to choose a mesh with a finer grid at the gusset plates and at the ends of the angle in order to model, more accurately, the distribution of stresses that takes place in this zone. Refinement of the mesh at the ends of the specimens was also necessary to model different weld lengths. The global axes were taken such that the cross-section of the angles was in the x-y plane. Finite element meshes used to model all the test specimens are shown in Figures 4-1 to 4-14.

The load was applied at the ends of the gusset plate in the form of concentrated nodal loads. In order to allow for a uniform stress distribution at the end of the gusset plate, which is line 2 in the model, the loads were applied through a layer of fully linear elastic elements which are bounded between lines 1 and 2 in Figures 4-1 to 4-14. These fully linear elastic elements were added to the model to prevent local yielding at the points where the concentrated loads are applied and to transform these point loads to uniform distributed pressure at the end of the gusset plate. The distance between lines 1 and 2 was taken equal to the gusset plate unconnected length, L_g.

While modelling Trahair et al. test specimens, it was found, through the testing of several models, that residual stresses had no significant effect on the ultimate load carrying

capacity of the single-angle member connected by one leg. Thus, only two eight-node plate elements with six degrees of freedom assigned at each node were used in the analysis of Trahair et al. test specimens. A typical finite element model of Trahair et al. test specimen A-1-1 is shown in Figure 4-15.

During the course of this research, the University Computer Centre Mainframe was upgraded. The speed and capacity of the new system permitted the use of a more refined mesh, doubling the number of nodes, while keeping the computer run time about the same. For that reason it was decided to use a finer mesh for the modelling of the test specimens and for the parametric study.

For the angles, it was decided to use eight four-node plate elements per leg. Discretizing the leg into eight strips of elements along the length enabled the modelling of residual stresses (although these were neglected later). From the pilot runs, it was found that an element aspect ratio less than three had to be maintained for all the elements in order to have consistent results.

Thus the procedure followed to choose the relevant mesh for this problem was as follows: (i) a convergence test was carried out for the regular mesh and the appropriate number of elements was selected, and (ii) then more refined meshes were created at the end elements of the angle and the gusset plate to make it possible to model the stress distribution and the exact lengths of the welds.

4.4.2 Material Modelling

The simple linear elastic, perfectly plastic stress-strain relationship was used for modelling the mechanical properties of the steel. ABAQUS uses the Von Mises yield

criterion for isotropic metals in the plasticity modelling of the material properties. In that model the yield surface acts as a failure surface with no strain hardening parameters. Both Young's modulus of elasticity and the yield stress obtained from the tension tests were used in the analysis of the experimental test specimens. Fully linear elastic material was used for the elements bounded by lines 1 and 2 at the end of the gusset plate, as shown in Figures 4-1 to 4-14.

4.4.3 Initial Out-of-Straightness

The coordinates of the nodes of the model were defined taking into consideration the initial out-of-straightness of the angle. When modelling the experimental test specimens, the actual measured initial out-of-straightness was used. For Trahair et al. test specimens and for the parametric study, an assumed ideal initial out-of-straightness was used. This ideal initial out-of-straightness was assumed to have a parabolic shape with maximum value of L/1000 at the mid-height of the angle.

4.4.4 Boundary Conditions

Boundary conditions were imposed on two different groups of nodes in the model. The first group included all the nodes on lines 1 and 2 at the end of the gusset plate, shown in Figures 4-1 to 4-14. At these nodes, the displacements in both the x and y directions were prevented but the vertical displacements in the z-direction were allowed. The three rotations about the global axes were prevented to represent the fixed end conditions at the end of the test specimen. The second group of nodes with imposed boundary conditions were the nodes at mid-height of the angle. For these nodes the displacement in the z-direction, as well as the

rotations about the x and y axes, were prevented. These boundary conditions represent the plane of symmetry at mid-height of the test specimen.

A literature survey was conducted to determine if there is any published research in which a finite element model was used to model a weld subjected to both shear forces and bending moments perpendicular to the plane of weld. This survey revealed that the weld is either neglected and the material is considered to be continuous, or the weld material is assumed to be very rigid (Girard et al. 1995; Lipson et al. 1978). The latter assumption was used in this study.

The modelling of the weld was performed using the multi-point constraints (MPC) feature in ABAQUS. This option allows the imposing of constraints between specified degrees-of-freedom in the model. A BEAM MPC was used between all the welded nodes on the gusset plate and the corresponding nodes on the angle. This option connected two adjacent weld nodes together with a very stiff beam.

4.4.5 Verification of the Mesh

In order to verify and validate the nonlinear finite element models presented in this chapter, an extensive experimental study was conducted. The finite element models presented herein were validated and substantiated using the results of the 51 ultimate strength tests carried out through the experimental part of this research. The nonlinear finite element model was also verified using Trahair et al. (1969) test results as mentioned in Chapter 2. The results obtained from ABAQUS showed a very good agreement with all experimental test results as discussed later in the following chapters.

4.4.6 Residual Stresses

Residual stresses develop in hot rolled sections as a consequence of the differential cooling process. Residual stresses affect the ultimate load carrying capacity by initiating yielding of some parts of the member before the others. It has been shown previously (Elgaaly et al. 1992; Usami and Galambos 1971) that the residual stresses affect the ultimate load carrying capacity of single-angle compression members connected by one leg by about five percent or less. In spite of this, it was decided to check the effect the initiation of yielding of some parts of the angle before others has on the load carrying capacity of the angles being studied. The residual stresses were modelled as an initial stress in the angle plate elements in the z-direction. As part of the analysis procedure, ABAQUS performed an equilibrium check on the model to ensure that the model was in equilibrium under the imposed initial stresses. The ECCS (1985) recommendations regarding residual stresses were adopted in this study and are illustrated in Figure 4-16.

CHAPTER V

EVALUATION OF DESIGN PRACTICES

5.1 General

In this chapter, the Trahair et al. (1969) experimental test results are presented and compared to the compressive resistances calculated in accordance with different accepted design approaches and the requirements of the CSA steel standard, the AISC specification, and the ASCE standard for transmission towers as well as other design methods recommended by previous research. The background of these design approaches was discussed in detail in Chapter II. The objective of this chapter is to show the great variance in the approach used and in the load carrying capacities obtained using different design practices. It will be shown that there is a significant difference between the experimental results and the computed load carrying capacities. The experimental test results were also used to verify the finite element model.

5.2 Properties

5.2.1 Geometric Properties

Only Series A and Series B of Trahair et al. (1969) experimental test specimens were considered in this study. Series A specimens were 51 x 51 x 6.4 mm (2 x 2 x 1/4 in.) angles of ASTM A242 steel, Series B specimens were the same size angles but A36 steel. The

geometric properties of the angles were calculated based on the idealized rectangular cross section in which the toe and the fillet radii are omitted. The following formulae were used to calculate different cross section properties using the values tabulated in the CISC Handbook (see Figure 1-4).

$$A_g = t\ (b_x + b_y - t) \tag{5-1}$$

$$x = \frac{b_y^2 + t\ (b_x - t)}{2\ (b_x + b_y - t)} \tag{5-2}$$

$$y = \frac{b_x^2 + t\ (b_y - t)}{2\ (b_x + b_y - t)} \tag{5-3}$$

$$I_x = \frac{1}{3}\ [\ t\ (b_x - y)^3 + b_y\ y^3 - (b_y - t)\ (y-t)^3] \tag{5-4}$$

$$I_y = \frac{1}{3}\ [\ t\ (b_y - x)^3 + b_x\ x^3 - (b_x - t)\ (x-t)^3] \tag{5-5}$$

$$C_w = \frac{t^3\ (b_x - \frac{t}{2})^3 + t^3\ (b_y - \frac{t}{2})^3}{36} \tag{5-6}$$

$$J = \frac{1}{3}\ [t^3\ (b_x - \frac{t}{2}) + t^3\ (b_y - \frac{t}{2})] \tag{5-7}$$

$$I_{xy} = \frac{-b_x\ b_y\ t\ (b_x - t)\ (b_y - t)}{4\ (b_x + b_y - t)} \tag{5-8}$$

$$I_v = I_x \sin^2\omega + I_y \cos^2\omega + I_{xy} \sin(2\omega) \tag{5-9}$$

$$\tan(2\omega) = \frac{2I_{xy}}{I_y - I_x} \tag{5-10}$$

$$r_x = \sqrt{\frac{I_x}{A_g}}, \quad r_y = \sqrt{\frac{I_y}{A_g}}, \quad r_v = \sqrt{\frac{I_v}{A_g}}, \quad r_u = \sqrt{\frac{I}{A}} \tag{5-11}$$

where A_g is the gross cross-sectional area; b_x and b_y are the widths of the two angle legs parallel to the x and y axes, respectively; t is the angle thickness; I_x, I_y, I_w, and I_z are the moments of inertia about the x, y, w, and z axes, respectively; C_w is the warping constant; r_x, r_y, r_w, and r_z are the geometric radii of gyration about the x, y, w, and z axes, respectively, J is the torsional constant, I_{xy} is the product of inertia about the x and y axes; and ω is the angle between the z axis and the y axis.

5.2.2 Mechanical Properties

Two tension tests and two stub column tests were carried out to determine the mechanical properties of the material in the angles. The tension and compression tests gave comparable results. The average modulus of elasticity of Series A was found to be 202 700 MPa (29,400 ksi) and the average yield stress was 351 MPa (50.9 ksi). For Series B the corresponding values were 206 200 MPa (29,900 ksi) and 294 MPa (42.7 ksi). These average values were used in the calculation of the failure loads.

5.3 Comparison of Design Approaches

5.3.1 Finite Element Analysis

Figure 5-1 shows the experimental failure loads for the fixed and hinged Series A

specimens. Also shown are the finite element failure loads for these specimens calculated using ABAQUS for the fixed and hinged end condition cases. It can be observed from the Figure 5-1 that there is very good agreement between the experimental and the theoretically predicted finite element results for both the fixed and hinged end condition cases. The differences between the finite element and experimental failure loads are within 7% for the hinged specimens. For the fixed specimens, these differences were within 6% except for two test results where the difference was 16%. The experimental test results for these two specimens are not consistant with the others. It can be concluded that the finite element analysis is a good tool for predicting the ultimate load carrying capacity of this type of structural elements.

5.3.2 Simple-Column Approach

The ultimate load carrying capacities were determined using the simple-column approach assuming the angle to be a concentrically loaded pin-ended member. The ultimate load carrying capacities were calculated in accordance with Clause 13.3.1 of the Canadian Standard CAN/CSA-S16.1-M89 (CSA 1989) using a resistance factor, ϕ , of 1.0. The effective length factor was taken as 1.0 and the minimum radius of gyration, r_z, was used to determine the slenderness parameter, λ. The computed load carrying capacities are in a reasonable agreement (within 12% difference) with the experimental results of the very slender hinged specimens, λ>2.0, but greatly underestimate the load carrying capacity of the fixed ended specimens for the same slenderness parameter range. This reasonable agreement is expected since, for slender pin-ended columns, the load eccentricity becomes less significant and end conditions become the most significant factor affecting the load carrying capacity.

For the remainder of the slenderness parameters the compressive resistances lie between the results obtained for the two limiting cases of end conditions, except for the very short fixed-ended specimens. The simple-column approach tends to be unconservative at low slenderness ratios. It overestimates the load carrying capacity by about 12% for $\lambda = 0.75$. The fact that the simple-column design approach overestimates the experimental failure loads of short angles has been noted before in the literature (Woolcock and Kitipornchai 1986). Engineers, when designing short angles, must be aware of the fact that the simple column approach overestimates the load carrying capacity of these angles.

5.3.3 AISC Beam-Column Approach

Also shown in Figure 5-1 are the ultimate load carrying capacities computed using the beam-column procedure outlined in the AISC Manual of steel construction, load and resistance factor design (1986, 1994). In this procedure the member is considered to be pinned, the effective length factor is equal to 1.0, and the absolute sum of interaction terms was used. The resistance factor, ϕ, was taken as 1.0 for both bending and axial compression. The procedure outlined in the 1994 Manual gives a higher compressive resistance than the procedure used in the 1986 Manual, but not significantly higher. The predicted load carrying capacity is higher by about 3% for $\lambda = 2.67$. The increase in the load carrying capacity becomes more significant as the column gets shorter. For $\lambda = 0.74$, the AISC 1994 Manual gives a compressive resistance that is higher by about 16% than that predicted by using the 1986 Manual. It can be noted from the figure that the AISC beam-column procedure significantly underestimates the ultimate load carrying capacity when compared with the experimental test results. The approach outlined in the 1994 AISC Manual underestimates

the load carrying capacity of the hinged specimens by about 50% for the entire range of the slenderness parameter, λ.

5.3.4 ASCE Standard

Figure 5-2 shows a comparison between the experimental failure loads of Series A and the compressive resistances calculated in accordance with the ASCE standard "Design of latticed steel transmission structures" (ASCE 1991). The equations used to calculate the ultimate load carrying capacity are based on the results of a large number of experimental results obtained from tests on steel transmission towers. As can be observed, the ultimate load carrying capacities obtained by using ASCE standard fall between the experimental failure loads obtained for Series A fixed specimens and those that have pinned end conditions. Falling between the two limiting cases of boundary conditions is expected since fixed end conditions in transmission towers cannot be achieved as inevitable rotations occurs at the ends of the angle members that are usually connected to flexible members. For very slender angles the ASCE standard estimation of the failure load is in reasonable agreement with the experimental results of the hinged case while for very short angles a reasonable agreement is achieved for the fixed case.

5.3.5 Woolcock and Kitipornchai Procedure (1986)

Woolcock and Kitipornchai (1986) suggested a procedure that uses a uniaxial beam-column interaction equation for buckling and bending in the plane perpendicular to the connected leg of an angle in trusses. The out-of-plane bending moments at the ends of the strut are considered. They suggested the use of a specific eccentricity which was to the centre

of the connected leg as explained in Chapter II. The following interaction equation was used:

$$\frac{P_u}{\phi_c P_n} + \frac{P_u \left(c_y - \frac{t}{2}\right)}{\phi_b M_{nx}} \leq 1.0 \qquad (5\text{-}1)$$

Figure 5-3 shows the load carrying capacities calculated using this procedure. In that figure, the calculated compressive resistances are plotted against the length of the Series A specimens instead of the slenderness parameter, λ. This was done since for the same angle specimen the slenderness ratio is not the same for the simple-column approach and for the Woolcock and Kitipornchai method. Woolcock and Kitipornchai procedure is based on the geometric radius of gyration about the y-axis, r_y, while the simple-column approach is based on the radius of gyration about the minor principal axis, r_z.

5.3.6 Series B Specimens

The results were essentially the same for Series B specimens. Figure 5-4 shows the experimental results compared against those predicted by the simple-column, AISC, and ASCE design approaches. The same conclusions can be drawn from the comparison of these results and hence will not be discussed further.

5.4 Evaluation of Current Design Practices

As can be noted from above, the computed ultimate load carrying capacities values vary greatly according to the approach used. In most cases, the predicted load carrying capacities also differ significantly from the experimental test results.

The simple-column approach is not correct although it gives a much better estimate

of the load carrying capacity in some cases. It does not reflect the behavior of this type of structural members. The single-column approach tends to be unconservative at low slenderness ratios when compared to all other design approaches. The angle is not concentrically loaded and the effective length factor is not 1.0. The slenderness ratio should be modified to reflect the eccentricity of the load and the restraining moment at the ends of the angle as is done with the ASCE procedure.

The assumption that the angle bends about the minor axis of the angle is another incorrect assumption as the angle is attached by one leg. At the ends of an angle member attached to a gusset plate, for example, the bending must take place about an axis parallel to the welded leg. At the mid-height of the specimen, the bending takes place about an axis that lies in between the minor z-axis and the axis parallel to the welded leg. The location of that axis is dependent on the angle length and the restraining moment provided by the gusset plate. As noted from previous research, the deflection in the x-direction, perpendicular to the attached leg, have been measured in the laboratory and have been determined to be about 2.5 to 5 times the deflection in the y-direction. The location of the axis of bending of the angle also varies along the length of the angle member from one that is parallel to the welded leg to one that gets closer to the minor z axis. The angle is not concentrically loaded. The angle does not buckle about the minor axis, the z axis, since it is connected by one leg.

Although the AISC beam-column approach seems to reflect, more logically, the behavior of single-angle compression members connected by one leg since it considers the eccentricity of the applied load, it greatly underestimates the load carrying capacity of this type of structural member. It underestimates even the load carrying capacities of the hinged-ended specimens by about 50% over the entire slenderness parameter range. This occurred

although the hinged-ended match to a great extent the assumption provided to use the interaction beam-column equation.

The AISC beam-column interaction equation was developed for a wide flange section, a doubly symmetric section, where one of the four corners is critical for moments about both principal axes simultaneously. For singly symmetric and unsymmetric sections, the points of maximum stress for bending about both the principal axes moments usually do not coincide. Adluri and Madagula (1992) suggested a modification to the AISC LRFD beam-column interaction equation to be used with single-angle compression members to reduce this problem. They recommended the use of 2/3 rather than 8/9 as a modifier to the flexural terms of the interaction expression as explained in Chapter II. This flexural terms modifier was evaluated using a resistance factor, ϕ, of 0.9 although it should have been evaluated using a resistance factor of 1.0. Figure 5-5 shows a comparison between the load carrying capacity obtained using the interaction equation in AISC Manual of Steel Construction (1986, 1994) and the modification suggested by Adluri and Madagula (1992) applied to the interaction equations of the 1994 AISC Manual of Steel Construction. The modification suggested by Adluri and Madagula to the interaction equation resulted in compressive resistances that are slightly higher (6-14%) than those obtained using the AISC Manual (1994) for the entire slenderness parameter range. The computed compressive resistances are still significantly lower than the experimental results.

Woolcock and Kitipornchai's suggested design procedure assumes a certain value for the eccentricity to be considered in a uniaxial interaction equation. Obviously, this is incorrect as the eccentricity of the load is a function of the end restraints. The end restraints, in turn, depends on the properties of the gusset plate or tee section connected to the angle.

On the other hand, the load carrying capacities of fixed-ended single-angle members vary significantly by changing the gusset plate dimensions. Changing the gusset plate dimensions changes the restraining moments provided by the gusset plates at the ends of the angle. This changes the apparent location of the load in a way so that it gets closer to the centroid. That is why the simple-column approach yields results that are much better in many cases than those predicted using the AISC beam-column approach. The ultimate load carrying capacity would increase considerably if, for example, the gusset plate thickness or width is doubled. This would shift the experimental test results curve higher. The difference between the fixed-ended and hinged-ended specimens test results would be reduced if the width and/or thickness of the gusset plate of the fixed-ended specimens is decreased.

It can be concluded that none of the current design practices can predict accurately the ultimate load carrying capacity of single-angle compression members connected by one leg. There is no published research that relates the gusset plate dimensions to the ultimate load carrying capacity of single-angle members. Such a study is crucial to define the most influential design parameters. These parameters would eventually be extensively studied to determine their effects and to include them in a design procedure. This will be the scope of the remainder of this research.

CHAPTER VI

EXPERIMENTAL STUDY AND VERIFICATION OF THE FINITE ELEMENT MODEL

6.1 General

The experimental program was carried out to study the behavior of single-angle compression members welded by one leg. The experimental program was designed to study the effect of gusset plate dimensions, the amount of weld and weld pattern used in connecting the angle to the gusset plate on the behavior and ultimate load carrying capacity of single-angle compression members welded by one leg to a gusset plate. The mode of failure, lateral deflections and cross-sectional rotations at mid-height were observed. The experimental program was also used to verify the results obtained from the nonlinear finite element model so that the latter could be used for an extensive parametric study and to develop design curves and design equation for this type of structural element. In this chapter, the experimental results obtained from the 51 ultimate strength tests discussed earlier in Chapter III are presented and discussed. The ultimate load carrying capacities and load-deflection and load-strain curves obtained from the finite element analysis are presented and compared with those obtained from experimental test results.

6.2 Properties

6.2.1 Geometric Properties

Steel angles of nominal dimensions 64 x 64 x 7.9 mm (2½ x 2½ x 5/16 in.) were used to build the specimens. The angles were cut to proper lengths from 6.1 m (20 ft.) long pieces. For the theoretical computations, the geometric properties of the angles were calculated based on the idealized rectangular cross-sectional elements in which the toe and the fillet radii were omitted. The formulae given in Section 5.1 were once again used to calculate cross-sectional properties.

The actual dimensions, measured in the laboratory, varied from the nominal dimensions by -0.2 to 1.1% for the angle leg widths and by -2.5% to 2.2% for the angle leg thicknesses. For convenience the nominal dimensions of angles were used for all theoretical and finite elements calculations. Tables 6-1 to 6-3 show the actual dimensions of the test specimens along with the number of the 6.1 m (20 ft.) angle piece from which they were cut.

6.2.2 Mechanical Properties

A total of fifteen pieces of angles, 6.1 m (20 ft.) long, were used to fabricate the test specimens. Fifteen tension tests were carried out to determine the mechanical properties of each of the angles used in this experimental investigation. The tension specimens were prepared in accordance with the requirements of CAN/CSA-G40.20-M92, "General requirements for rolled or welded structural quality steel" (1992). The dimensions of these tension test specimens are given in Figure 3-11. Young's modulus of elasticity of the angles was determined by using strain gauges, one on each side of three tension test specimens. The actual cross section dimensions of the tension specimens were measured before testing and

were used to calculate the mechanical properties of the angles.

Table 6-4 shows the tension test data obtained for the tension specimens cut from each of the fifteen angle pieces. As can be seen from Table 6-4, the average Young's modulus of elasticity was found to be 207 000 MPa and was used in all the theoretical computations. The yield stress varied from 344.8 to 417.1 MPa. Due to the significant difference in these values, the actual yield stress for each individual angle was used in the theoretical analysis. Three tension test specimens were taken from the webs of each of the W530 x 82 (W21 x 55) and the W530 x 123 (W21 x 83) split to make the tee sections used in the specimens to represent the end gusset plates. As can be seen from Tables 6-5 and 6-6, the average yield stress was 413.4 and 386.6 MPa, and the Young's modulus of elasticity was found to be 203 400 and 204 100 MPa for the W530 x 82 (W21 x 55) and the W530 x 123 (W21 x 83), respectively. These values were used in all the theoretical computations.

6.2.3 Initial out-of-straightness

The initial out-of-straightness of each angle leg was measured as explained earlier in Chapter III. Tables 6-7 to 6-9 list the measured initial out-of-straightness for the slender, longer intermediate length, and shorter intermediate length specimens, respectively. The initial out-of-straightness ranged from L/930 to L/9130 for the slender specimens, L/1000 to L/4960 for the longer intermediate length specimens, L/1830 to L/4125 for the shorter intermediate length specimens. For the angles used in the test specimens in the experimental program, the out-of-straightness, in general, decreased as the length of the angle decreased. The out-of-straightness of an angle leg was, in most cases, in a direction towards the angle centroid.

6.3 Experimental and Theoretical Results of Test Specimens

6.3.1 Ultimate Load Carrying Capacities

Tables 6-10 to 6-14 list the ultimate load carrying capacities obtained from the experimental program and from the finite element analysis. Although the theoretical failure loads obtained from the finite element analysis are, in general, higher than the experimental failure loads, the agreement is quite good. For the slender specimens the difference ranged from +2.6% to +8.5%, for the longer intermediate length specimens from -1.1 to +6.1%, and for the shorter intermediate length specimens from -3.8% to +8.7%. It can be concluded that the finite element analysis can be used to predict, with a reasonable degree of accuracy, the ultimate load carrying capacity of single-angle compression members welded by one leg to a gusset plate.

Tables 6-15 to 6-17 make a comparison of the experimental failure loads and the compressive resistances as predicted by using the two generally accepted design approaches, the simple-column approach and the beam-column approach. The simple-column approach, as explained before, assumes that the angle is a concentrically loaded column that buckles about the minor principal axis of the angle, the z axis. The effective length factor is usually assumed to be 1.0 and this assumption is used in all calculations. The resistance factor, ϕ, was taken as 1.0. In the beam-column approach the load was assumed to act at the centre of the gusset plate and, once again, the resistance factors were taken as 1.0.

For the slender specimens the simple-column approach underestimates the ultimate load carrying capacity by about 32 to 44%. For the longer intermediate length specimens, the simple-column approach underestimates the load carrying capacity by about 20 to 30%, but for the shorter intermediate length specimens the simple-column approach overestimates the

load carrying capacity by as much as 16%. The beam-column approach predicts a load carrying capacity that is only about 50%, or less, of the actual experimental load carrying capacity. This approach is not widely used by design engineers since it provides a very conservative estimate of the load carrying capacity and since it involves tedious calculations for a structural member that is considered by most practicing engineers to be a very simple member.

6.3.2 Failure Modes

All the specimens failed in a similar manner. Increasing the compressive load caused some yielding to occur at the ends of the gusset plate. This was followed by the development of a plastic hinge at the ends of the gusset plates as the applied load increased. A typical plastic hinge after the completion of testing can be seen in Figures 6-1 and 6-2 for specimens S-D-1 and L-I-3, respectively. The yielding of the gusset plate was followed by some yielding near the angle ends. Large lateral deflections of the angle at mid-height caused yielding near the toes of the angle legs which soon propagated toward the heel and then towards the ends of the angles. However, for slender angles, yielding of the angle was limited to the tips at mid-height only and occurred due to the large lateral deflections that developed after reaching the ultimate load carrying capacity. Figure 6-3 shows the deflected shape of Specimen L-D-2 during testing. For the shorter intermediate length specimens, yielding of the angle at mid-height started before the ultimate load was reached and kept propagating toward the ends of the angle until the ultimate load was reached. This behavior was observed during the application of the load by watching the cracking of the whitewash. This failure mechanism was confirmed by the finite element analysis and by the load-strain curves discussed later in

this chapter. Figure 6-4 shows the yielding of the connected leg of Specimen S-D-2. Figures 6-5 to 6-7 show the deflected shape at ultimate load, predicted using the finite element method, of Specimens L-A-1, M-A-1, and S-A-1, respectively.

6.3.3 Load-Deflection Curves

Figures 6-8 to 6-10 show the mid-height load-deflection and load-rotation curves obtained from experimental testing and finite element analysis for specimens L-A-1, M-A-1, and S-A-1, respectively. These are typical for all the specimens. The same curves are shown in Appendix A for all the 51 specimens tested in this study. This is a convenient method to represent and to make a comparison of the experimental and finite element results. As can be observed, there is a good agreement between the experimental and theoretical results. It is interesting to mention that the agreement between the theoretical and experimental lateral deflections is better than that observed between the theoretical and experimental rotations. It is easier to model the more slender angles than the shorter angles as material nonlinearity becomes more predominant in shorter columns. Figure 6-10, however, indicates that good results were obtained for even the shorter specimens. All the load versus deflection and rotation curves indicate a typical biaxial beam-column behavior where deflections in the x and y directions and the cross-sectional rotation start increasing from the early stages of loading and increase excessively as the load is increased. There is no bifurcation of the equilibrium, that is, no buckling occurs, but failure occurs due to inelastic instability after some yielding have taken place. The amount of yielding depends on the angle slenderness ratio.

Table 6-18 shows the x to y deflection ratios obtained from experimental testing, refer to Figure 6-11 for the definition of the x and y directions, for all the test specimens at ultimate

loads and at working loads, using a load factor of 1.4. Table 6-19 lists the same results obtained from finite element analysis for the theoretical specimens using an initial out-of-straightness of L/1000 and a 300 MPa yield stress. As can be observed from the load-deflection curves and from Tables 6-18 and 6-19, the predominant deflection is the one in the direction perpendicular to the gusset plate, the x direction. The deflection in the plane of the gusset plate was relatively small but did increase once the ultimate load was reached. For slender specimens, the lowest x to y deflection ratio observed at ultimate load was that of specimen L-F-2 and was 5.1. At a working load, using a factor of 1.4, the lowest x to y deflection ratio observed was that for specimen L-I-1 and was 6.3. For shorter intermediate length specimens, the lowest x to y deflection ratio observed was that of specimen S-H-3 and was 9.7 at ultimate load. At a working load, using a factor of 1.4, the lowest x to y deflection ratio observed was for specimen S-I-1 and was 8.1. Figure 6-12 shows the location of the deflected cross-section, as obtained from finite element analysis, at mid-height and quarter point for Specimens L-A-1, M-A-1, and S-A-1, respectively. It can be seen that the predominant deflection is the one that is perpendicular to the gusset plate. Figure 6-13 makes a comparison between the finite element analysis and experimental results for the location of the deflected cross section at mid height for Specimens L-A-1, M-A-1, and S-A-1, respectively. Good agreement is again observed between the finite element analysis and experimental testing.

6.3.4 Load-Rotation Curves

Load-rotation curves are plotted for all the test specimens and shown in Appendix A. As can be observed, there is a good agreement between the experimental and theoretical

results. The rotation always occurred in the positive direction shown in Figure 6-11. Rotation of the angle cross-section at mid-height was very small until the ultimate load was reached. At the ultimate load, the experimentally measured rotations ranged from 2.8° to 5.3° for slender specimens, 2.8° to 4.0° for the longer intermediate length specimens, and 1.7° to 2.8° for the shorter intermediate length specimens. This small rotation of the cross section at mid-height can be observed in Figure 6-13 which shows the location of the experimental and finite element deflected cross-section at ultimate load at mid-height for Specimens L-A-1, M-A-1, and S-A-1, respectively.

6.3.5 Failure Axis

As can be concluded from the discussion above, all the specimens failed by flexural buckling about an axis falling between the minor principal axis, the z axis, and the geometric axis parallel to the gusset plate, the y axis. However, the failure axis is always very close to the y axis. The failure axis is illustrated in Figure 6-14. The location of the failure axis can be obtained from Table 6-18 which shows the x to y deflection ratios for all the test specimens at ultimate loads and at working loads, using a load factor of 1.4. For slender specimens, the angle α is always less than 11° at working loads and decreases to 7° or less at ultimate loads. The decrease is due to the increase in the y deflection as the ultimate load is approached. For shorter intermediate length specimens, this angle is always less than 5°. Figure 6-15 shows the location of the failure axis, as obtained from the finite element analysis, with respect to the y-axis along the angle height for Specimens L-A-1, M-A-1, and S-A-1. This failure axis changes along the specimen height from one that is parallel to the connected leg at a section adjacent to the weld to one oriented as shown in Figure 6-14 at mid-height.

Table 6-19 shows the x to y deflection ratios for all test specimens obtained from the finite element modeling of specimens taking the initial out-of-straightness as L/1000 and the yield stress as 300 MPa. In general, the angle α is smaller than those observed in the tests.

6.3.6 Load-Strain Curves

In order to get more confidence in the finite element model, one slender specimen, L-A-3, and one of the shorter intermediate length specimens, S-A-3, were strain gauged as shown in Figure 3-9 to study the behavior of the gusset plate and the angle cross section at mid-height. This was also done to confirm the mode of failure observed by watching the cracking of the whitewash.

Figures 6-16 to 6-18 show the experimental strain measured at the end of the gusset plate of Specimen L-A-3 by strain gauges 5 to 10 which are located as shown in Figure 3-9. The strain at the same points as calculated by the finite element method is also shown in the same figures. There is a good agreement between the experimental and finite element results up to a load of about 75% of the experimental ultimate load. Beyond 75% of the ultimate load, the experimental strains are much higher than those obtained using the finite element method. This might be due to residual stresses in the gusset plate which are developed as a result of the welding and manufacturing process. No attempt was made to measure these residual stresses or account for them in the finite element analysis. It can be noted from the results that the gusset plate yielded first before the angle and developed a plastic hinge. However, the development of a plastic hinge did not take place until a load was reached which is near the ultimate load for slender specimens.

Figure 6-19 shows a comparison between the experimental and finite element strains

at points where strain gauges 1 and 4 are located at mid-height of the specimen L-A-3, as indicated by Figure 3.9. Comparing the finite element and experimental strains it can be observed that there is the same trend of high strain near the toe of the outstanding leg while the strain in the welded leg is almost linear. The high strain at the toe of the outstanding leg is due to the excessive large deflections observed at mid-height near the failure load after the development of the plastic hinges in the gusset plate. The angle failed due to geometric instability caused by large deflections at mid-height. This is be expected as the specimen is a slender specimen with a slenderness ratio, L/r_z, of 170.

Figures 6-20 to 6-22 show a comparison of the experimentally measured strains and those computed by the finite element method at the end of the gusset plate of the shorter intermediate length Specimen S-A-3 at the location of strain gauges 5 to 10. Good agreement exists between the experimental and finite element strains until the load reaches about 95% of the ultimate load except for strain gauge 6 where the experimental strains are about 30% higher than the finite element results. It can be noted also from the results that the gusset plate yielded first on the compression side at about 60% of the ultimate load and then on the tension side at about 80% of the ultimate load. The plastic hinges developed in the gusset plate of the shorter intermediate length specimens at a lower ratio of load to ultimate load than with the slender specimens.

Figure 6-23 compares the experimental and finite element strains for strain at locations of strain gauges 1 and 4 located at mid height of Specimen S-A-3, as indicated by Figure 3-9. The finite element strain is lower than the experimental strain when the load approaches the ultimate load. Excessive strains, due to large deflections, are observed near the failure load after the development of the plastic hinges in the gusset plate. From these curves the yielding

in the attached leg can be observed at mid-height. The angle failed inelastically due to the excessive deflections at mid-height.

From Figures 6-16 to 6-23 it can be concluded that a finite element analysis can be used to predict, with a reasonable degree of accuracy, the strains in the angles and in the gusset plates. This is true for all slenderness ratios studied in the experimental program. The good agreement between the experimental and finite element strains makes the finite element model a good, and economical, tool for studying the behavior of this type of compression member. Finite element analysis also eliminates the need for the time consuming and costly installation of strain gauges for further studies of this type of member.

6.4 Effect of Gusset Plate Dimensions

One of the objectives of the experimental program was to get some data to determine the effect of gusset plate dimensions and weld pattern on the behavior of single-angle compression members connected by one leg. Three different gusset plate parameters were investigated: the unconnected length of the gusset plate L_g, the gusset plate thickness t_g, and the gusset plate width B_g. As these specimens vary in their yield stress and initial out-of-straightness, a finite element modeling of these specimens was conducted using a yield stress of 300 MPa and a sinusoidal initial out-of-straightness of L/1000 about the z-axis so that the effect of the parameter under consideration can be assessed. These specimens will be referred to as "theoretical specimens." In the following sections the effect of changing gusset plate dimensions on the ultimate load carrying capacity and behavior of single-angles are discussed.

6.4.1 Effect of Gusset Plate Unconnected Length, L_g

The effect of changing the gusset plate unconnected length can be observed by comparing the results of Type A and Type B specimens where the unconnected gusset length is 20 mm and 40 mm, respectively. Tables 6-10 and 6-13 show the ultimate load carrying capacities of these specimens. Increasing the unconnected gusset plate length from 20 mm to 40 mm reduced the average experimental ultimate load carrying capacity by about 3.5% and 3.9% for the slender and the shorter intermediate length specimens, respectively. For the theoretical specimens, shown in Column 7 of Tables 6-10 and 6-13, the finite element analysis indicated a reduction of 2.8% and 1.7% in the ultimate load carrying capacity of the slender and the shorter intermediate length specimens, respectively. This indicates an insignificant decrease in the ultimate load carrying capacity.

Figures 6-24 to 6-26 show the effect of changing different gusset plate dimensions on the behavior of the theoretical test specimens. As can be seen from these figures, increasing the unconnected gusset plate length weakened the end restraint provided by the gusset plate. This resulted in a small increase in lateral deflections and cross-sectional rotations of the single-angle. The same observations can be noticed from Figures 6-27 to 6-29 for the shorter intermediate length specimens.

As increasing this parameter increases the size of the gusset plate and decreases the angle strength, the 40 mm unconnected length in Type B specimens provided a reasonable upper limit for studying this parameter. As already observed, doubling the unconnected gusset length reduced the load carrying capacity by less than 3.3%. Since this reduction is insignificant, the effect of the unconnected gusset length on the ultimate load carrying can be neglected as long as it remains within practical limits. The gusset plates of Type A and Type

B specimens yielded and a plastic hinge developed and was observed.

An unconnected gusset plate length of 20 mm is a reasonable minimum value for this design parameter as enough room must be provided to allow the weld to be placed at the end of angle. The 20 mm dimension also satisfies the seismic design recommendation of Astaneh-Asl et al. (1986). In that research it was recommended that an unconnected gusset plate length of at least two times the gusset thickness should be provided to ensure the free formation of plastic hinges and to improve the ductility of gusset plates used with double-angle bracing members.

6.4.2 Effect of Gusset Plate Thickness, t_g

The effect of increasing the gusset plate thickness was studied using Type A and Type F test specimens. Type F specimens had the same dimensions as Type A specimens except for the gusset plate thickness which was taken as 12.7 mm instead of 10.2 mm. Tables 6-10, 6-12, and 6-13 show the ultimate load carrying capacities for Type A and Type F specimens. For slender specimens, increasing the gusset plate thickness from 10.2 mm to 12.7 mm increased the averaged experimental failure loads by about 16%. The finite element analysis of the theoretical specimens indicated an increase of about 12.7%. For the longer and shorter intermediate length specimens, the increase in the experimental failure load was 8.5% and 6.6%, respectively. The increase in the ultimate load of the theoretical specimens was 9.9% and 7.4% for the longer and shorter intermediate length specimens, respectively. Increasing the gusset plate thickness increased the gusset plate stiffness and hence the restraining moment provided by the gusset plate at the ends of the angle. The increase in the ultimate load carrying capacity becomes greater as the angle slenderness parameter increases. This

increase is of a significant value, especially if a wider range of gusset plate thicknesses is considered, and should be an explicit term in any design equation for this type of compression members. This conclusion is confirmed by the results of a parametric study presented and discussed in the following chapter. From experimental observation and finite element results it was noticed that the gusset plate yielded first and a plastic hinge developed in Type F specimens as well as in Type A specimens.

Figures 6-24 to 6-32 show the effect of changing the gusset plate thickness on the behavior of the theoretical test specimens. As can be seen from Figures 6-24 to 6-26, for slender specimens, increasing the gusset plate thickness increased the end restraint provided by the gusset plate. This decreased all lateral deflections and cross-sectional rotations of the single-angle member. The same observations can be noticed from Figures 6-27 to 6-32 for the shorter and longer intermediate length specimens.

6.4.3 Effect of Gusset Plate Width, B_g

The effect of increasing the gusset plate width was studied using Type A and Type J test specimens. Type J specimens were similar to Type A specimens except for the gusset width which was take as 225 mm instead of 150 mm. Tables 6-10, 6-12, and 6-13 show the ultimate load carrying capacities for Type A and Type J specimens. For slender specimens, increasing the gusset plate width from 150 mm to 225 mm increased the experimental failure loads by about 12.9%. The finite element analysis of theoretical specimens indicated an increase of about 7.4%. For the longer and shorter intermediate length specimens, the increase in the experimental averaged ultimate load was found to be 5.5% and 9.9%, respectively. The increase in the ultimate load carrying capacity for the theoretical specimens

was 4.5% and 7.9% for the longer and shorter intermediate length specimens, respectively. This increase is significant, especially if a wider range of gusset plate widths is considered, and hence should be considered in any design equation for this type of compression members. From experimental observation and finite element results it was noticed that the gusset plate yielded first and a plastic hinge developed in Type J specimens as well as in Type A specimens. The yielding of Type J specimens was more localized toward the angle than toward the gusset plate ends.

Figures 6-24 to 6-32 show the effect of changing gusset plate width on the behavior of the theoretical test specimens. As can be seen from Figures 6-24 to 6-26, increasing the gusset plate width increased the end restraint provided by the gusset plate. As a result, all lateral deflections and cross-sectional rotations of the single-angle decreased. The same observations can be noticed from Figures 6-27 to 6-32 for the shorter and longer intermediate length specimens.

6.5 Effect of Weld Length, L_w

The effect of increasing the weld was studied using Type A and Type D test specimens. Type D specimens were exactly the same as Type A specimens except that the weld length was designed to attach an axially loaded angle with an assumed effective length factor of 0.8 instead of 1.0. Tables 6-10 and 6-13 show the ultimate load carrying capacities for Type A and Type D specimens. As can be seen from Columns 4 and 7 in these tables, the increase in the ultimate load carrying capacity was insignificant and may be neglected. For slender specimens, increasing the total weld length from 70 to 104 mm increased the

experimental failure loads by about 1.6%. The finite element analysis indicated an increase of about 0.6% in the theoretical specimens. For the shorter intermediate length specimens, the increase in the experimental failure loads and ultimate loads obtained from the finite element analysis for the theoretical specimens was in the order of was -0.1% and 2.5%, respectively. The change in the ultimate load carrying capacity due to increasing the weld length is insignificant and can be neglected in any further parametric study. The failure mechanism occurred as in all specimens by developing a plastic hinge in the gusset plates followed by excessive deformation at mid-height and the development of yielding in short specimens which, with increasing the load, propagated toward the angle ends. The increase if the weld length reinforced the angle slightly by strengthening the angle cross-section in a zone that is not critical in the failure mechanism.

For the slender specimens, no effect of the weld length was observed on the lateral deflections and cross-sectional rotations at mid-height as shown in Figures 6-33 to 6-35. For the shorter intermediate length specimens, referring to Figures 6-36 to 6-38, no effect on the angle deflections and rotations was noticed until a load of about 65% of the ultimate load was reached. The cross-sectional deflection and rotation was slightly decreased when the weld length increased.

As for the gusset plate unconnected length, increasing the weld length increases the size of the gusset plate. This increase in the weld length is accompanied by a very slight increase in the ultimate load carrying capacity which makes the connection more expensive. Therefore, the minimum weld required to sustain the ultimate load carrying capacity of the angle should be used.

6.6 Effect of Weld Pattern Used in the Connection

The effect of changing the weld pattern was studied using Type F, Type H, and Type I test specimens. Type F specimens had weld that was balanced about the centre of the connected leg, referred to as "equal weld". Type I specimens were exactly the same as Type A specimens except that the weld was arranged such that it was balanced about the projection of the centroid on the connected leg, refer to Figures 3-3 and 3-4. Type H specimens were identical to Type I specimens except for the weld pattern which was unbalanced about the projection of the centroid on the connected leg. Tables 6-11 and 6-14 show the ultimate load carrying capacities for Type F, Type I, and Type H specimens. As can be seen from Columns 4 and 7 in these tables, the increase in the ultimate load carrying capacity was insignificant and may be neglected. For slender specimens, using balanced welds in the connection increased the experimental failure loads by about 2.7% when compared with using equal welds. Using unbalanced welds instead of equal welds increased the experimental failure loads by about 1.1% . The finite element analysis of the theoretical indicated an increase of about 1.9% and 2.4%, respectively. For the shorter intermediate length specimens, using balanced welds in the connection instead of equal welds resulted in an increase in the experimental failure loads and ultimate loads obtained from the finite element analysis for the theoretical specimens in the order of 4.0% and 1.8%, respectively. The increase was 2.5% and 1.8% when unbalanced welds were used instead of equal welds. The change in the ultimate load carrying capacity due to using balanced or unbalanced welds is insignificant and can be neglected in any further parametric study. Using different weld patterns did not affect the failure mechanism.

Changing the weld pattern affects the load eccentricity in the plane of the gusset

takes place in the plane perpendicular to the gusset plate, any eccentricity in the plane of the gusset plate has an insignificant effect on the ultimate load carrying capacity.

Figures 6-39 to 6-44 show the effect of using different weld patterns on the lateral deflections and cross-sectional rotations at mid-height for the slender and shorter intermediate length specimens. For slender specimens, no effect of the weld pattern was observed on the lateral deflections and cross-sectional rotations at mid-height as shown in Figures 6-39 to 6-41. For the shorter intermediate length specimens, referring to Figures 6-42 to 6-44, no effect on the angle deflection in the x direction and rotations was noticed. The weld pattern affected only the lateral deflection in the y direction at the beginning of loading.

As the weld pattern does not have a significant effect on the ultimate load carrying capacity or behavior of single-angle compression members connected by one leg, the weld should be arranged in a way that makes the gusset plate area as small as possible to reduce the cost of such structural element.

CHAPTER VII

PARAMETRIC STUDY AND DESIGN EQUATION

7.1 General

It was shown in Chapters V and VI that the ultimate load carrying capacity of a single-angle compression member welded to a gusset plate by one leg is, in general, considerably higher than that predicted by using the two generally accepted design approaches, the simple-column and the beam-column approaches. Both approaches neglect several important design parameters of the members being considered. The most important of these parameters are the dimensions of the gusset plate. The dimensions of the gusset plate affect the end restraint provided at the ends of the angle.

It was shown in Chapters V and VI that the finite element method gives results that agreed reasonably well with the experimental results. This good agreement was a green light to conduct a parametric study using that method. In this chapter, the results of a detailed parametric study that involved more than 1800 models of single-angle compression members attached by one leg to gusset plates is presented and discussed. The parametric study involved a study of the effect of initial out-of-straightness, residual stresses, Young's modulus of elasticity, and the width, thickness and unconnected length of the gusset plate. A study of the effect of varying these parameters is required to get a better understanding of the behavior of these members so that a design equation can be developed for this type of structural

element.

For the parametric study a 64 x 64 x 7.9 mm (2½ x 2½ x 5/16 in.) angle was used in all cases. A gusset plate with a width of twice the angle leg width and a thickness of 0.2 times the angle leg width was used when studying the effect of varying the initial out-of-straightness, residual stresses, Young's modulus of elasticity, and the unconnected length of the gusset plate. The thickness of the gusset plate was expressed as a function of the angle width because of the significant effect that property has on the bending stiffness of the angle. The thickness of the 64 x 64 mm (2½ x 2½ in.) angle was varied from 3.2 mm (0.125 in.) to 12.7 mm (0.5 in.) to produce a large database of angles with different design parameters so that a design equation that covers all width-to-thickness ratios, b/t, of angles listed in the CISC Handbook (1995) could be developed. The yield stress of the angle and the gusset plate was taken as 300 MPa in all cases. The projection of the centroid of the angle on the gusset plate was aligned with the centroid of the gusset plate. The parametric study will be discussed in detail in the following sections.

7.2 Slenderness ratio

The slenderness ratio is the most important parameter in predicting the strength of a single-angle compression member. The simple-column and AISC beam-column approaches use the radius of gyration about the minor principal axis to calculate the ultimate load carrying capacity. In some other cases, Woolcock and Kitipornchai (1986) for example, the load carrying capacity was calculated using the radius of gyration about one of the geometric axes, the one that is parallel to the connected leg. It should be pointed out that the use of this slenderness ratio requires some explanation since it does not conform to the normal concept

of a slenderness ratio. The slenderness ratio is calculated using the radius of gyration about an axis of bending which is the same axis at all cross sections in the compression member. This is not true for angles attached by one leg to a gusset plate. The axis of bending in the angle adjacent to the welds must be about an axis parallel to the gusset plate. Considering that the axis of bending is determined from the deflections in the x and y directions at other cross sections away from the connection, it was explained in the previous chapter that the failure axis rotates until at mid-height it would be something like the axis shown in Figure 6-14. As cross sections that range from a section adjacent to the connection to one at mid-height of the compression member are considered, the failure axis rotates towards, but never coincides with, the z axis. The location of the failure axis at mid-height depends on the restraint provided to the angle by the element to which the angle is attached and on the angle length. The gusset plate in this study provides a lot of restraint to the angle and therefore the failure axis is close to the y axis. Thus it is not possible to calculate a slenderness ratio for a single-angle attached by one leg to a gusset plate in the traditional sense. With the gusset plates providing enough end restraint to the angle to buckle about an axis close to the y-axis, it is suggested that the slenderness ratio be calculated about the geometric axis parallel to the gusset plate, the y axis.

As for all structural columns, the slenderness ratio is a very significant factor in determining the ultimate load carrying capacity. Figure 7-1 shows the failure load versus slenderness ratio for an equal-leg angle with a leg width of 64 mm (2½ in.). The angle thickness was varied to plot the curves for different width-to-thickness ratios. Decreasing the slenderness ratio, L/r_z, from 300 to 50 increases the load carrying capacity by 277, 258, and 230% for angles with width-to-thickness ratios of 5, 12, and 20, respectively.

7.3 Parametric Study on Angle Properties

The objective of this section is to study the influence of different parameters related to the strength of equal-leg single-angle compression member to determine whether or not their effect on the ultimate load carrying capacity should be considered in a design procedure.

7.3.1 Effect of the Initial Out-of-Straightness

The effect of an initial out-of-straightness on the ultimate load carrying capacity was studied and the results are shown in 7-2. The initial out-of-straightness, sinusoidal in shape, was taken in a direction perpendicular to the minor principal axis, the z axis. Four different slenderness ratios, L/r_z, ranging from 80 to 300, were used in the study. A maximum slenderness ratio of 300 was used although Clause 10.2.1 of CAN/CSA-S16.1-94, "Limit states design of steel structures" (CSA 1994), limits the slenderness ratio of a compression member to 200. As explained above, it is a common practice to calculate the slenderness ratio based on r_z, the radius of gyration about the minor principal axis. For angles welded to gusset plates by one leg, as has been shown in Chapter VI, the predominant deflection is in the x direction, a direction perpendicular to the connected leg. Thus it might be argued that a slenderness ratio based on r_y, the radius of gyration about the geometric axis parallel to the gusset plate, should be used for this type of angle members. For equal-leg angles the ratio of r_y to r_z is 1.5. Thus if L/r_z is 300, L/r_y would be 200, the maximum allowed by S16.1

As can be seen from Figure 7-2, changing the initial out-of-straightness from L/4000 to L/250 decreases the load carrying capacity by about 13%, 12%, 11%, and 8% for L/r_z of 300, 200, 140, and 80, respectively. The reduction in the ultimate load carrying capacity varies almost linearly with the magnitude of out-of-straightness. The effect of initial out-of-

straightness becomes more significant as the slenderness ratio of the angle increases. Initial out-of-straightness of L/4000 to L/1000 covers most of the initial out-of-straightness measured in the experimental study. As can be shown from Figure 7-2, changing the initial out-of-straightness from L/4000 to L/1000 affects the load carrying capacity by only 3% for the slenderness ratios, L/r_z, ranging from 80 to 300. This small reduction in the ultimate load carrying capacity is negligible when compared to the effect of changing other parameters. The initial out-of-straightness was taken as L/1000 in the rest of this parametric study and its effect on the ultimate load carrying capacity was not explicitly included in the proposed design equation. However, it must be emphasized that the load reduction that occurs due to an initial out-of-straightness of L/1000 is included in the equation but because of the small effect of changing the out-of-straightness the design equation does not include the out-of-straightness as a specific term.

7.3.2 Effect of Residual Stresses

The exact distribution of residual stresses depends on many factors such as the straightening and cooling processes, etc. In this study, the standard ECCS (1985) residual stress distribution shown in Fig. 4.16 was adopted to study the effect of residual stresses. As noted before from previous research, the effect of residual stresses was found to be negligible for the type of structural member studied in that research. Elgaaly et al. (1992) reported on the behavior and load carrying capacity of single angles connected by one leg to truss chords which were tee sections. In order to determine the effect these residual stresses had on the ultimate load carrying capacity, Elgaaly et al. carried out a sensitivity analysis in which the maximum value of the residual stresses was varied from 0 to $0.3F_y$. It was concluded that the

effect of the residual stresses on the ultimate load carrying capacity was 5% or less. Usami and Galambos (1971) also concluded that the effect of residual stresses on the ultimate load carrying capacity was insignificant and negligible since the effect was 4% or less.

Since the gusset plates in this study provided more end restraint than did the end connection in previous research, it was believed to be advisable to check the effect of residual stresses on the compression members being considered in this research. The finite element results indicated that the effect of residual stresses for the angles under consideration was found to be 3% or less for slenderness ratios, L/r_z, ranging from 80 to 300. Thus, the effect of residual stresses was neglected throughout the rest of this study.

7.3.3 Effect of Young's Modulus of Elasticity

The effect of varying Young's modulus of elasticity for both the angle and the gusset plate on the ultimate load carrying capacity is shown in Figure 7-3 for four slenderness ratios. In this figure the modulus of elasticity has been varied over a range that is greater than what would be expected from results of tension tests. This was done so that the effect of changing the modulus of elasticity would be more apparent. Figure 7-3 shows that the ultimate load carrying capacity increases almost linearly as Young's modulus of elasticity increased. As Young's modulus of elasticity decreases, the lateral deflection increases since both the rotational restraint provided by the gusset plates and the angle stiffness decrease. Since slender columns are more sensitive to changes in end conditions, the effect of changing Young's modulus of elasticity is a little greater for slender angles than for shorter ones. Changing Young's modulus of elasticity from 180 000 to 220 000 MPa increased the ultimate load carrying capacity by 13%, 10%, 8%, and 3% for slenderness ratios, L/r_z, of 300, 200,

140, and 80, respectively. As the practical variation in Young's modulus of elasticity for steel is limited to a range of about 195 000 to 205 000 MPa its effect on the ultimate load carrying capacity can be neglected. The modulus of elasticity was taken as 200 000 MPa in the rest of the study.

7.4 Parametric Study on Gusset Plate Properties

Three gusset plate parameters were investigated; the unconnected length of the gusset plate, and the thickness and width of the gusset plate. Since it is not practical to get sufficient data from an experimental program, the finite element method was used to extend the experimental results and this proved to be successful.

7.4.1 Effect of Unconnected Gusset Plate Length, L_g

The effect of the unconnected gusset plate length on the ultimate load carrying capacity was studied on an 64 x 64 x 7.9 mm angle (2½ x 2½ x 5/16 in.) connected to a gusset plate with a width of twice the angle leg width and a thickness of 0.2 times the angle leg width. The unconnected length of the gusset plate has been defined as the distance from the end of the angle to the section at which a plastic hinge forms. In the experimental specimens, this section is the beginning of the fillet at the end of the stem of the tee section. Figure 7-4 shows that increasing the gusset plate unconnected length decreases the ultimate load carrying capacity since it reduces the amount of end restraint provided by the gusset plate to the angle. Changing the gusset plate unconnected length from 10 to 80 mm (i.e. from 0.8 t_g to 6.3 t_g, where t_g is the gusset plate thickness) decreased the load carrying capacity by about 11, 8, 7, and 7% for L/r_z of 300, 200, 140, and 80, respectively. The reduction in the

ultimate load carrying capacity varied almost linearly with the increase in the magnitude of the unconnected gusset plate length. Although this reduction seems significant, the practical minimum unconnected gusset length should not be less than twice the gusset plate thickness. This minimum distance was suggested by Astaneh et al. (1986) to ensure that a plastic hinge can develop in the gusset plate to satisfy seismic design requirements. The unconnected gusset length should also provide enough room for the welder to place the weld at the end of the angle. This would be in the order of 20 mm. In other words, the practical range of this parameter is usually two to three times the gusset plate thickness. It can be shown that going from two to three times the gusset plate thickness reduces the load carrying capacity by about 4% for all slenderness ratios. This is a small reduction in the ultimate load carrying capacity and therefore can be neglected. The unconnected gusset plate length was taken as three times the gusset plate thickness in the rest of this parametric study and its effect on the ultimate load carrying capacity was not explicitly included in the proposed design equation as a specific term.

7.4.2 Effect of Gusset Plate Thickness, t_g

The gusset plate thickness is the most important factor when determining the load carrying capacity of single-angle compression members connected by one leg to gusset plates. Figures 7-5 to 7-8 show the effect of changing the gusset plate thickness on the ultimate load carrying capacity for different slenderness ratios and gusset plate widths. Gusset plate widths of 1.5, 2, 2.5, 3, and 4 times the angle leg width were considered. The gusset plate thickness was varied from 0.1 to 0.45 times the angle width. The latter is an extreme value that might not be practical for a real structure, but it was used to obtain a clear understanding of the

behavior of these members. For an angle with a slenderness ratio, L/r_z of 300, changing the gusset thickness from 0.1 to 0.45 times the angle width increases the load carrying capacity by 95% when the width of the gusset plate, B_g, is twice the angle width. The increase is 99%, 103%, and 64% for the slenderness ratios of 200, 140 and 80, respectively. When the gusset plate width is four times the angle width, changing the gusset plate thickness from 0.1 to 0.45 times the angle leg width increases the load carrying capacity by 86%, 90%, 99%, and 66% for slenderness ratios, L/r_z, of 300, 200, 140, and 80, respectively. Figures 7-7 and 7-8 show that increasing the gusset plate thickness increases the ultimate load carrying capacity significantly until a certain point. At that point, any further increase in the gusset plate thickness results only in a slight increase in the ultimate load carrying capacity and the curve becomes flatter. This indicates that the angle is near a fixed-ended condition. The point at which any further increase in the gusset plate thickness does not produce a significant increase in the ultimate load carrying capacity is also dependent on the gusset plate width, angle length, and the angle leg to thickness ratio. The point after which any increase in the gusset plate thickness produces less significant increase in the ultimate load carrying capacity can be clearly seen in Figures 7-5 when the gusset plate width to angle leg width ratio, B_g/b, is 3.0 or higher and in Figure 7-6 when the gusset plate width to angle leg width ratio, B_g/b, is 2.5 or higher. For angles with slenderness ratio of 200 and 300, shown in Figures 7-7 and 7-8, the two regions can be clearly seen for all gusset plate widths.

It must be noted that during the preparation of the design curves, discussed later in this chapter, for very short angles of slenderness ratio L/r_z of 50 and width-to-ratio of 5, that when the gusset plate is too thin the excessive deformations in the gusset plate resulted in failure due to local buckling of the gusset plate prior to the failure of the angle. This

observation was noticed only for the range below the slenderness ratios and width-to-thickness ratios mentioned. Based on the parametric study, the following minimum gusset plate thickness is proposed to prevent failure due to local buckling in the gusset plate and to assure that failure occurs due to excessive deflection at mid-height in the angle:

$$\frac{t_g}{b} \geq 0.1\ C_1\ C_2\ (\frac{B_g}{b} - 1) \qquad (7\text{-}1a)$$

where

$$C_1 = (\frac{80 - L/r_z}{30}) \geq 0$$
$$C_2 = (\frac{8 - b/t}{3}) \geq 0 \qquad (7\text{-}1b)$$

C_1 and C_2 must be greater than zero otherwise their value is set to zero. It can be concluded from the design curves given in Appendix B, for angles with width-to-thickness ratio, b/t, of 8 and higher, no failure due to local buckling is observed. No failure due to local buckling is also observed for angles with width-to-thickness ratio, b/t, of 5 when the slenderness ratio, L/r_z, is 80 or higher. This fact is considered and included in the two constants C_1 and C_2 of Equation 7-1a. As can be seen from equation 7-1b, it can only be greater than zero if the slenderness ratio, L/r_z, is less than 80 and the width-to-thickness ratio of the angle, b/t, is less than 8. For example, for an angle with a slenderness ratio, L/r_z, of 50 and a width-to-thickness ratio, b/t, of 5, both C_1 and C_2 are equal to 1.0. If the gusset plate width to angle leg thickness ratio, B_g/b, is equal to 2.0 then t_g should be greater than 0.1 times the angle leg width in order to prevent failure due to local buckling in the gusset plate. If the slenderness

ratio is 80 or higher, C_1 will always be zero. That means that t_g/b must be greater than zero in order to prevent failure due to local buckling of the gusset plate. As any gusset plate must have a thickness, which in turn will be greater than zero, failure due to local buckling of the gusset plate prior to the failure of the angle member will not occur.

7.4.3 Effect of Gusset Plate Width, B_g

The gusset plate width is the second most influential factor that affects the load carrying capacity. This is confirmed by the experimental study. Figures 7-9 to 7-12 show the effect of changing the gusset plate width on the ultimate load carrying capacity for four different slenderness ratios. The gusset plate width was varied from 1.5 to 4 times the angle width. For an angle with slenderness ratio, L/r_z, of 300, changing the gusset width from 1.5 to 4 times the angle width increases the load carrying capacity by 13% for a gusset plate thickness, t_g, of 0.1 times the angle width. The increase is 15%, 18%, and 16% for the slenderness ratios of 200, 140 and 80, respectively. When the gusset plate thickness is 0.2 times the angle leg width, changing the gusset plate width from 1.5 to 4 times the angle leg width increases the load carrying capacity by 22%, 26%, 34%, and 24% for slenderness ratios, L/r_z, of 300, 200, 140, and 80, respectively. As can be noted from Figures 7-9 to 7-12, increasing the gusset plate width beyond a certain value has less effect on the ultimate load carrying capacity. This is evident in Figure 7-11 and 7-12. As can be noted from the curves, the maximum gusset width that should be considered in a design equation is 4 times the angle leg width. The effect of gusset plate width is also dependent on the gusset plate thickness as these two gusset plate properties have a significant effect on the development of the plastic hinge in the gusset plate.

7.5 Empirical equation for the ultimate load carrying capacity

A huge database of ultimate load carrying capacities as a function of different design parameters was obtained from the extensive parametric study carried out through this research. The database included about 1800 combination of properties. The results of this parametric study are converted to the design curves shown in Appendix B. From the parametric study it was obvious that the ultimate load carrying capacity of equal-leg single-angle compression members attached by one leg to a gusset plate is governed by the following parameters: (i) slenderness ratio with respect to the axis parallel to the connected leg, (ii) the gusset plate thickness, (iii) the gusset plate width, and (iv) the angle leg width-to-thickness ratio. By knowing the value of these four parameters the ultimate load carrying capacity can be obtained by interpolation from the proper design curves given in Appendix B.

With the rapid development of computers, design engineers prefer dealing with design equations over design curves as they can be easily coded in a computer program to calculate the ultimate load carrying capacity or develop design curves. Therefore, an empirical equation was developed using statistical methods to obtain the best fit for the data obtained from the parametric study. The slenderness ratio is considered with respect to the y axis, the axis parallel to the gusset plate. This empirical equation is applicable for the following range of parameters: (i) slenderness ratios, L/r_y, of 50 to 200, (ii) ratios of gusset plate width to angle leg width, B_g/b, of 1.5 to 4, (iii) ratios of gusset plate thickness to angle leg width, t_g/b, of 0.1 to 0.25, and (iv) angle leg width-to-thickness ratio, b/t, of 5 to 20.

The ultimate load carrying capacity of single-angle compression members connected by one leg to a gusset plate that satisfy the conditions mentioned above can be predicted using the following empirical equation:

$$C_r = K_a A_g F_y \tag{7-2}$$

where A_g is the area of the angle member, F_y is the specified yield stress of the angle, and K_a is a non-dimensional constant where

$$\begin{aligned} K_a &= K_{a1} K_{a2} K_{a3} * 10^{-3} \\ K_{a1} &= a_1 + a_2 (\frac{B_g}{b}) + a_3 (\frac{B_g}{b})^2 \\ K_{a2} &= b_1 + b_2 (\frac{t_g}{b}) + b_3 (\frac{t_g}{b})^2 \\ K_{a3} &= c_1 + c_2 (\frac{L}{r_y}) + c_3 (\frac{L}{r_y})^2 * 10^{-5} \end{aligned} \tag{7-3}$$

the dimensionless constants a_1, a_2, a_3, b_1, b_2, b_3, c_1, c_2, and c_3, in Equation 7-2, are listed as a function of the angle leg-to-thickness ratio in Table 7-1; L is the length of the angle; b is the angle leg width; r_y is the radius of gyration of the angle cross-section about the axis parallel to the connected leg; and t_g and B_g are the thickness and width of the gusset plate, respectively. If the yield stress of the gusset plate is higher than that of the angle the design equation would give a conservative result.

It must be noted that when designing an equal-leg single angle with a width-to-thickness ratio, b/t, that is not listed in Table 7-1, the equation constants cannot be interpolated from the values listed in the table. The ultimate load carrying capacity must be calculated twice for the two width-to-thickness ratio values and then, by interpolation, K_a can be obtained for the proper width-to-thickness ratio.

Although this equation seems to be cumbersome, it can be easily programmed and even for hand calculations it is much shorter and easier to use than the beam-column approach. Table 7-2 shows some statistics about the errors that results from using the

proposed equation compared with the finite element results, the design curves of Appendix B. It can be noticed from the table that for an angle with a width-to-thickness ratio varying from 5 to 20 that 72~80% of the results predicted by this equation are within 5% of the finite element results. More than 91% of all the predictions of the ultimate load carrying capacity are within an error margin of 8%, and 95% of the results are within an error margin of 10%.

In order to assess the validity of the proposed design equation in predicting the ultimate load carrying capacity, it was imperative to compare it with experimental test results reported previously. Figure 7-13 makes a comparison between the experimental test results (Series A) reported by Trahair et al. (1969) and the ultimate load carrying capacities as predicted by the proposed design equation. As shown in that figure, the proposed design equation provides a much better estimate of the ultimate load carrying capacity than other current design practices discussed in detail in Chapter V. For a slenderness ratio, L/r_y, of 84, the experimental failure load is 108.5 kN. The ultimate load carrying capacity as predicted by the simple-column approach is 60.8 kN while the AISC LRFD beam-column approach (1994) predicts a value of 29.5 kN. The proposed design equation gives a much better estimate, 104.0 kN, of the ultimate load carrying capacity.

7.6 Gusset Plates of Irregular Shape

The majority of gusset plates are not rectangular in shape as assumed in developing the proposed design equation but the proposed design equation is applicable to commonly used gusset plates. To convert a gusset plate of irregular shape to an equivalent rectangular one, similar to that used in developing the design curves, the gusset plate width, B_g, should be measured at the location where a plastic hinge can develop. Figure 7-14 shows an angle

bracing member welded to a gusset plate of a practical shape. It is evident that a plastic hinge can develop in the region bounded by lines I-I and II-II. A finite element analysis was conducted twice for the bracing member shown in Figure 7-14, once for the actual gusset plate shape and for an equivalent rectangular gusset plate with a width, B_g, of 194 mm. This width was measured at line II-II where a plastic hinge can develop.

Table 7-3 compares the results obtained from the finite element analysis and the empirical equation for three different lengths of angle. The difference in compressive resistances of the angles for these three cases is small. It is noted that the finite element and empirical equation results are in good agreement irrespective of the shape of the gusset plate.

Figure 7-15 shows the variation of the ultimate load carrying capacity with the unconnected gusset plate length, the distance measured from line I-I to II-II in Figure 7-14. For all different slenderness ratios, the gusset plate is capable of developing a plastic hinge as long as the unconnected gusset plate length is greater than the gusset plate thickness. This observation is in a good agreement with that reported by Astaneh et al. (1986). Astaneh et al. recommended an unconnected gusset plate length of twice the gusset plate thickness be used to provide sufficient distance for the plastic hinge to form. For the case of $L/r_z = 80$, the end restraint has less effect on the load carrying capacity than for slender columns. A sudden change in the slope of the curve is evident in Figure 7-15 when the unconnected gusset plate length increased from zero to 1.0 times the gusset plate thickness, which is 9.5 mm. This is the zone behind which a plastic hinge is difficult to form. If the angle is extended beyond line I-I, a negative unconnected gusset plate length, the gusset plate does not yield across the entire width of the gusset plate. As mentioned in Section 7.4.1, the proposed design equation is developed for the case where the unconnected gusset plate length is three times the gusset

plate thickness. This satisfies the seismic design requirements. This is also a lower bound for the ultimate load carrying capacity. Figures 7-16 and 7-17 show the stress distribution in the gusset plate for the angle with a slenderness ratio, L/r_y, of 109 at ultimate load for the tension side and the compression side, respectively. It can be seen that the gusset plate yielded in both tension and compression across the entire width on both sides of the gusset plate between lines I-I and II-II shown in Figure 7-14. Figure 7-18 and 7-19 show the stress distribution in the angle connected leg and outstanding leg, respectively. It can be shown from these figures that the angle almost yielded at mid-height in both tension and compression.

7.7 Design Examples

7.7.1 Illustrative Example I

In this example the application of the recommended design equation to a gusset plates of an irregular practical shape is demonstrated. Consider the 64 x 64 x 7.9 mm (2½ x 2½ x 5/16 in.) angle bracing member shown in Figure 7-14. The thickness of the gusset plate is 9.5 mm (3/8 in.).

Consider the length of the angle to be 3725 mm. Thus (i) $b/t = 63.5/7.9 = 8.0$, (ii) $B_g/b = 194/63.5 = 3.06$, (iii) $t_g/b = 9.5/63.5 = 0.15$, and (iv) $L/r_y = 3725/19.3 = 193.0$.

Then, $K_{a1} = 4.89 + 2.23 \times 3.06 - 0.27 \times 3.06^2 = 9.19$

$K_{a2} = 24.4 + 50.0 \times 0.15 + 103 \times 0.15^2 = 34.22$

$K_{a3} = 2.45 - 0.0176 \times 193.0 + 3.84 \times 193.0^2 \times 10^{-5} = 0.484$

$K_a = 9.19 \times 34.22 \times 0.484 \times 10^{-3} = 0.152$

This results in a $C_r = 0.152 \times 945 \times 300 \times 10^{-3} = 43.2$ kN

A finite element model was developed to obtain a solution for this example, as mentioned in Section 7.6, and it resulted in a failure load of 40.9 kN. The value obtained from using an idealized equivalent rectangular shape is 43.2 kN.

7.7.2 Illustrative Example II

This example illustrates the interpolation process required when the angle width-to-thickness ratio, b/t, is not listed in Table 7-1. Consider an angle 64 x 64 x 6.4 mm (2½ x 2½ x ¼ in.) and 2100 mm in length. The angle is connected to a gusset plate that is 12.7 mm (0.5 in.) thick and of 190 mm (7.5 in.) width. To determine the ultimate load carrying capacity of this angle, the four design parameters should be calculated as follows: (i) b/t = 63.5/6.35 = 10, (ii) B_g/b = 190/63.5 = 3, (iii) t_g/b = 12.7/63.5=0.2, and (iv) L/r_y = 2100/19.53 = 107.5. As b/t=10 which is not listed in Table 7-1, K_a will be determined first for b/t = 8 and then for b/t =12. The constant K_a will then be determined for b/t=10 by linear interpolation.

For b/t=8, $K_{a1} = 4.89 + 2.23 \times 3.0 - 0.27 \times 3.0^2 = 9.15$

$K_{a2} = 24.4 + 50.0 \times 0.2 + 103 \times 0.2^2 = 38.52$

$K_{a3} = 2.45 - 0.0176 \times 107.5 + 3.84 \times 107.5^2 \times 10^{-5} = 1.00$

$K_a = 9.15 \times 38.52 \times 1.00 \times 10^{-3} = 0.353$

For b/t=12, $K_{a1} = 6.64 + 2.91 \times 3.0 - 0.37 \times 3.0^2 = 12.04$

$K_{a2} = 20.0 + 87.0 \times 0.2 + 21.7 \times 0.2^2 = 38.27$

$K_{a3} = 2.06 - 0.0146 \times 107.5 + 3.06 \times 107.5^2 \times 10^{-5} = 0.84$

$K_a = 12.04 \times 38.27 \times 0.84 \times 10^{-3} = 0.387$

By interpolation K_a=0.370 for b/t = 10.

Thus $C_r = 0.37 \times 766 \times 300 \times 10^{-3} = 85.0$ kN. This compressive resistance is about 3.6% less than the value obtained from the finite element solution which is 88.2 kN.

It must be noted that, as mentioned in section 7.5, K_a cannot be interpolated from Table 7-1 to get the constants for a b/t ratio not listed in the Table. It is obviously a simple matter to program this empirical equation for a computer solution to obtain a solution for any of the parameters considered in this research.

CHAPTER VIII

CONCLUSIONS AND RECOMMENDATIONS

8.1 Conclusions

In this research the behavior and load carrying capacity of single-angle compression members attached by one leg to a gusset plate was studied. Several design approaches were investigated and compared with experimental results from this study and from previous research. The finite element analysis was also used to predict the behavior and ultimate load carrying capacity of the experimental specimens. The finite element analysis was further used to conduct a parametric study on this type of structural member. A database of 1800 cases of angles with different design parameters was generated using the finite element method and used to develop design curves and an empirical design equation for this type of structural member. The following conclusions can be drawn from this research:

1. The simple-column design approach, as adopted by most Canadian engineers, seems to be based on assumed behavior under load which is not correct.
2. The AISC beam-column approach, although more accurately reflects the behavior of single-angles, greatly underestimates the ultimate load carrying capacity of such members.
3. The simple-column design approach also underestimates but gives a more reasonable prediction of the load carrying capacity of such members when compared with the

AISC beam-column approach. However, it overestimates the load carrying capacity of single angles with small slenderness ratios. Caution must be exercised when designing these angles of small slenderness ratio.

4. The finite element model used in this research can be used to predict, reasonably accurately, the behavior and ultimate load carrying capacity of single-angle compression members attached by one leg to a gusset plate.
5. Failure is primarily due to excessive deflection in a direction perpendicular to a gusset plate.
6. The traditional concept of a slenderness ratio is not, in the strictest sense, applicable to these angles since the axis of bending varies from one cross section to another along the angle height. The slenderness ratio, for practical reasons, should be based on the radius of gyration about a geometric axis parallel to the gusset plate as most of the displacement occurs in a direction perpendicular to this geometric axis.
7. The effect of residual stress on the ultimate load carrying capacity of these compression members is not significant (did not exceed 3%).
8. For the range of out-of-straightness measured in the experimental part of this study, the effect of the out-of-straightness on the ultimate load carrying capacity did not exceed 4%.
9. The effect on the ultimate load carrying capacity of varying Young's modulus of elasticity over the range normally determined from tension tests on coupons taken from angles is insignificant.
10. Placing the welds at the angle end in such a way that the welds are balanced about the projection of the centroid on the connected leg is not necessary. The weld pattern

used in the connection between the angle and gusset plate does not have a significant effect on the ultimate load carrying capacity.

11. The minimum amount of weld based on the weld strength should be used at the end of the connection. Increasing the amount of weld does not have any significant effect on the ultimate load carrying capacity.

12. The practical range for the unconnected gusset plate length is usually 2 to 3 times the thickness of the gusset plate. This distance allows for the formation of a plastic hinge in the gusset plate prior to the failure of the angle and allows enough room for the weld to be placed. In this practical range, the effect of the unconnected gusset plate length on the ultimate load carrying capacity is negligible.

13. The gusset plate thickness is the most important parameter that affects the load carrying capacity of this type of structural member. This is due to the effect that the gusset plate thickness has on the restraining moment provided by the gusset plate at the ends of the angle member.

14. For angles with small slenderness ratio and large angle leg width-to-thickness ratio, the gusset plate thickness should be enough to prevent local buckling of the gusset plate prior to the failure of the angle member. A limitation on the gusset plate thickness was developed and proposed. It allows the angle to fail due to large deflections and not because of the buckling of the gusset plate.

15. The gusset plate width is the second most important parameter that affects the load carrying capacity. In general, there is little advantage in making the width of the gusset plate more than four times the angle leg width.

16. Design curves and an empirical equation have been developed which can be used to

predict the load carrying capacity of a single-angle compression member attached to a gusset plate by one leg. The equation gives a much better estimate of the load carrying capacity than all other design approaches. The equation, although not difficult to use, may seem lengthy and in a format which a design engineer would find undesirable. However, the equation is easy to program and much shorter for hand calculations when compared with the AISC beam-column procedure.

8.2 Recommendations for Further Research

The present study is carried out for equal-leg single angles. Research should be conducted to expand this work to include unequal-leg angles.

REFERENCES

Adluri, S. M. R., and Madugula, M. K. S. 1992. ***Eccentrically loaded steel angle struts***. Engineering Journal, American Institute of Steel Construction, **31**(2): 59-66.

AISC. 1994. ***Manual of steel construction, load and resistance factor design***, American Institute of Steel Construction, 2nd edition, Chicago, IL.

AISC. 1989. ***Manual of steel construction, allowable stress design***, American Institute of Steel Construction, 9th edition, Chicago, IL.

AISC. 1986. ***Manual of steel construction, load and resistance factor design***, American Institute of Steel Construction, 1st edition, Chicago, IL.

ASCE. 1991. ***Design of latticed steel transmission structures***, Standard ANSI/ASCE 10-90, American Society of Civil Engineers, New York.

ASCE. 1988. ***ASCE Manual No. 52, Guide for design of steel transmission towers***, American Society of Civil Engineers, 2nd edition, New York.

Astaneh, A., Goel, S. C., and Hanson, R. D. 1986. ***Earthquake-resistant design of double-angle bracings***. Engineering Journal, American Institute of Steel Construction. 23(4):133-147.

ASTM. 1989. ***Metals test methods and analytical procedures***, American Society for Testing and Materials, Section 3, Vol. 03.01, Philadelphia, pp. 131-161.

Bleich, F. 1952. ***Buckling strength of metal structures***, McGraw-Hill, New York.

BSI. 1985. ***Structural use of steelwork in buildings. Part 1: Code of practice for design in simple and continuous construction; hot rolled sections.*** British Standards Institutions, London, England.

CISC. 1995. ***Handbook of steel construction***, Canadian Institute of Steel Construction, Willowdale, Ontario.

Column Research Council. 1966. ***The guide to design criteria for metal compression members***, 2nd edition, Ed. Bruce G. Johnston. Wiley & Sons, New York, N.Y.

CSA. 1994. ***Limit state design of steel structures***, Standard CAN/CSA-S16.1-94, Canadian Standards Association, Rexdale, Ontario.

CSA. 1994. ***Antennas, towers, and antenna-supporting structures***, Standard S37-94, Canadian Standards Association, Rexdale, Ontario.

CSA. 1992. ***General requirements for rolled or welded structural quality steel***, Standard CAN/CSA-G40.20-M92, Canadian Standards Association, Rexdale, Ontario.

CSA. 1989. ***Welded steel construction (metal arc welding)***, Standard CAN/CSA-W59-M89, Canadian Standards Association, Rexdale, Ontario.

ECCS. 1985. ***Recommendations for angles in lattice transmission towers***, Working Group 8.1, Technical Committee 8, European Convention for Constructional Steel Work, Brussels, Belgium.

Elgaaly, M., Davids, W., and Dagher, H. 1992. ***Non-slender single angle struts***, Engineering Journal, American Institute of Steel Construction, **29**(2): 49-58.

Elgaaly, M., Davids, W., and Dagher, H. 1991. ***Behaviour of single-angle-compression members***, ASCE Journal of Structural Engineering, **117**(12): 3720-3741.

Galambos, T. V. 1968. ***Structural members and frames***, Prentice-Hall, Englewood Cliffs, N.J.

Gibson, G. J., and Wake, B. T. 1942. ***An investigation of welded connections for angle tension members***, Welding Journal, January, 44-49.

Girard, C., Picard, A., and Farad, M. 1995. ***Finite element modelling of shear lag effects in an HSS welded to a gusset plate.*** Canadian Journal of Civil Engineering, **22**(4): 651-659

Hibbitt, Karlson, and Sorenson, Inc. 1994. ***ABAQUS Version 5.4.*** Hibbitt, Karlson, and Sorenson, Inc., Providence, R.I.

Leigh, J. M., and Galambos, T. V. 1972. ***The design of compression webs in long span steel joists***, Research Report, No. 21, Structural Division, Civil and Environmental Engineering Department, Washington University, St. Louis, Missouri.

Lipson, S. L., and Haque, M. I. 1978. ***Elastic-plastic analysis of single-angle bolted-welded connection using the finite element method***. Computers and Structures, **9:** 553-545.

Sakla, S. S. S. 1992. ***Balanced and unbalanced welds for angle compression members***, M.A.Sc. Thesis, University of Windsor, Windsor, Ontario.

Timoshinko, S. P., and Gere, J. M. 1961. ***Theory of elastic stability***, McGraw-Hill, New York.

Trahair, N. S. 1969. ***Restrained elastic beam-columns***, ASCE Journal of Structural Division, **95**(ST12): 2641-2664.

Trahair, N. S., Usami, T., and Galambos, T. V. 1969. ***Eccentrically loaded single angle columns***, Research Report No. 11, Structural Division, Civil and Environmental Engineering Department, Sever Institute of Technology, Washington University, St. Louis, Missouri.

Usami, T., and Galambos, T. V. 1971. ***Eccentrically loaded single angle columns***, International Association for Bridge and Structural Engineering, Zurick, 153-184.

Woolcock, S. T., and Kitipornchai, S. 1980. ***The design of single angle struts***, Steel Construction, Australian Institute of Steel Construction, **14**(4): 2-23.

Woolcock, S. T., and Kitipornchai, S. 1986. ***Design of single angle web struts in trusses***, ASCE Journal of Structural Engineering, **112**(6): 1327-1345.

Table 3-1. Dimensions of test specimens

Specimen[1]	Gusset plate			Angle length	Weld length	Weld pattern
	Width B_g (mm)	Thickness t_g (mm)	Unconnected length L_g (mm)	L (mm)	L_w (mm)	
(1)	(2)	(3)	(4)	(6)	(7)	(8)
L-A	150	10.2	20	2100	35	equal
L-B	150	10.2	40	2100	35	equal
L-D	150	10.2	20	2100	52	equal
L-F	150	12.7	20	2100	35	equal
L-H	150	12.7	20	2100	16/54	unbalanced
L-I	150	12.7	20	2100	54/16	balanced
L-J	225	10.2	20	2100	35	equal
M-A	150	10.2	20	1550	60	equal
M-F	150	12.7	20	1550	60	equal
M-J	225	10.2	20	1550	60	equal
S-A	150	10.2	20	990	78	equal
S-B	150	10.2	40	990	78	equal
S-D	150	10.2	20	990	154	equal
S-F	150	12.7	20	990	78	equal
S-H	150	12.7	20	990	32/124	unbalanced
S-I	150	12.7	20	990	124/32	balanced
S-J	225	10.2	20	990	78	equal

[1] The first letter refers to the length of the angle member. L, M, and S refer to specimens with angle lengths of 2100, 1550, and 990 mm, respectively. The second letter refers to specific gusset plate dimensions, for example, A refers to a gusset plate with a 150 mm width, a 10.2 mm thickness, and a 20 mm unconnected length. When a number follows the notation the number indicates the number of the specimen of the same type.

Table 6-1. Nominal dimensions of slender specimens

		Angle			Gusset
Specimen	Taken from piece	Width b_1 (mm)	Width b_2 (mm)	Thickness t (mm)	Plate thickness t_g (mm)
(1)	(2)	(3)	(4)	(5)	(6)
L-A-1	3	63.82	63.70	7.88	10.20
L-A-2	1	63.84	63.74	7.90	10.24
L-A-3	4	63.92	63.86	7.88	10.18
L-B-1	1	63.90	64.00	7.94	10.22
L-B-2	2	63.84	63.94	7.98	10.18
L-B-3	5	63.38	64.04	7.74	10.26
L-D-1	4	64.02	63.98	7.88	10.22
L-D-2	3	64.00	63.60	7.82	10.14
L-D-3	2	63.80	64.02	7.84	10.22
L-F-1	7	64.02	64.18	8.02	12.46
L-F-2	5	64.18	63.80	7.90	12.48
L-F-3	6	63.52	64.20	7.84	12.28
L-H-1	15	63.82	63.98	7.96	12.64
L-H-2	8	63.50	63.88	7.90	12.52
L-H-3	7	64.21	63.90	7.74	12.66
L-I-1	10	63.88	64.18	7.94	12.48
L-I-2	9	63.64	63.56	7.82	12.44
L-I-3	9	63.72	63.82	7.90	12.68
L-J-1	11	63.82	64.02	7.84	10.38
L-J-2	11	63.84	63.56	8.07	10.18
L-J-3	10	63.94	63.82	7.96	10.28

Table 6-2. Nominal dimension of longer intermediate length specimens

		Angle			Gusset
Specimen	Taken from piece	Width b_1 (mm)	Width b_2 (mm)	Thickness t (mm)	Plate thickness t_g (mm)
(1)	(2)	(3)	(4)	(5)	(6)
M-A-1	9	63.58	63.78	8.00	10.18
M-A-2	8	63.74	63.88	7.98	10.20
M-A-3	10	63.88	63.98	7.92	10.22
M-F-1	7	63.76	63.52	7.88	12.44
M-F-2	5	63.68	64.15	7.92	12.34
M-F-3	6	63.94	64.12	7.92	12.58
M-J-1	11	64.10	63.86	7.92	10.34
M-J-2	2	64.06	63.74	7.84	10.14
M-J-3	4	63.98	63.96	7.90	10.26

Table 6-3. Nominal dimension of shorter intermediate length specimens

		Angle			Gusset
Specimen	Taken from piece	Width b_1 (mm)	Width b_2 (mm)	Thickness t (mm)	Plate thickness t_g (mm)
(1)	(2)	(3)	(4)	(5)	(6)
S-A-1	15	64.00	63.74	8.02	10.18
S-A-2	12	63.72	64.00	7.94	10.20
S-A-3	14	63.86	64.02	7.90	10.26
S-B-1	15	63.92	64.08	8.02	10.38
S-B-2	12	63.96	63.70	8.00	10.32
S-B-3	13	64.12	63.78	7.72	10.22
S-D-1	15	64.04	63.82	7.86	10.24
S-D-2	12	63.46	64.12	7.90	10.22
S-D-3	14	63.84	64.12	7.70	10.26
S-F-1	15	63.60	64.20	7.76	12.62
S-F-2	12	63.76	63.92	7.74	12.32
S-F-3	12	64.10	63.48	8.06	12.24
S-H-1	14	63.82	63.98	7.94	12.48
S-H-2	13	63.86	63.98	7.82	12.34
S-H-3	13	63.90	63.82	7.87	12.22
S-I-1	13	63.60	63.74	7.74	12.56
S-I-2	13	63.74	63.82	7.92	12.64
S-I-3	14	63.92	63.94	7.78	12.36
S-J-1	7	63.98	64.08	7.74	10.19
S-J-2	12	64.10	63.96	8.07	10.28
S-J-3	14	63.96	64.00	8.02	10.20

Table 6-4. Results of angles tensile test coupons

Taken from piece No. (1)	Width b (mm) (2)	Thickness t (mm) (3)	Yield stress (MPa) (4)	Young's modulus (MPa) (5)
1	12.80	7.60	356.7	198 400
2	11.06	7.86	376.2	
3	11.09	7.64	349.4	207 400
4	12.96	7.71	376.3	215 200
5	11.79	7.65	344.8	
6	11.44	7.67	367.0	
7	12.91	7.89	390.7	
8	11.84	7.87	398.2	
9	11.41	7.90	417.1	
10	12.18	7.92	404.3	
11	11.24	7.90	382.9	
12	11.42	7.83	381.1	
13	11.94	7.65	354.7	
14	8.30	7.94	400.6	
15	11.40	7.91	374.8	
Average			378.3	207 000

Table 6-5. Results of W530 x 82 (W21 x 55) tensile test coupons

Coupon No. (1)	Width b (mm) (2)	Thickness t (mm) (3)	Yield stress (MPa) (4)	Young's modulus (MPa) (5)
1	12.71	9.20	423.3	206 200
2	12.92	9.16	404.7	200 300
3	12.86	9.08	412.2	203 700
Average			413.4	203 400

Table 6-6. Results of W530 x 123 (W21 x 83) tensile test coupons

Coupon No. (1)	Width b (mm) (2)	Thickness t (mm) (3)	Yield stress (MPa) (4)	Young's modulus MPa (5)
1	12.78	12.00	386.7	207 300
2	12.86	11.86	381.6	203 400
3	12.76	11.98	391.4	201 600
Average			386.6	204 100

Table 6-7. Initial out-of-straightness of slender specimens

Specimen (1)	Yield stress (MPa) (2)	Welded leg Top 1/4 (mm) (3)	Welded leg Mid. (mm) (4)	Welded leg Btm 1/4 (mm) (5)	Outstanding leg Top 1/4 (mm) (6)	Outstanding leg Mid. (mm) (7)	Outstanding leg Btm 1/4 (mm) (8)
L-A-1	349.4	0.08	0.40	0.14	1.12	1.56	1.22
L-A-2	356.7	0.42	0.68	0.48	1.52	1.8	1.46
L-A-3	376.3	0.06	0.78	0.35	1.10	1.54	1.24
L-B-1	356.7	0.18	0.38	0.22	1.56	1.78	1.60
L-B-2	376.2	0.28	0.56	0.32	0.94	1.08	0.84
L-B-3	344.8	0.74	1.06	0.90	1.58	2.00	1.48
L-D-1	376.3	0.78	0.84	0.50	1.28	1.6	1.16
L-D-2	349.4	0.20	0.28	0.28	1.10	1.48	0.80
L-D-3	376.2	0.24	0.30	0.04	0.82	1.50	0.84
L-F-1	390.7	0.28	0.49	0.34	0.68	0.98	0.62
L-F-2	344.8	0.16	0.30	0.10	-0.12	-0.20	0.00
L-F-3	367.0	-0.10	-0.16	0.02	0.10	0.16	0.02
L-H-1	374.8	0.17	0.33	0.23	0.22	0.34	0.16
L-H-2	398.2	-0.38	-0.64	-0.40	-0.24	-0.10	-0.06
L-H-3	390.7	0.33	0.46	0.27	0.74	1.00	0.84
L-I-1	404.3	0.28	0.50	0.08	0.40	0.58	0.38
L-I-2	417.1	0.00	-0.30	-0.06	0.08	-0.12	0.02
L-I-3	417.1	0.00	-0.28	0.08	-0.16	-0.36	-0.08
L-J-1	382.9	0.15	0.21	0.05	1.20	1.54	1.22
L-J-2	382.9	0.50	0.66	0.42	0.85	1.07	0.73
L-J-3	404.3	0.00	-0.15	-0.02	-0.46	-0.30	-0.34

Table 6-8. Initial out-of-straightness of longer intermediate length specimens

Specimen (1)	Yield stress (MPa) (2)	Welded leg Top 1/4 (mm) (3)	Welded leg Mid. (mm) (4)	Welded leg Btm 1/4 (mm) (5)	Outstanding leg Top 1/4 (mm) (6)	Outstanding leg Mid. (mm) (7)	Outstanding leg Btm 1/4 (mm) (8)
M-A-1	417.1	0.14	0.18	0.12	0.10	0.30	0.14
M-A-2	398.2	0.13	0.20	0.10	0.16	0.24	0.18
M-A-3	404.3	0.11	0.16	0.08	0.24	0.42	0.20
M-F-1	390.7	0.08	0.28	0.08	0.28	0.62	0.34
M-F-2	344.8	0.16	0.26	0.00	0.60	1.50	0.66
M-F-3	367.0	0.02	0.16	0.06	0.10	0.28	0.14
M-J-1	382.9	0.16	0.24	0.18	0.16	0.32	0.20
M-J-2	376.2	0.14	0.32	0.26	0.20	0.40	0.30
M-J-3	376.3	0.14	0.28	0.22	0.18	0.40	0.24

Table 6-9. Initial out-of-straightness of shorter intermediate length specimens

Specimen	Yield stress	Welded leg			Outstanding leg		
		Top 1/4	Mid.	Btm 1/4	Top 1/4	Mid.	Btm 1/4
	(MPa)	(mm)	(mm)	(mm)	(mm)	(mm)	(mm)
(1)	(2)	(3)	(4)	(5)	(6)	(7)	(8)
S-A-1	374.8	0.16	0.30	0.06	0.24	0.32	0.14
S-A-2	381.1	0.18	0.30	0.18	0.20	0.30	0.18
S-A-3	400.6	0.14	0.28	0.12	0.22	0.30	0.20
S-B-1	374.8	0.16	0.31	0.14	0.30	0.40	0.25
S-B-2	381.1	0.18	0.28	0.16	0.19	0.33	0.23
S-B-3	354.7	0.08	0.22	0.14	0.17	0.25	0.17
S-D-1	374.8	-0.06	-0.12	-0.06	0.20	0.30	0.10
S-D-2	381.1	0.01	0.19	0.09	0.12	0.22	0.04
S-D-3	400.6	0.08	0.20	0.06	0.15	0.25	0.17
S-F-1	374.8	0.08	0.25	0.12	0.14	0.48	0.10
S-F-2	381.1	0.16	0.30	0.20	0.11	0.28	0.16
S-F-3	381.1	0.08	0.24	0.10	0.04	0.16	0.02
S-H-1	400.6	0.02	0.24	0.08	0.18	0.36	0.28
S-H-2	354.7	0.14	0.24	0.20	0.14	0.25	0.12
S-H-3	354.7	0.14	0.26	0.08	0.04	0.38	0.14
S-I-1	354.7	0.04	0.10	0.06	0.04	0.22	0.06
S-I-2	354.7	0.08	-0.06	0.02	0.10	0.26	0.04
S-I-3	400.6	0.18	0.22	0.10	0.08	0.16	0.06
S-J-1	390.7	0.04	0.22	0.06	0.24	0.40	0.22
S-J-2	381.1	0.04	0.22	0.10	0.14	0.28	0.08
S-J-3	400.6	0.08	0.24	0.08	0.20	0.36	0.16

Table 6-10. Experimental and finite element results for slender specimens (Type A, B, D, F, and J gusset plate)

Specimen	$P_{expt.}$ (kN)	Average $P_{expt.}$ (kN)	Avg. $P_{expt.}$ / Avg. $P_{expt.\ A}$ [1]	$P_{theo.}$ (kN)	$\frac{P_{theo}-P_{expt}}{P_{expt}}$ (%)	$P_{theo.}$ OOS=L/1000 (kN)	$\frac{P_{theo,\ L/1000}}{P_{theo.\ L/1000\ A}}$ [2]
(1)	(2)	(3)	(4)	(5)	(6)	(7)	(8)
L-A-1	89.3			95.7	7.2	82.9	
L-A-2	90.1	89.6	1.000	93.8	4.1	82.9	1.000
L-A-3	89.5			96.6	7.9	82.9	
L-B-1	85.8			92.4	7.7	80.6	
L-B-2	86.5	86.5	0.965	93.3	7.9	80.6	0.972
L-B-3	87.3			90.6	3.8	80.6	
L-D-1	89.1			96.7	8.5	83.4	
L-D-2	92.1	91.1	1.016	97.3	5.6	83.4	1.006
L-D-3	92.0			98.1	6.6	83.4	
L-F-1	103.7			109.4	5.5	93.4	
L-F-2	101.2	103.3	1.153	109.7	8.4	93.4	1.127
L-F-3	105.1			108.3	3.0	93.4	
L-J-1	99.3			104.1	4.8	89.0	
L-J-2	100.2	101.2	1.129	104.1	3.9	89.0	1.074
L-J-3	104.1			106.8	2.6	89.0	

[1] Ratio of average experimental failure load to average experimental failure load for slender specimens with a gusset plate width of 150 mm, thickness of 10.2 mm, and an unconnected length of 20 mm (a type A gusset plate).

[2] Ratio of finite element failure load of a specimen with an out-of-straightness (OOS) of L/1000 to finite element failure load for a slender specimen with the same out-of-straightness and a gusset plate width of 150 mm, thickness of 10.2 mm, and an unconnected length of 20 mm (a type A gusset plate). F_y = 300 MPa.

Table 6-11. Experimental and finite element results for slender specimens (Type F, H, and I gusset plate)

Specimen	P_{expt} (kN)	Average P_{expt} (kN)	Avg. P_{expt} / Avg. P_{expt} [1]	P_{theo} (kN)	$\frac{P_{theo}-P_{expt}}{P_{expt}}$ (%)	P_{theo}, OOS=L/1000 (kN)	$\frac{P_{theo,\ L/1000}}{P_{theo,\ L/1000\ F}}$ [2]
(1)	(2)	(3)	(4)	(5)	(6)	(7)	(8)
L-F-1	103.7			109.4	5.5	93.4	
L-F-2	101.2	103.3	1.000	109.7	8.4	93.4	1.000
L-F-3	105.1			108.3	3.0	93.4	
L-H-1	102.8			110.6	7.6	95.6	
L-H-2	108.7	104.4	1.011	113.7	4.6	95.6	1.024
L-H-3	101.8			109.7	7.8	95.6	
L-I-1	103.5			111.6	7.8	95.2	
L-I-2	106.7	106.1	1.027	113.1	6.0	95.2	1.019
L-I-3	108.2			113.1	4.5	95.2	

[1] Ratio of average experimental failure load to average experimental failure load for slender specimens with a gusset plate width of 150 mm, thickness of 12.7 mm, and an unconnected length of 20 mm (a type F gusset plate).

[2] Ratio of finite element failure load of a specimen with an out-of-straightness (OOS) of L/1000 to finite element failure load for a slender specimen with the same out-of-straightness and a gusset plate width of 150 mm, thickness of 12.7 mm, and an unconnected length of 20 mm (a type F gusset plate). F_y = 300 MPa.

Table 6-12. Experimental and finite element results for longer intermediate length specimens

Specimen	$P_{expt.}$ (kN)	Average $P_{expt.}$ (kN)	$\frac{\text{Avg. } P_{expt.}}{\text{Avg. } P_{expt.\ A}}$ [1]	$P_{theo.}$ (kN)	$\frac{P_{theo}-P_{expt}}{P_{expt}}$ (%)	$P_{theo.}$ OOS=L/1000 (kN)	$\frac{P_{theo.\ L/1000}}{P_{theo.\ L/1000\ A}}$ [2]
(1)	(2)	(3)	(4)	(5)	(6)	(7)	(8)
M-A-1	131.4			136.5	3.9	110.6	
M-A-2	128.7	130.7	1.000	136.5	6.1	110.6	1.000
M-A-3	132.1			135.0	2.2	110.6	
M-F-1	146.1			146.4	0.2	121.5	
M-F-2	135.0	141.8	1.085	140.1	3.8	121.5	1.099
M-F-3	144.3			145.5	0.8	121.5	
M-J-1	141.0			139.4	-1.1	115.5	
M-J-2	137.2	137.9	1.055	138.6	1.0	115.5	1.045
M-J-3	135.4			138.6	2.4	115.5	

[1] Ratio of average experimental failure load to average experimental failure load for slender specimens with a gusset plate width of 150 mm, thickness of 10.2 mm, and an unconnected length of 20 mm (a type A gusset plate).

[2] Ratio of finite element failure load of a specimen with an out-of-straightness (OOS) of L/1000 to finite element failure load for a slender specimen with the same out-of-straightness and a gusset plate width of 150 mm, thickness of 10.2 mm, and an unconnected length of 20 mm (a type A gusset plate). F_y = 300 MPa.

Table 6-13. Experimental and finite element results for shorter intermediate length specimens (Type A, B, D, F, and J gusset plate)

Specimen	$P_{expt.}$ (kN)	Average P_{expt} (kN)	Avg. $P_{expt.}$ / Avg. $P_{expt.}$ A [1]	$P_{theo.}$ (kN)	$\frac{P_{theo}-P_{expt}}{P_{expt}}$ (%)	$P_{theo.}$ OOS=L/1000 (kN)	$\frac{P_{theo.\ L/1000}}{P_{theo.\ L/1000\ A}}$ [2]
(1)	(2)	(3)	(4)	(5)	(6)	(7)	(8)
S-A-1	163.3			174.4	6.4	141.2	
S-A-2	161.9	163.5	1.000	176.4	8.2	141.2	1.000
S-A-3	165.4			181.2	8.7	141.2	
S-B-1	156.0			170.4	8.5	138.8	
S-B-2	160.7	157.2	0.961	172.4	6.8	138.8	0.983
S-B-3	155.0			165.0	6.1	138.8	
S-D-1	160.0			173.3	8.3	144.7	
S-D-2	163.1	163.3	0.999	174.1	6.7	144.7	1.025
S-D-3	166.8			178.7	7.1	144.7	
S-F-1	172.9			184.8	6.4	151.6	
S-F-2	179.2	174.4	1.066	185.0	3.1	151.6	1.074
S-F-3	171.1			185.8	7.9	151.6	
S-J-1	180.6			193.2	6.5	152.4	
S-J-2	176.7	179.8	1.099	191.6	7.8	152.4	1.079
S-J-3	182.1			196.4	7.3	152.4	

[1] Ratio of average experimental failure load to average experimental failure load for slender specimens with a gusset plate width of 150 mm, thickness of 10.2 mm, and an unconnected length of 20 mm (a type A gusset plate).

[2] Ratio of finite element failure load of a specimen with an out-of-straightness (OOS) of L/1000 to finite element failure load for a slender specimen with the same out-of-straightness and a gusset plate width of 150 mm, thickness of 10.2 mm, and an unconnected length of 20 mm (a type A gusset plate). F_y = 300 MPa.

Table 6-14. Experimental and finite element results for shorter intermediate length specimens (Type F, H, and I gusset plate)

Specimen	P_{expt} (kN)	Average P_{expt} (kN)	Avg. P_{expt} / Avg. $P_{expt,F}$ [1]	P_{theo} (kN)	$\frac{P_{theo}-P_{expt}}{P_{expt}}$ (%)	P_{theo}, OOS=L/1000 (kN)	$\frac{P_{theo,\ L/1000}}{P_{theo,\ L/1000,F}}$ [2]
(1)	(2)	(3)	(4)	(5)	(6)	(7)	(8)
S-F-1	172.9			184.8	6.4	151.6	
S-F-2	179.2	174.4	1.000	185.0	3.1	151.6	1.000
S-F-3	171.1			185.8	7.9	151.6	
S-H-1	179.3			193.2	7.8	154.4	
S-H-2	176.4	178.8	1.025	178.8	1.4	154.4	1.018
S-H-3	180.8			178.0	-1.5	154.4	
S-I-1	180.1			173.2	-3.8	154.4	
S-I-2	179.6	181.3	1.040	174.0	-3.1	154.4	1.018
S-I-3	184.3			183.2	-0.6	154.4	

[1] Ratio of average experimental failure load to average experimental failure load for slender specimens with a gusset plate width of 150 mm, thickness of 12.7 mm, and an unconnected length of 20 mm (a type F gusset plate).

[2] Ratio of finite element failure load of a specimen with an out-of-straightness (OOS) of L/1000 to finite element failure load for a slender specimen with the same out-of-straightness and a gusset plate width of 150 mm, thickness of 12.7 mm, and an unconnected length of 20 mm (a type F gusset plate). F_y = 300 MPa.

Table 6-15. Experimental results and predicted compressive resistance of slender specimens using the two design approaches

Specimen (1)	Yield stress F_y (MPa) (2)	Expt. failure load $P_{expt.}$ (kN) (3)	Simple-column approach P_{sc} (kN) (4)	$\frac{P_{expt.}-P_{sc}}{P_{expt.}}$ % (5)	Beam-column approach P_{bc} (kN) (6)	$\frac{P_{expt.}-P_{bc}}{P_{expt.}}$ % (7)
L-A-1	349.4	89.3	60.0	+32.8	34.0	+61.9
L-A-2	356.7	90.1	60.1	+33.3	34.2	+62.0
L-A-3	376.3	89.5	60.5	+32.4	34.7	+61.2
L-B-1	356.7	85.8	58.2	+32.2	33.3	+61.2
L-B-2	376.2	86.5	58.5	+32.4	33.8	+60.9
L-B-3	344.8	87.3	58.0	+33.6	33.0	+62.2
L-D-1	376.3	89.1	60.5	+32.1	34.7	+61.1
L-D-2	349.4	92.1	60.0	+34.9	34.0	+63.1
L-D-3	376.2	92.0	60.5	+34.2	34.7	+62.3
L-F-1	390.7	103.7	60.7	+41.5	34.3	+66.9
L-F-2	344.8	101.2	59.9	+40.8	33.0	+67.4
L-F-3	367.0	105.1	60.3	+42.6	33.7	+67.9
L-H-1	374.8	102.8	60.4	+41.2	33.8	+67.1
L-H-2	398.2	108.7	60.8	+44.1	34.3	+68.4
L-H-3	390.7	101.8	60.7	+40.4	34.3	+66.3
L-I-1	404.3	103.5	60.8	+41.3	34.6	+66.6
L-I-2	417.1	106.7	61.0	+42.8	34.8	+67.4
L-I-3	417.1	108.2	61.0	+43.6	34.8	+67.8
L-J-1	382.9	99.3	60.6	+39.0	34.9	+64.9
L-J-2	382.9	100.2	60.6	+39.5	34.9	+65.2
L-J-3	404.3	104.1	60.8	+41.6	35.4	+66.0

Table 6-16. Experimental results and predicted compressive resistance of longer intermediate length specimens using the two design approaches

Specimen	Yield stress F_y (MPa)	Expt. Failure load $P_{expt.}$ (kN)	Simple-column approach P_{sc} (kN)	$\frac{P_{expt.}-P_{sc}}{P_{expt.}}$ %	Beam-column approach P_{bc} (kN)	$\frac{P_{expt.}-P_{bc}}{P_{expt.}}$ %
(1)	(2)	(3)	(4)	(5)	(6)	(7)
M-A-1	417.1	131.4	102.9	+21.7	53.4	+59.4
M-A-2	398.2	128.7	102.1	+20.7	52.6	+59.1
M-A-3	404.3	132.1	102.4	+22.5	52.8	+60.0
M-F-1	390.7	146.1	101.8	+30.3	50.8	+65.2
M-F-2	344.8	135.0	99.4	+26.4	48.3	+64.2
M-F-3	367.0	144.3	100.6	+30.3	49.6	+65.6
M-J-1	382.9	141.0	101.4	+28.1	51.8	+63.6
M-J-2	376.2	137.2	101.1	+26.3	51.5	+62.5
M-J-3	376.3	135.4	101.1	+25.3	51.5	+62.0

Table 6-17. Experimental results and predicted compressive resistance of shorter intermediate length specimens using the two design approaches

Specimen	Yield stress F_y (MPa)	Expt. failure load $P_{expt.}$ (kN)	Simple-column approach P_{sc} (kN)	$\frac{P_{expt.}-P_{sc}}{P_{expt.}}$ %	Beam-column approach P_{bc} (kN)	$\frac{P_{expt.}-P_{bc}}{P_{expt.}}$ %
(1)	(2)	(3)	(4)	(5)	(6)	(7)
S-A-1	374.8	163.3	186.3	-14.1	77.5	+52.5
S-A-2	381.1	161.9	187.6	-15.9	78.4	+51.6
S-A-3	400.6	165.4	191.5	-15.8	80.9	+51.1
S-B-1	374.8	156.0	178.1	-14.2	75.6	+51.5
S-B-2	381.1	160.7	179.3	-11.6	76.5	+52.4
S-B-3	354.7	155.0	174.2	-12.4	73.0	+52.9
S-D-1	374.8	160.0	186.3	-16.4	77.5	+51.6
S-D-2	381.1	163.1	187.6	-15.0	78.4	+51.9
S-D-3	400.6	166.8	191.5	-14.8	80.9	+51.5
S-F-1	374.8	172.9	186.3	-7.8	74.6	+56.9
S-F-2	381.1	179.2	187.6	-4.7	75.4	+57.9
S-F-3	381.1	171.1	187.6	-9.6	75.4	+55.9
S-H-1	400.6	179.3	191.5	-6.8	77.8	+56.6
S-H-2	354.7	176.4	181.9	-3.1	71.9	+59.2
S-H-3	354.7	180.8	181.9	-0.6	71.9	+60.2
S-I-1	354.7	174.1	181.9	-4.5	71.9	+58.7
S-I-2	354.7	179.6	181.9	-1.3	71.9	+60.0
S-I-3	400.6	184.3	191.5	-3.9	77.8	+57.8
S-J-1	390.7	180.6	189.5	-4.9	79.7	+55.9
S-J-2	381.1	176.7	187.6	-6.2	78.4	+55.6
S-J-3	400.6	182.1	191.5	-5.2	80.9	+55.6

Table 6-18. Ratio of deflections x/y for all test specimens obtained from experimental testing

Specimen	x/y ratio		Specimen	x/y ratio		Specimen	x/y ratio	
	W.L.[1]	U.L.[2]		W.L.[1]	U.L.[2]		W.L.[1]	U.L.[2]
L-A-1	10.6	6.8	M-A-1	39.8	12.6	S-A-1	66.0	32.0
L-A-2	21.0	8.6	M-A-2	24.3	9.7	S-A-2	12.0	130.4
L-A-3	7.9	5.2	M-A-3	17.4	7.9	S-A-3	17.1	53.0
L-B-1	12.6	7.1				S-B-1	101.2	17.5
L-B-2	8.5	5.9				S-B-2	201.0	101.0
L-B-3	8.5	5.8				S-B-3	27.6	41.7
L-D-1	210.0	11.4				S-D-1	61.4	21.4
L-D-2	19.6	8.2				S-D-2	36.1	39.
L-D-3	12.0	4.4				S-D-3	43.3	146.0
L-F-1	10.2	5.4	M-F-1	61.7	15.0	S-F-1	59.3	27.3
L-F-2	14.0	5.1	M-F-2	22.6	11.1	S-F-2	29.5	17.9
L-F-3	262.0	9.9	M-F-3	21.3	11.9	S-F-3	164.0	29.0
L-H-1	19.0	7.4				S-H-1	36.3	24.6
L-H-2	500.0	9.8				S-H-2	115.0	120.0
L-H-3	33.0	7.4				S-H-3	19.5	9.7
L-I-1	6.3	4.0				S-I-1	8.1	19.2
L-I-2	7.3	4.27				S-I-2	8.7	25.9
L-I-3	88.0	6.38				S-I-3	15.6	70.6
L-J-1	11.1	6.3	M-J-1	20.9	12.4	S-J-1	66.6	260.0
L-J-2	11.0	5.6	M-J-2	13.0	10.7	S-J-2	56.6	12.4
L-J-3	15.7	9.1	M-J-3	17.5	10.4	S-J-3	46.1	29.9

[1] W.L.: Ratio of deflections at working load when the working load is taken as the ultimate load divided by a factor of 1.4.
[2] U.L.: Ratio of deflections at ultimate load

Table 6-19: Ratio of deflections x/y for test specimens with an initial out-of-straightness of L/1000 obtained from finite element analysis for theoretical specimens (F_y=300 MPa)

Specimen	x:y ratio		Specimen	x:y ratio		Specimen	x:y ratio	
	W.L.[1]	U.L.[2]		W.L.[1]	U.L.[2]		W.L.[1]	U.L.[2]
L-A	17.4	10.1	M-A	87.0	29.5	S-A	23.0	31.5
L-B	17.5	10.5				S-B	21.6	35.1
L-D	15.3	10.3				S-D	25.4	32.3
L-F	17.4	9.1	M-F	87.3	21.9	S-F	21.2	30.5
L-H	10.0	8.3				S-H	25.0	63.7
L-I	7.7	7.4				S-I	113.0	45.0
L-J	19.7	10.2	M-J	102.0	28.7	S-J	17.0	20.0

[1] W.L.: Ratio of deflections at working load when the working load is taken as the ultimate load divided by a factor of 1.4.
[2] U.L.: Ratio of deflections at ultimate load

Table 7-1. Constants for empirical equation.

Angle b/t	Gusset plate width constants			Gusset plate thickness constants			Slenderness ratio constants		
	a_1	a_2	a_3	b_1	b_2	b_3	c_1	c_2	c_3
5	5.83	3.09	-0.36	25.2	25.0	119.0	1.78	-0.0128	2.80
8	4.89	2.23	-0.27	24.4	50.0	103.0	2.45	-0.0176	3.84
12	6.64	2.91	-0.37	20.0	87.0	21.7	2.06	-0.0146	3.06
16	7.63	2.65	-0.35	16.3	121.0	-78.3	2.05	-0.0145	3.04
20	7.09	2.23	-0.31	24.4	250.0	-315.0	1.32	-0.0091	1.86

Table 7-2. Errors attained by using the empirical equation compared with the finite element results.

b/t ratio	percentage of results within an error margin of		
	5%	8%	10%
5	80%	93%	97%
8	74%	91%	95%
12	75%	94%	98%
16	73%	96%	99%
20	72%	94%	99%

Table 7-3. A comparison of finite element results and those obtained from the empirical equation.

Angle length (mm)	Slender-ness ratio L/r_y	Finite element analysis of real gusset plate[1] C_r (kN)	Finite element analysis of equivalent rectangular gusset plate C_r (kN)	Load predicted by the proposed equation C_r (kN)
3725	193	40.9	40.0	43.2
2110	109	82.3	83.4	87.8
995	52	138.2	143.2	146.6

[1] Gusset plate dimensions are shown in Figure 7-14.

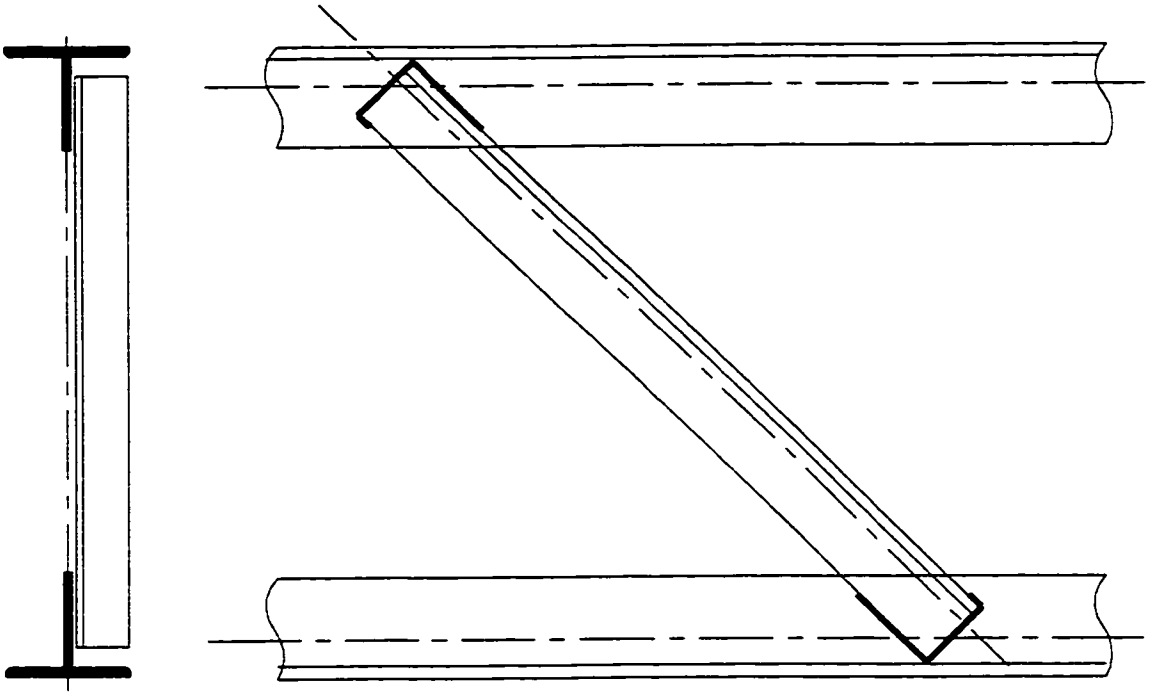

Figure 1-1. Single-angle web member welded to tee section chords

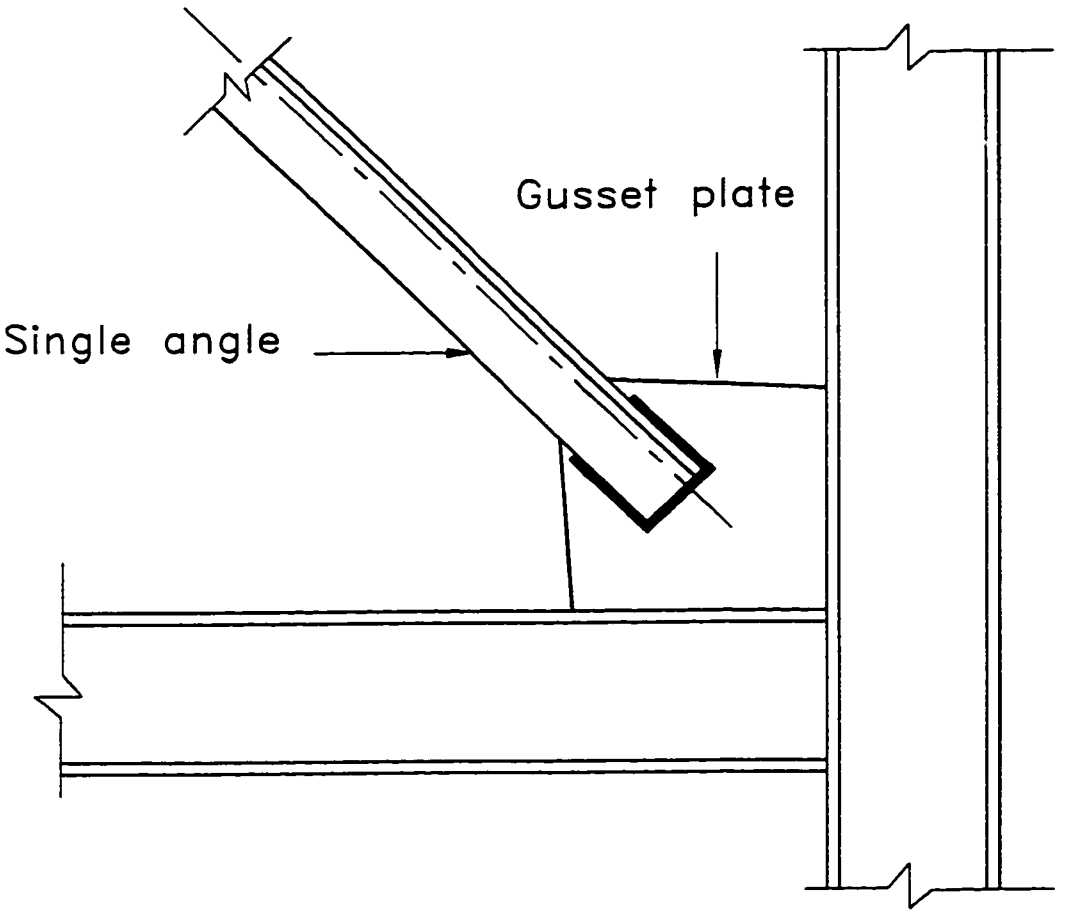

Figure 1-2. Gusset plate connection in a braced frame

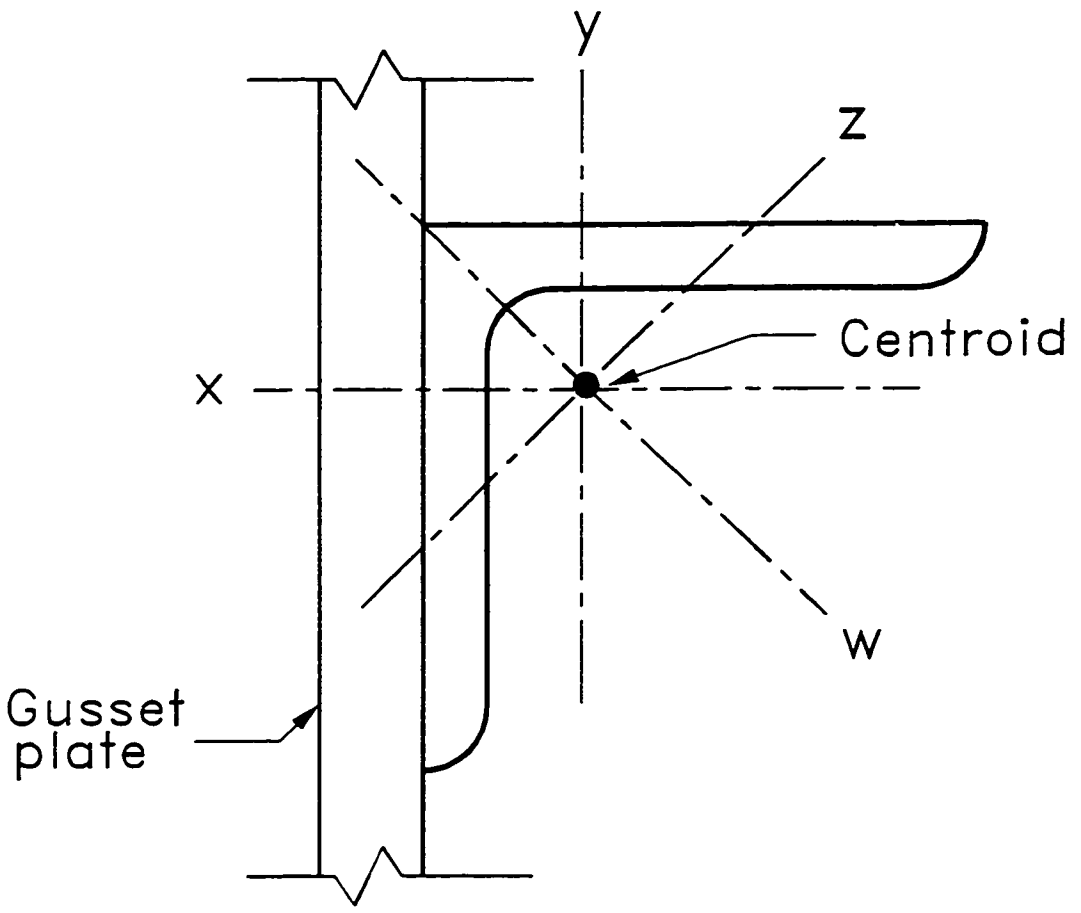

Figure 1-3. Simple-column design approach

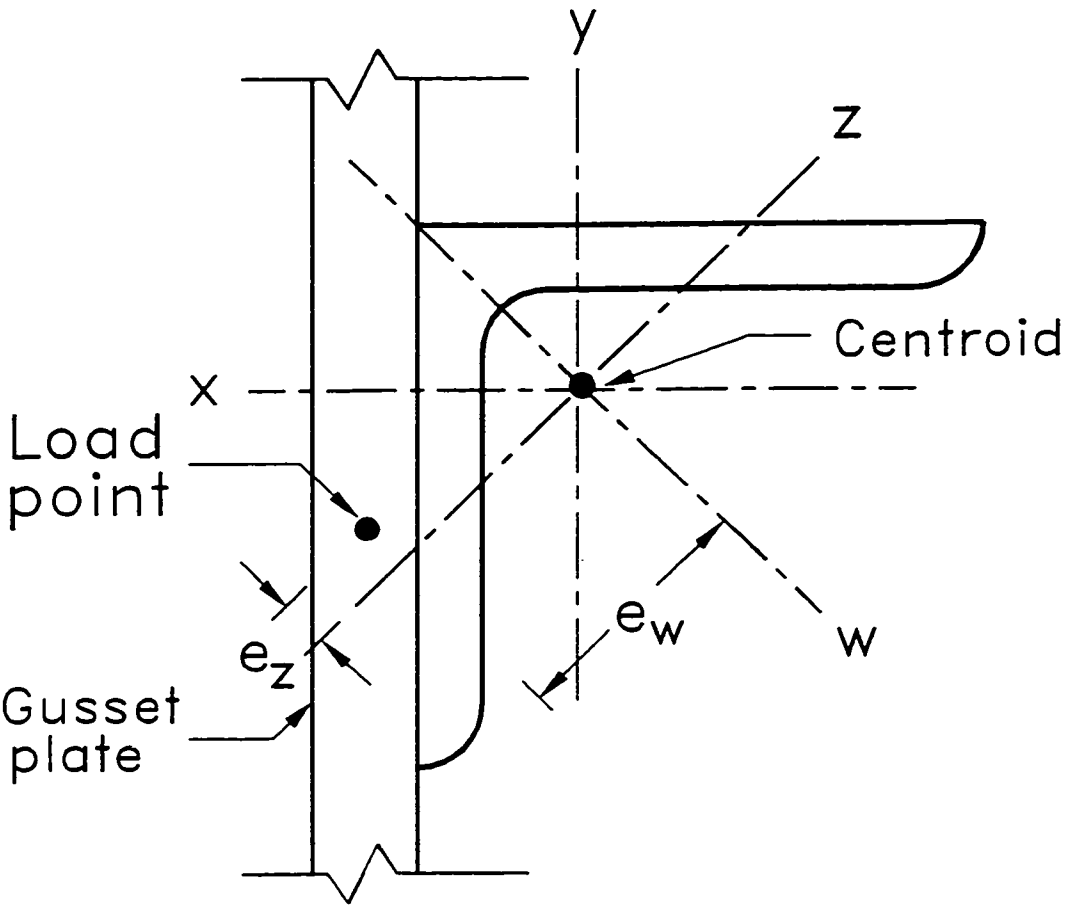

Figure 1-4. AISC beam-column design approach

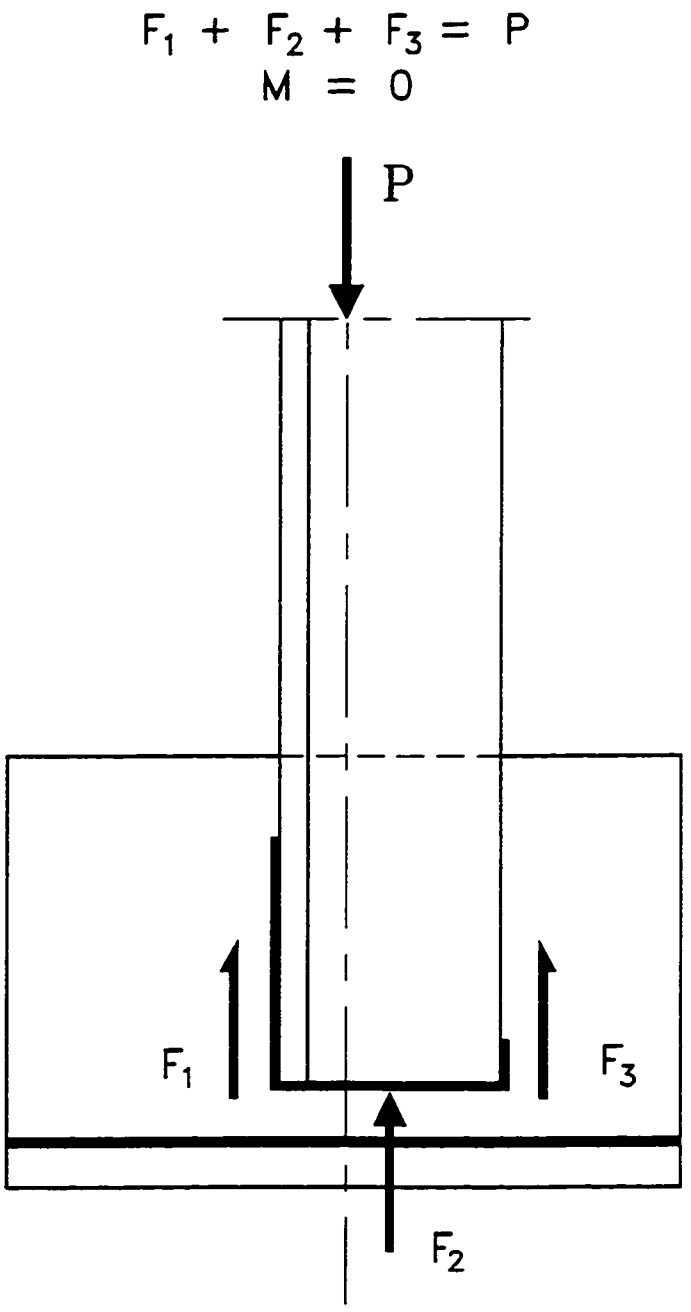

Figure 1-5. Balanced weld

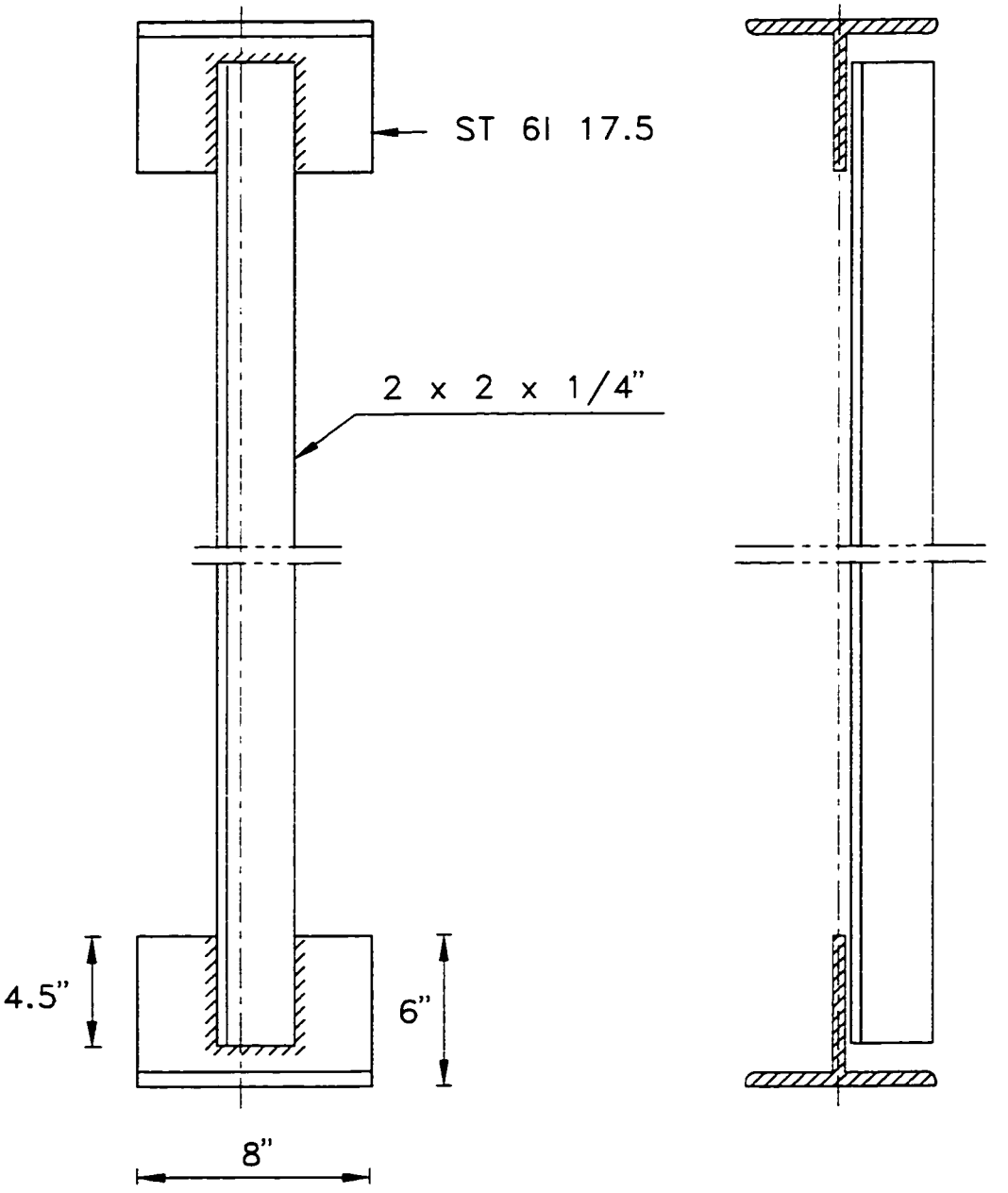

Figure 2-1. Test specimen (after Trahair et al. 1969)

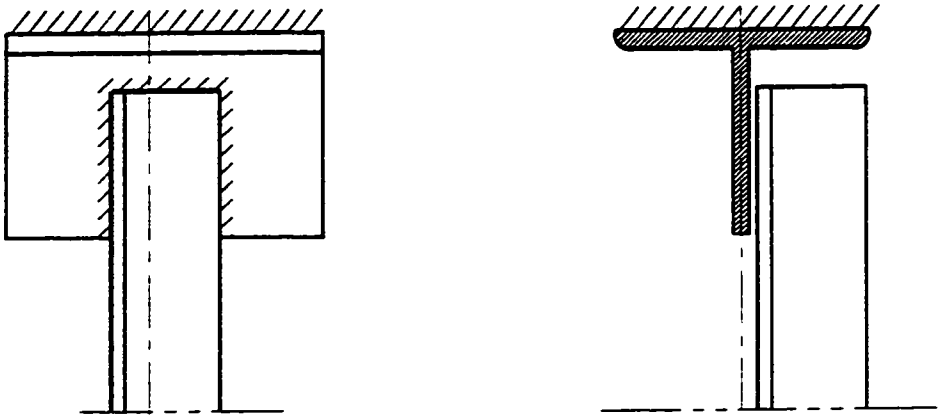

(a)

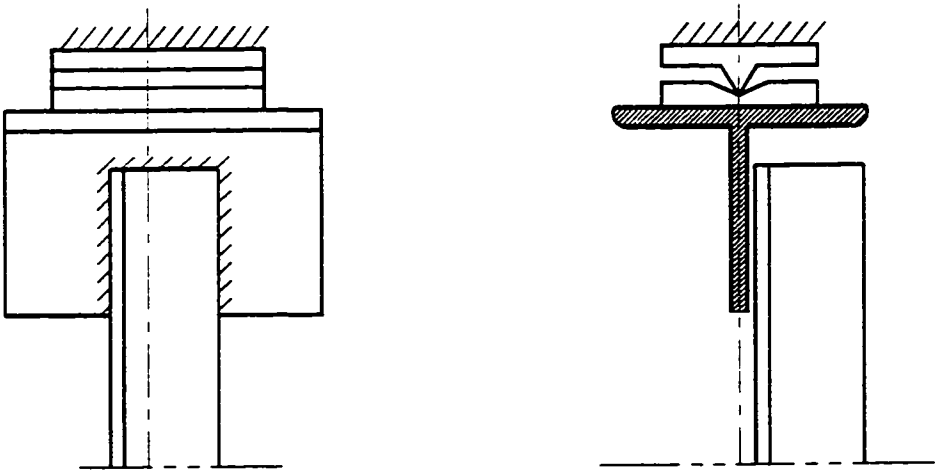

(b)

Figure 2-2. End conditions (after Trahair et al. 1969): (a) fixed ended, and (b) pin-ended

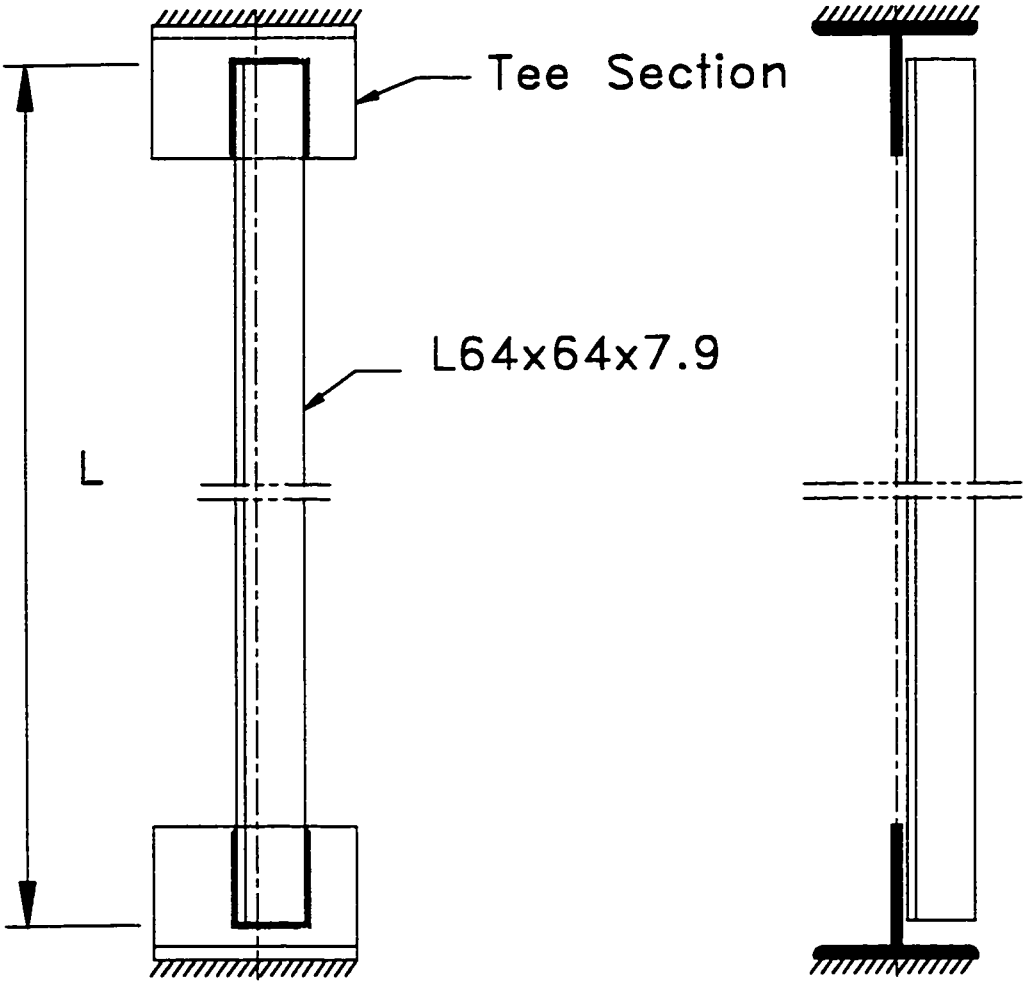

Figure 3-1. Typical test specimen

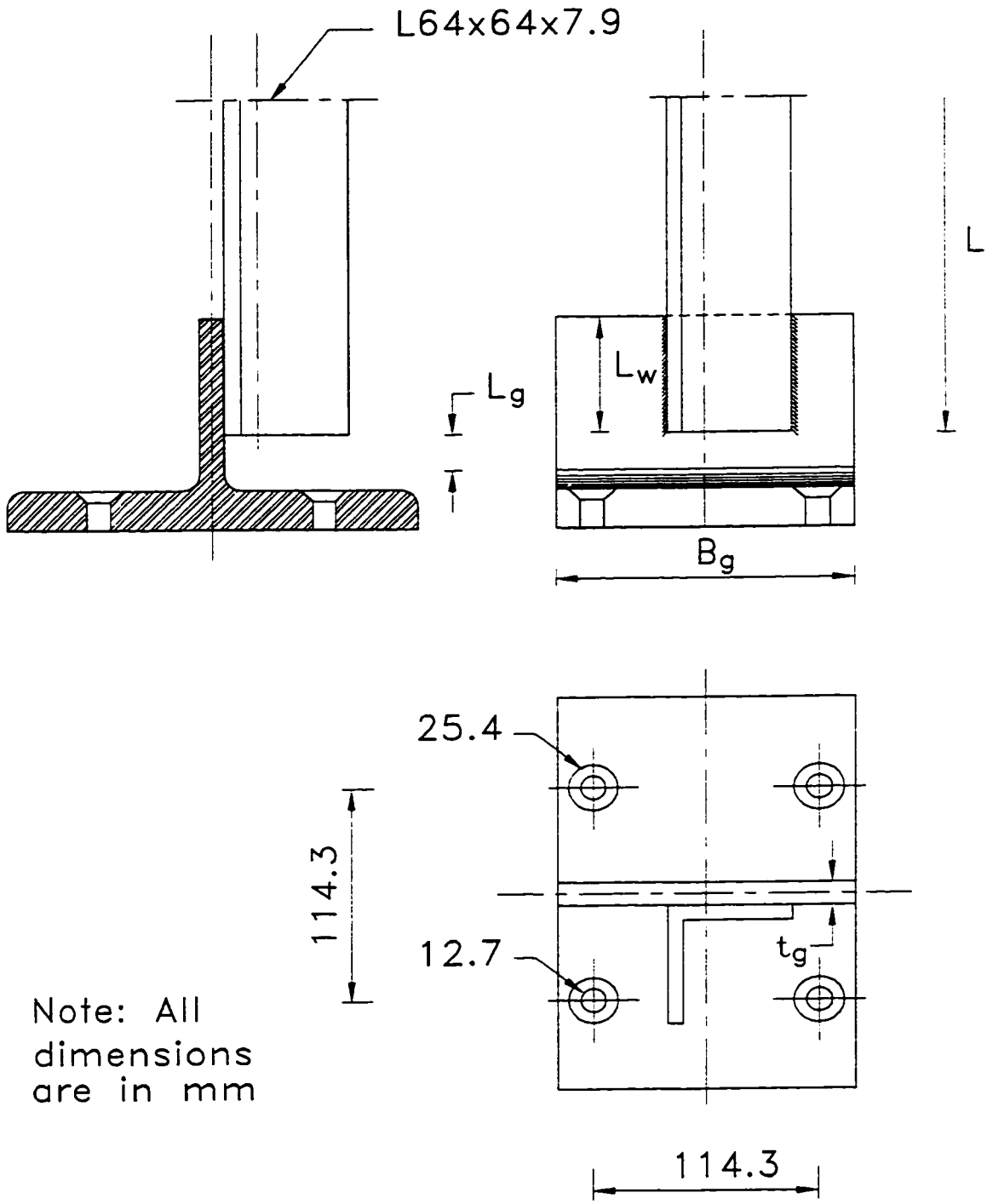

Figure 3-2. Details of the specimen ends

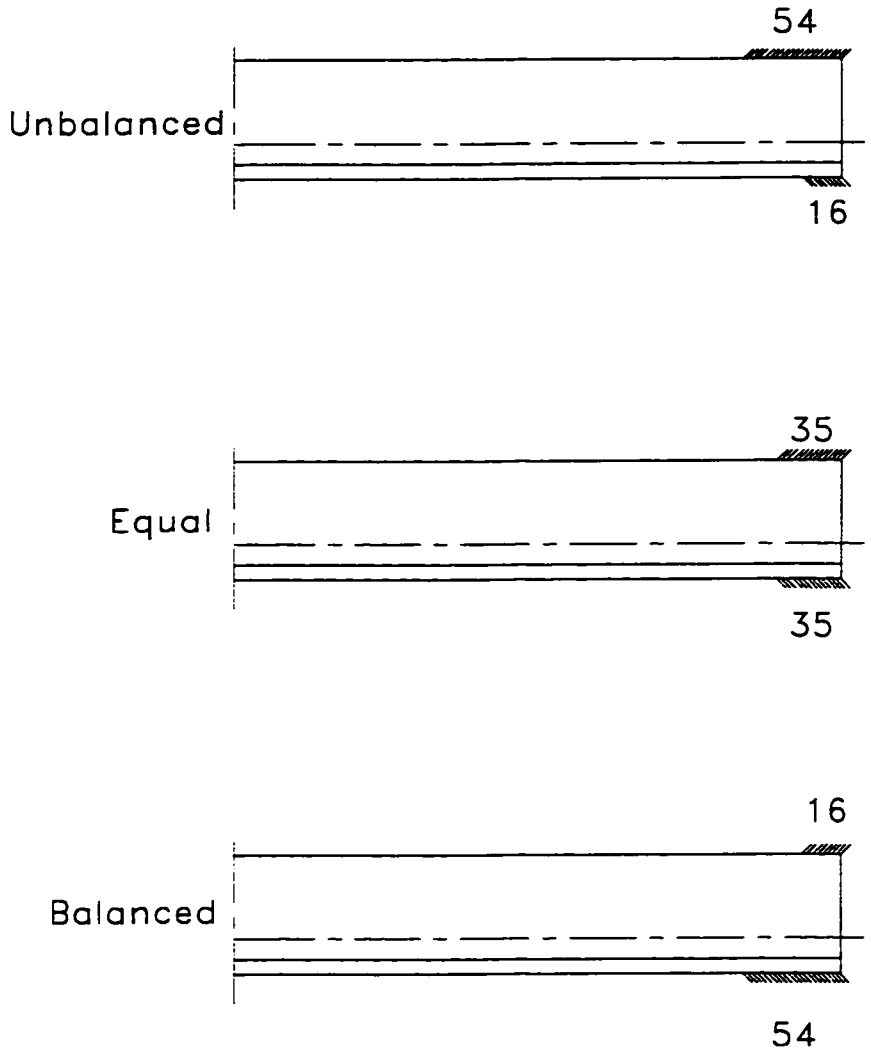

Figure 3-3. Weld pattern, slender specimens (dimensions in mm)

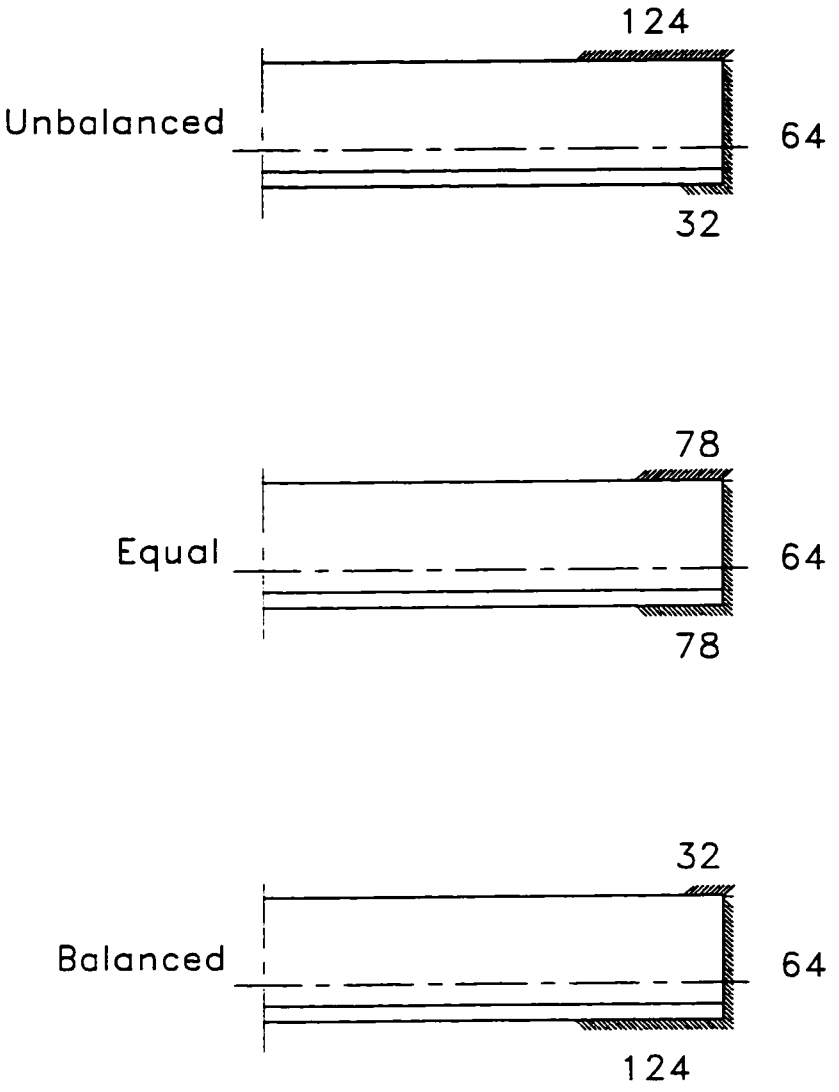

Figure 3-4. Weld pattern, shorter intermediate length specimens (dimensions in mm)

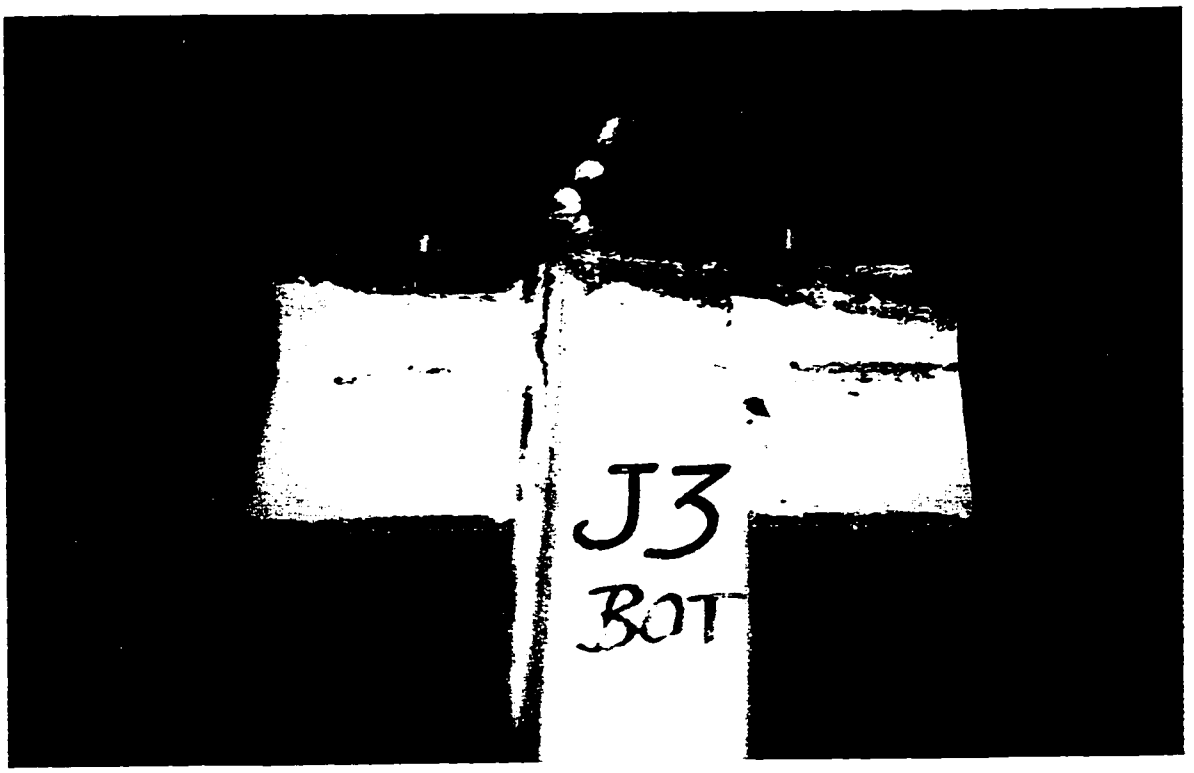

Figure 3-5. A close-up of one end of a test specimen

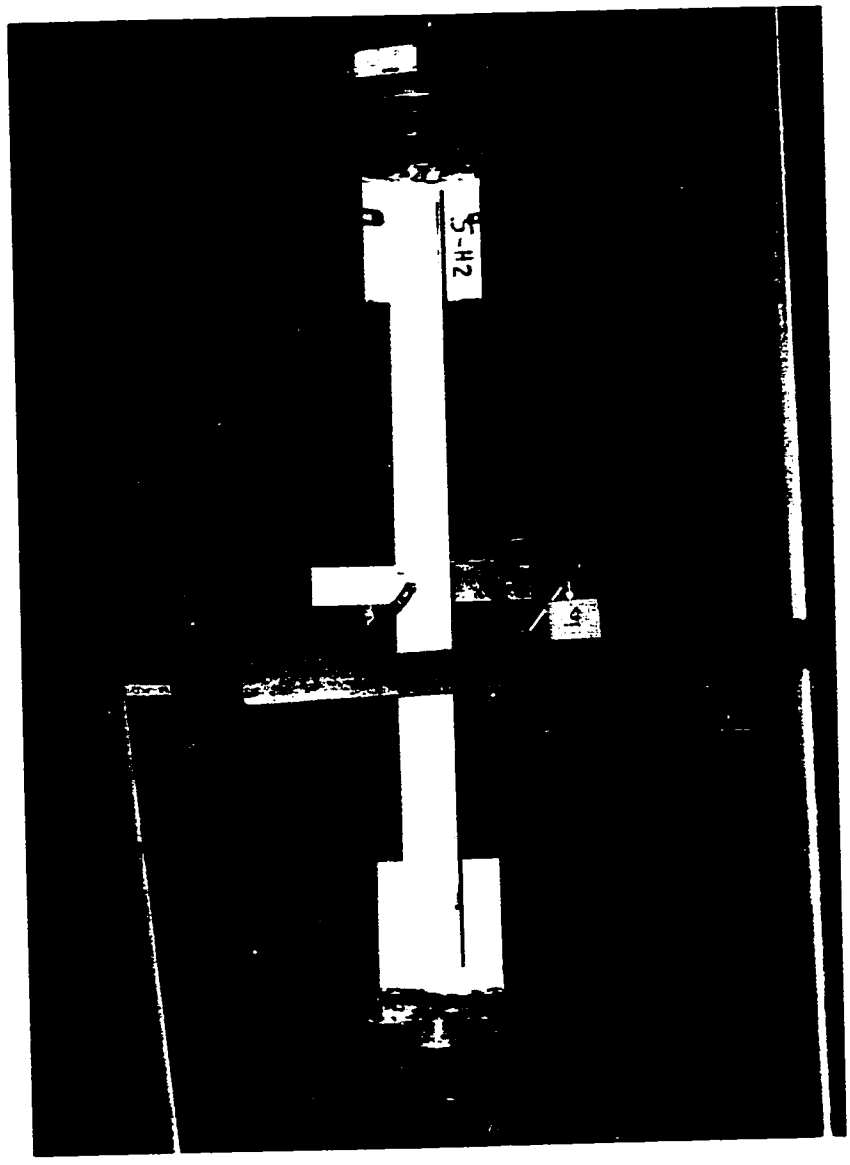

Figure 3-6. Test setup, shorter intermediate length specimen

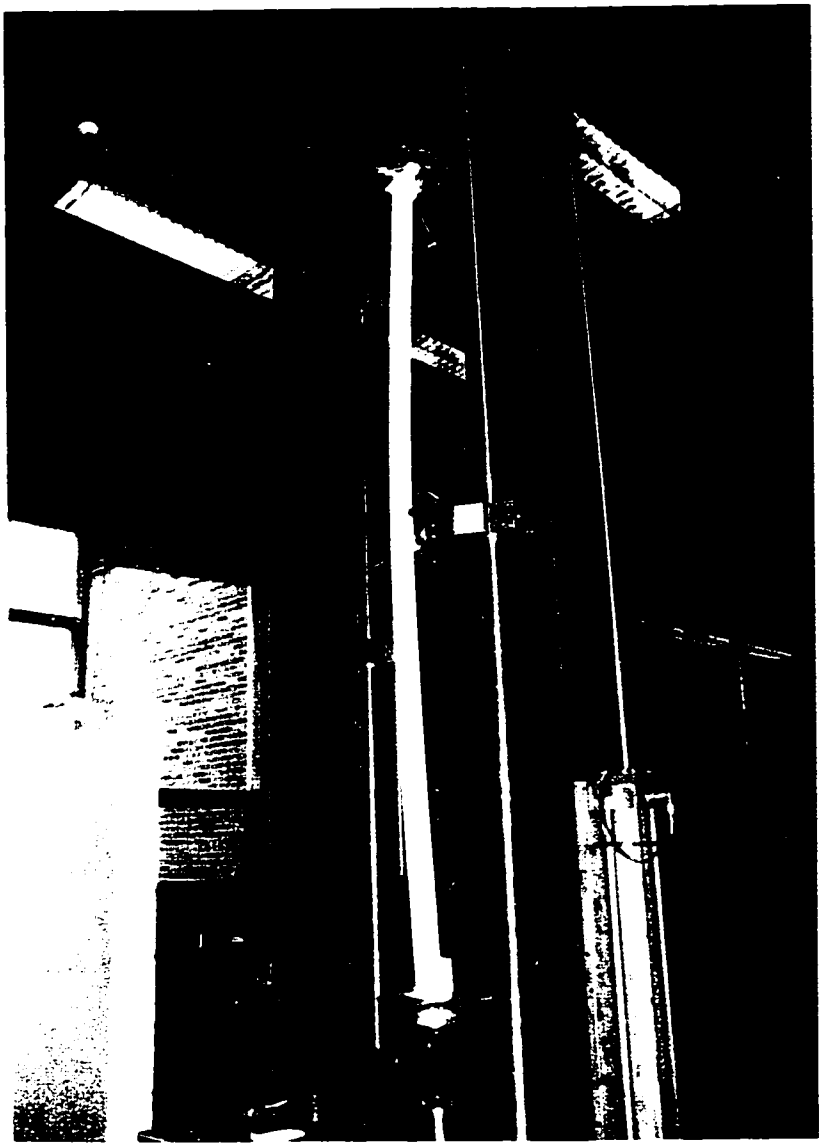

Figure 3-7. Test setup, slender specimen

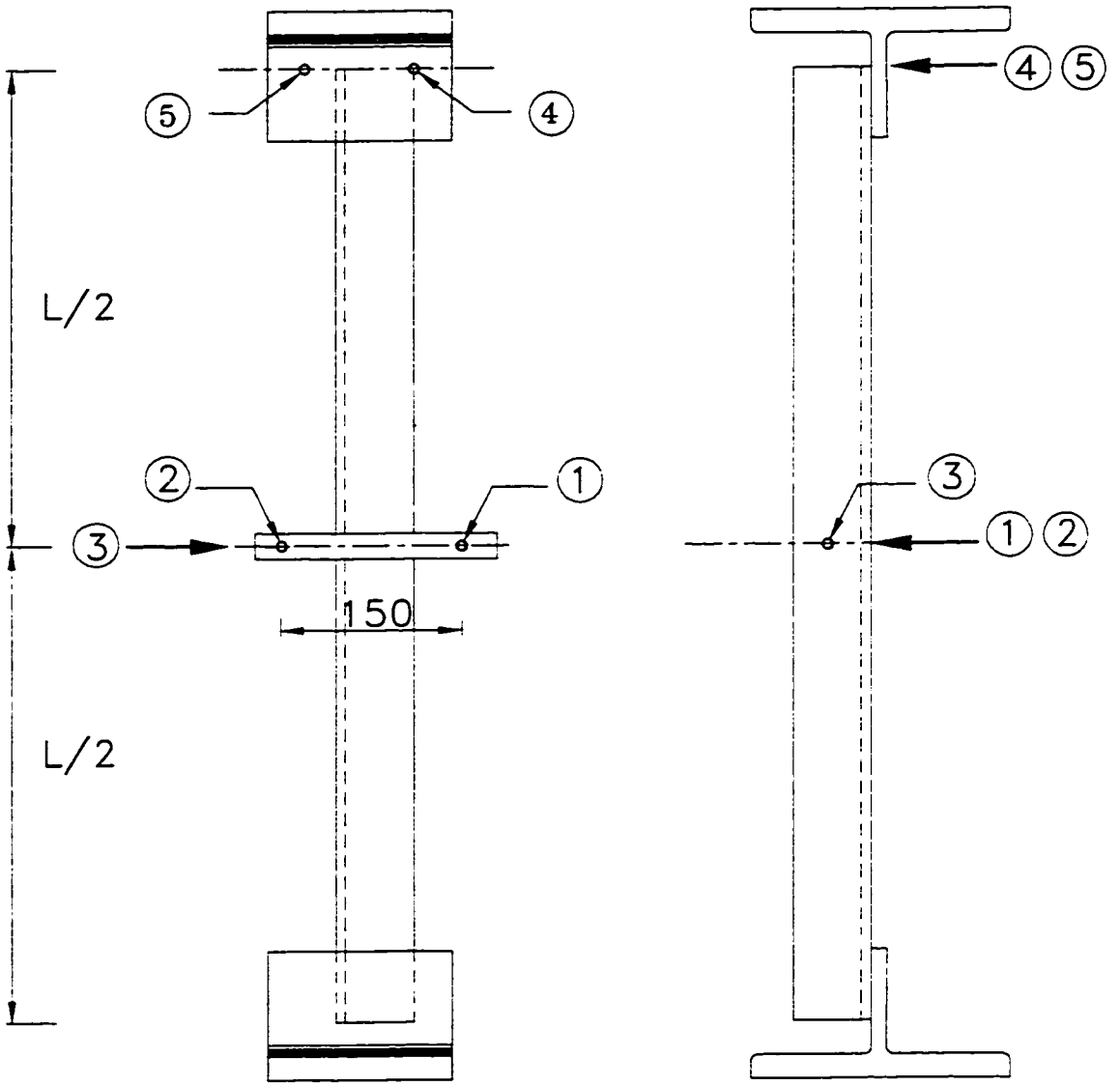

Figure 3-8. Location of dial gauges

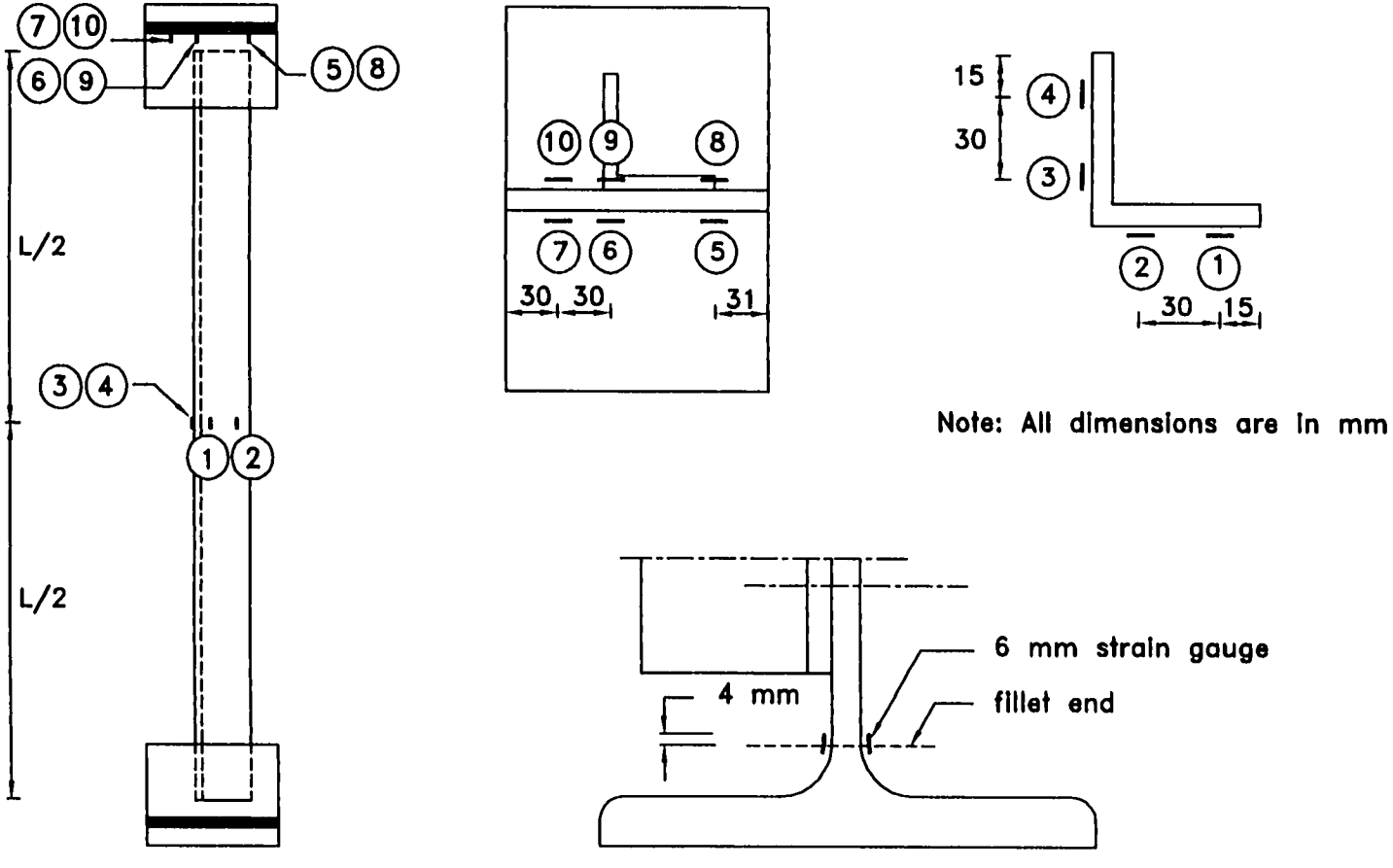

Figure 3-9. Location of strain gauges

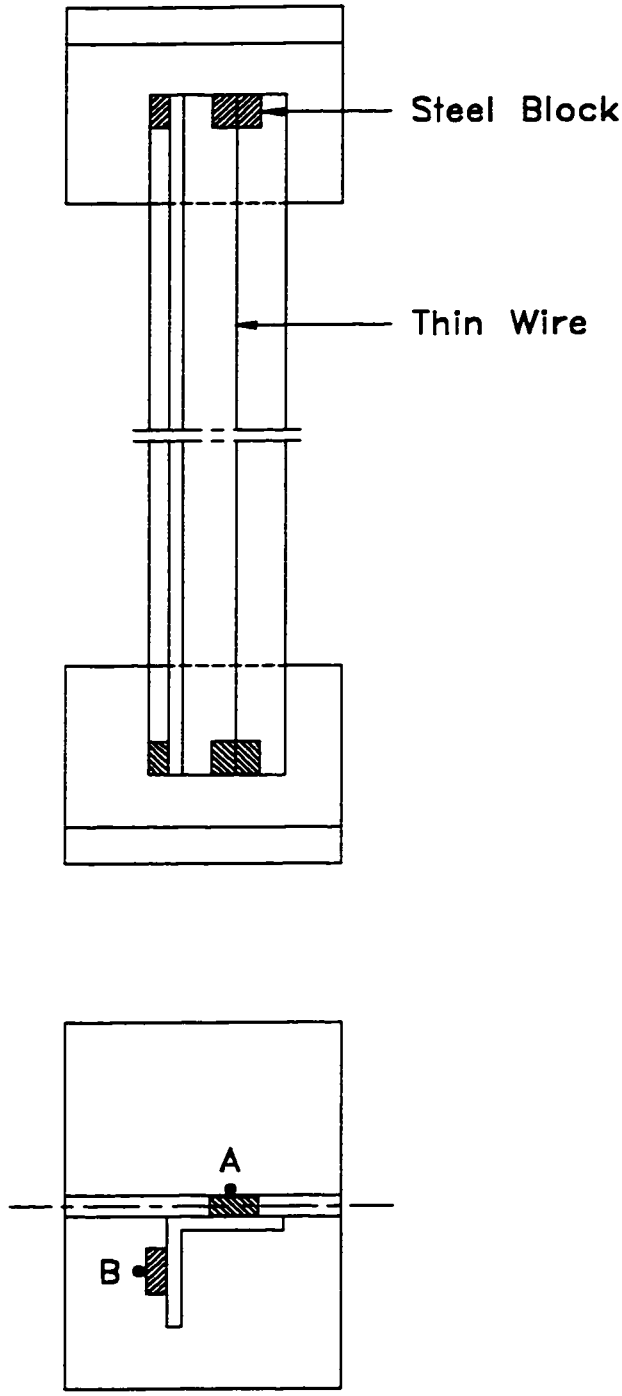

Figure 3-10. Out-of-straightness measurement

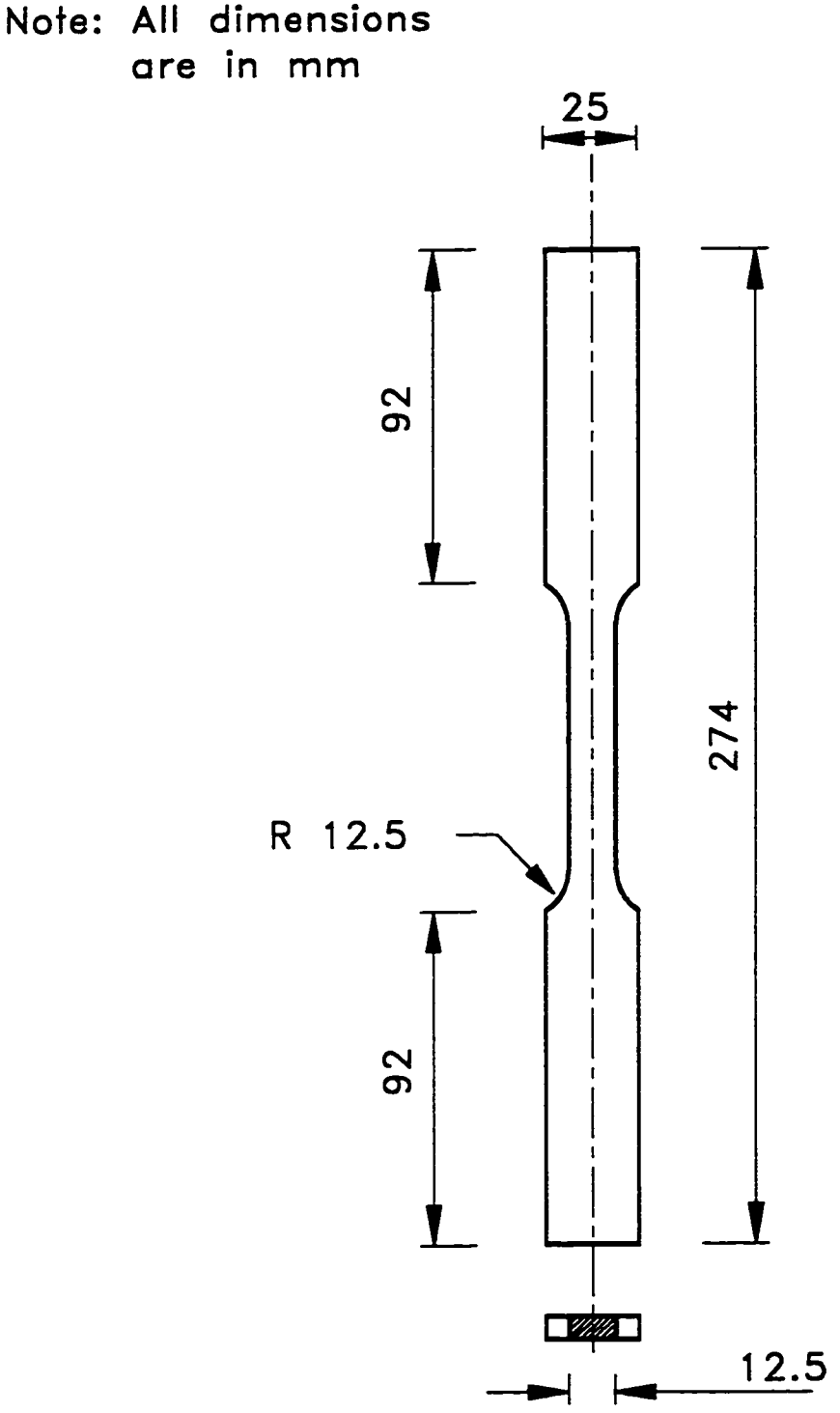

Figure 3-11. Tension test specimen

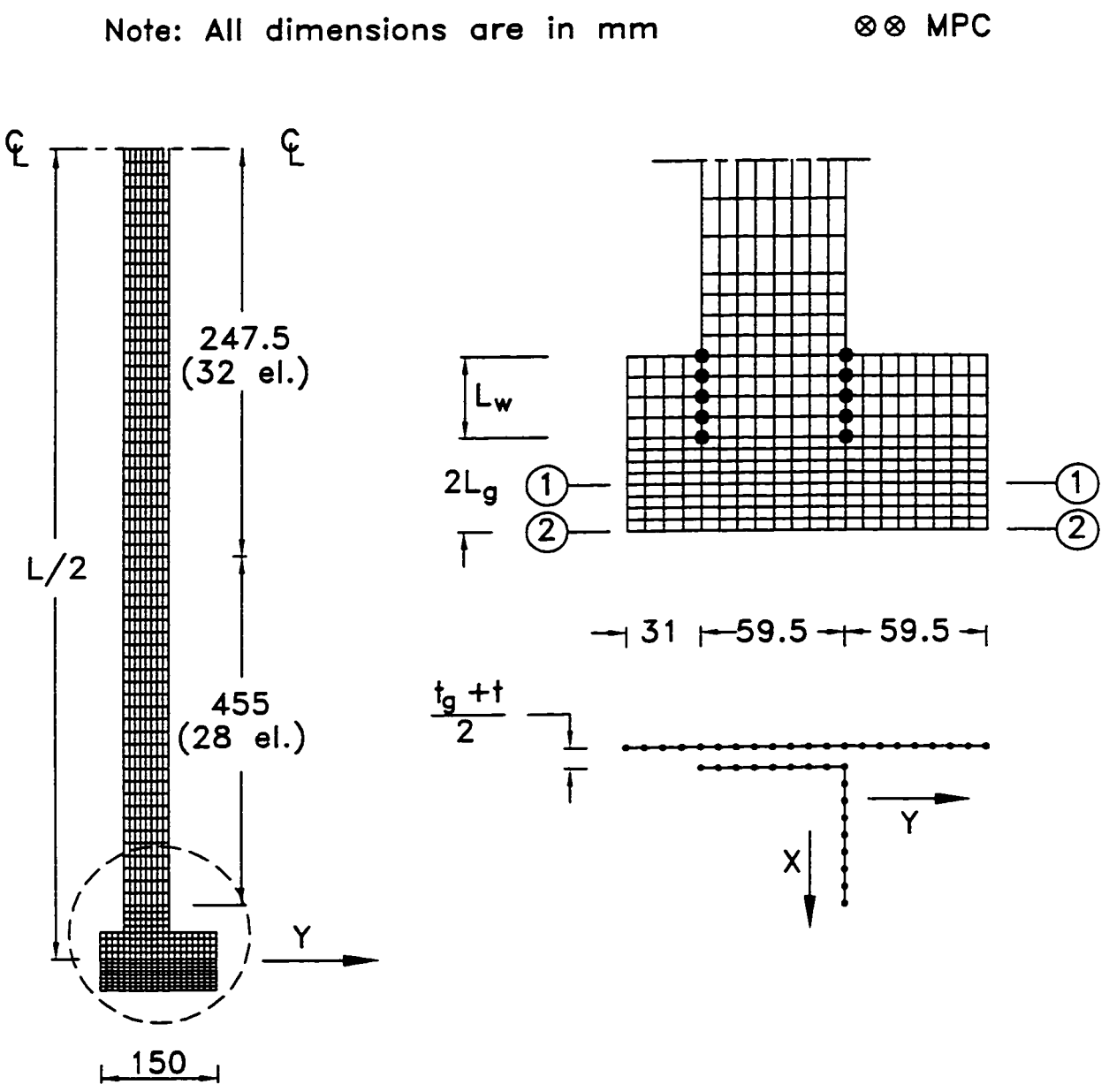

Figure 4-1. Typical finite element mesh for specimens L-A and L-F

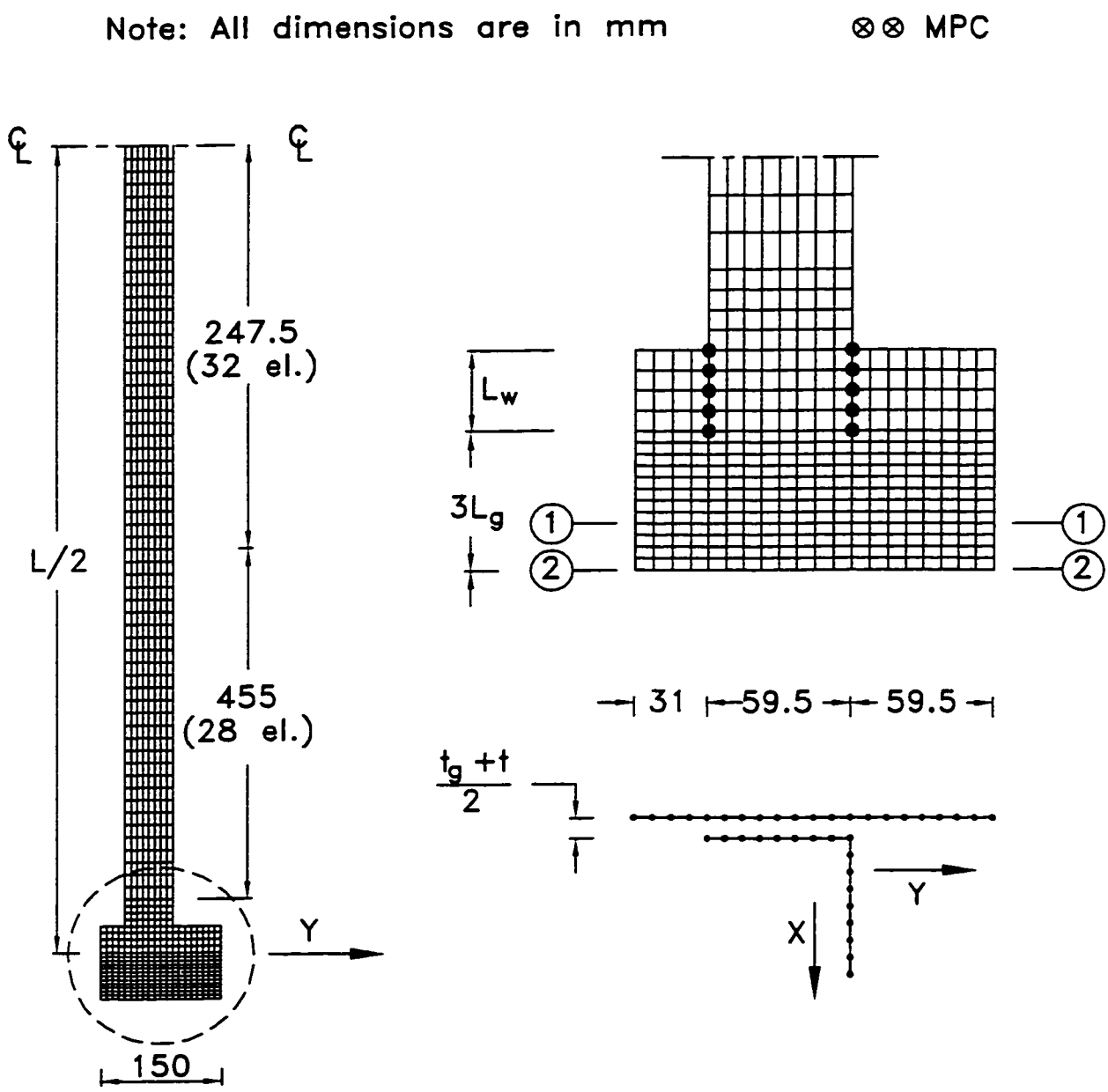

Figure 4-2. Typical finite element mesh for specimens L-B

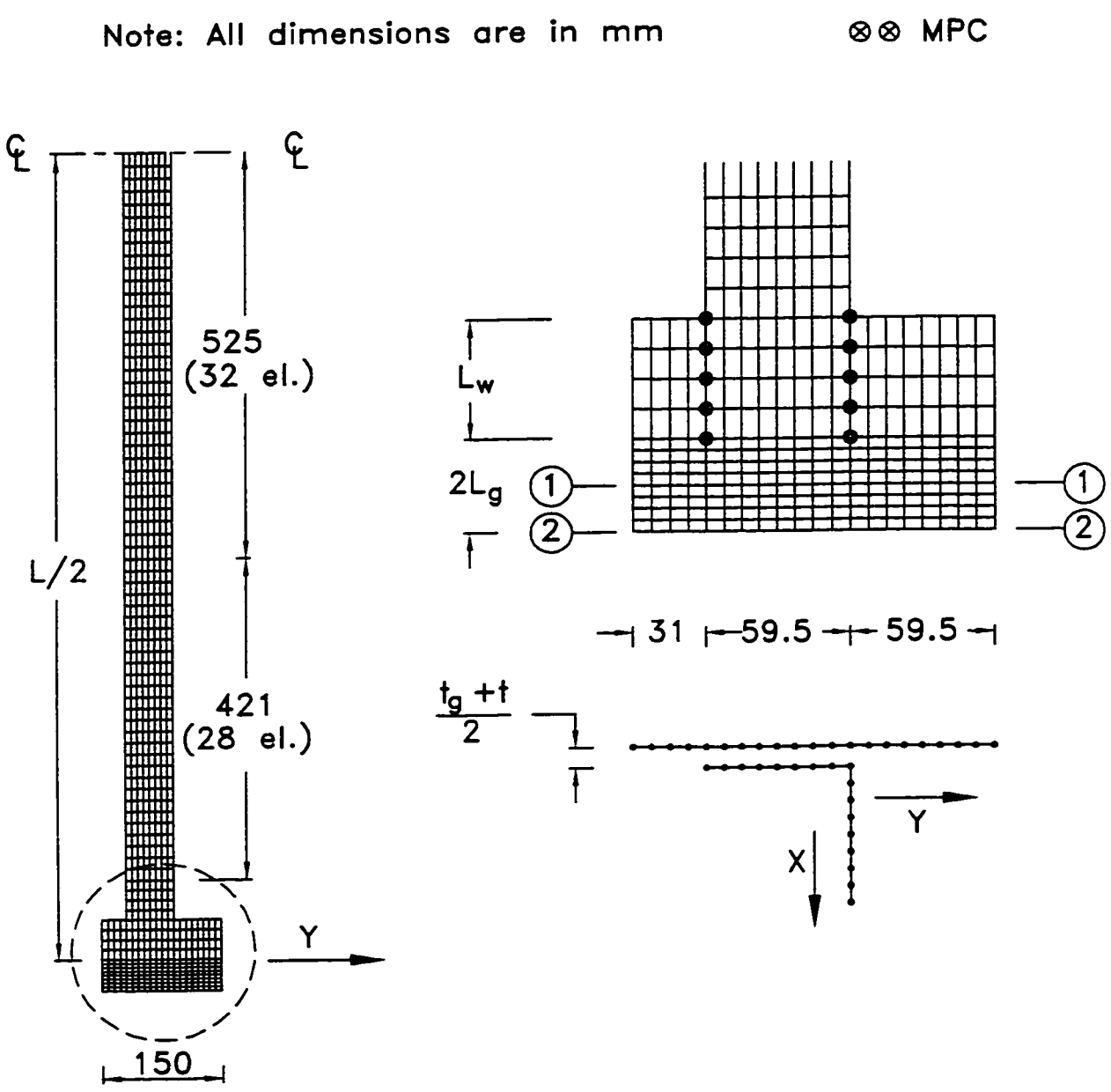

Figure 4-3. Typical finite element mesh for specimens L-D

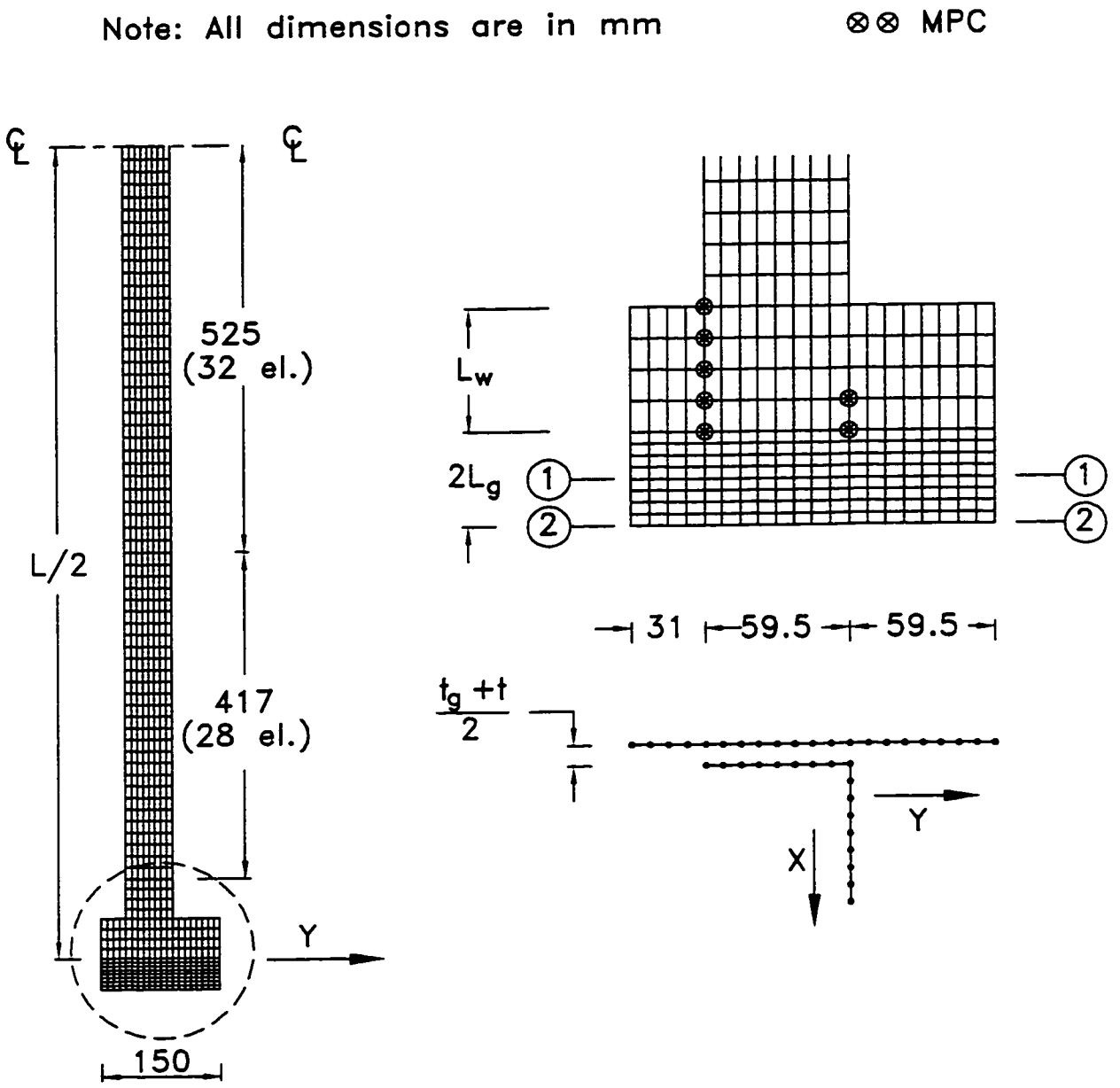

Figure 4-4. Typical finite element mesh for specimens L-H

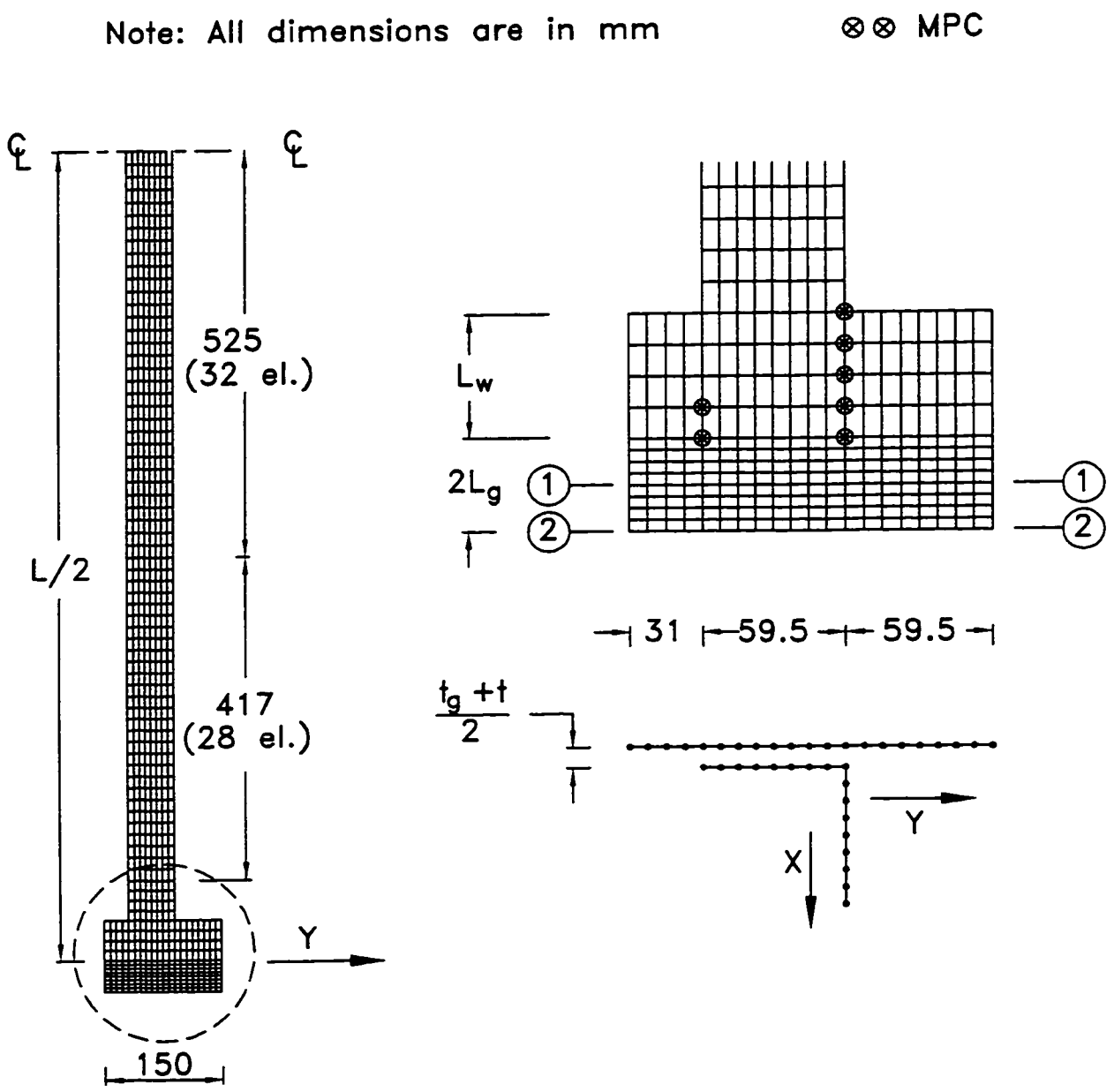

Figure 4-5. Typical finite element mesh for specimens L-I

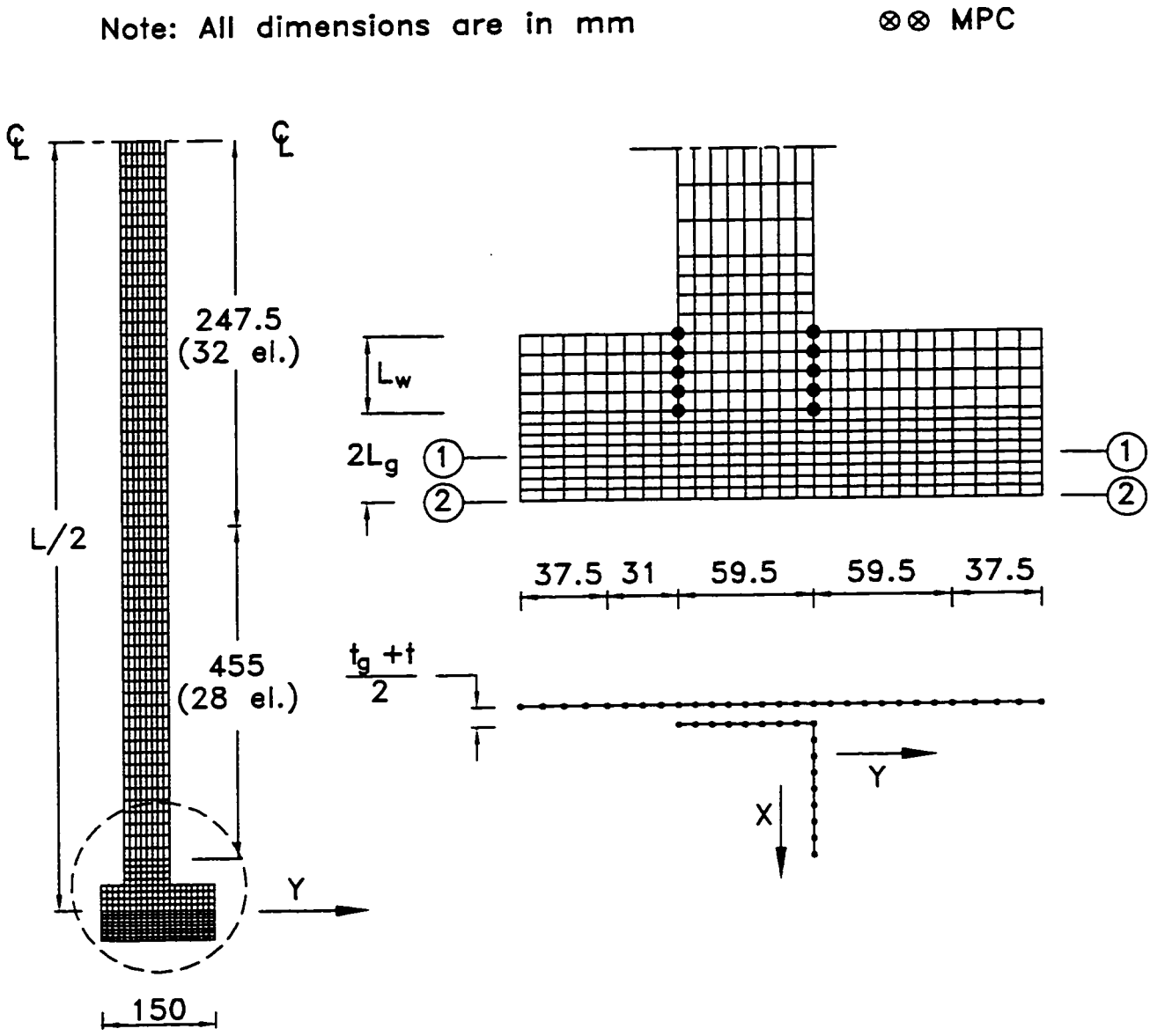

Figure 4-6. Typical finite element mesh for specimens L-J

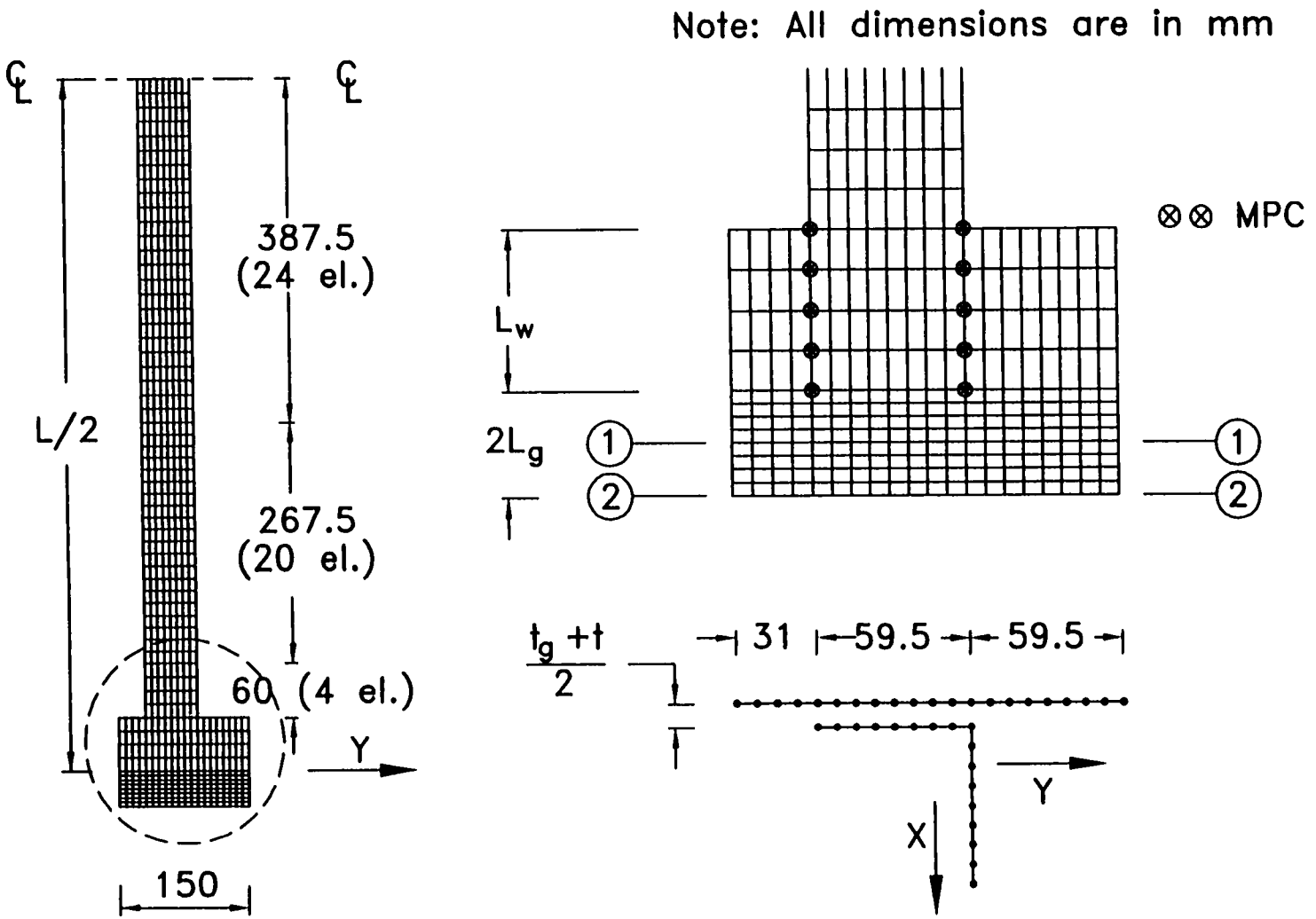

Figure 4-7. Typical finite element mesh for specimens M-A and M-F

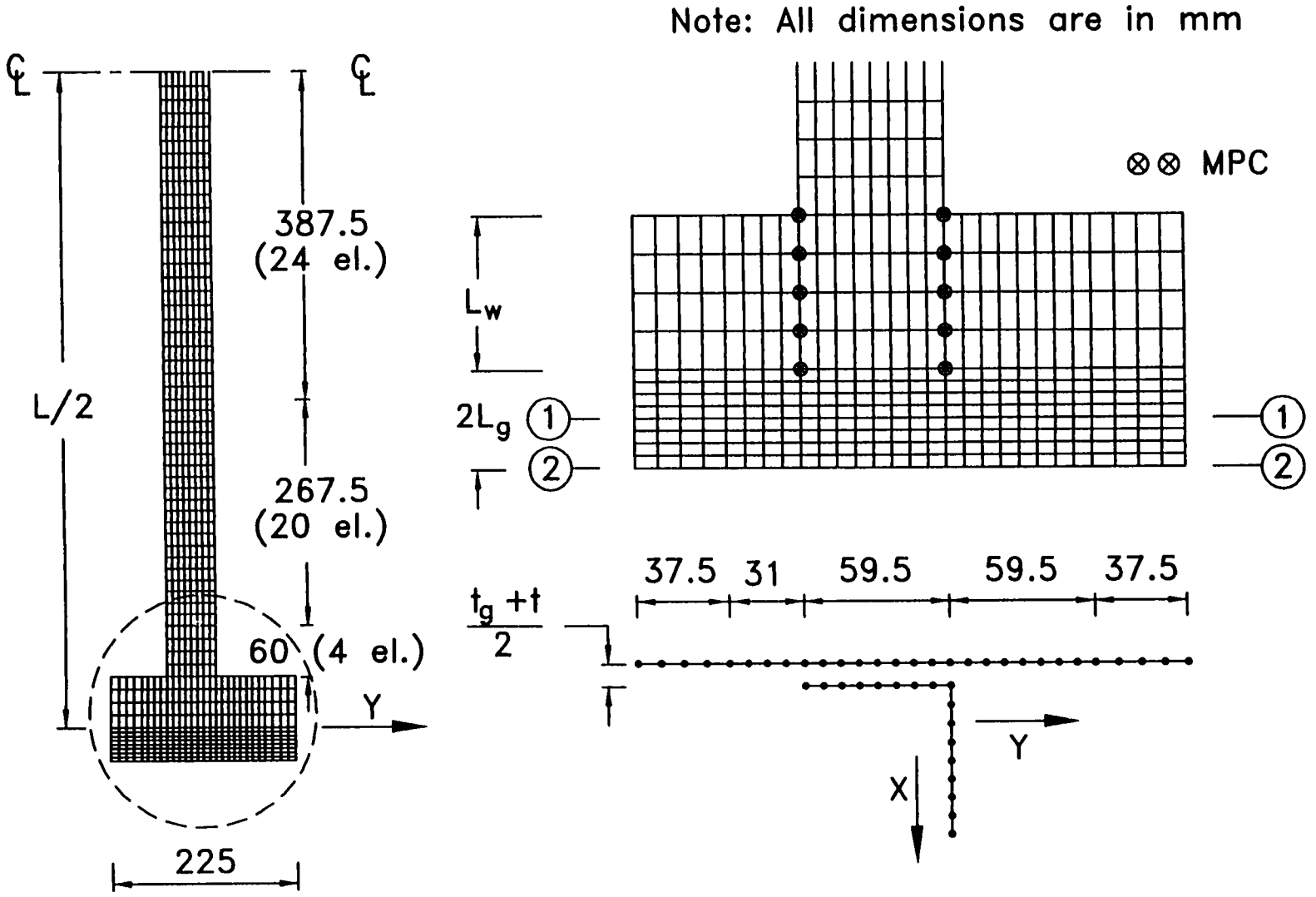

Figure 4-8. Typical finite element mesh for specimens M-J

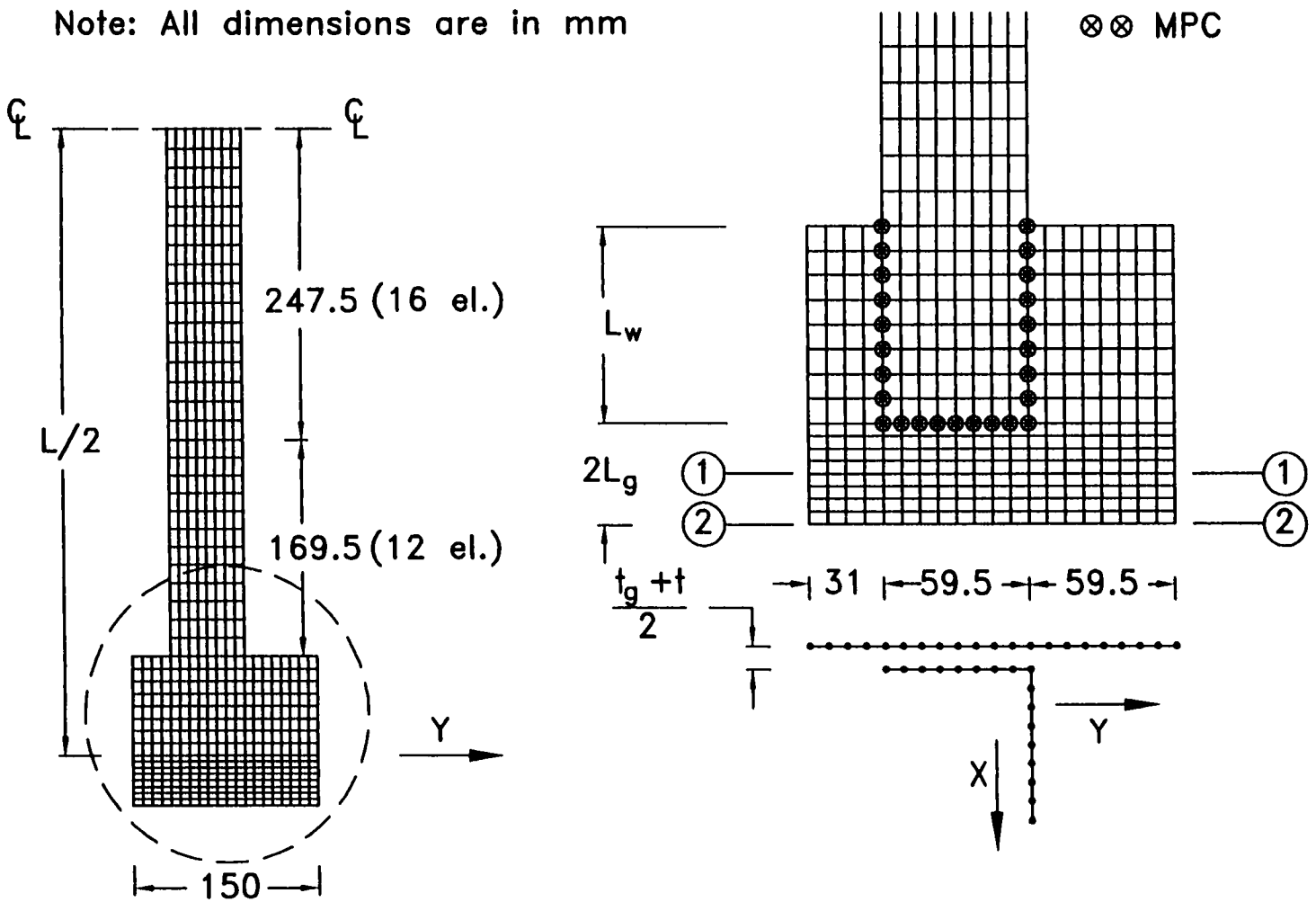

Figure 4-9. Typical finite element mesh for specimens S-A and S-F

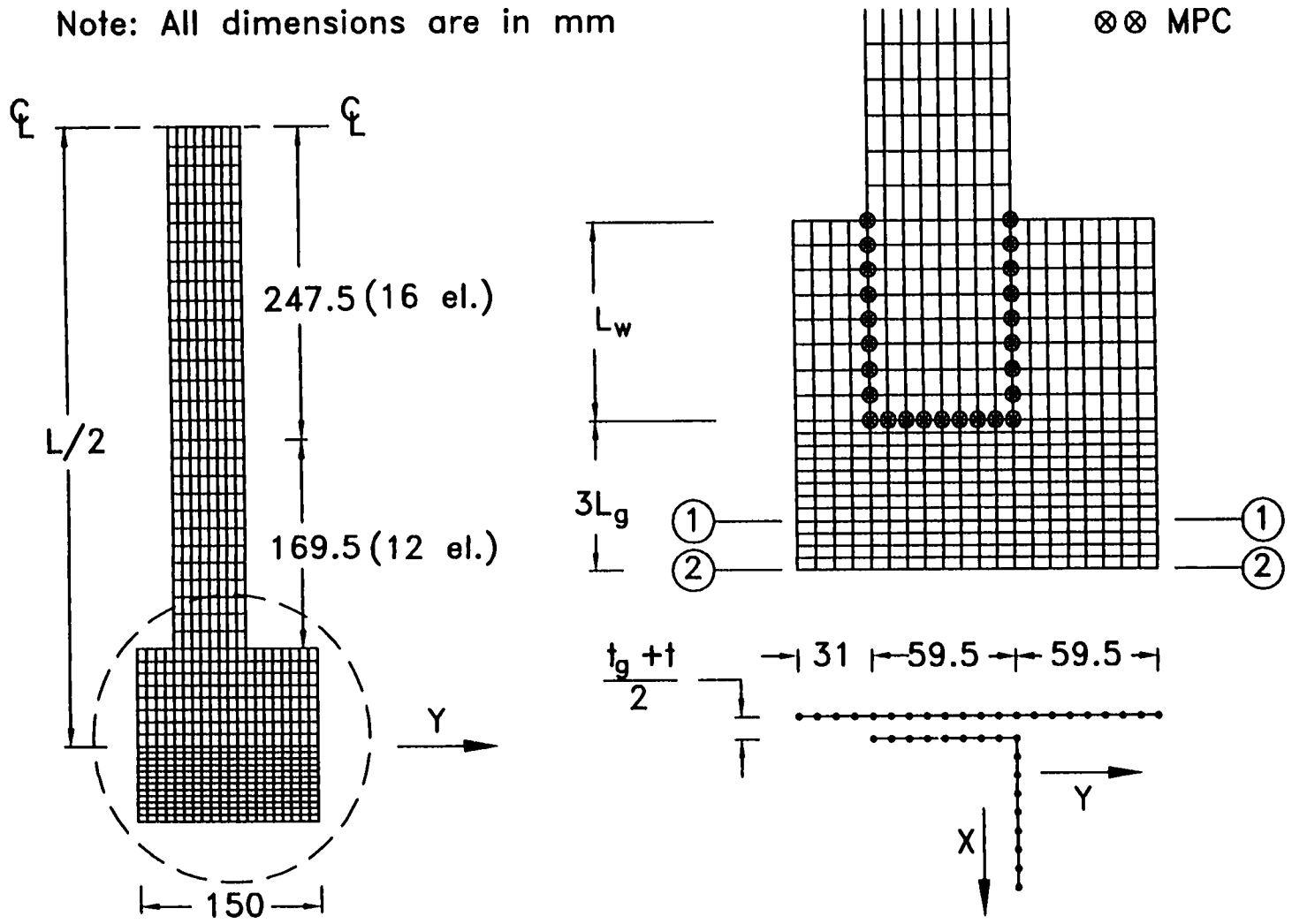

Figure 4-10. Typical finite element mesh for specimens S-B

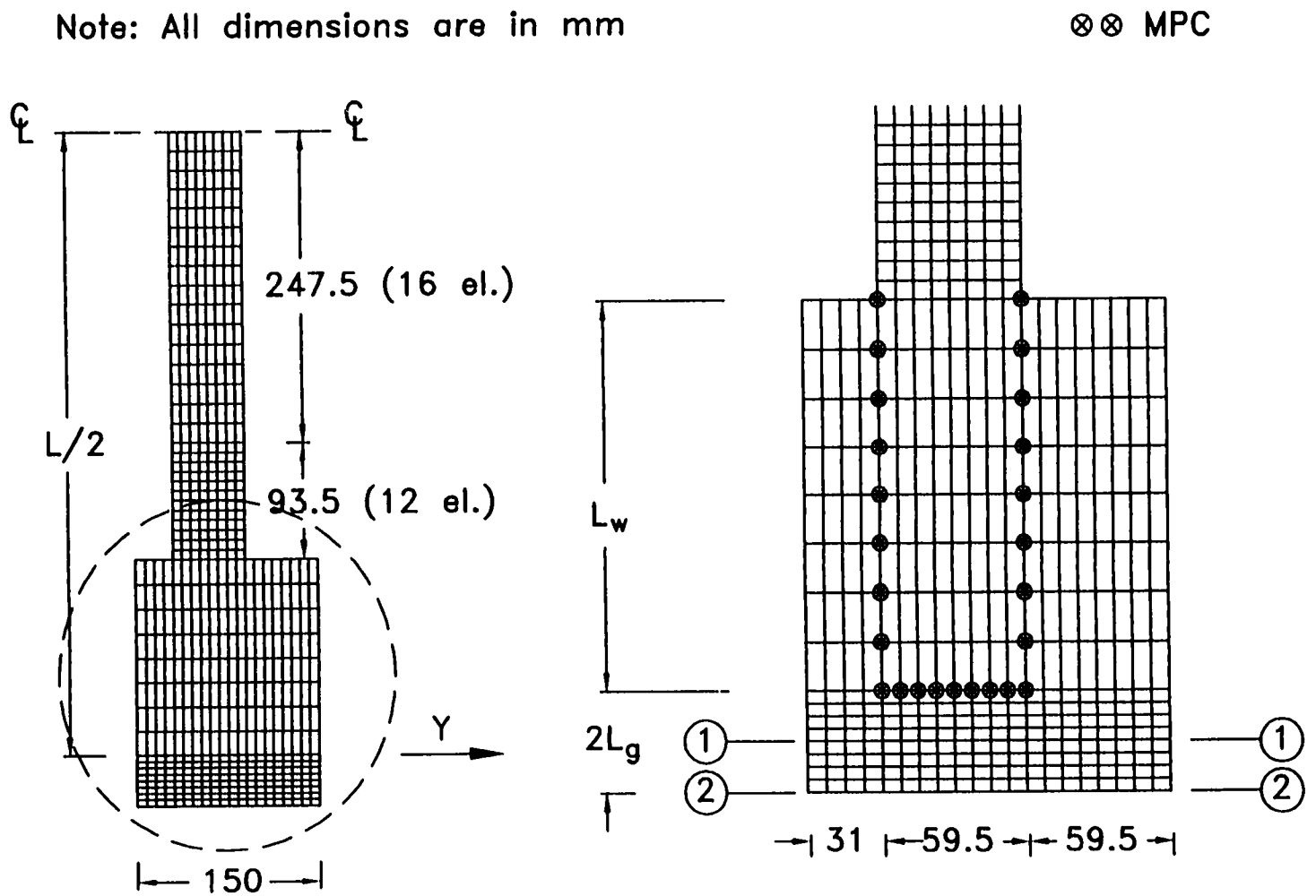

Figure 4-11. Typical finite element mesh for specimens S-D

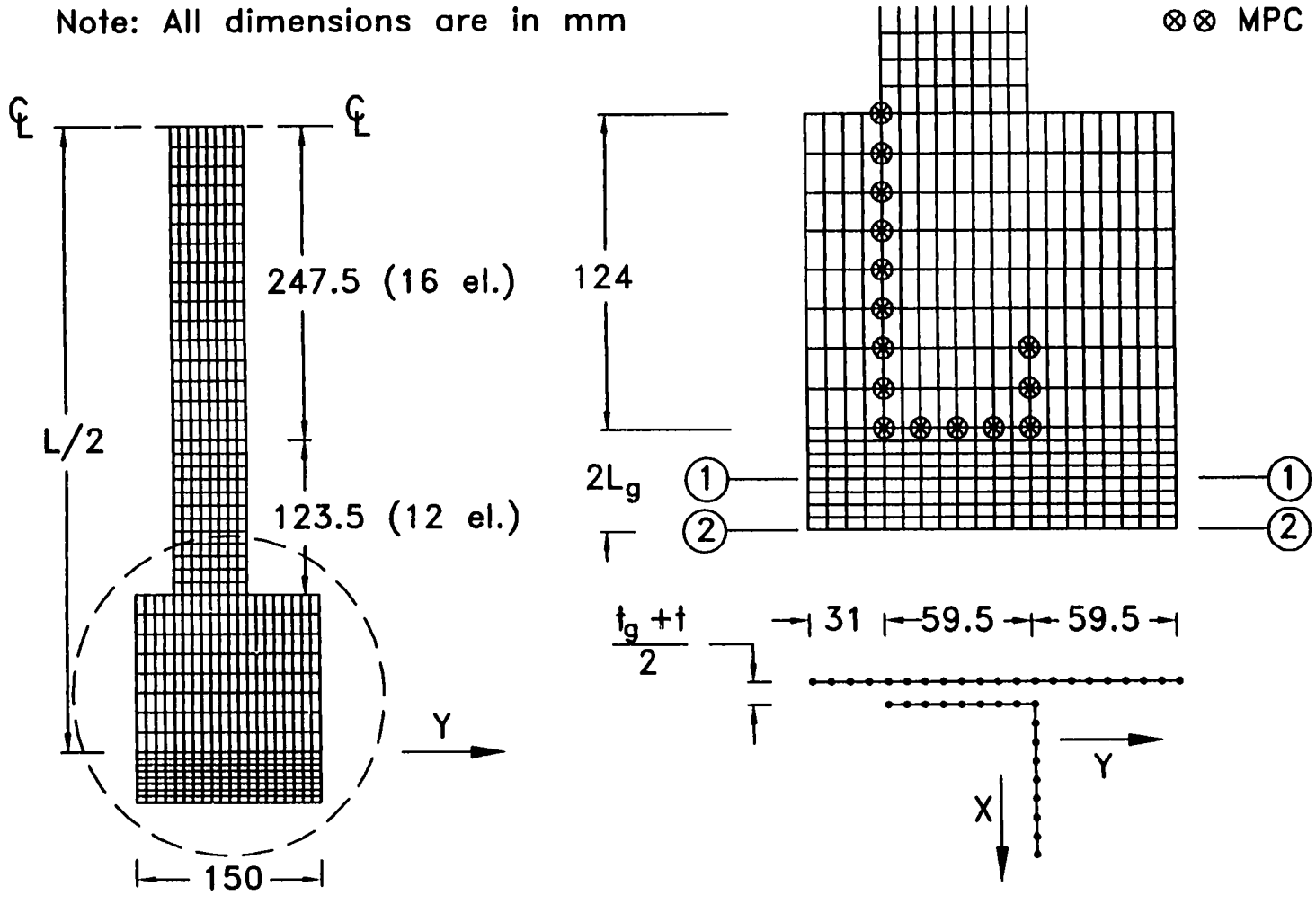

Figure 4-12. Typical finite element mesh for specimens S-H

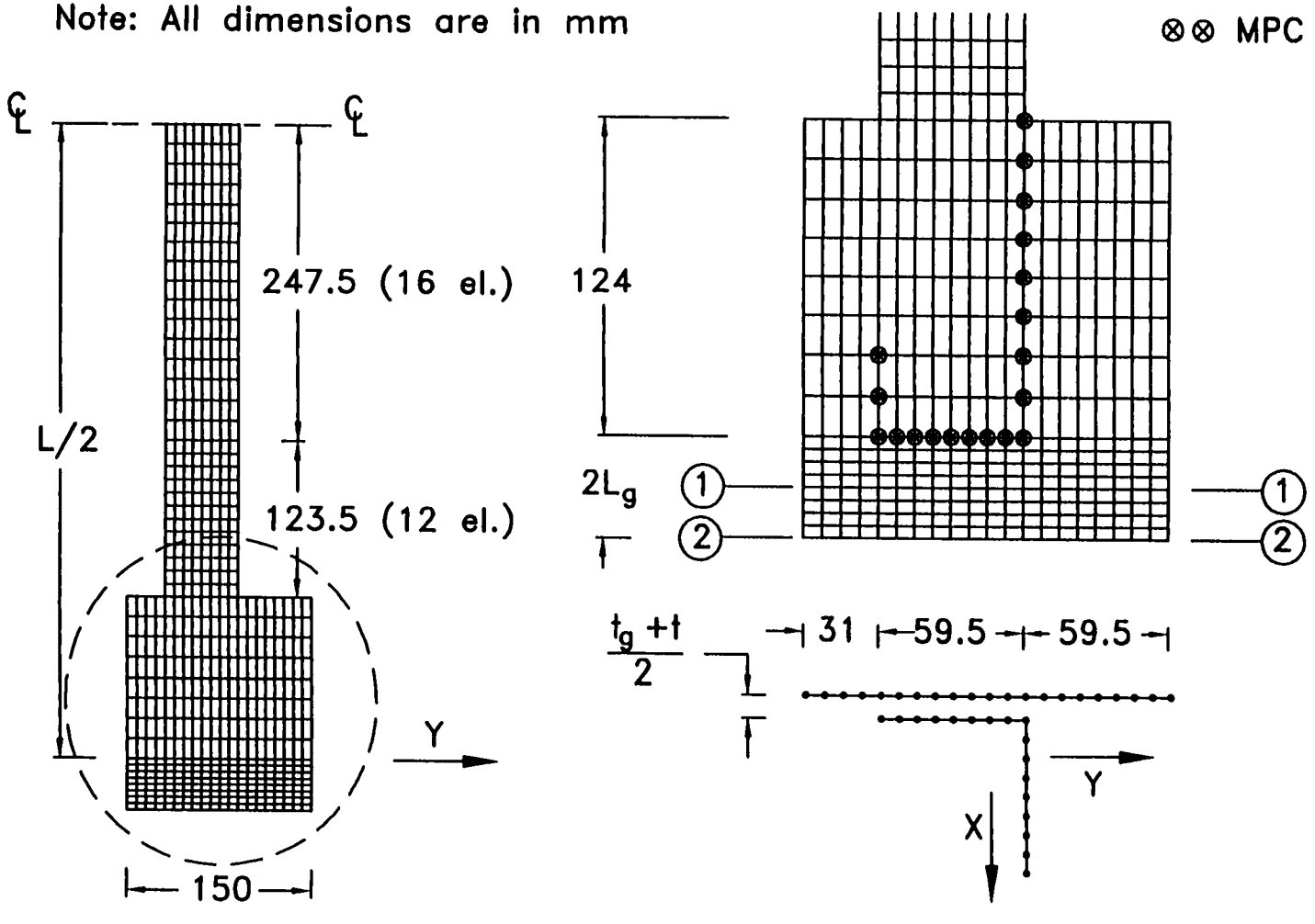

Figure 4-13. Typical finite element mesh for specimens S-I

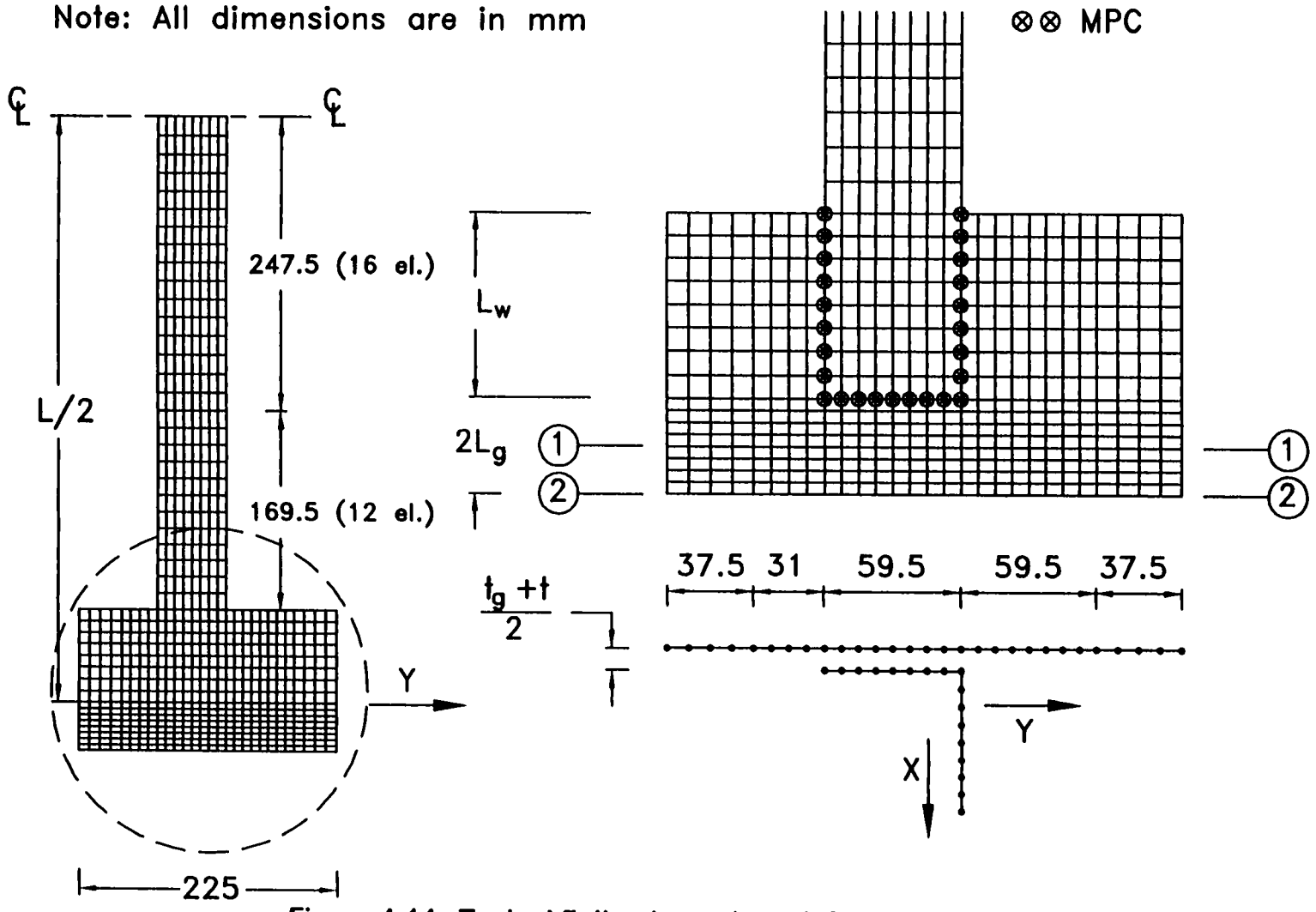

Figure 4-14. Typical finite element mesh for specimens S-J

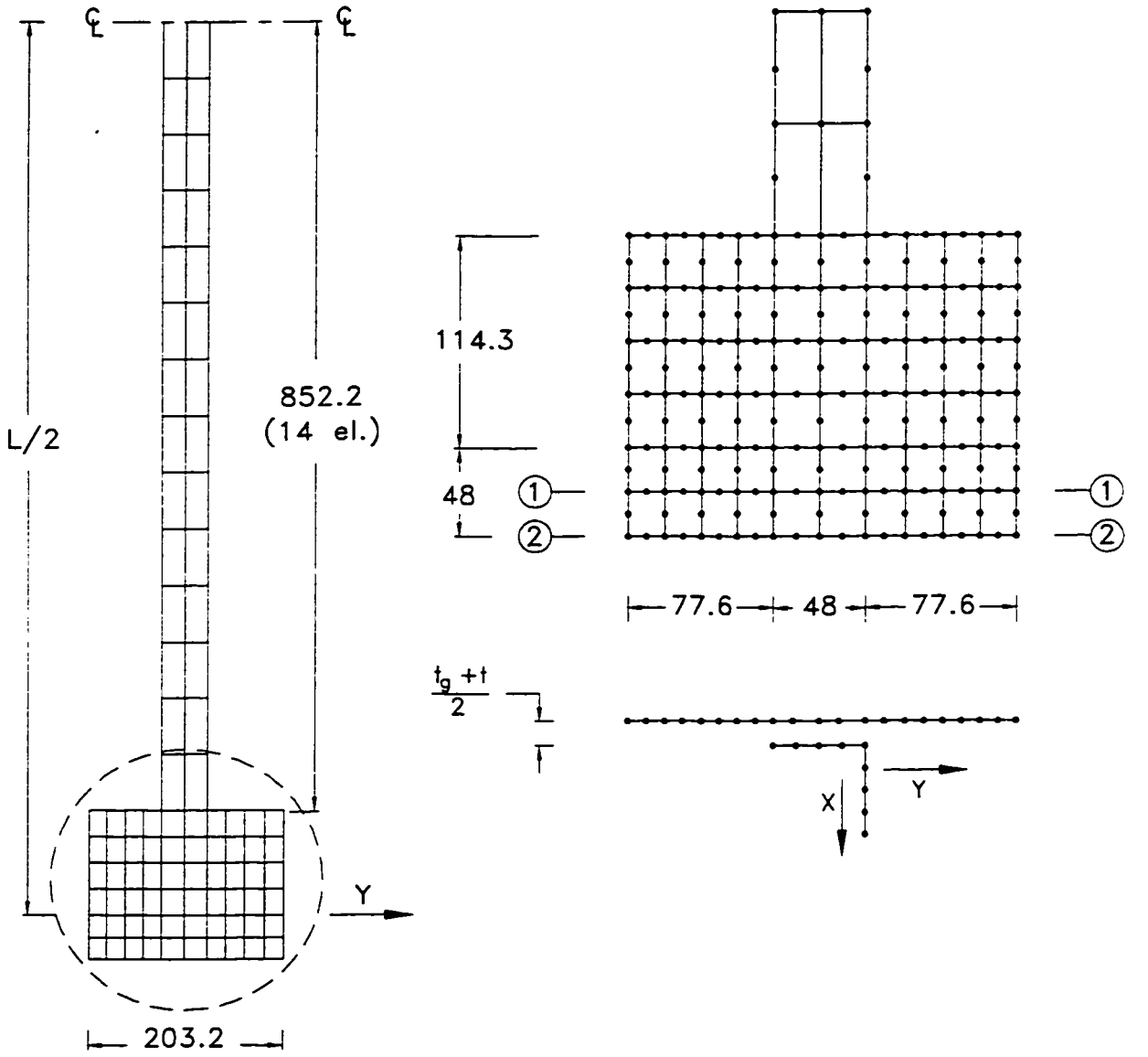

Figure 4-15. Typical finite element mesh for Trahair et al. test specimen A-1-1

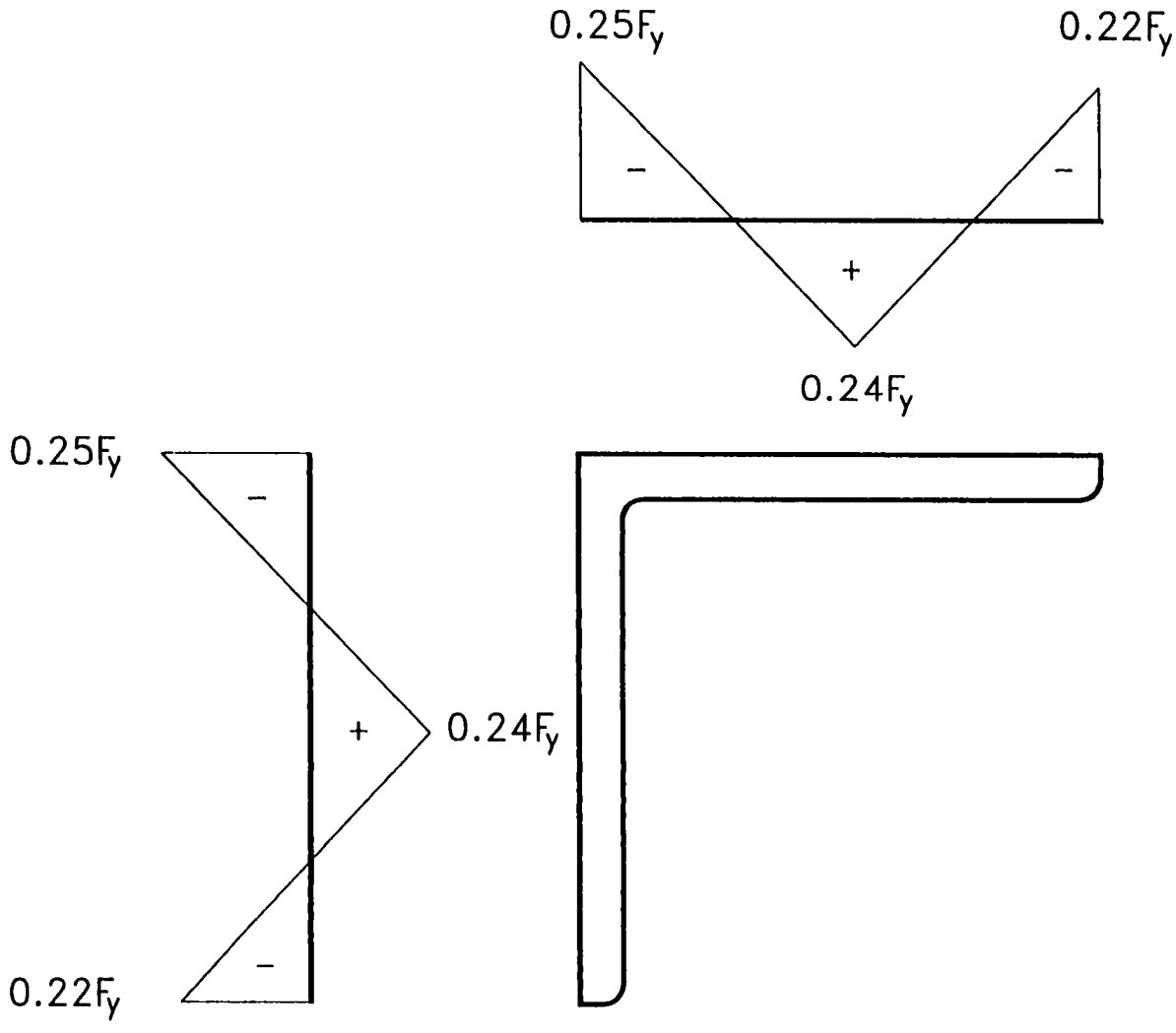

Figure 4-16. ECCS residual stresses

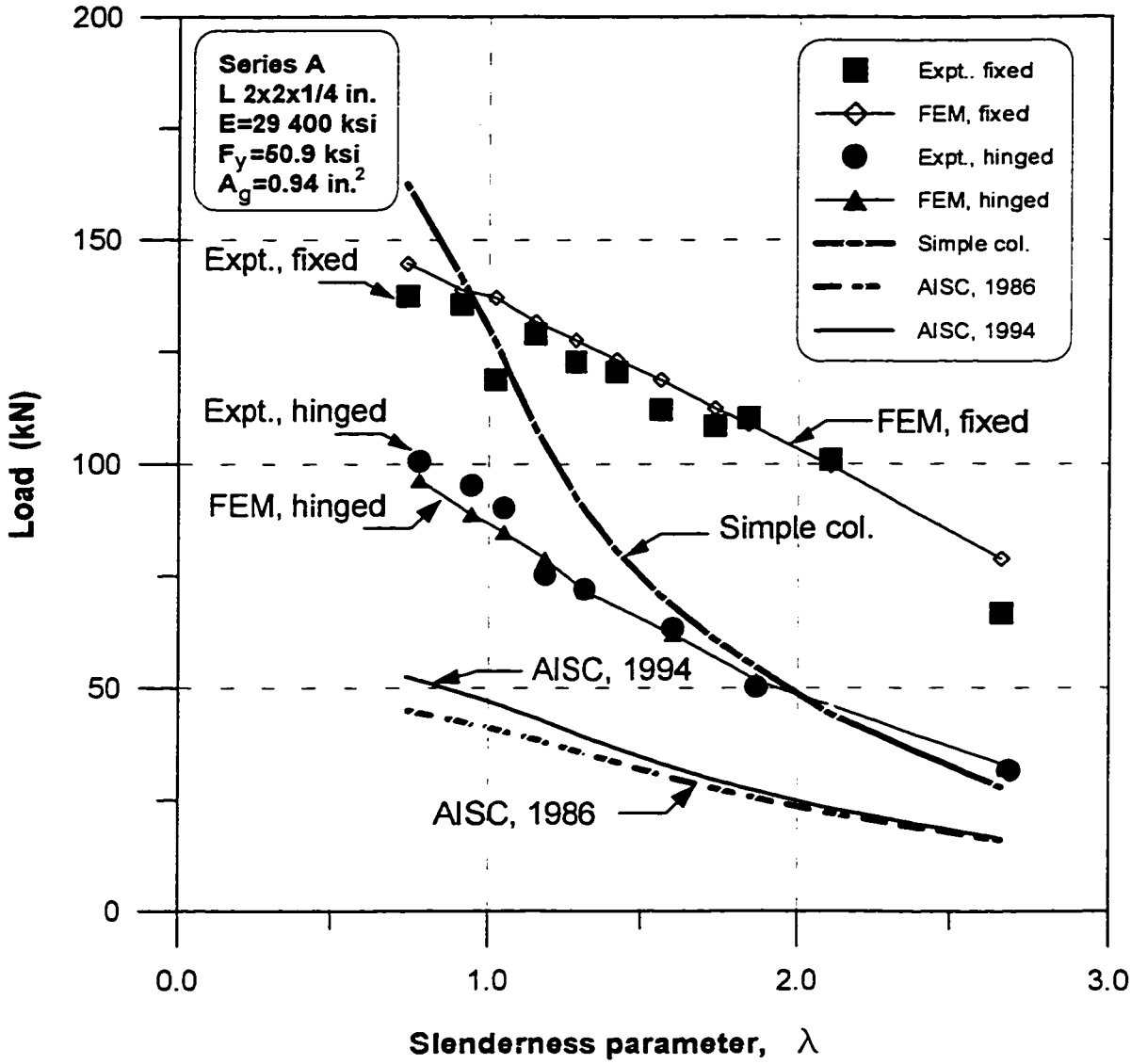

Figure 5-1. Comparison of experimental failure loads (Series A) and compressive resistances calculated in accordance with the simple-column and AISC approaches, and by the finite element method (FEM)

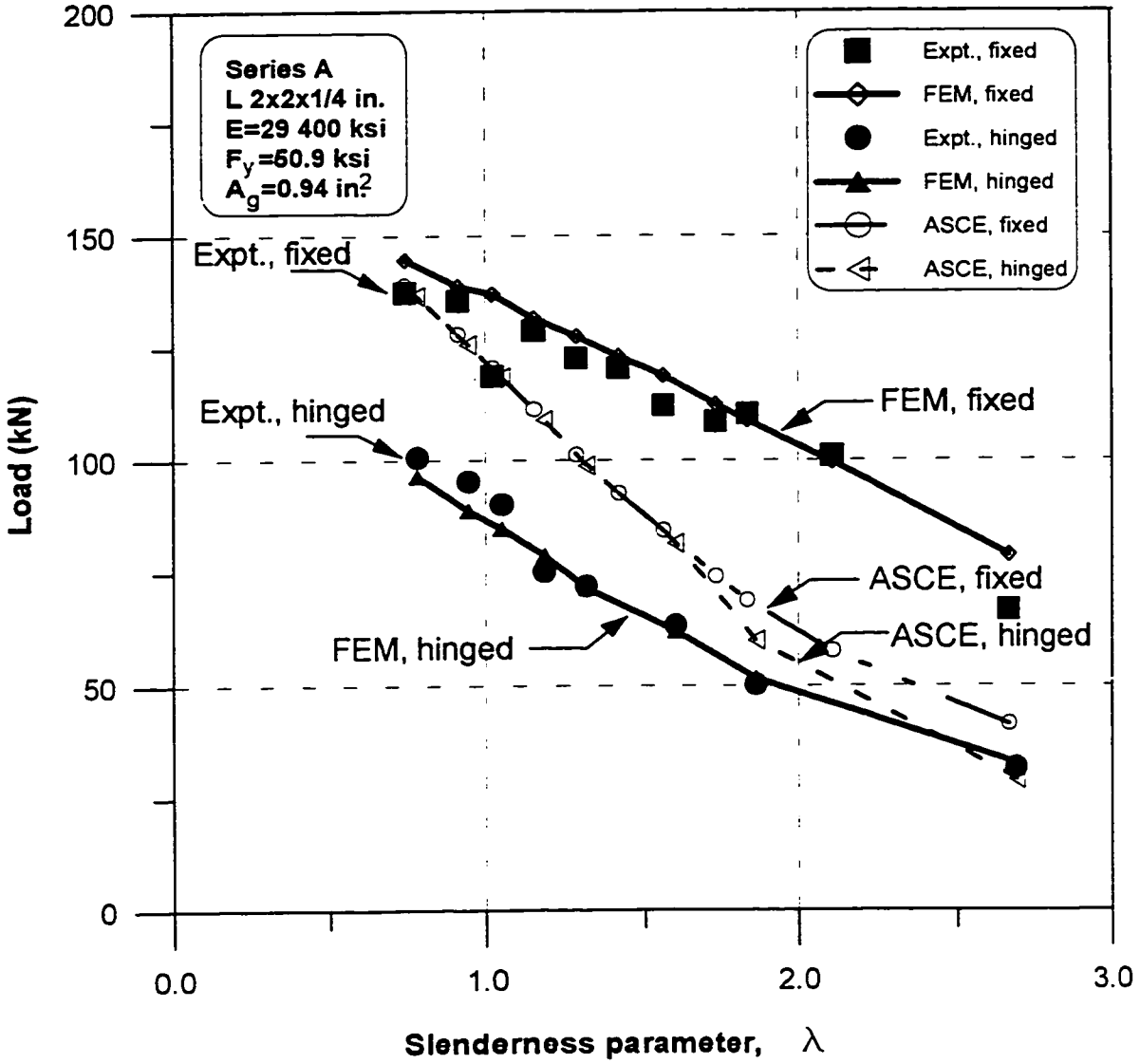

Figure 5-2. Comparison of experimental failure loads (Series A) and compressive resistances calculated by ASCE Standard

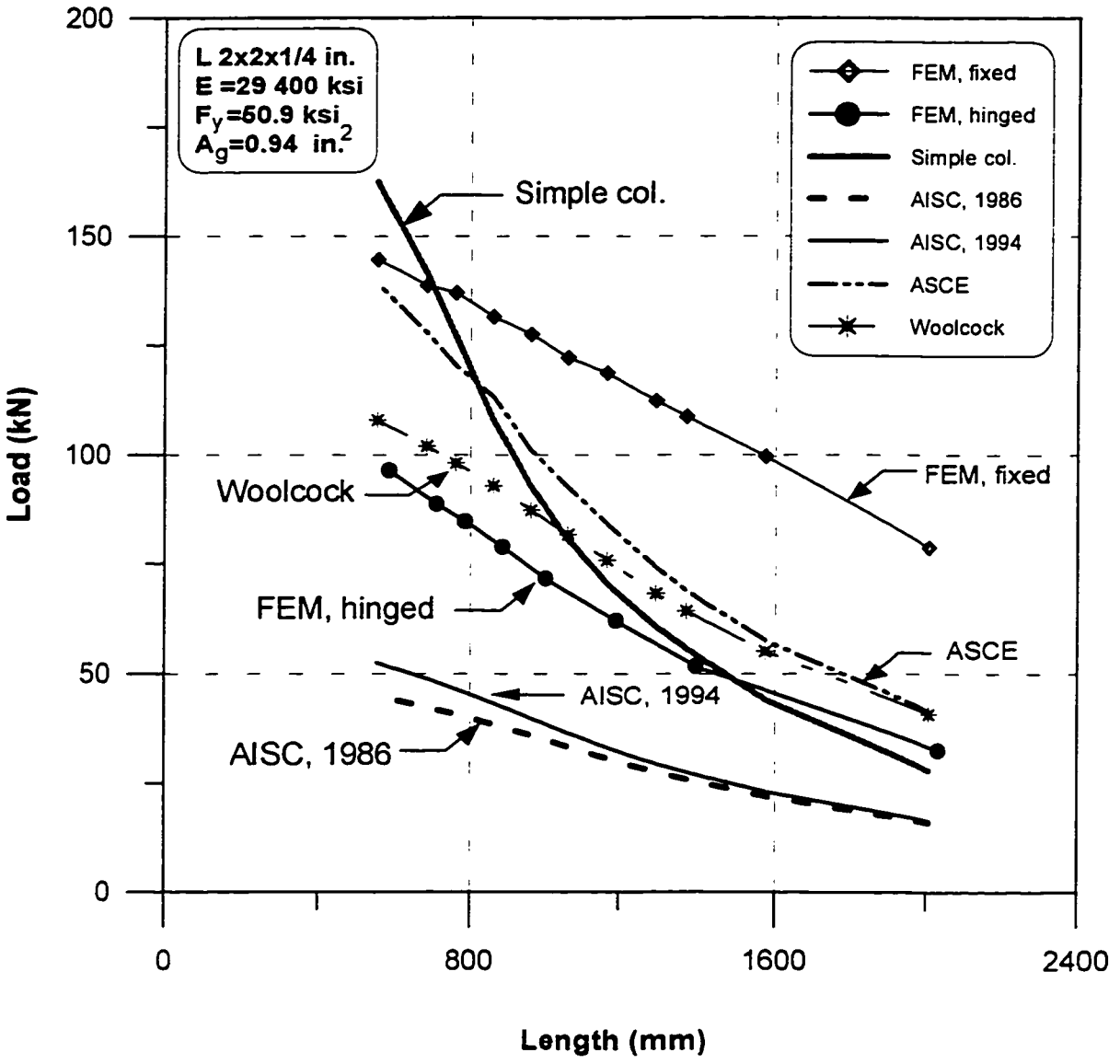

Figure 5-3. Comparison of predicted compressive resistances for Series A specimens

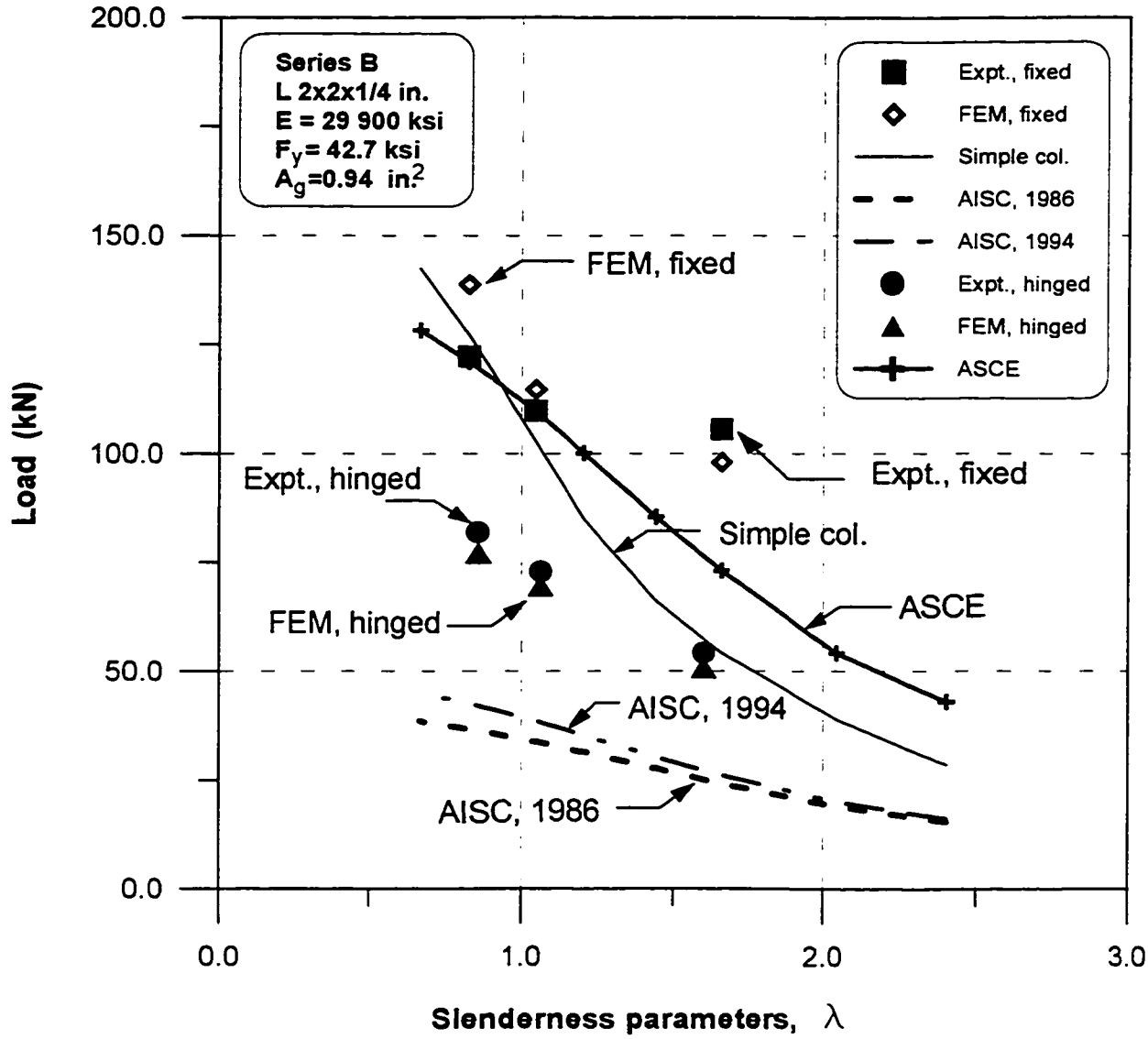

Figure 5-4. Comparison of experimental failure loads (Series B) and compressive resistances calculated in accordance with the simple-column and AISC approaches, and by the finite element method (FEM)

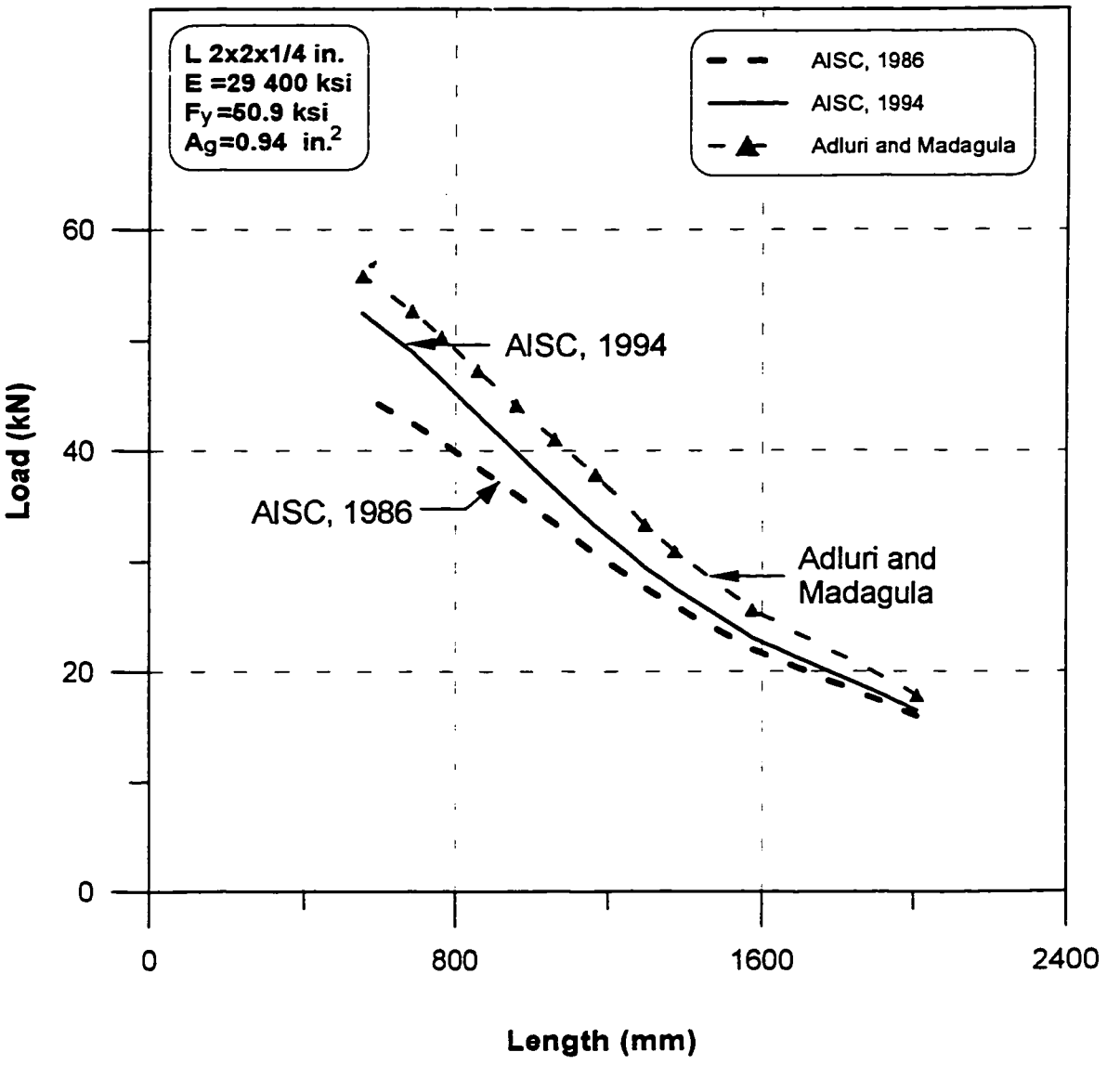

Figure 5-5. Comparison of predicted compressive resistances calculated by AISC approach, and Adluri and Madugula (1992)

Figure 6-1. Plastic hinge in gusset plate, Specimen S-D-1

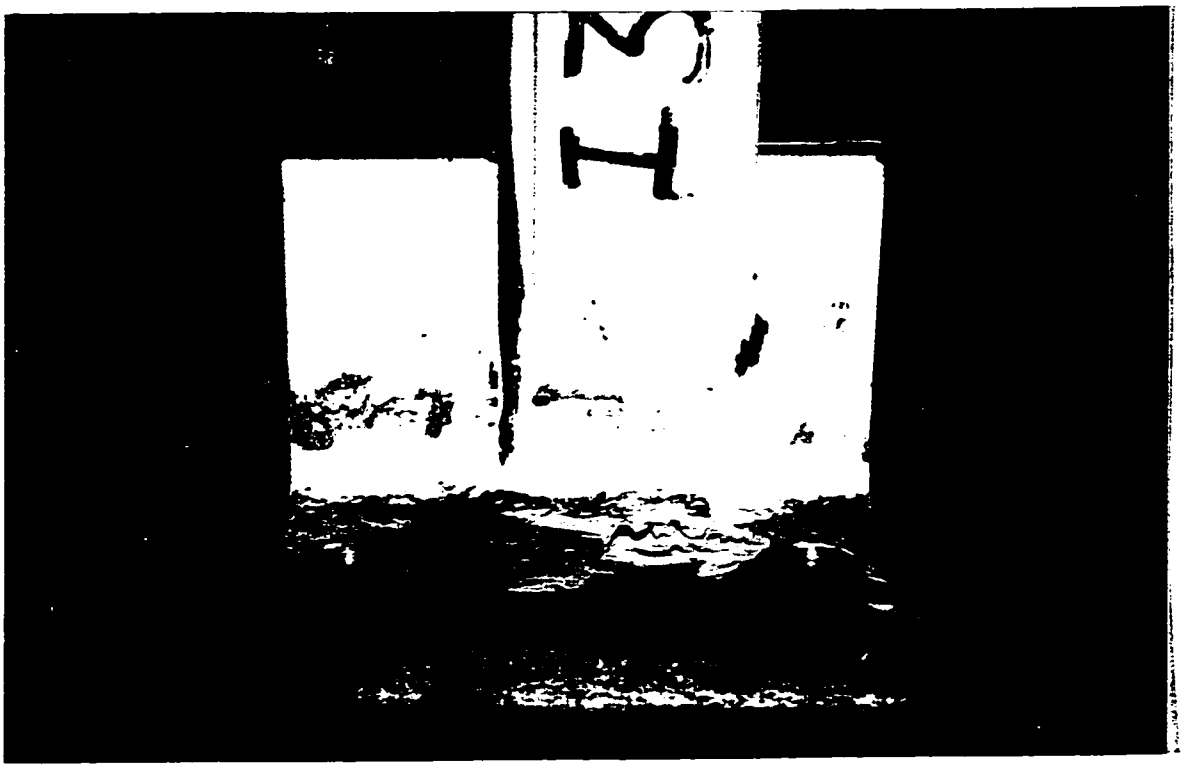

Figure 6-2. Plastic hinge in gusset plate, Specimen L-I-3

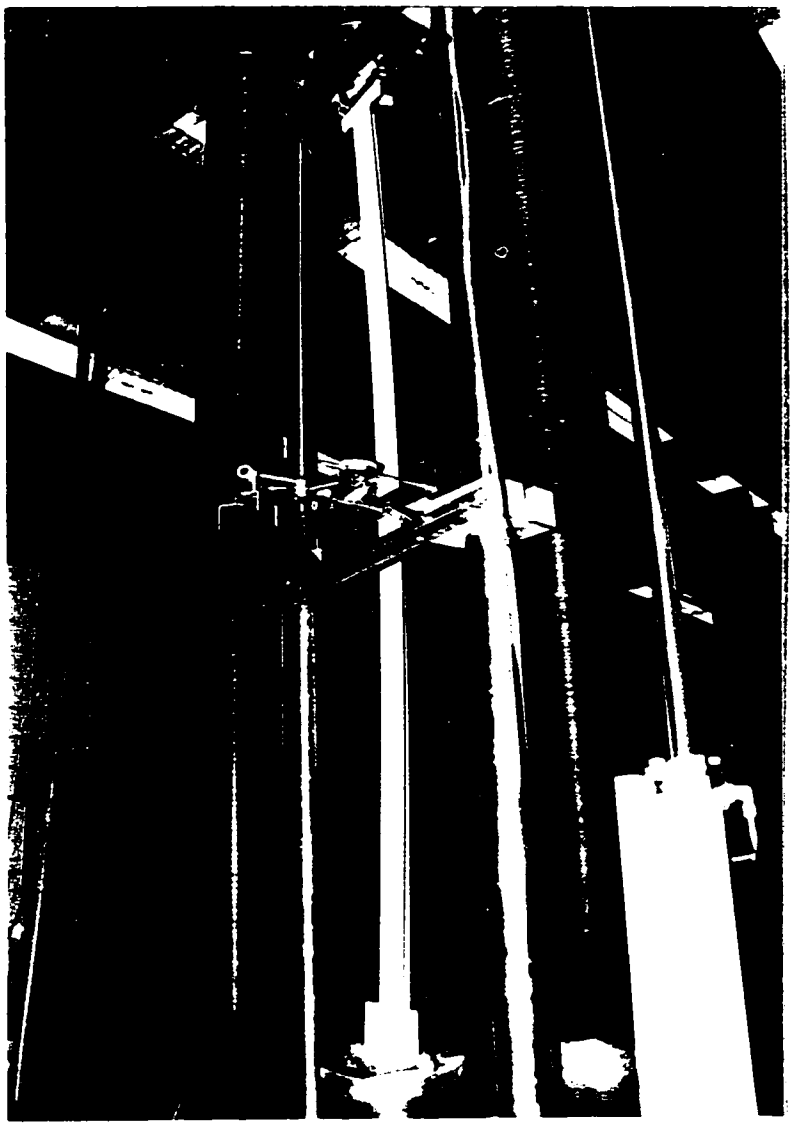

Figure 6-3. Deflected shape of Specimen L-D-2 during testing

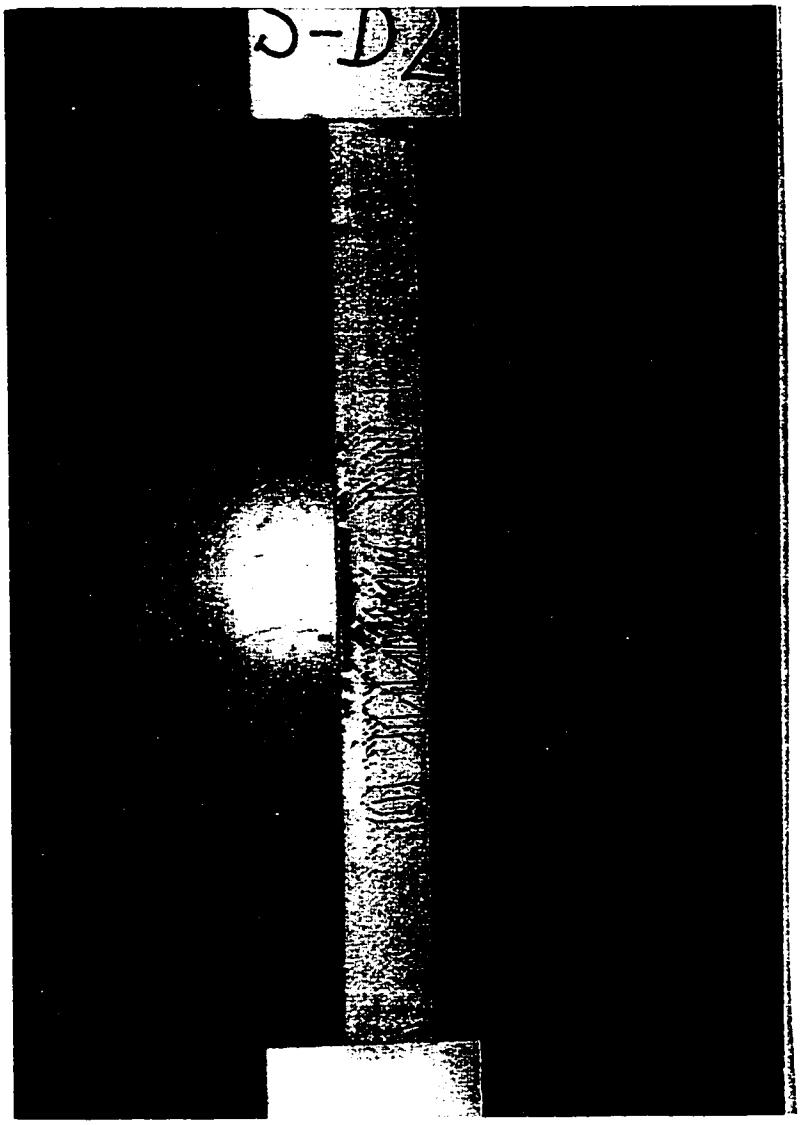

Figure 6-4. Yielding of angle leg, Specimen S-D-2

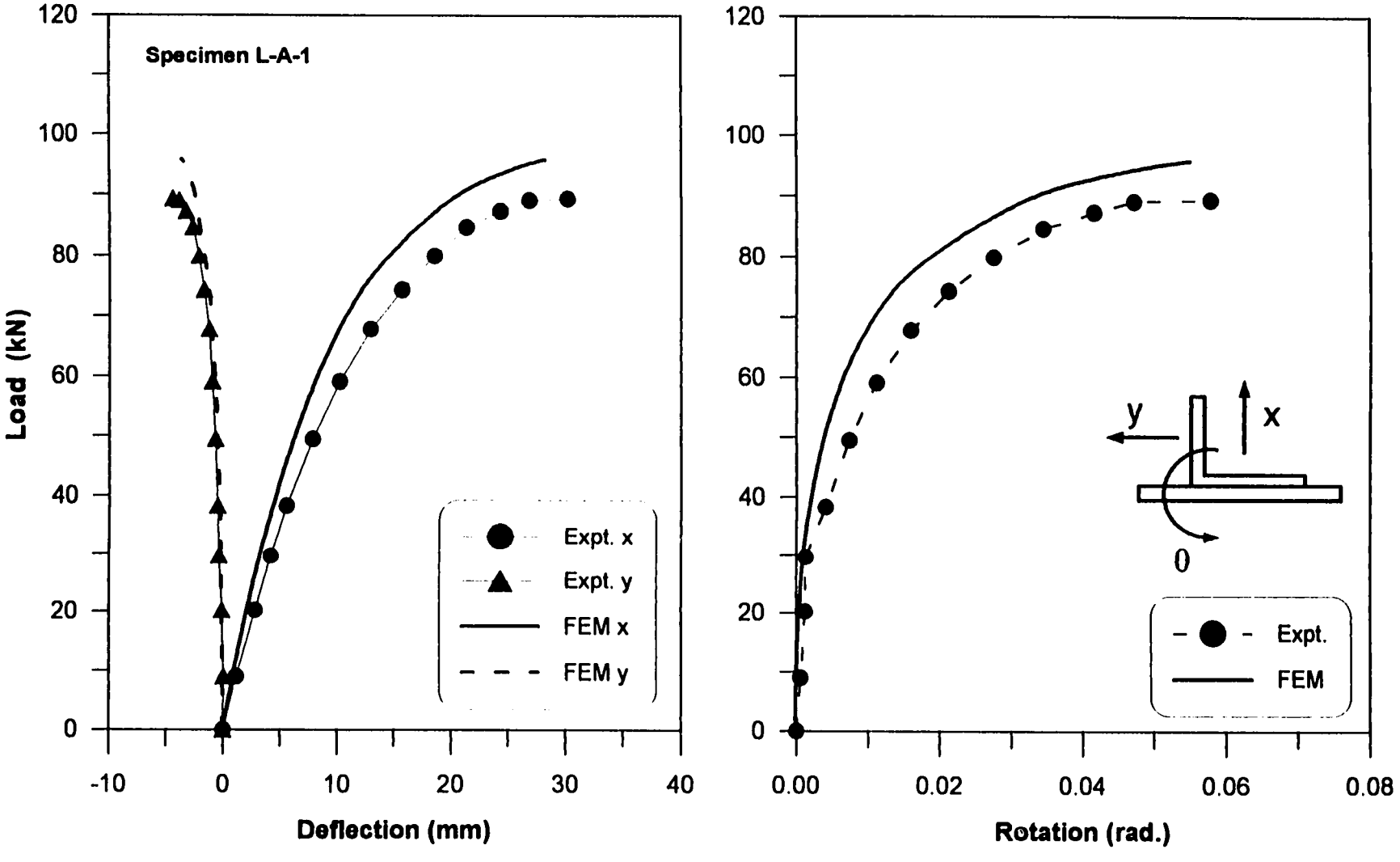

Figure 6-8. Load versus deflection and rotation for specimen L-A-1

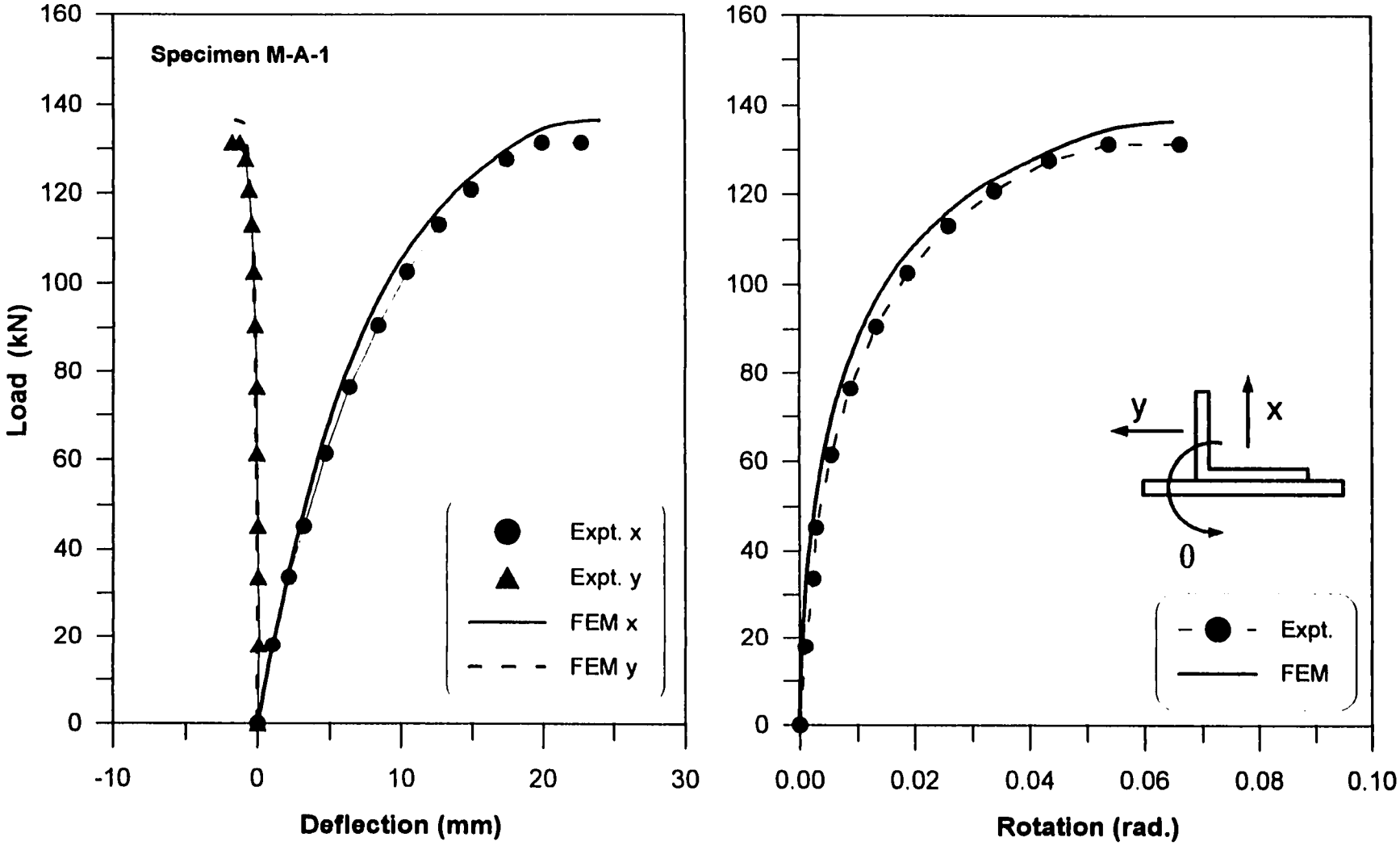

Figure 6-9. Load versus deflection and rotation for Specimen M-A-1

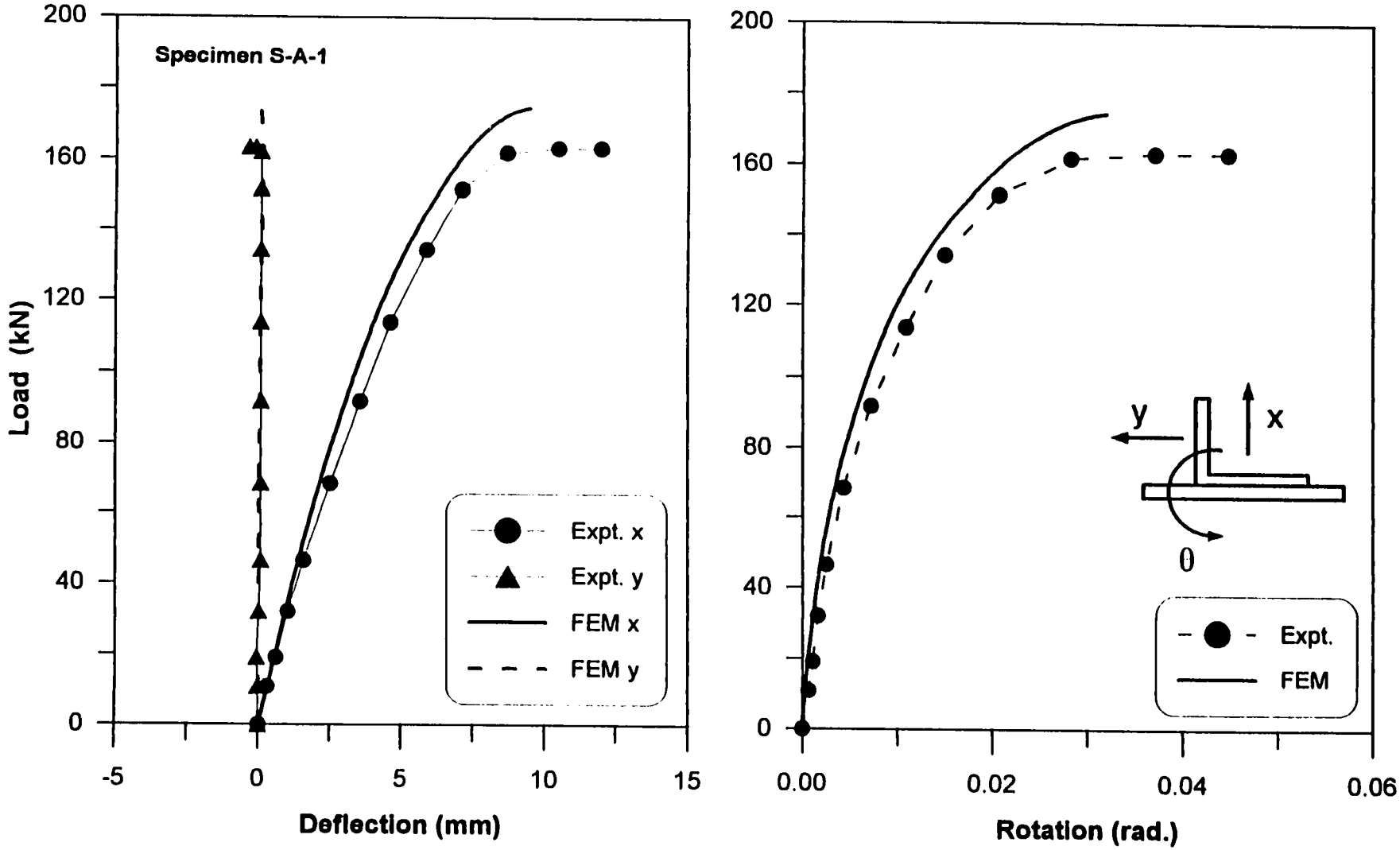

Figure 6-10. Load versus deflection and rotation for Specimen S-A-1

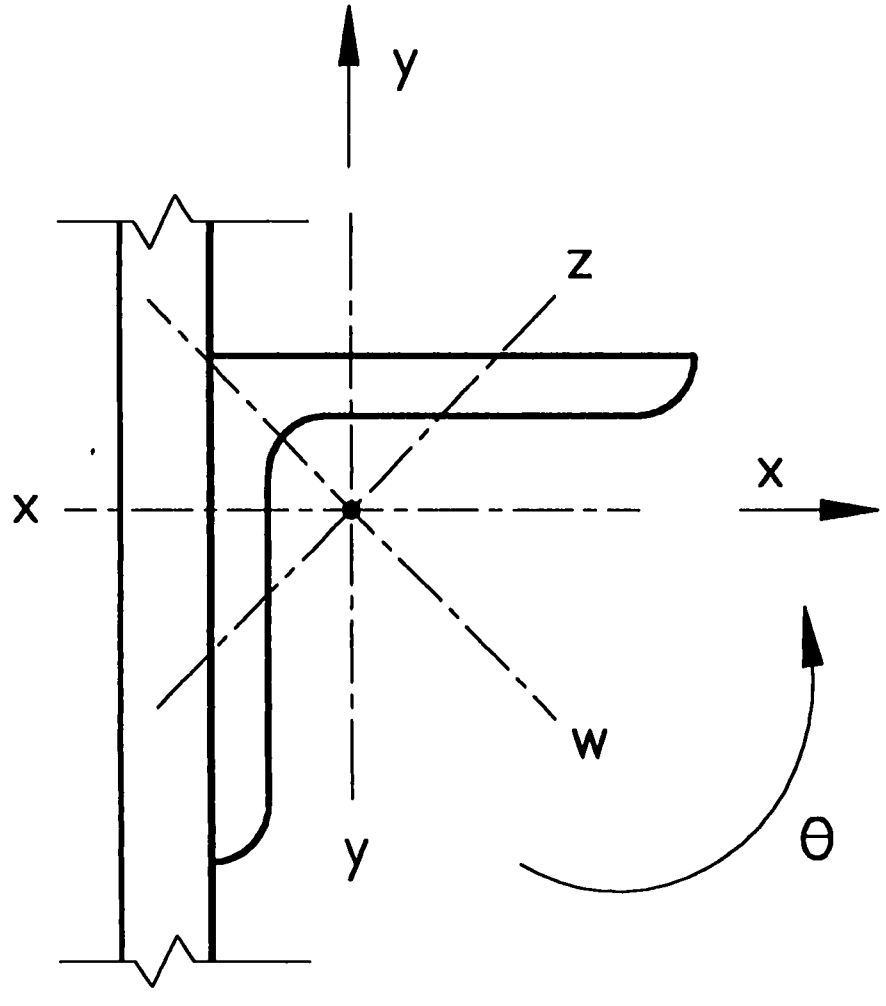

Figure 6-11. Designation of cross section deformations

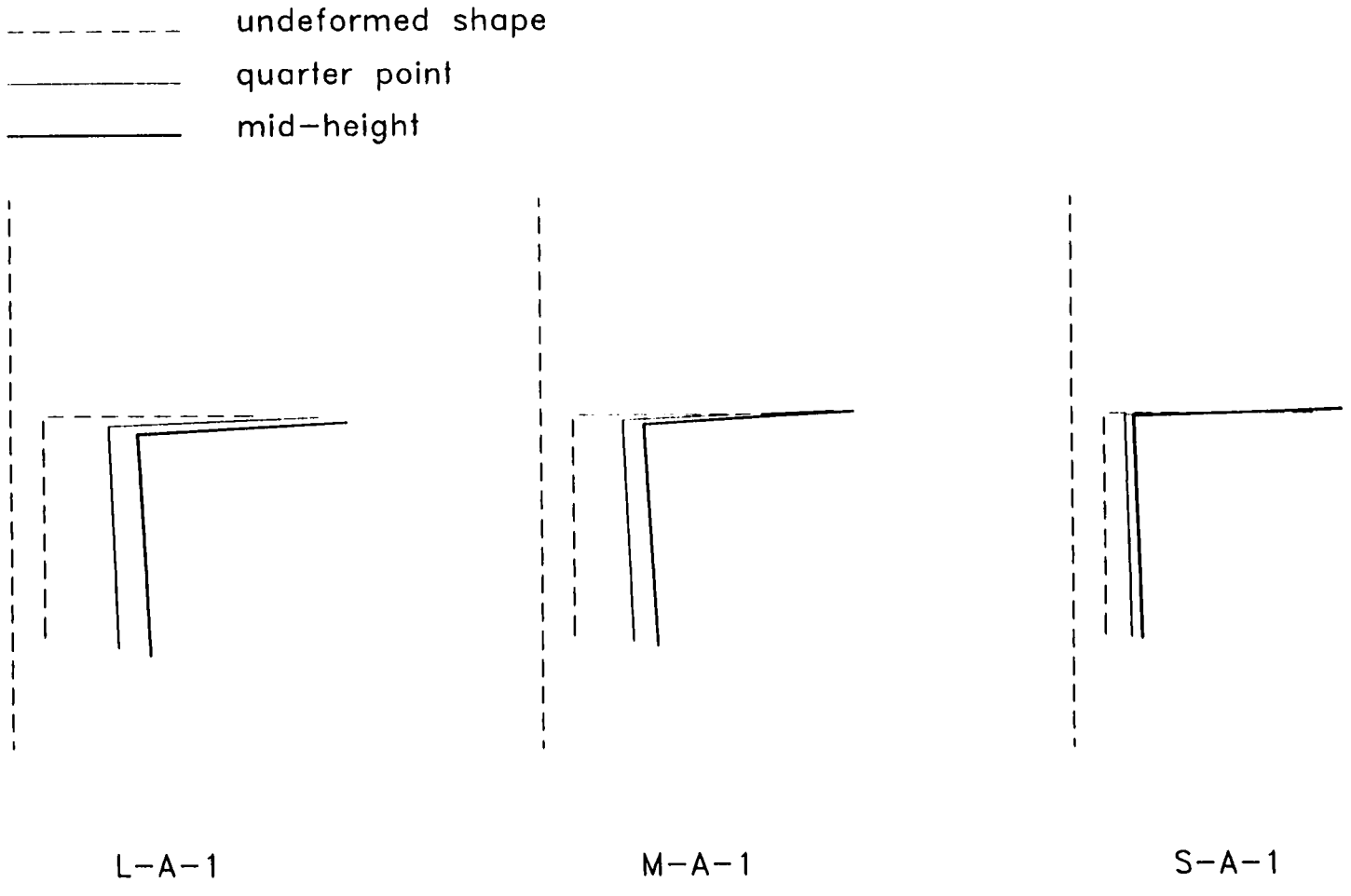

Figure 6-12. Cross section deflected shape as obtained from finite element analysis (Specimens L-A-1, M-A-1, and S-A-1)

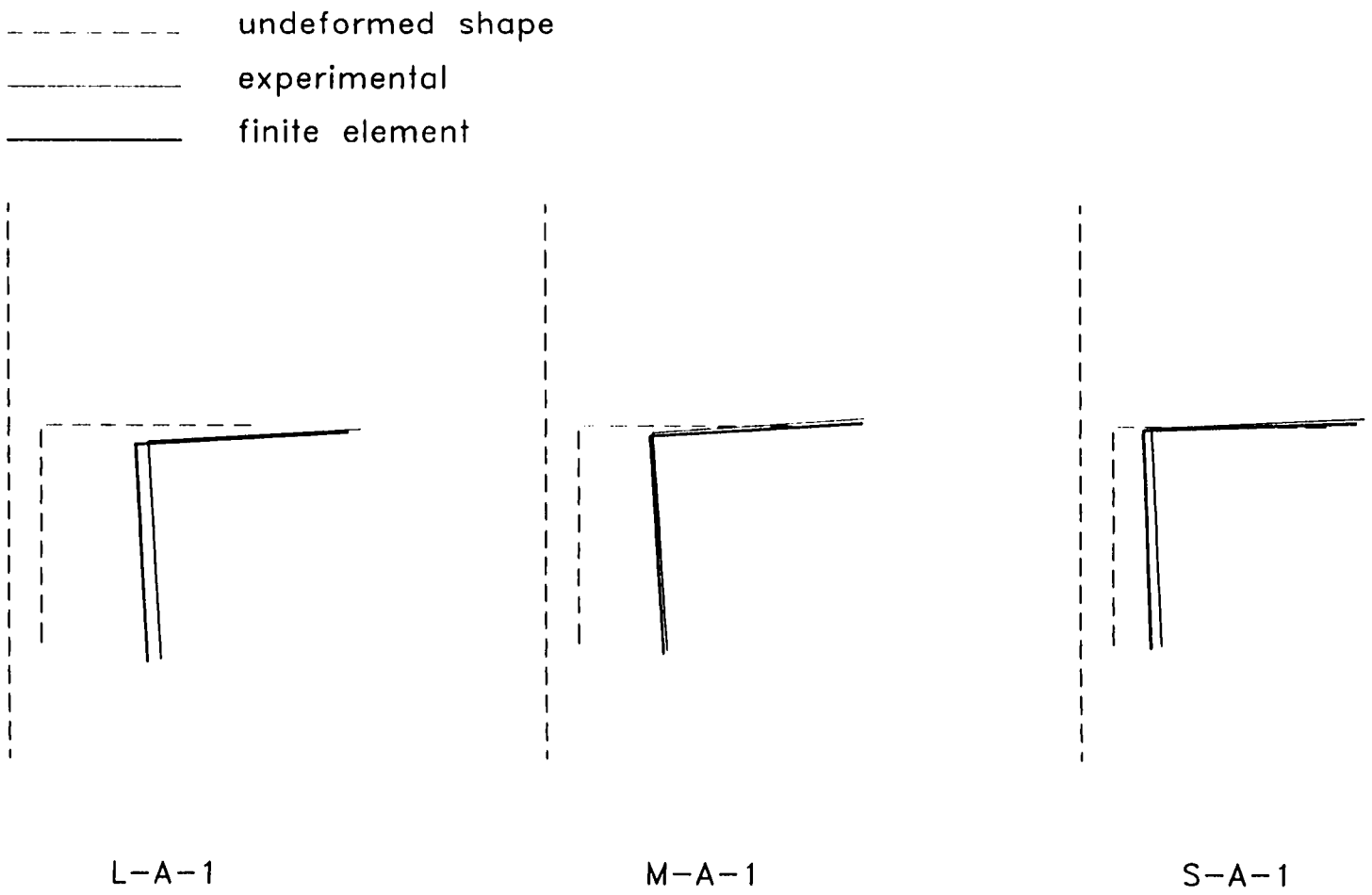

Figure 6-13. Cross section deflected shape at mid-height as obtained from finite element analysis and experimental tests (Specimens L-A-1, M-A-1, and S-A-1)

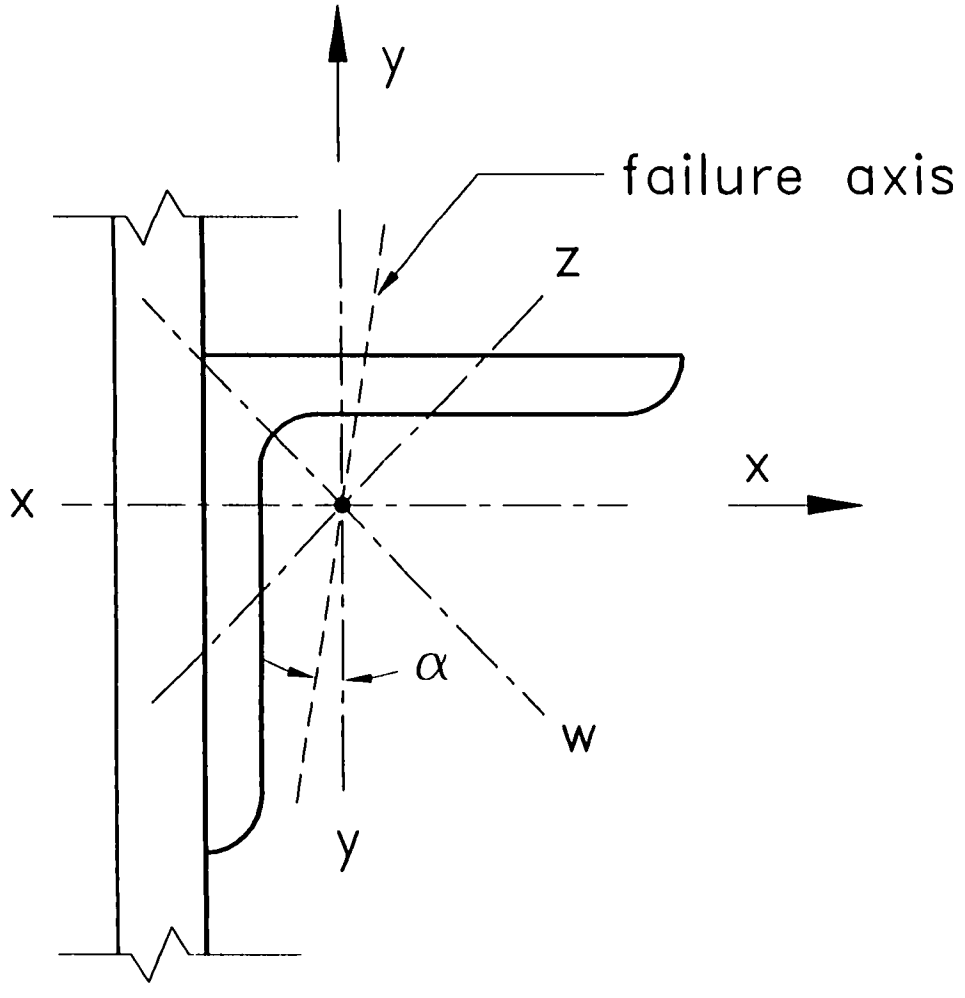

Figure 6-14. Failure axis

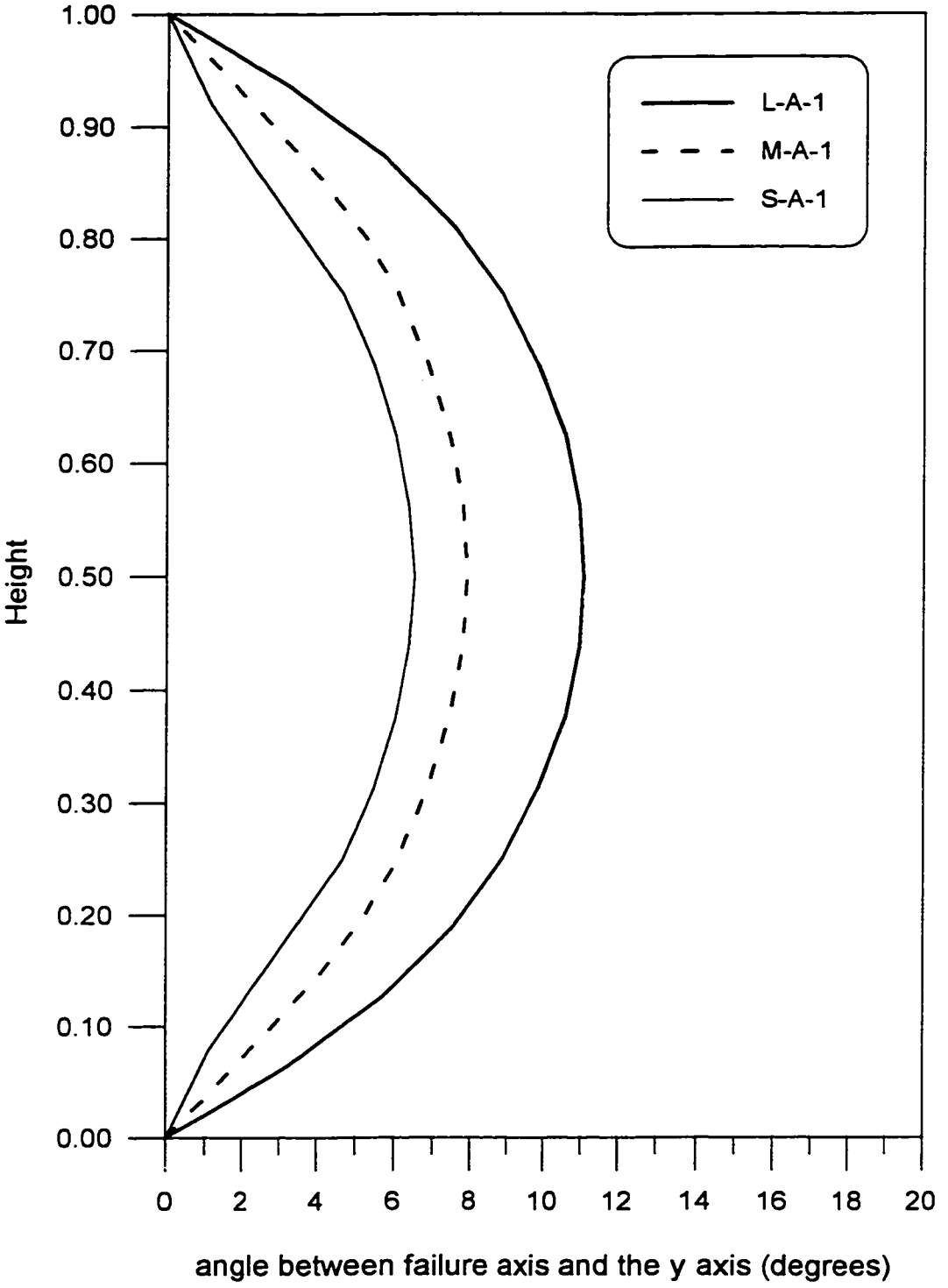

Figure 6-15. Angle between the failure axis and the y axis (Specimens, L-A-1, M-A-1, and S-A-1)

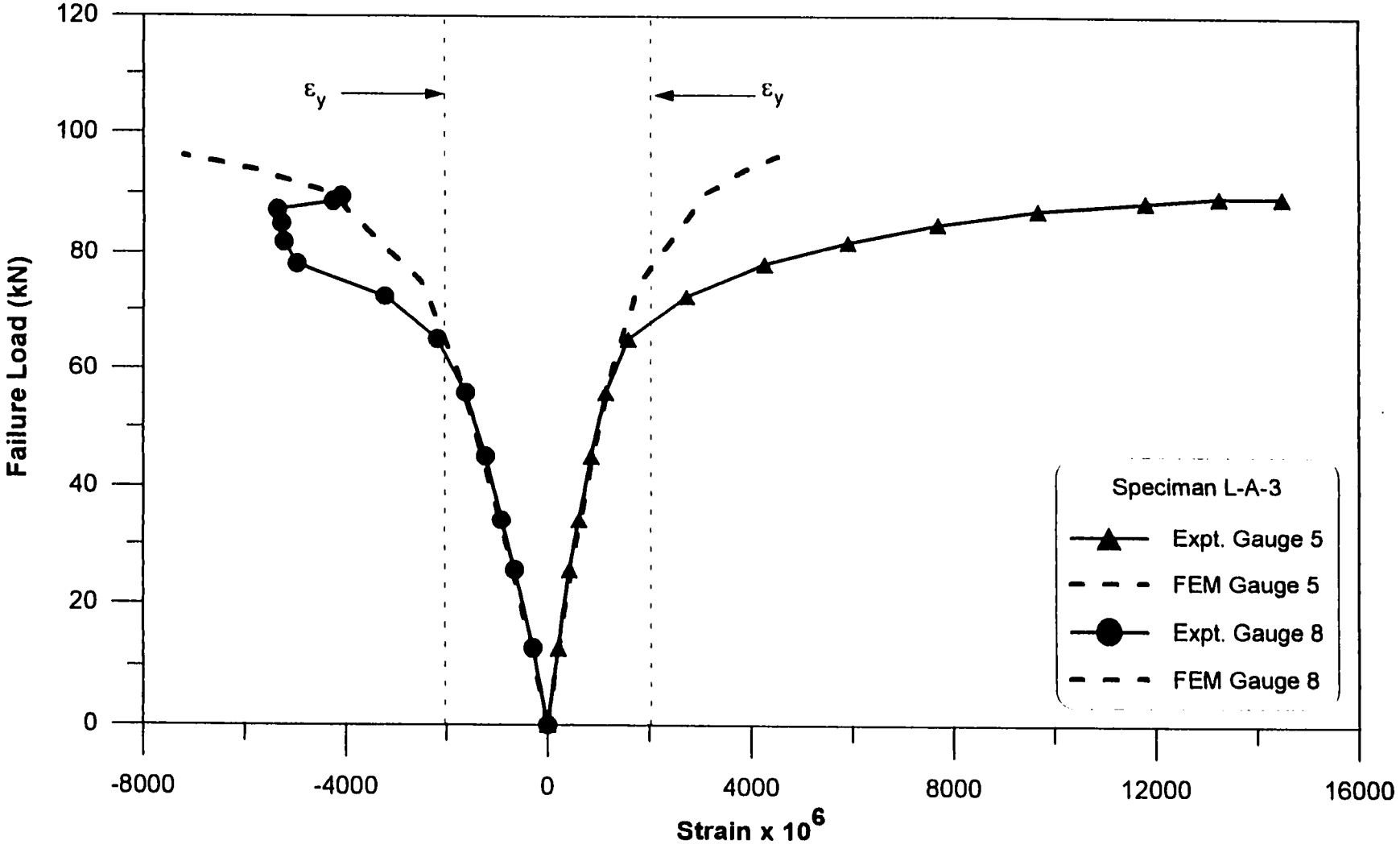

Figure 6-16. Load versus strain for Specimen L-A-3, Strain gauges 5 and 8

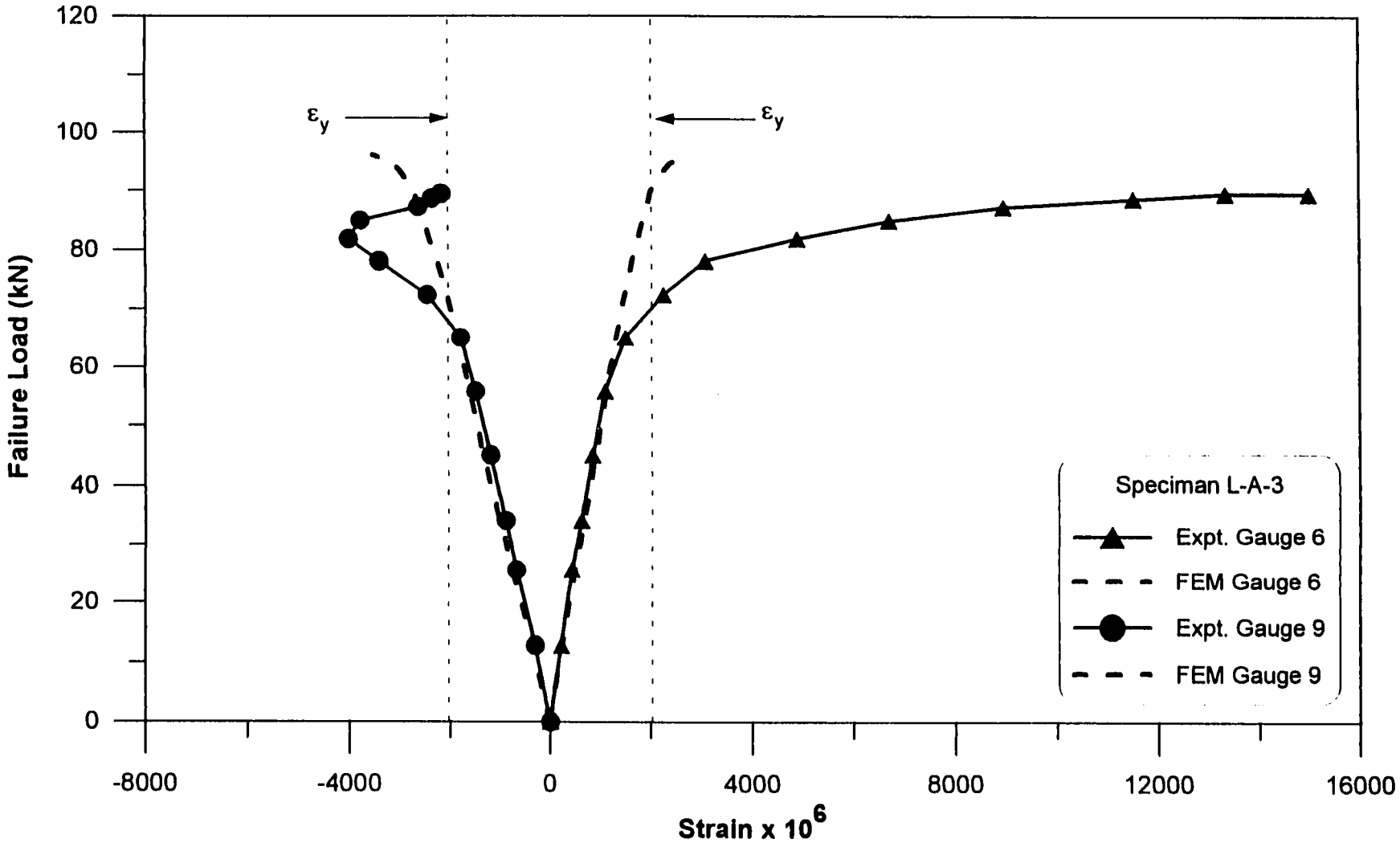

Figure 6-17. Load versus strain for Specimen L-A-3, Strain gauges 6 and 9

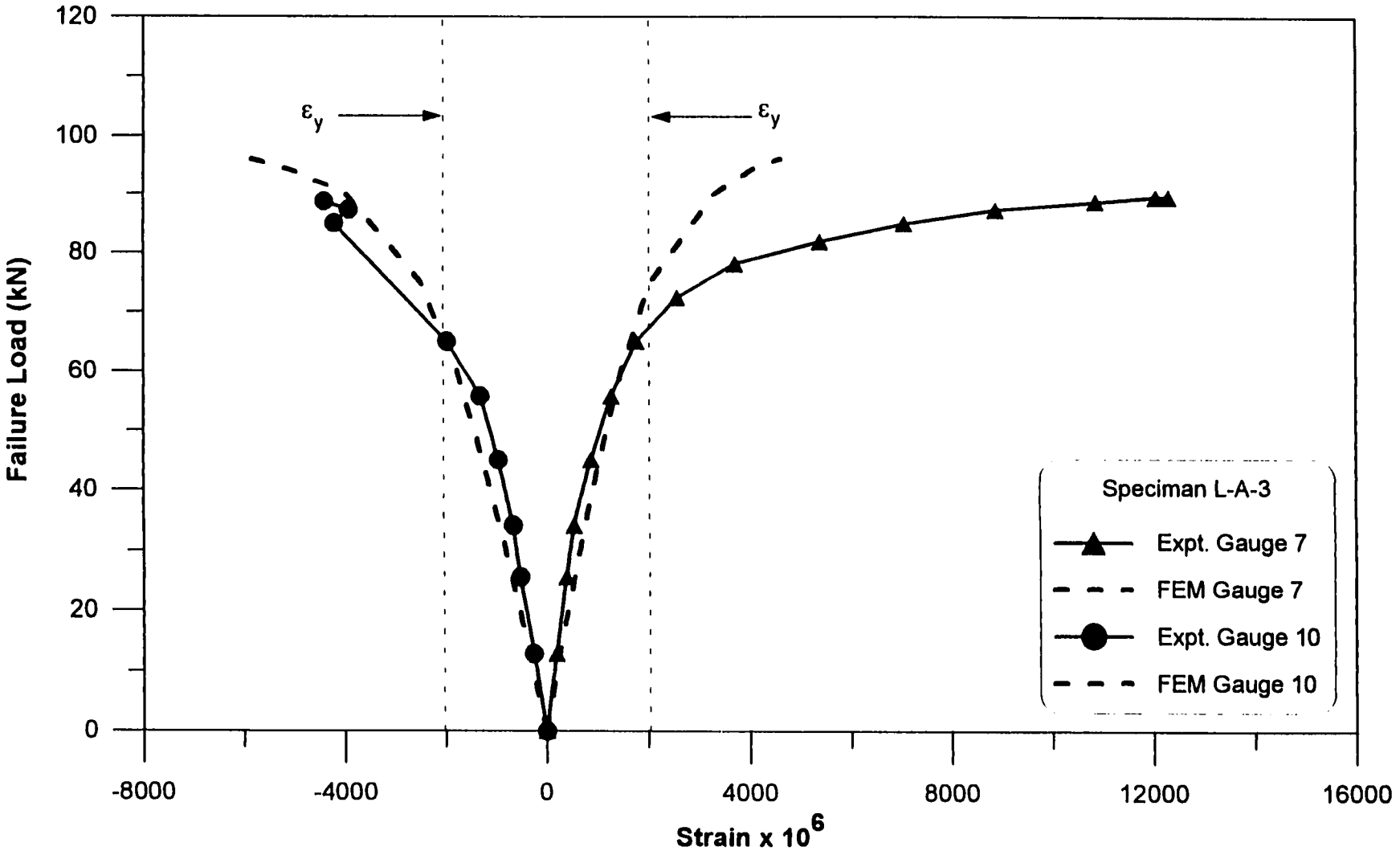

Figure 6-18. Load versus strain for Specimen L-A-3, Strain gauges 7 and 10

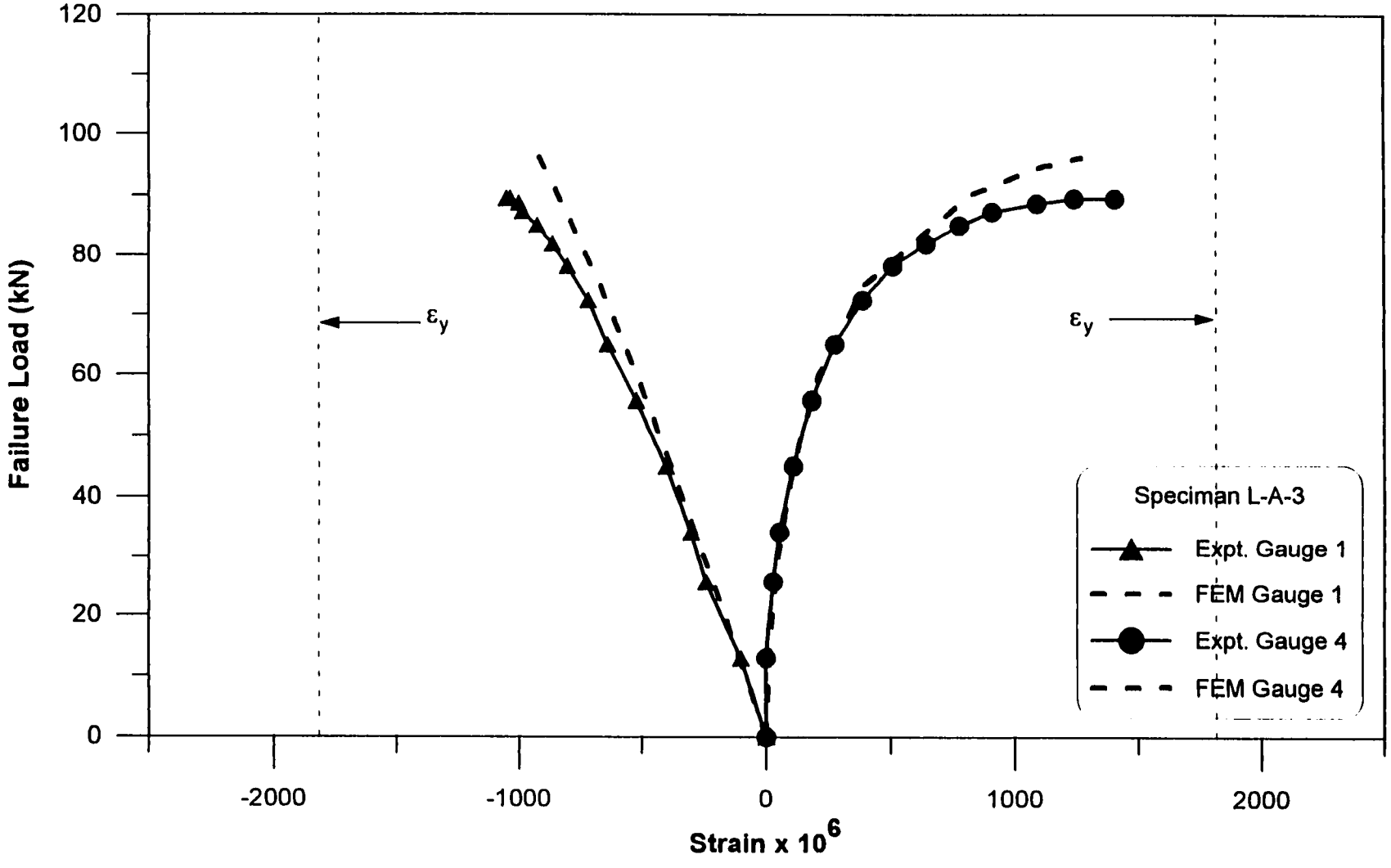

Figure 6-19. Load versus strain for Specimen L-A-3, Strain gauges 1 and 4

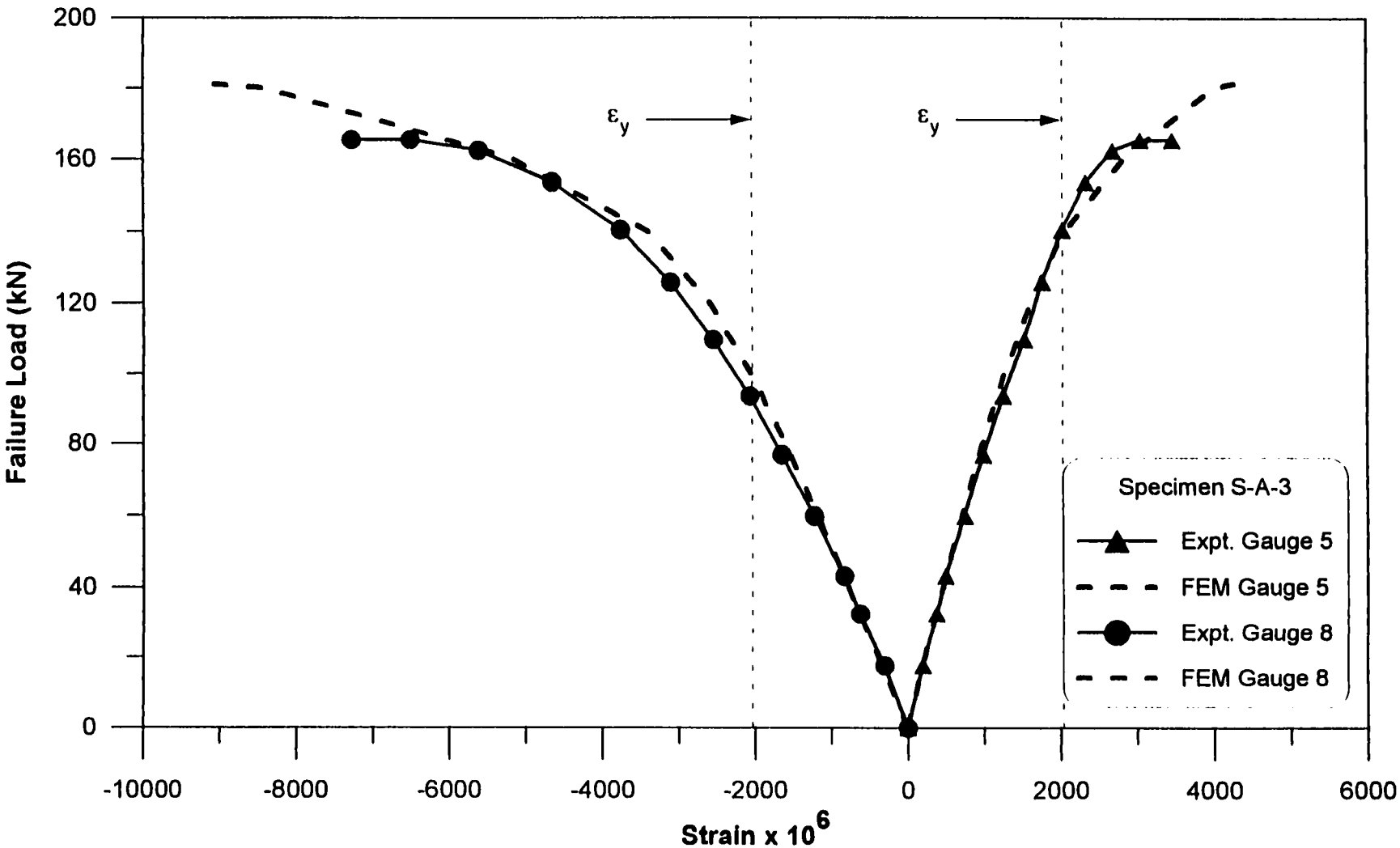

Figure 6-20. Load versus strain for Specimen S-A-3, Strain gauges 5 and 8

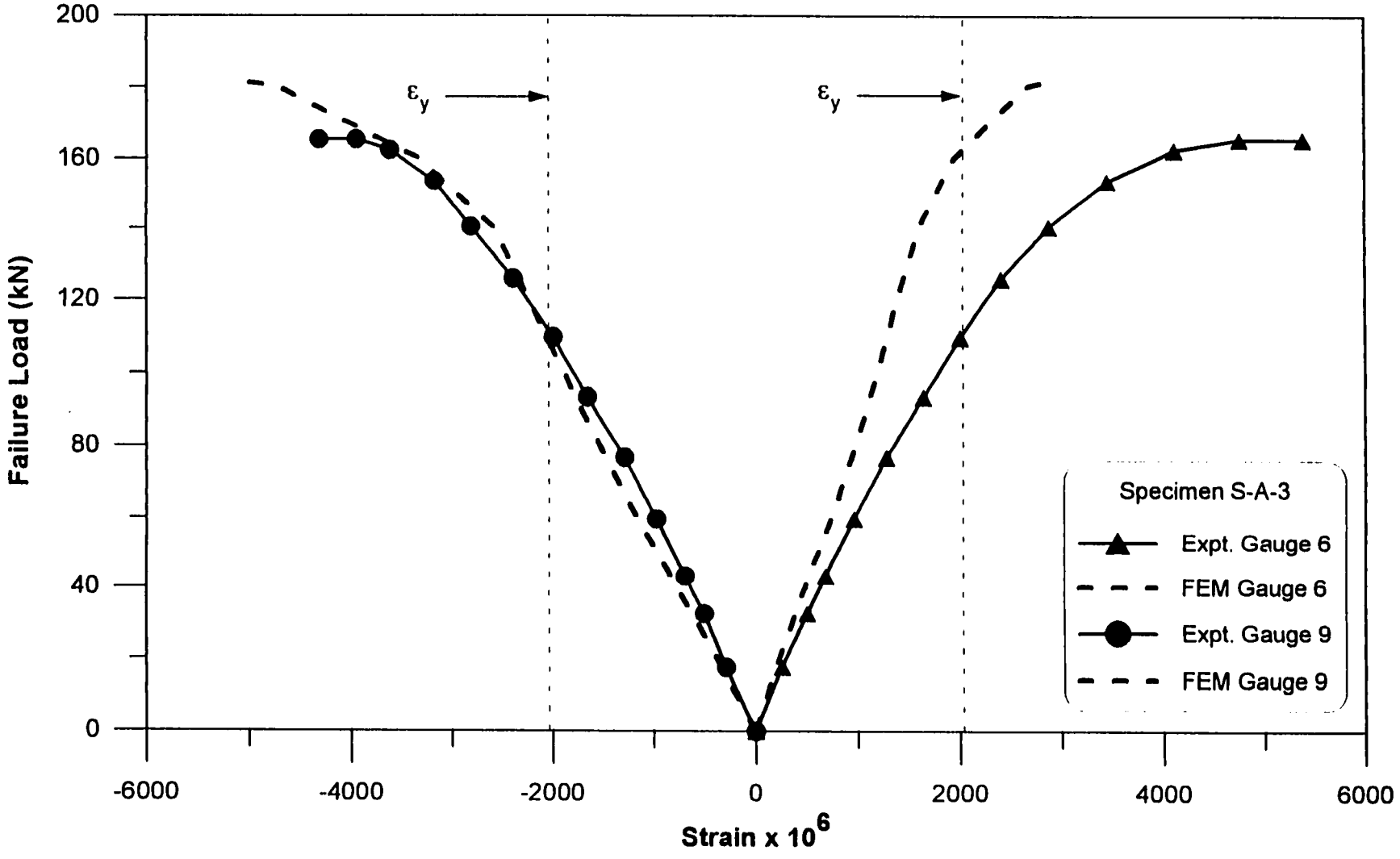

Figure 6-21. Load versus strain for Specimen S-A-3, Strain gauges 6 and 9

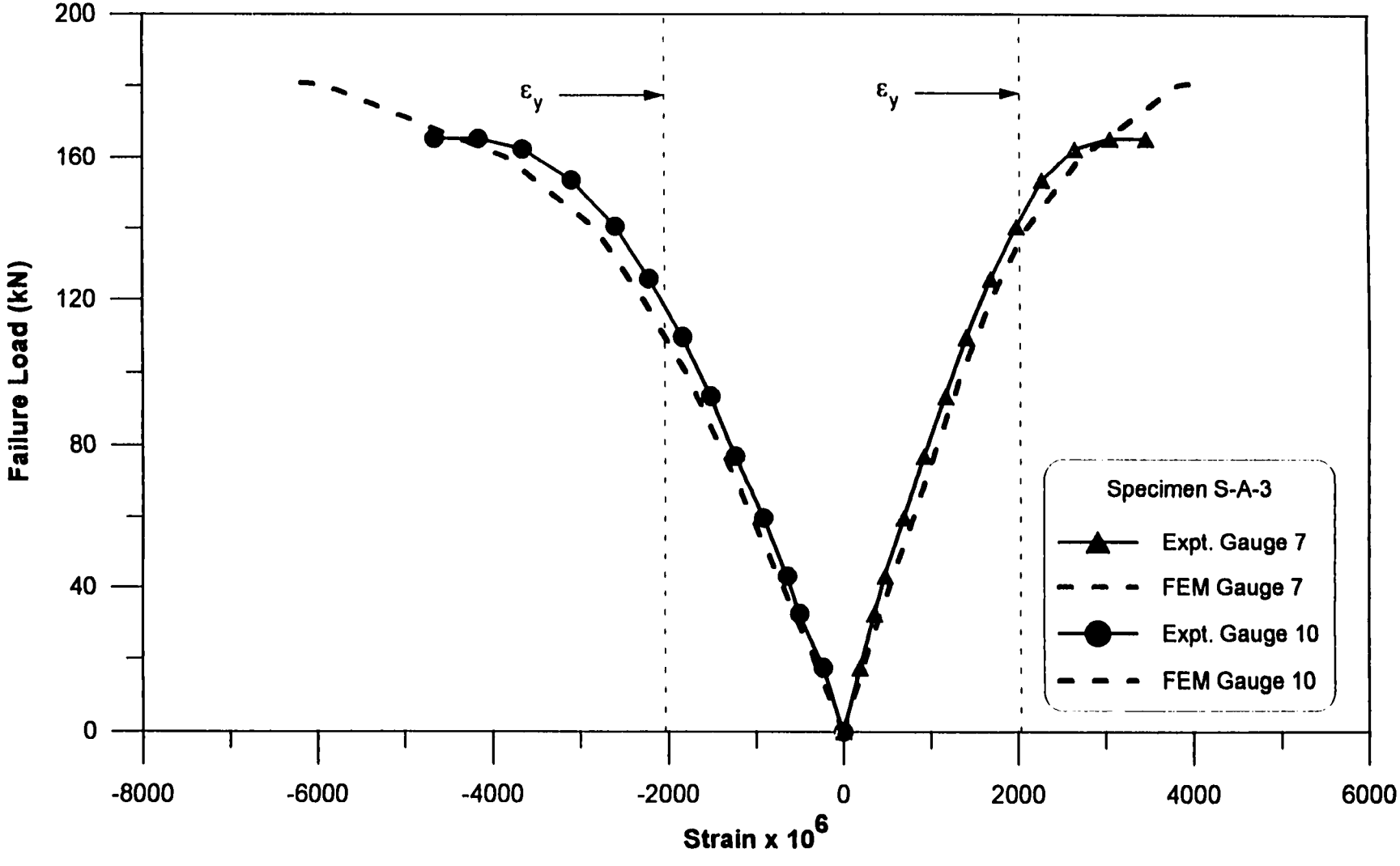

Figure 6-22. Load versus strain for Specimen S-A-3, Strain gauges 7 and 10

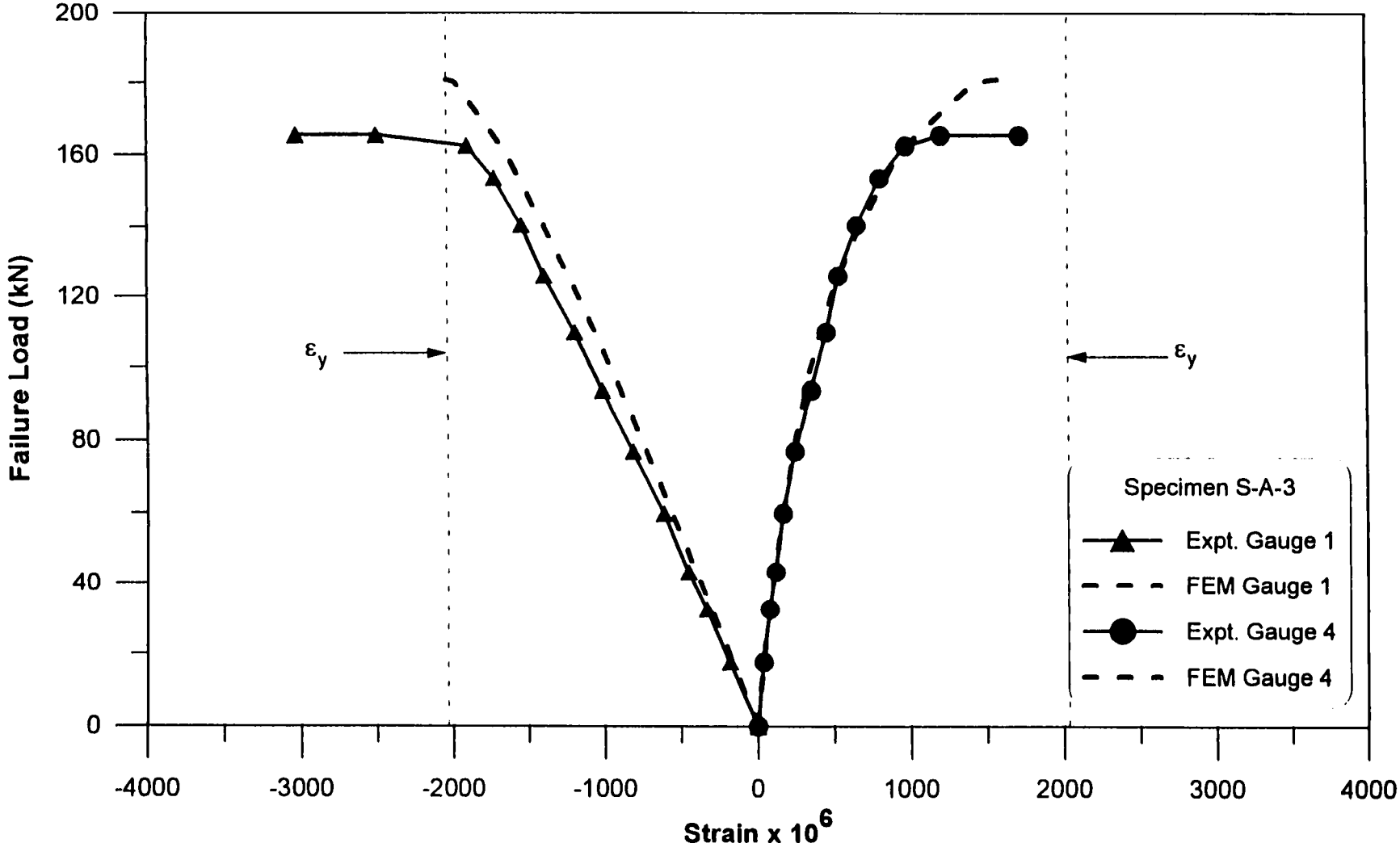

Figure 6-23. Load versus strain for Specimen S-A-3, Strain gauges 1 and 4

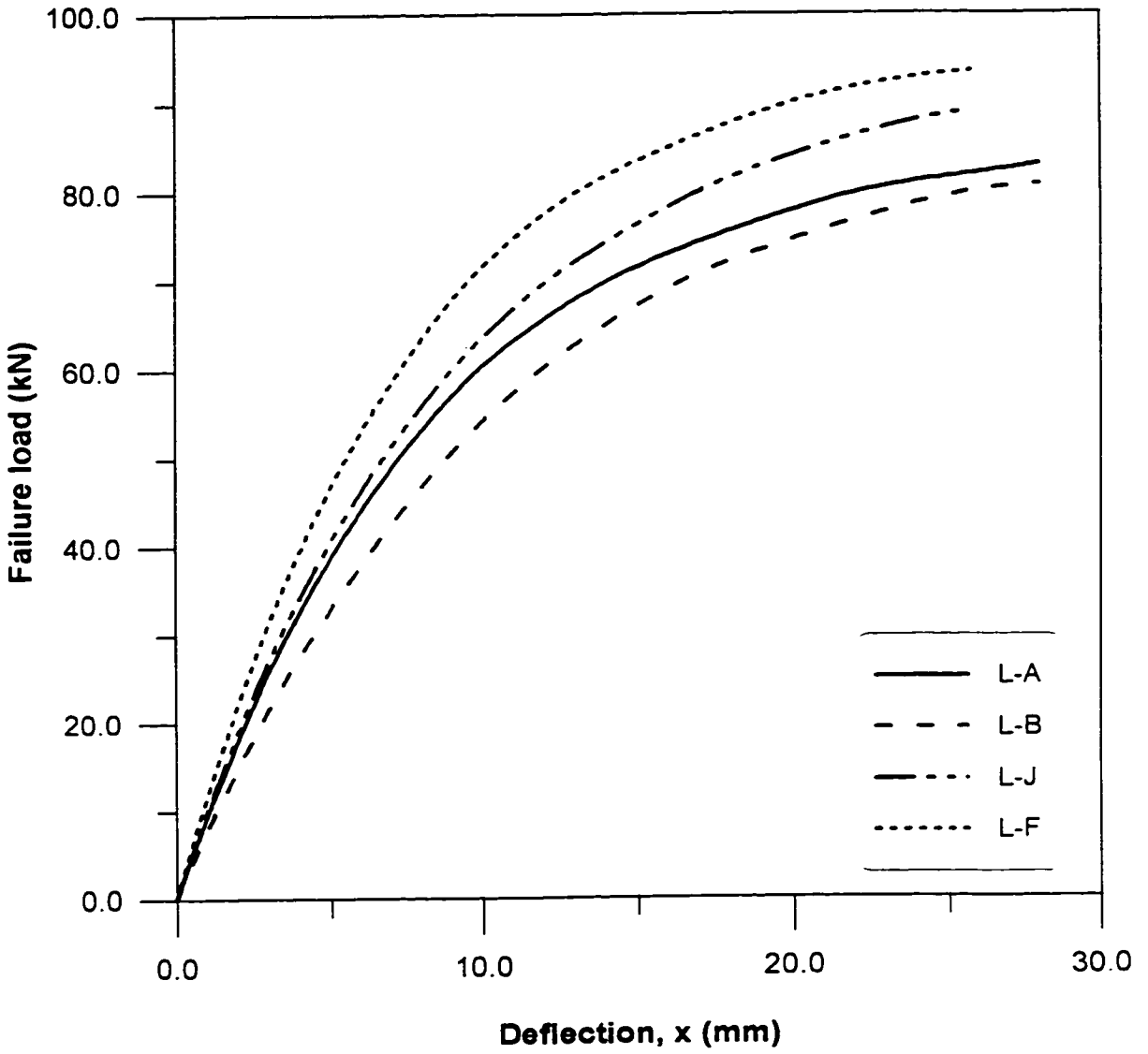

Figure 6-24. Load versus deflection in x direction for Type A, Type B, Type J, and Type F theoretical slender specimens

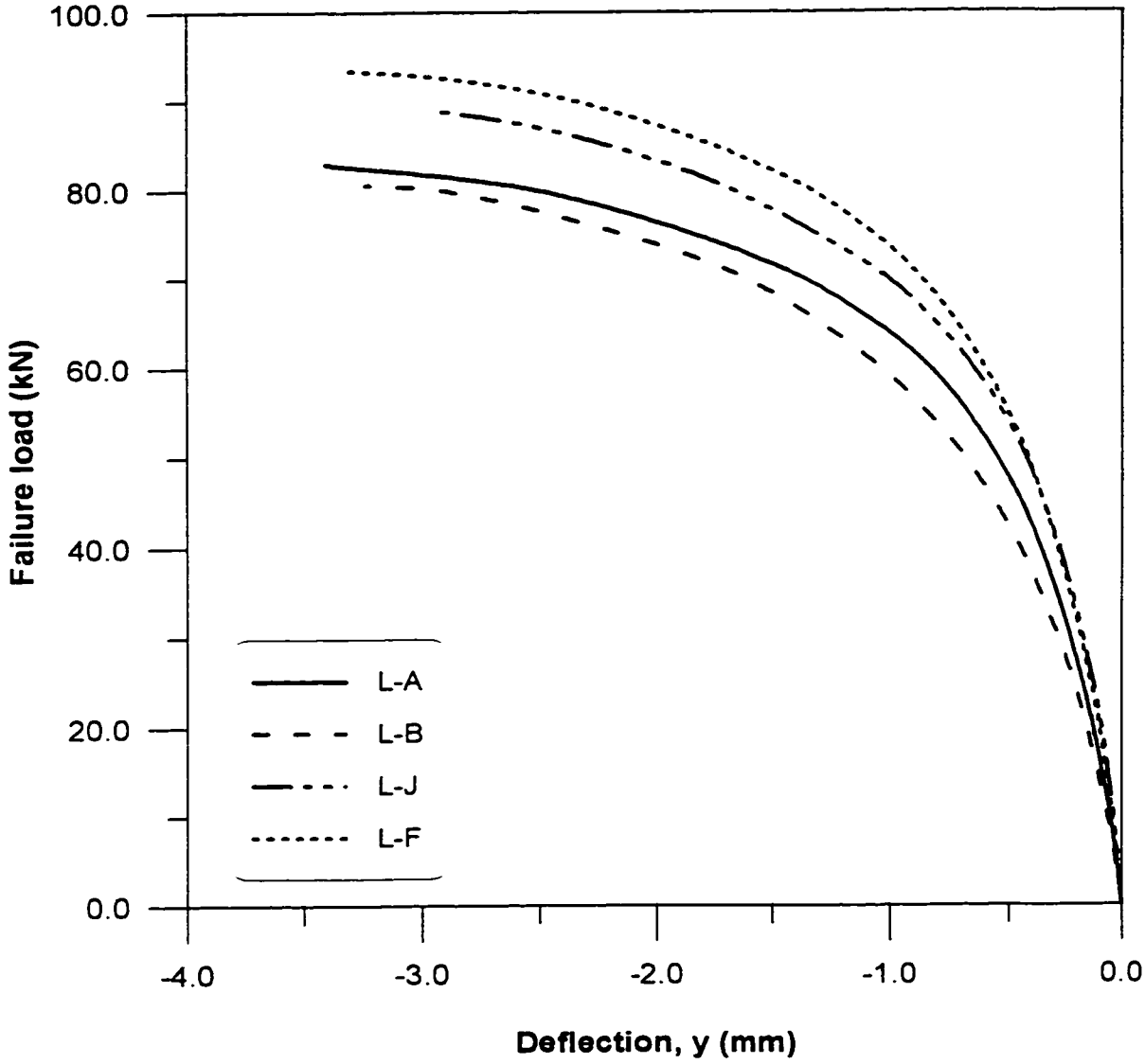

Figure 6-25. Load versus deflection in y direction for Type A, Type B, Type J, and Type F theoretical slender specimens

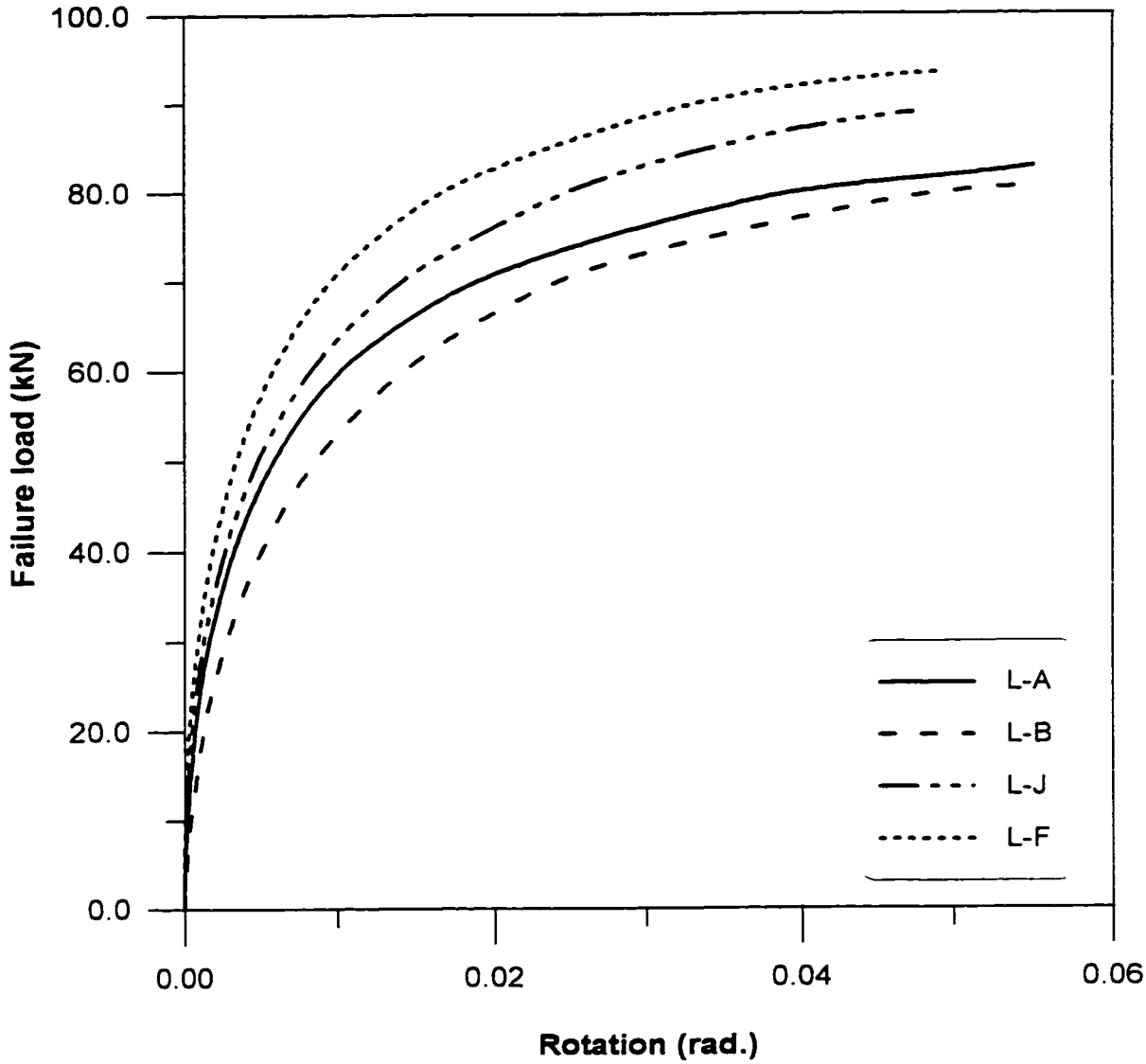

Figure 6-26. Load versus rotation for Type A, Type B, Type J, and Type F theoretical slender specimens

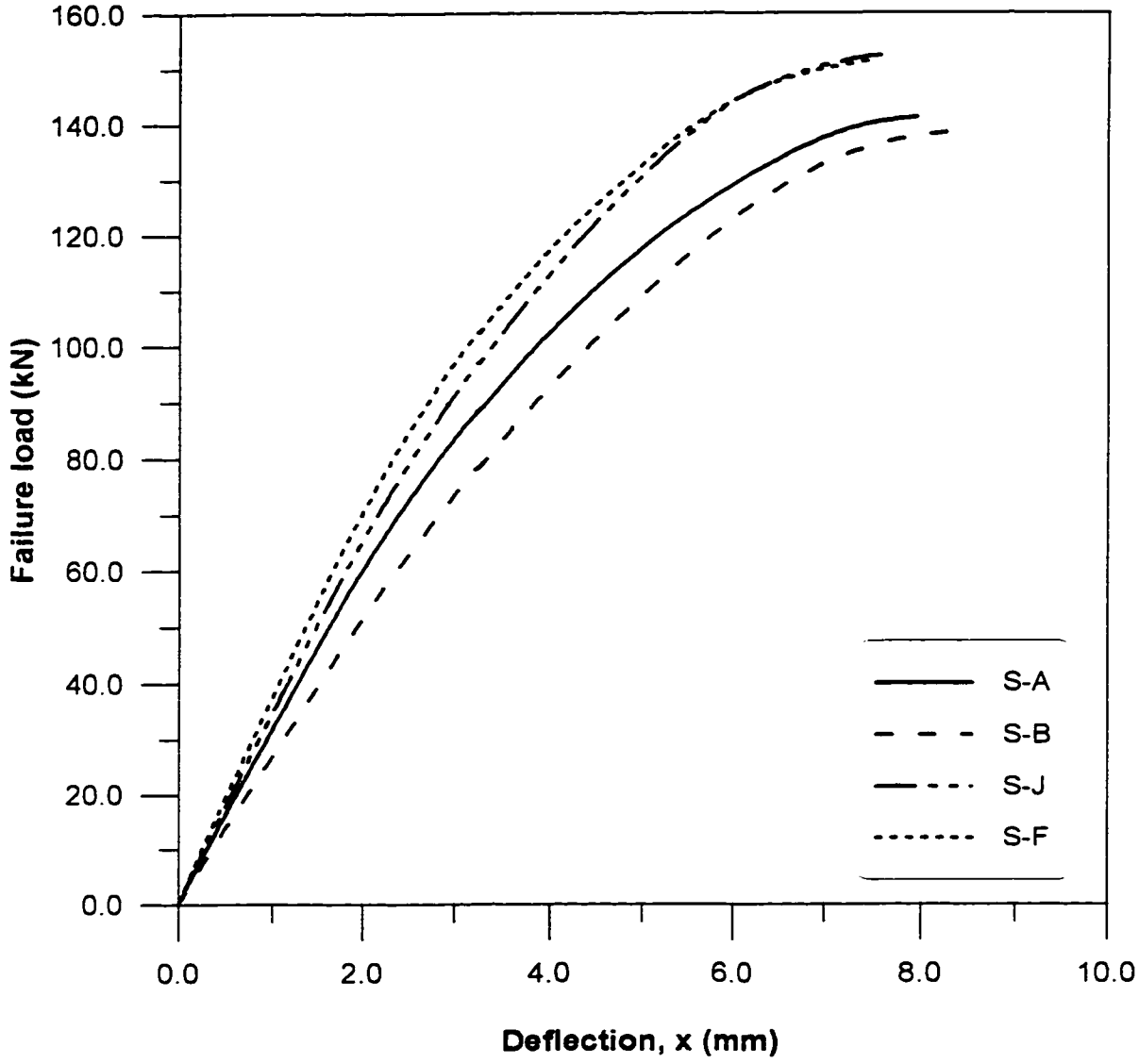

Figure 6-27. Load versus deflection in x direction for Type A, Type B, Type J, and Type F theoretical shorter intermediate length specimens

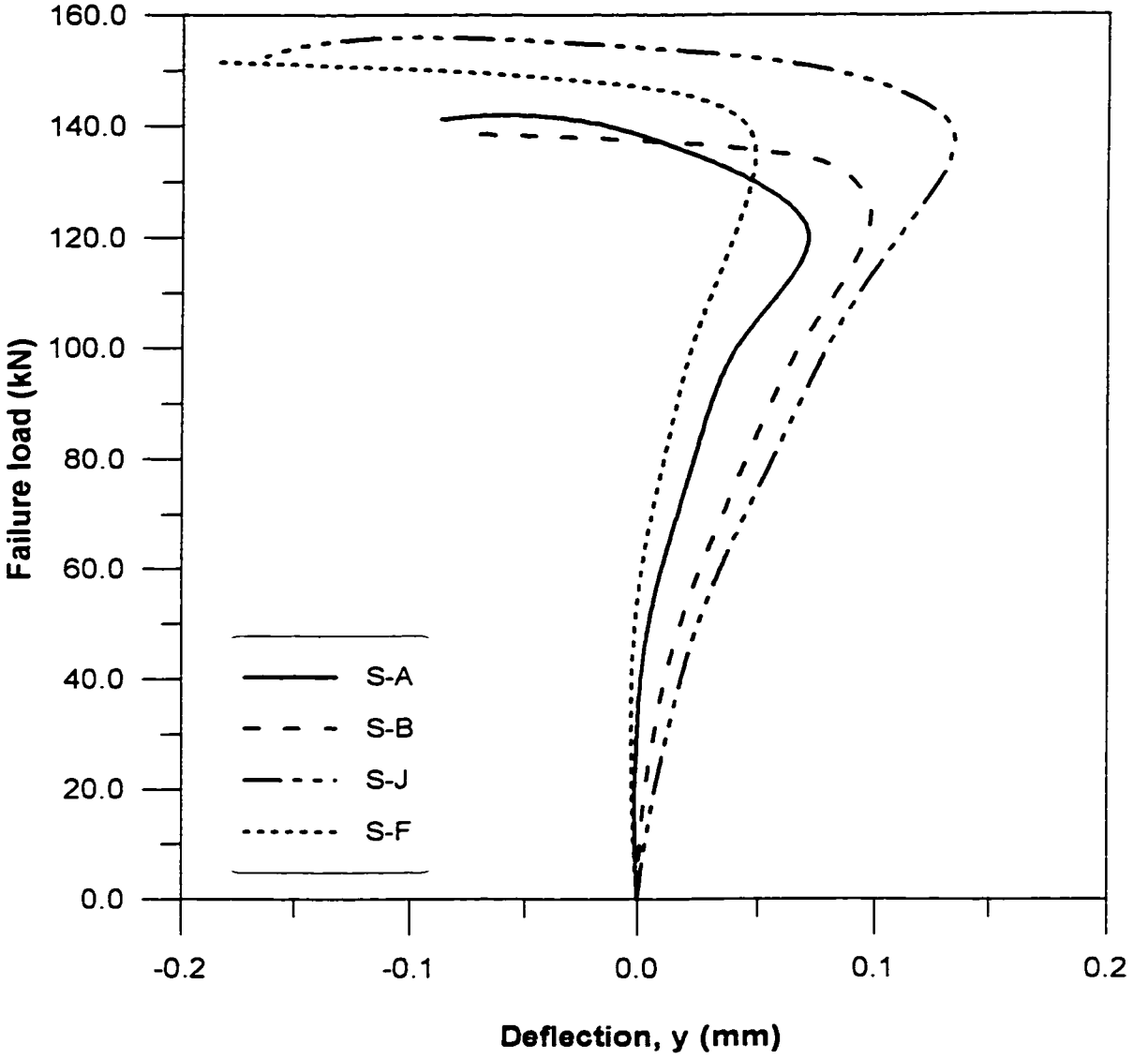

Figure 6-28. Load versus deflection in y direction for Type A, Type B, Type J, and Type F theoretical shorter intermediate length specimens

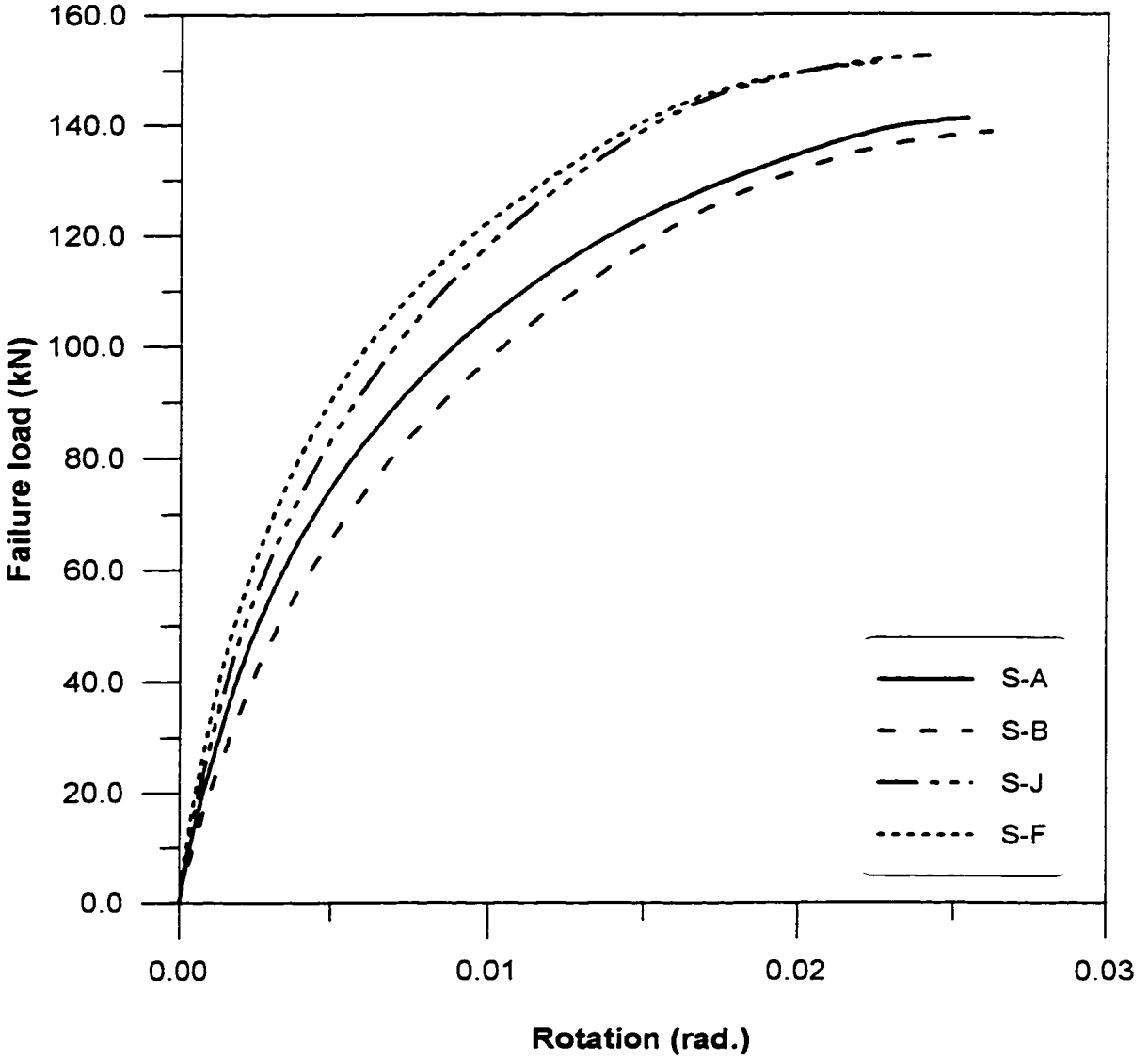

Figure 6-29. Load versus rotation for Type A, Type B, Type J, and Type F theoretical shorter intermediate length specimens

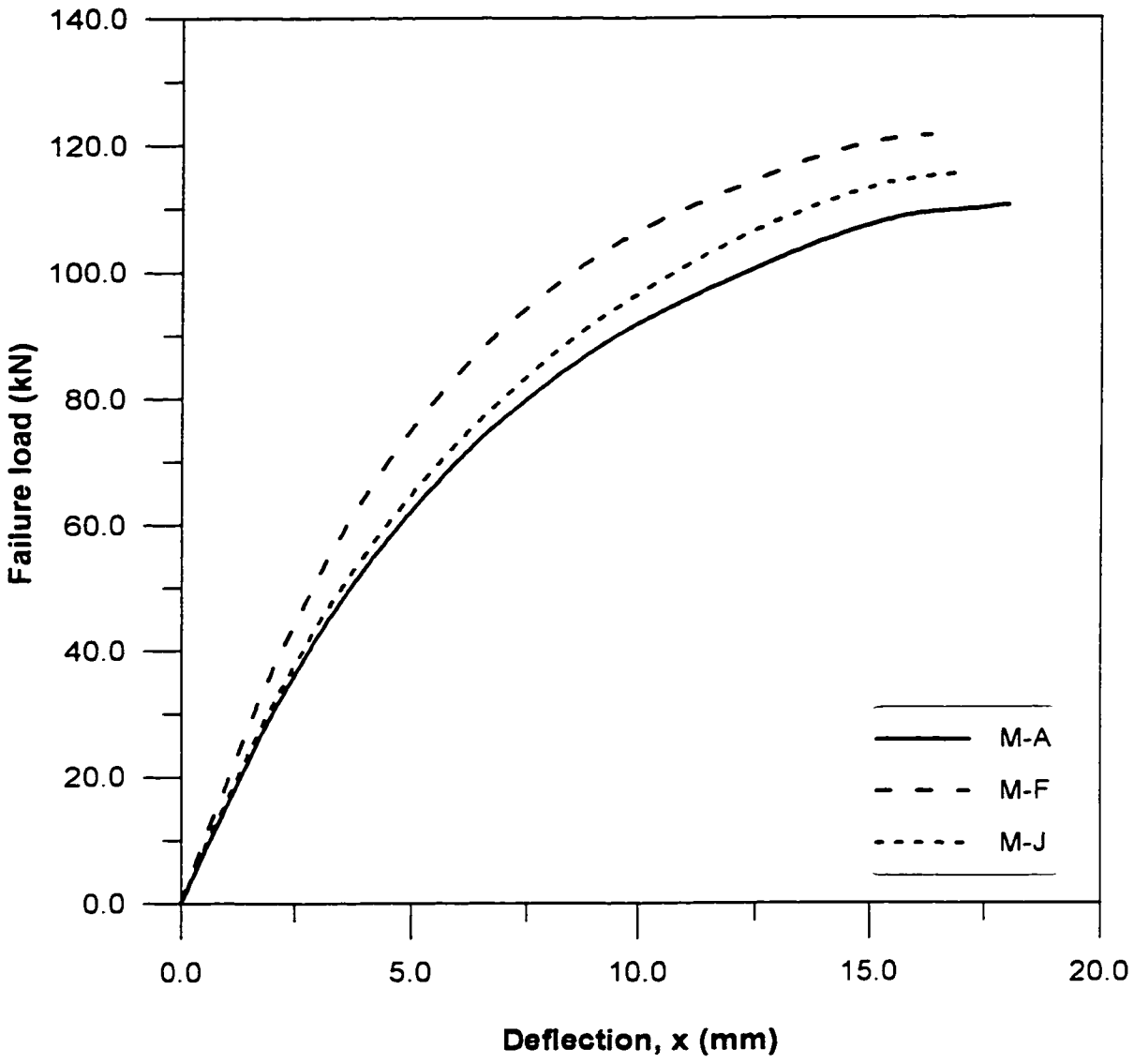

Figure 6-30. Load versus deflection in x direction for Type A, Type J, and Type F theoretical longer intermediate length specimens

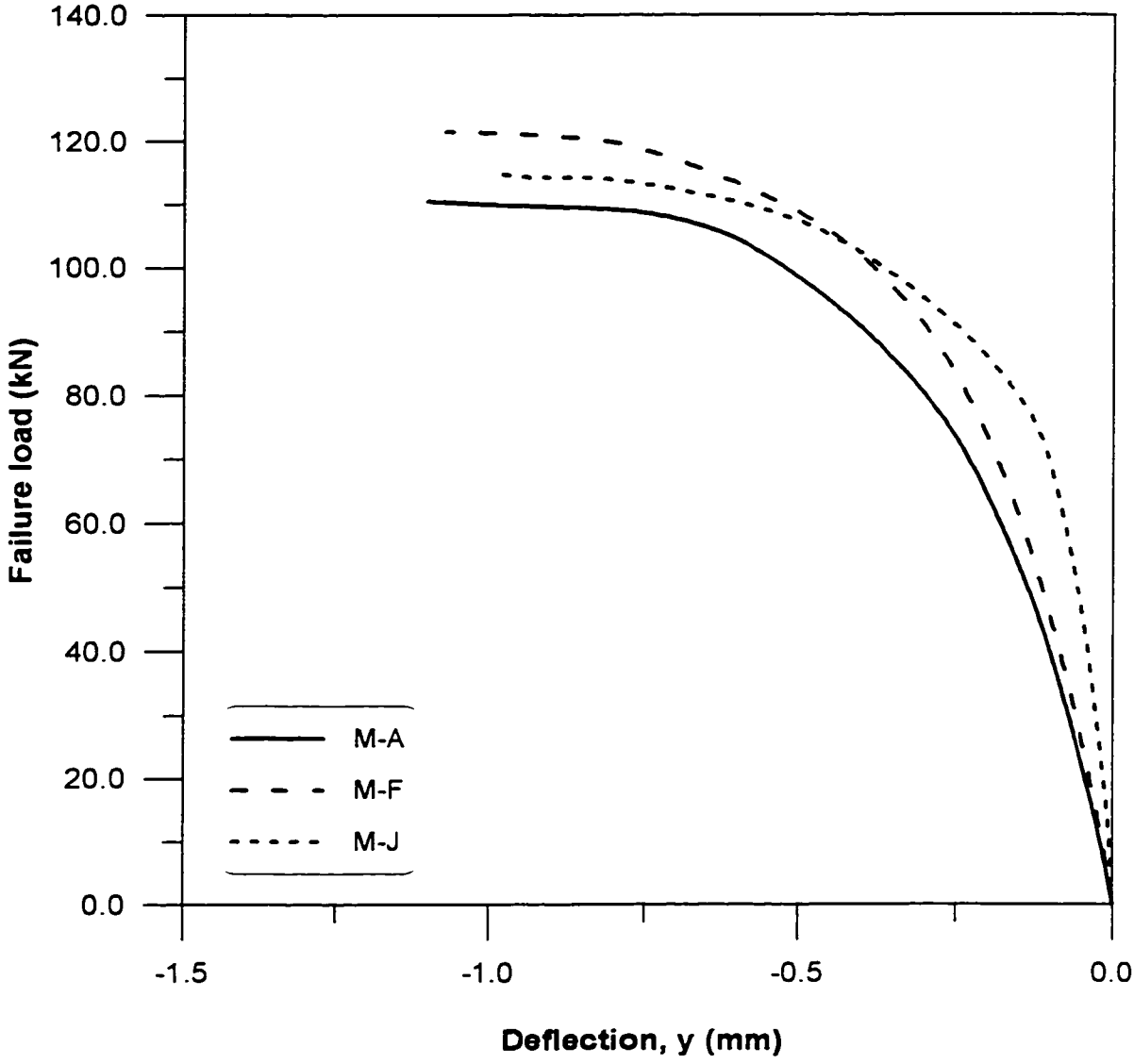

Figure 6-31. Load versus deflection in y direction for Type A, Type J, and Type F theoretical longer intermediate length specimens

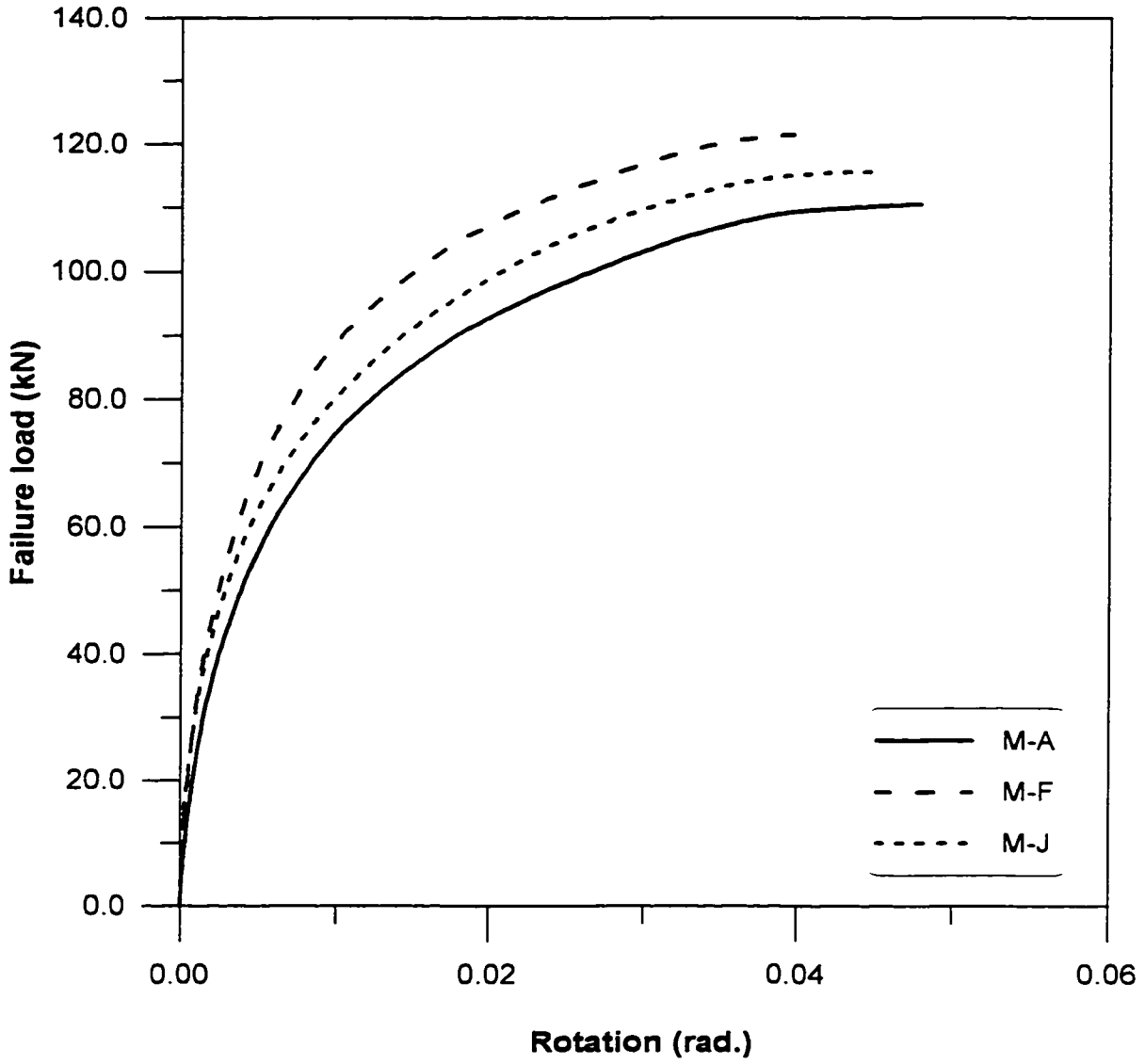

Figure 6-32. Load versus rotation for Type A, Type J, and Type F theoretical longer intermediate length specimens

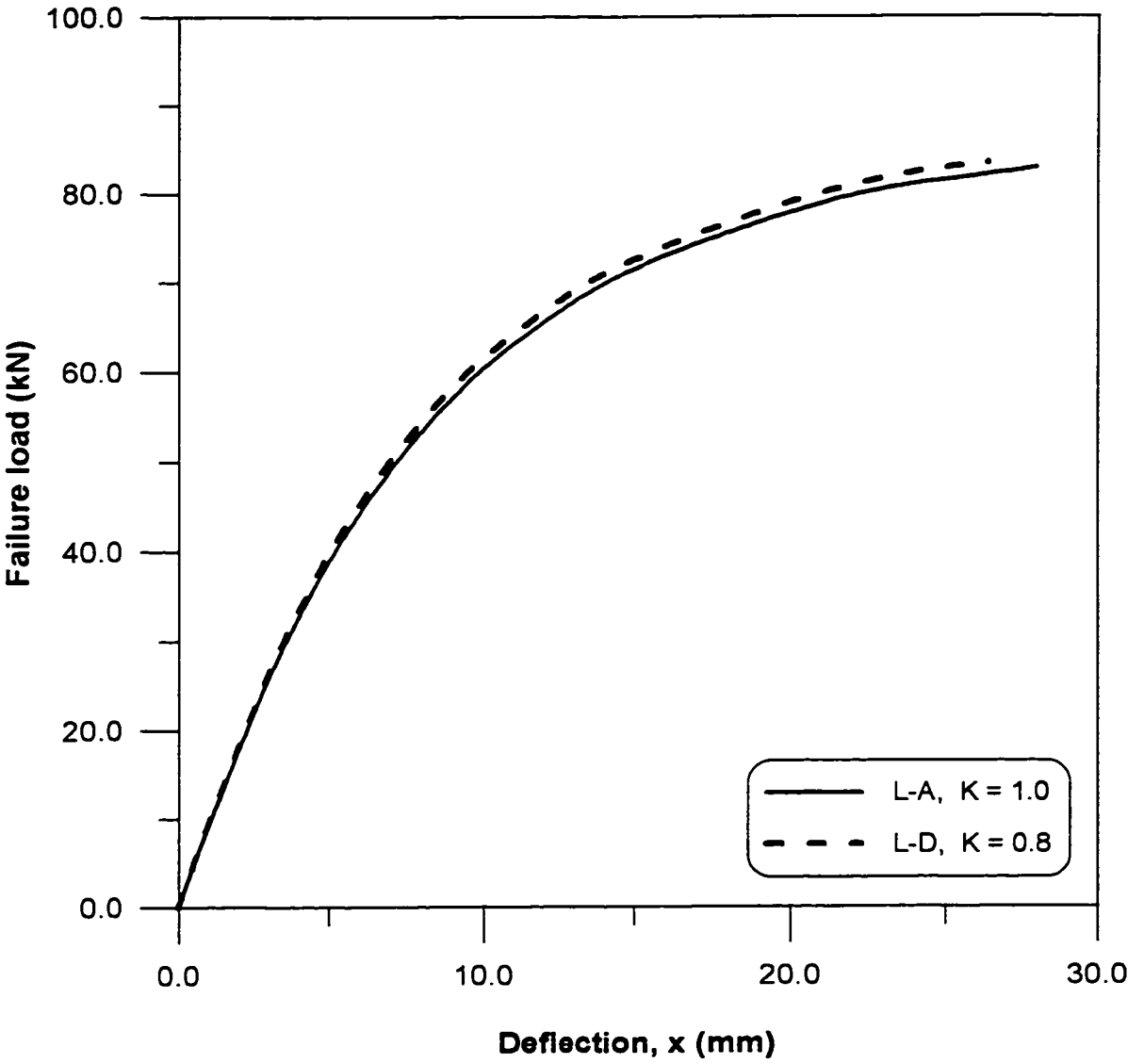

Figure 6-33. Effect of changing the weld length on the deflection in the x direction of slender specimens

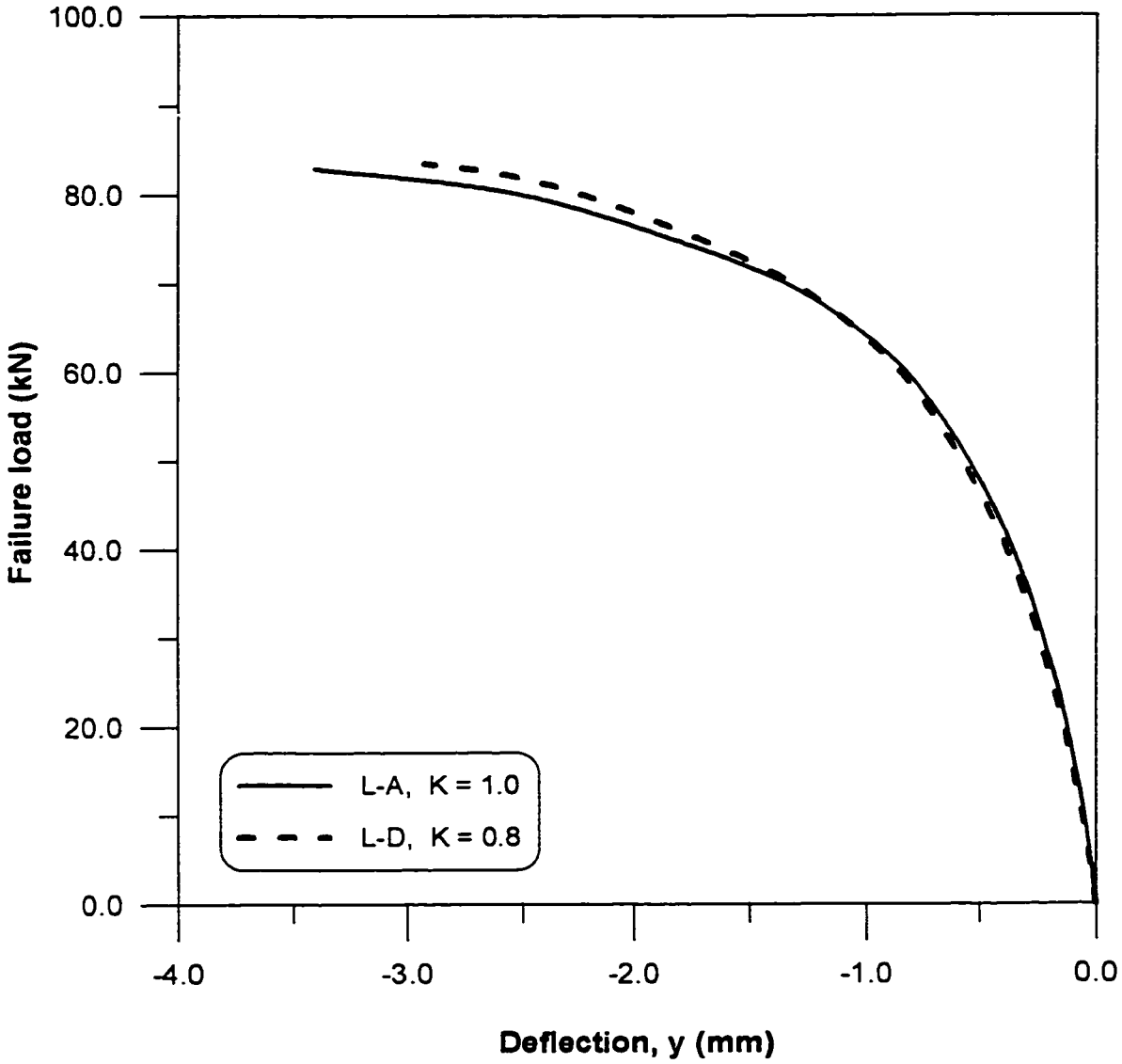

Figure 6-34. Effect of changing the weld length on the deflection in the y direction of slender specimens

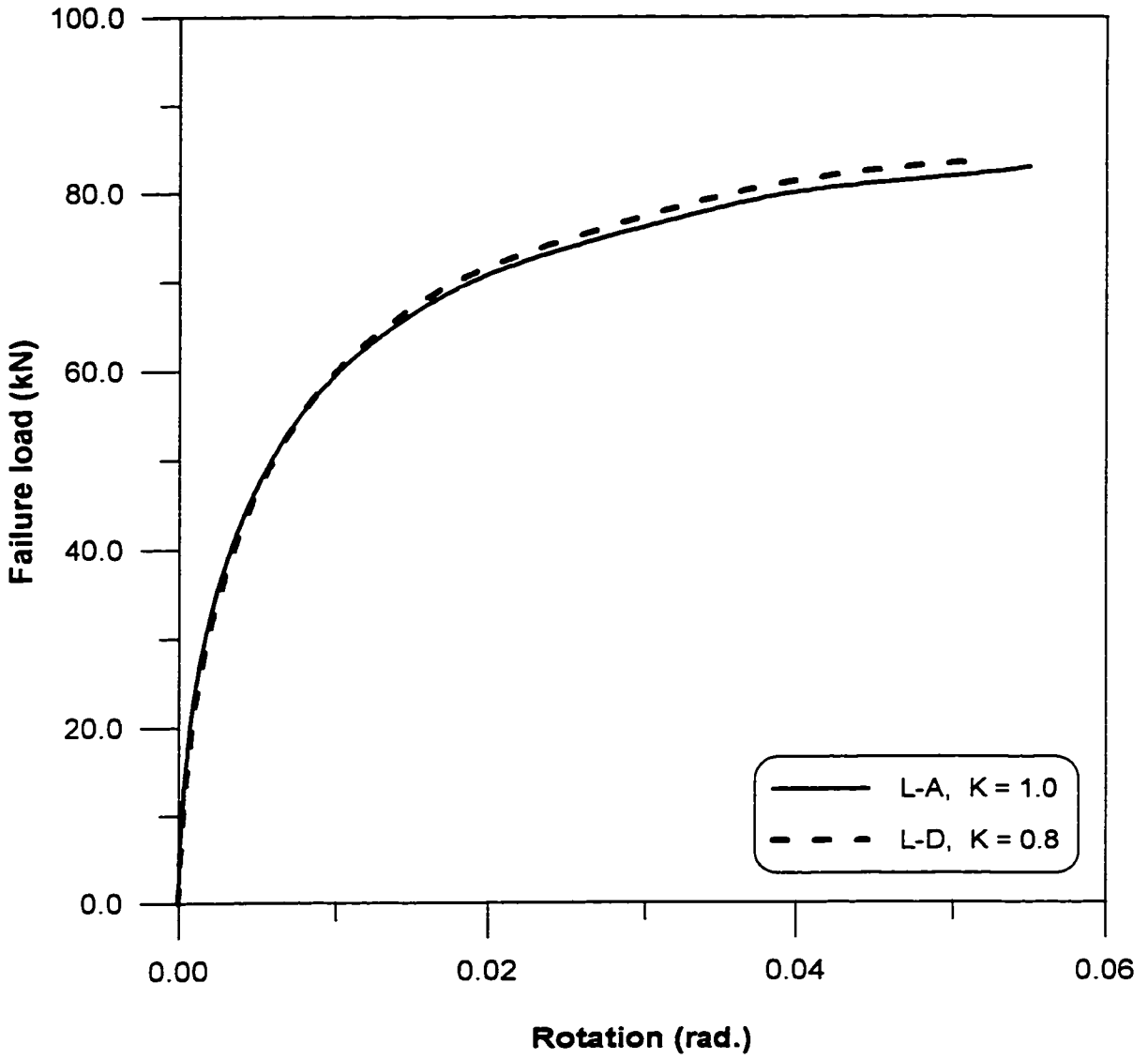

Figure 6-35. Effect of changing the weld length on the cross-sectional rotation of slender specimens

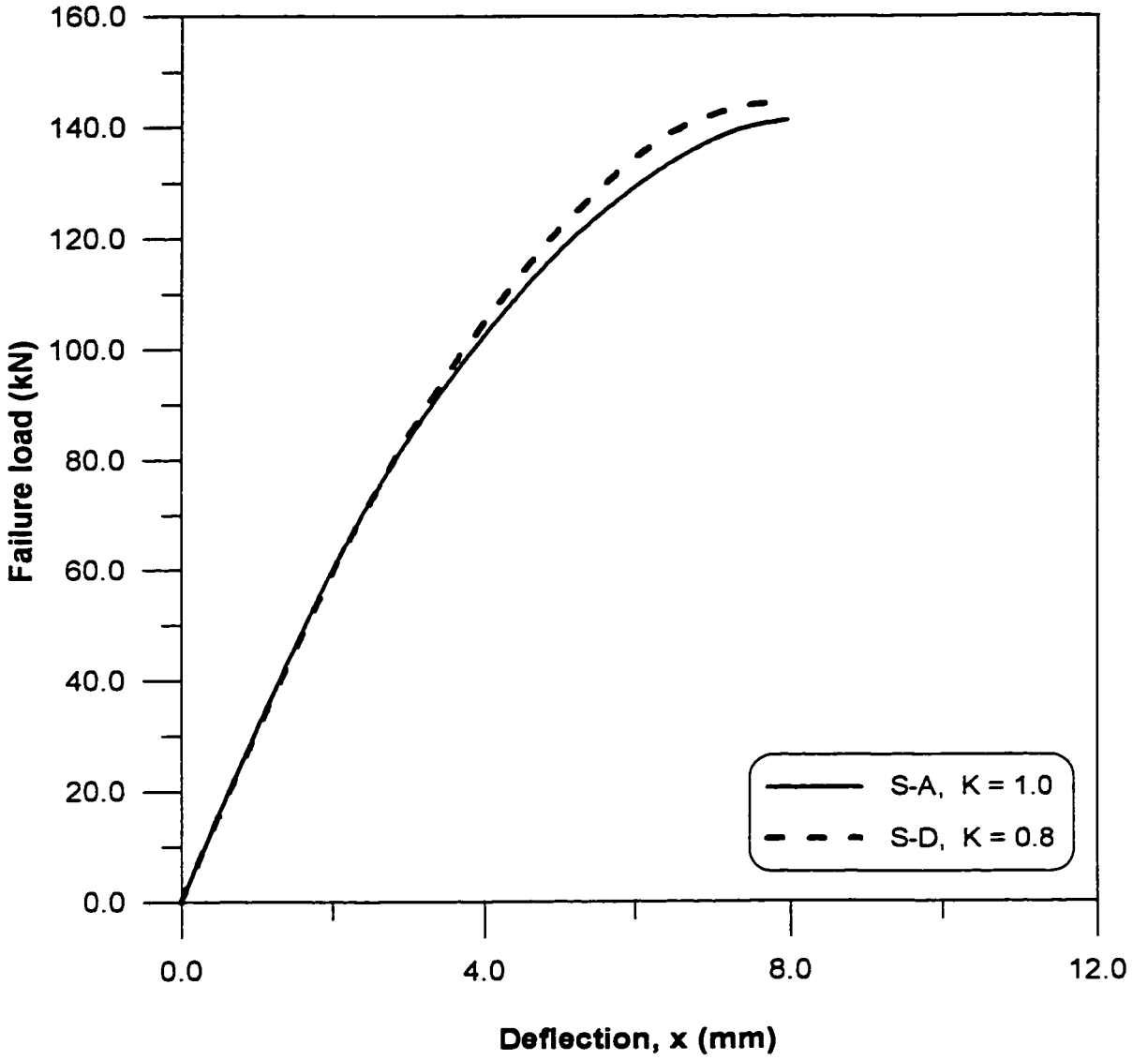

Figure 6-36. Effect of changing the weld length on the deflection in x direction of shorter intermediate length specimens

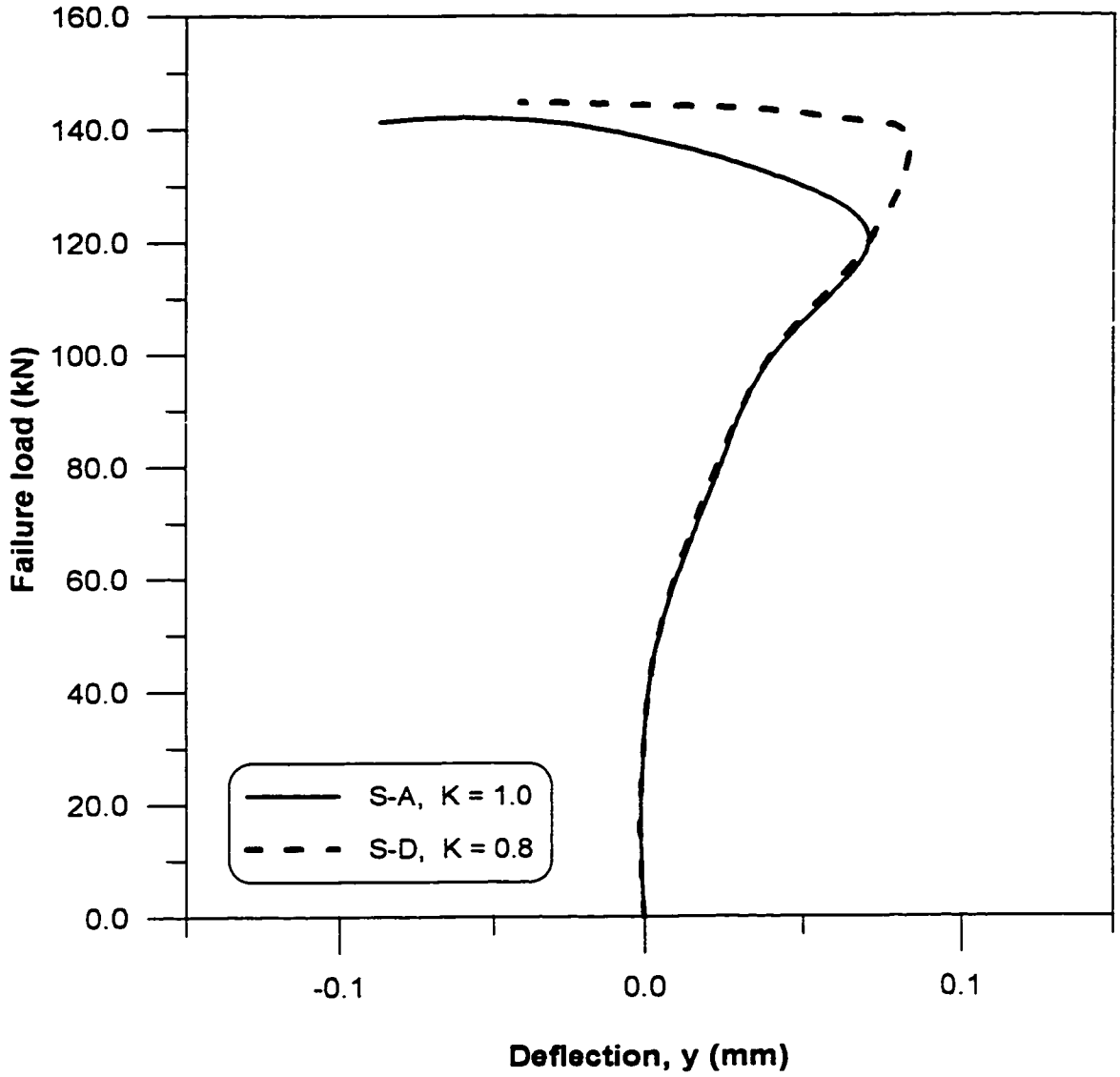

Figure 6-37. Effect of changing the weld length on the deflection in y direction of shorter intermediate length specimens

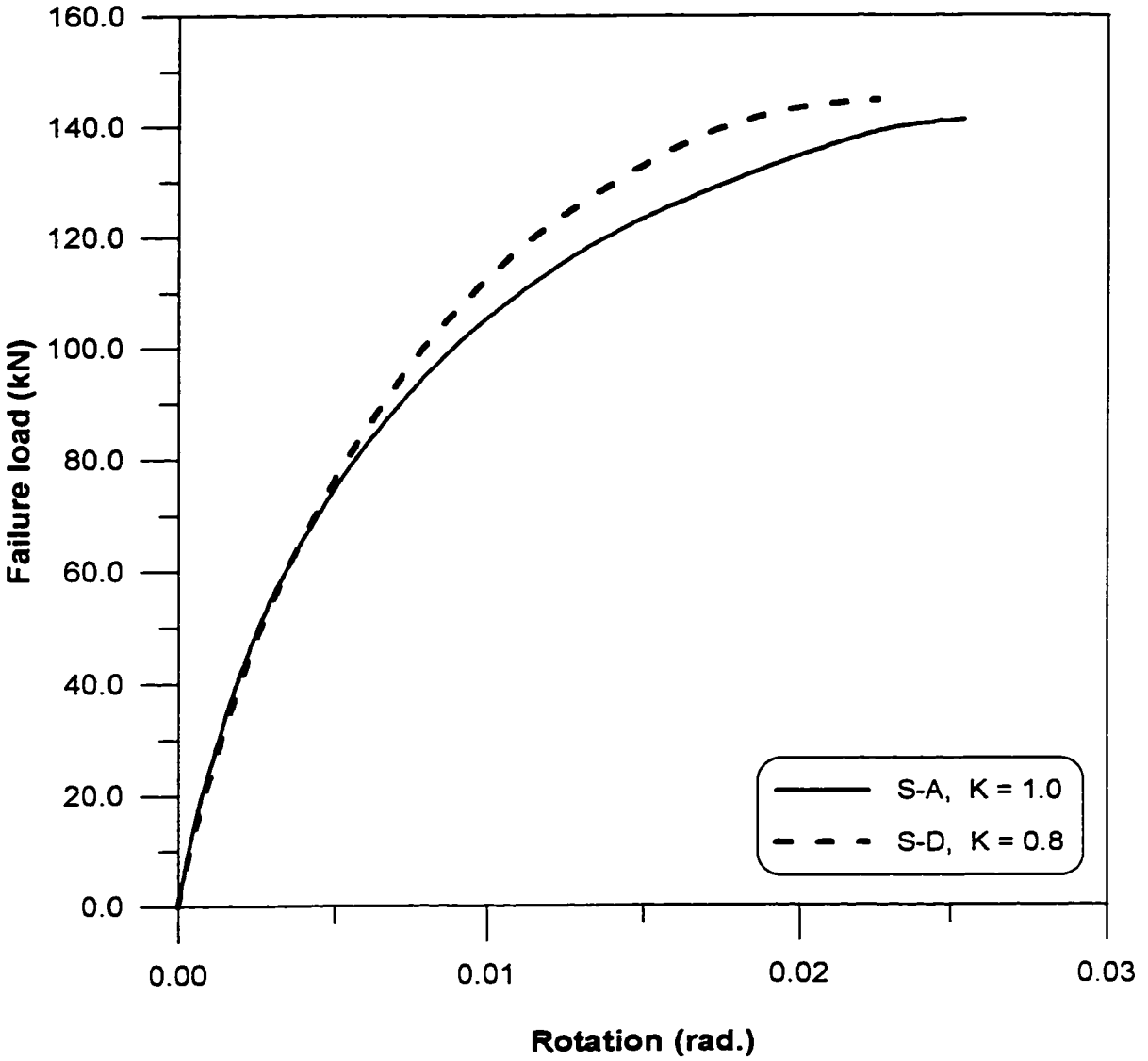

Figure 6-38. Effect of changing the weld length on the cross-sectional rotation of shorter intermediate length specimens

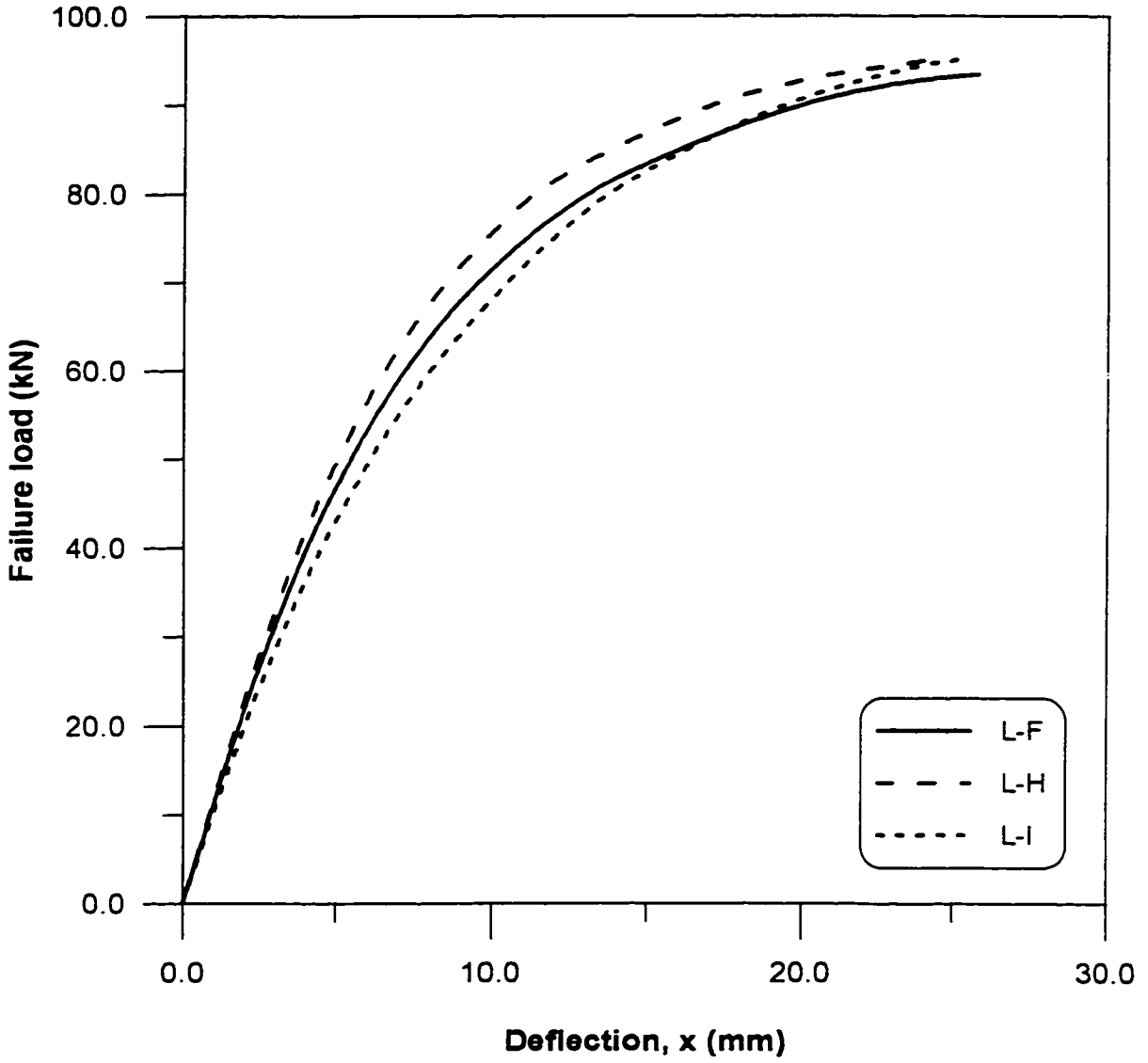

Figure 6-39. Load versus deflection in x direction for Type F, Type H, and Type I theoretical slender specimens

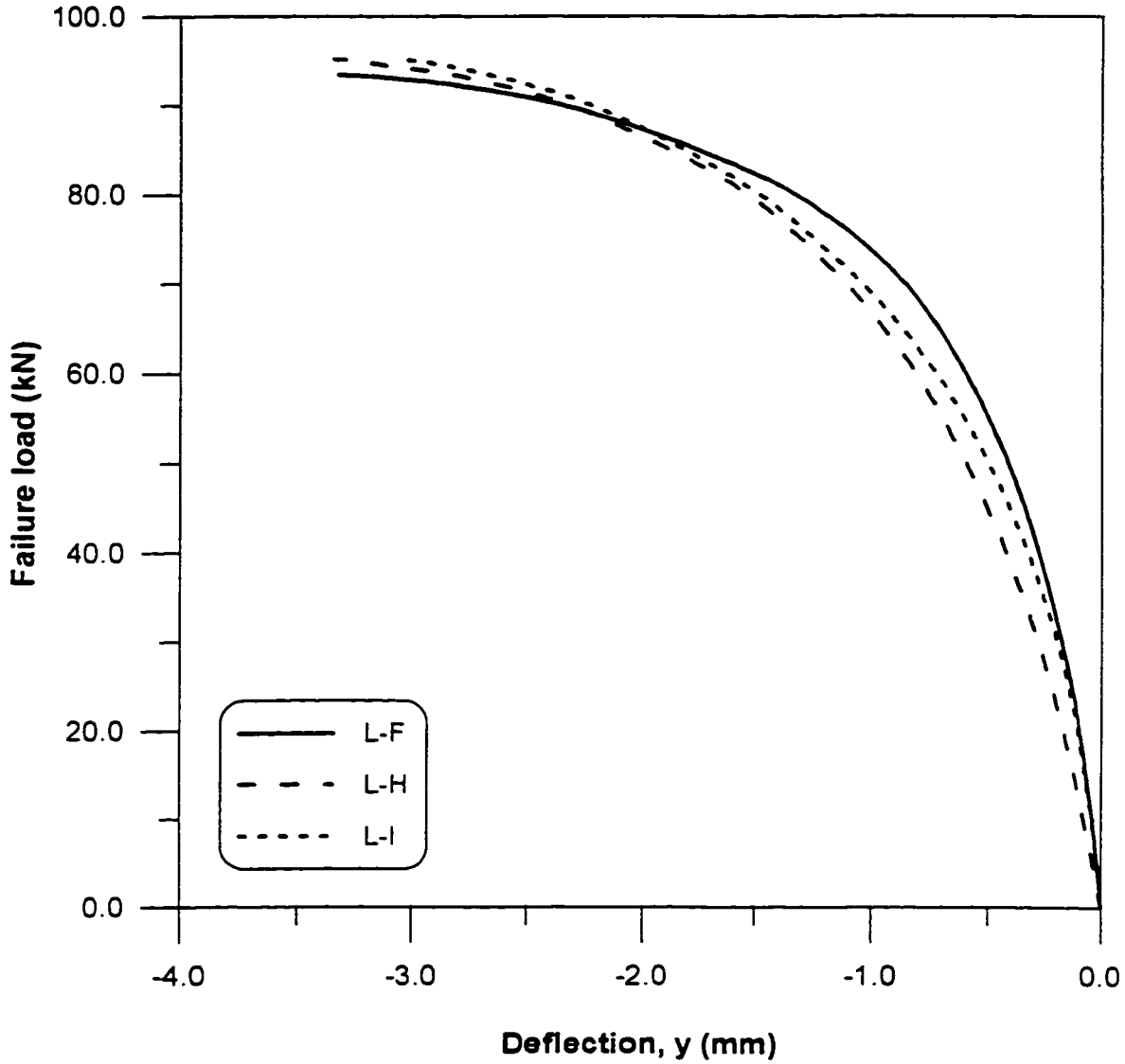

Figure 6-40. Load versus deflection in y direction for Type F, Type H, and Type I theoretical slender specimens

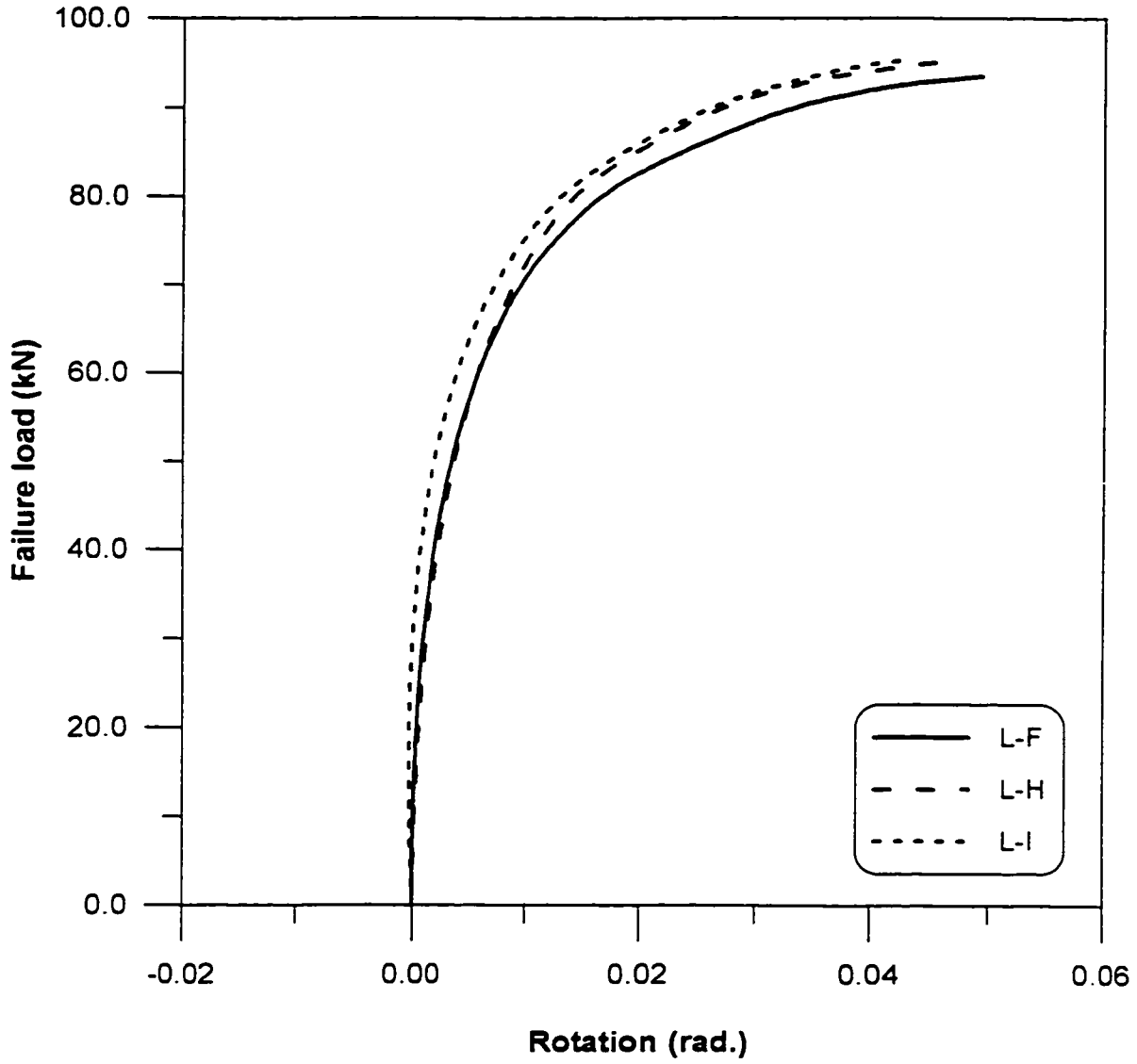

Figure 6-41. Load versus rotation for Type F, Type H, and Type I theoretical slender specimens

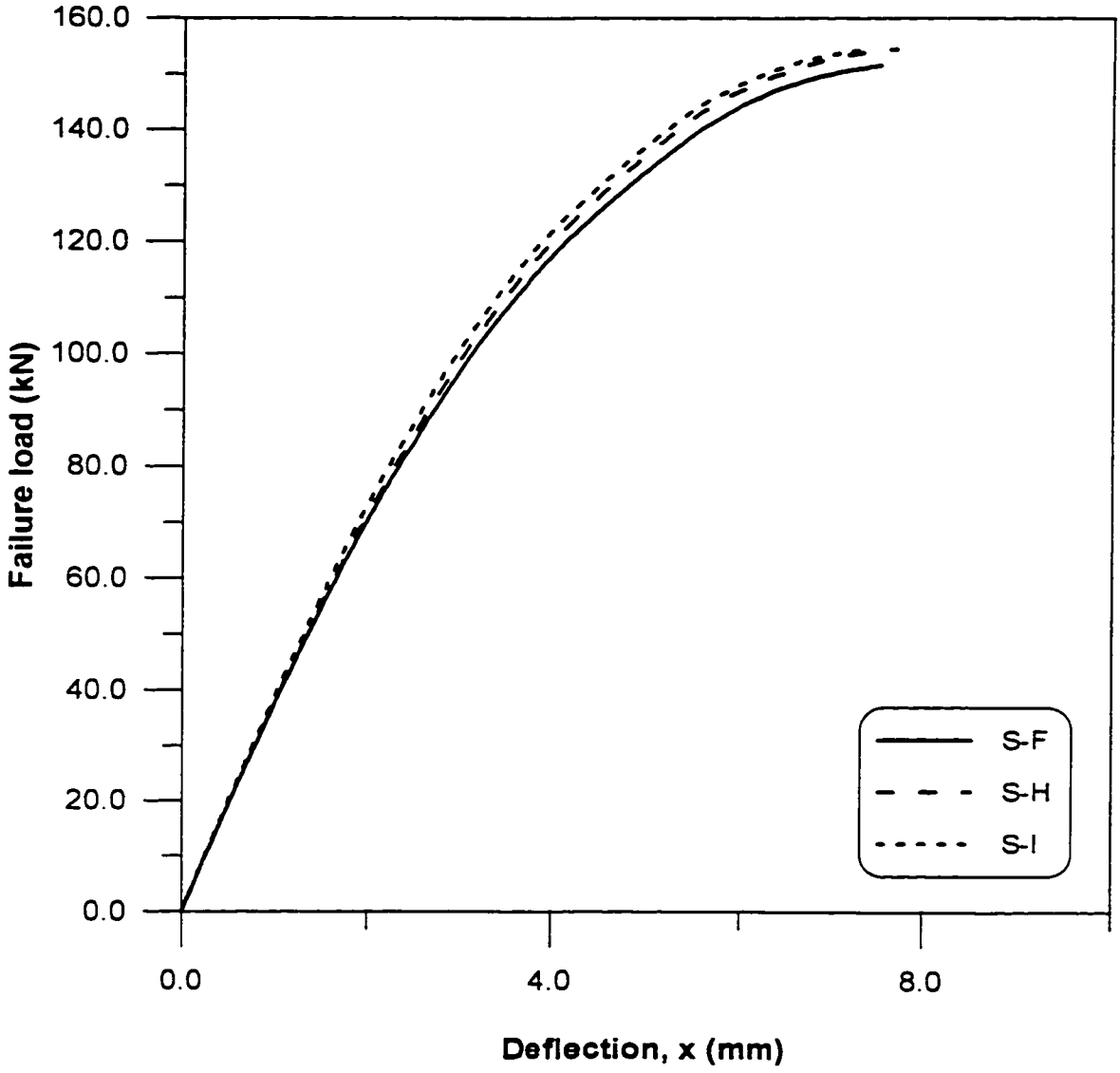

Figure 6-42. Load versus deflection in x direction for Type F, Type H, and Type I theoretical shorter intermediate length specimens

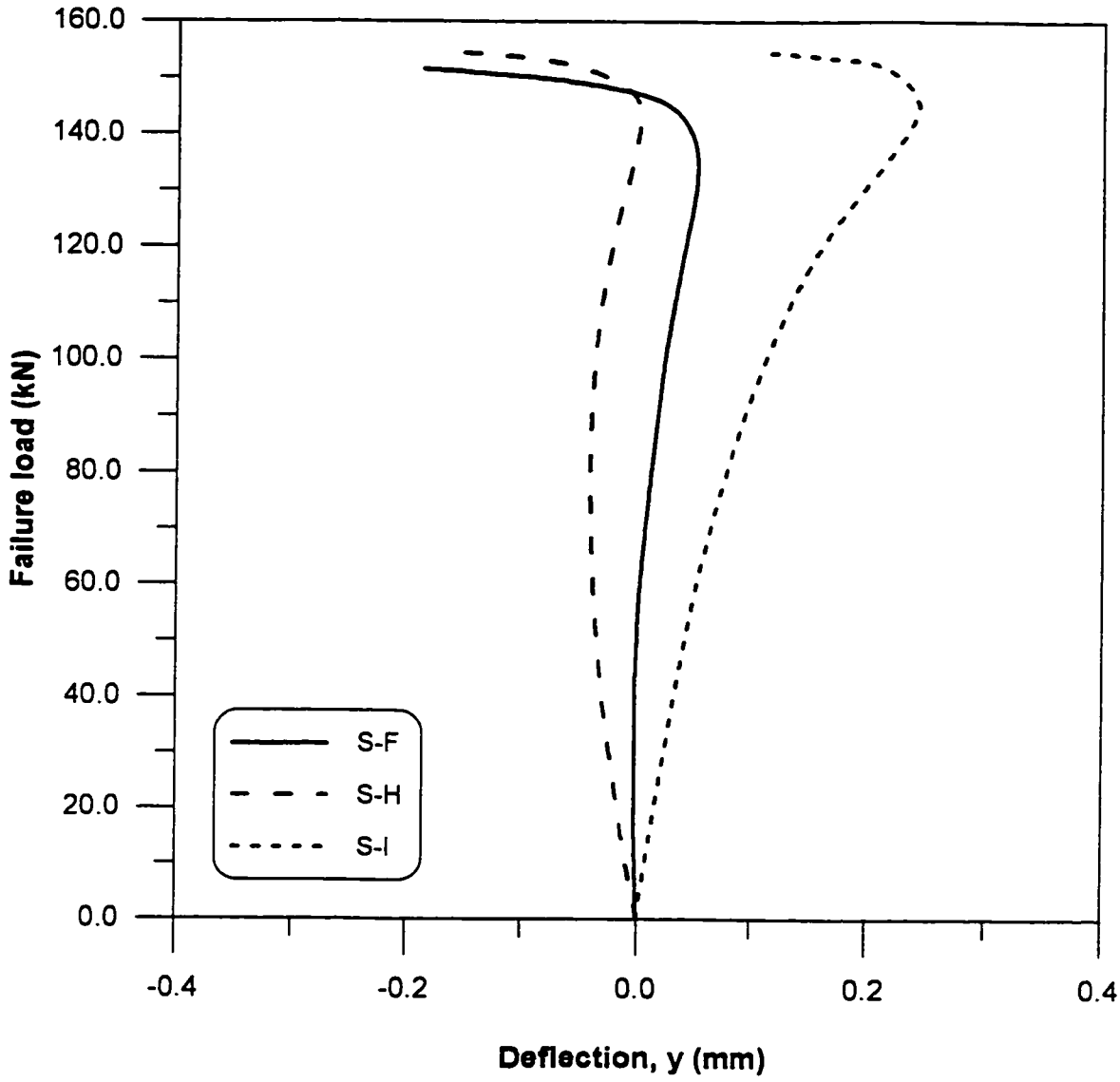

Figure 6-43. Load versus deflection in y direction for Type F, Type H, and Type I theoretical shorter intermediate length specimens

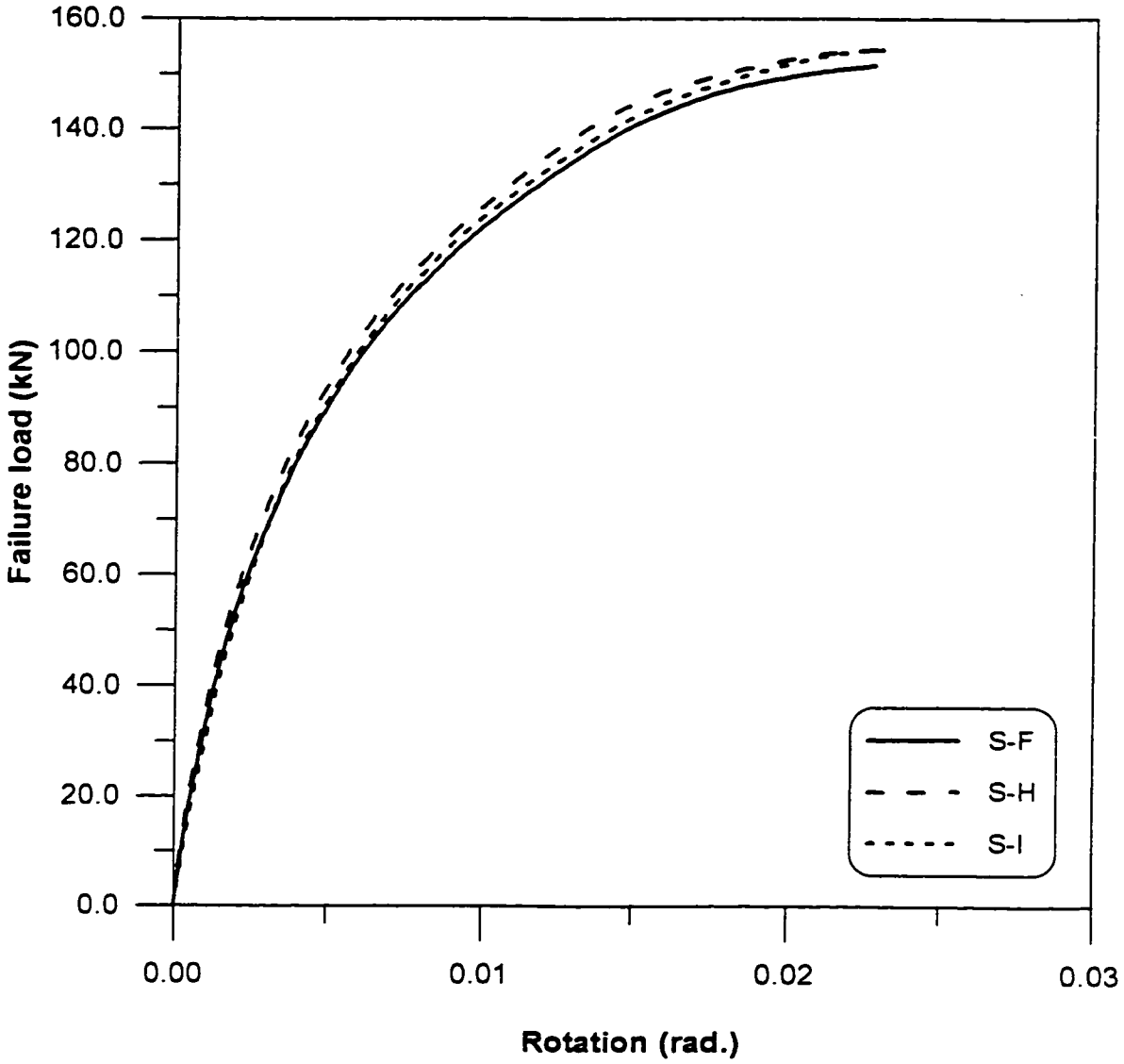

Figure 6-44. Load versus rotation for Type F, Type H, and Type I theoretical shorter intermediate length specimens

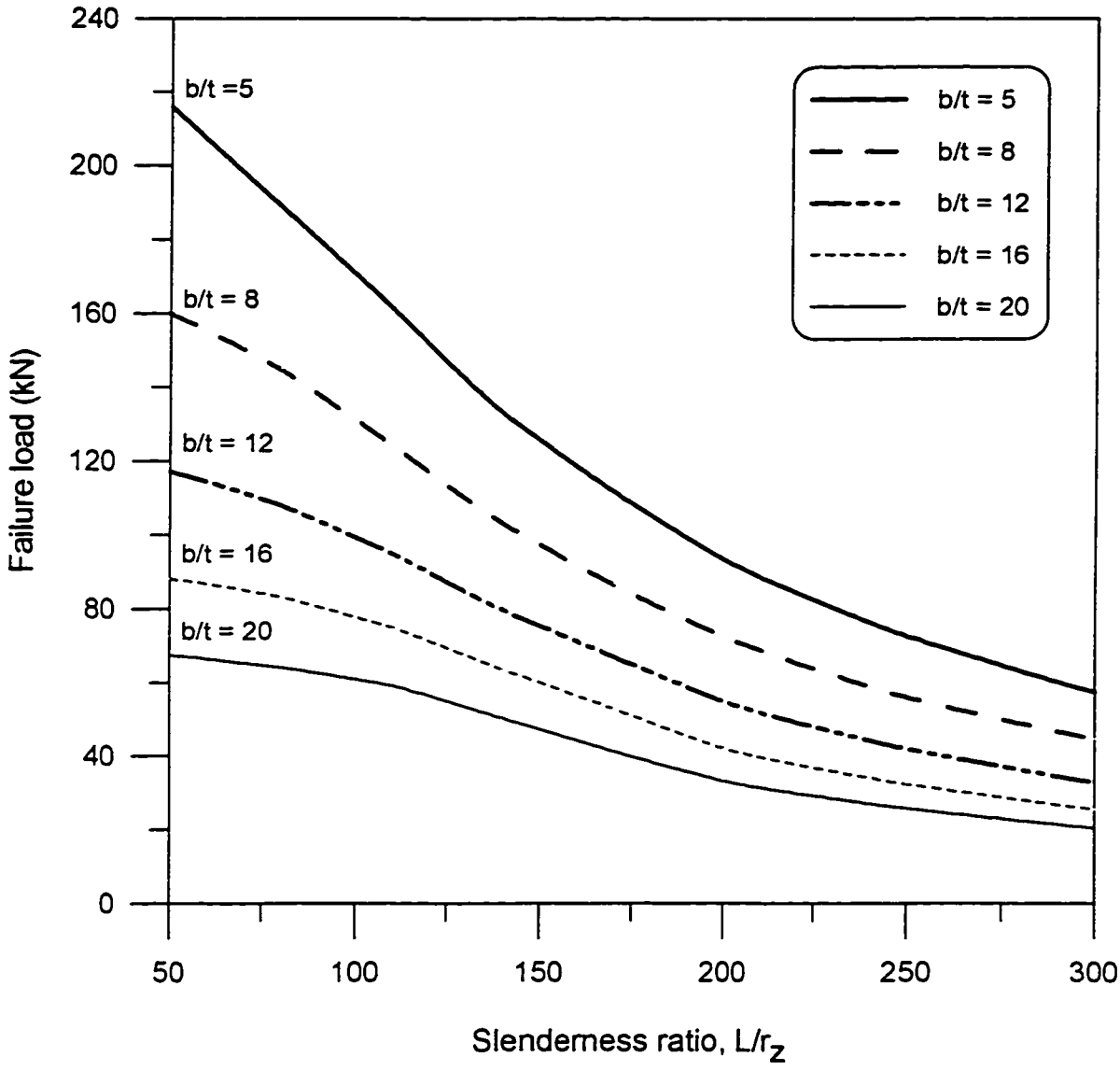

Figure 7-1. Effect of varying the slenderness ratio on the failure load

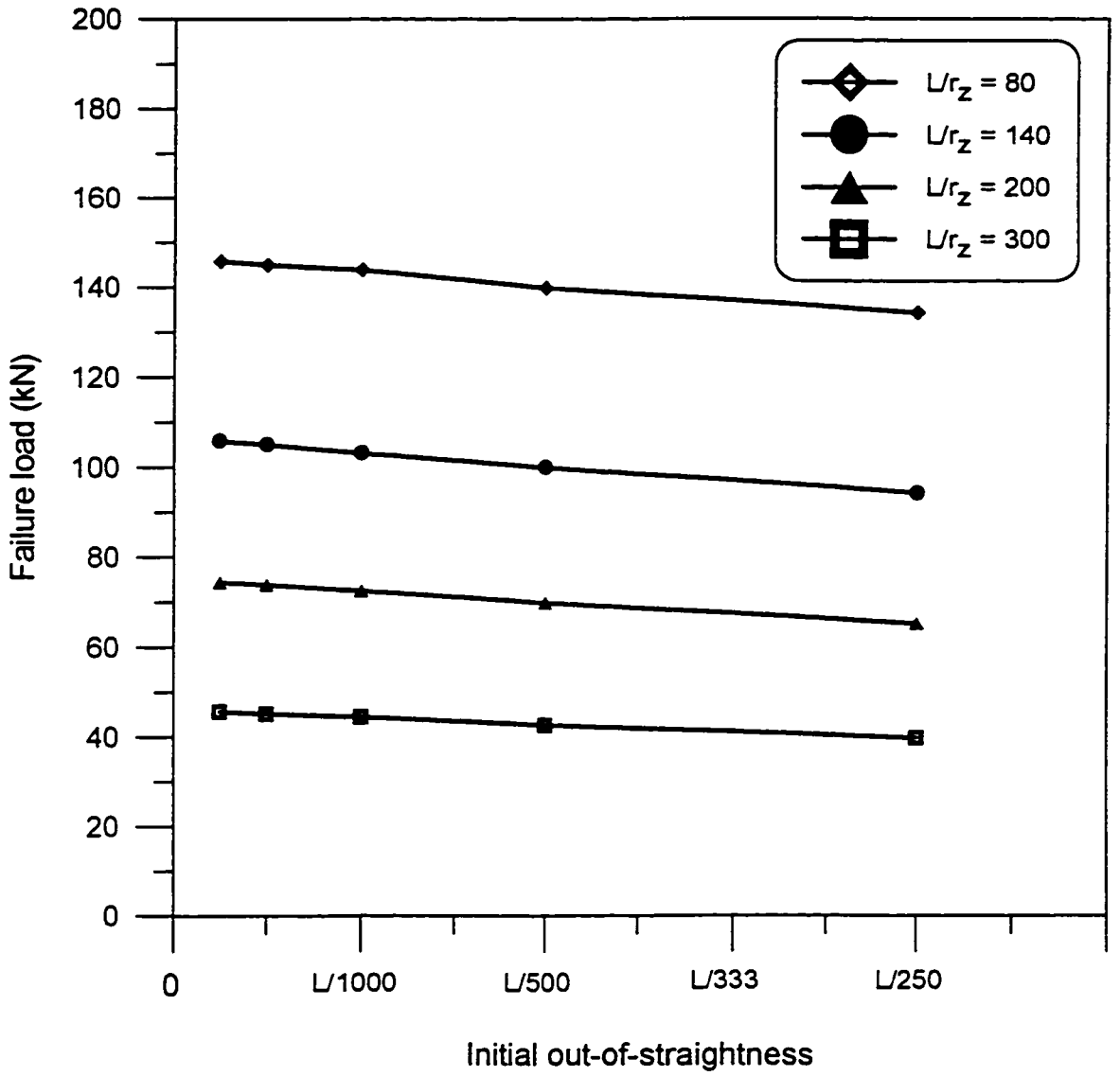

Figure 7-2. Effect of varying the initial out-of-straightness on the failure load

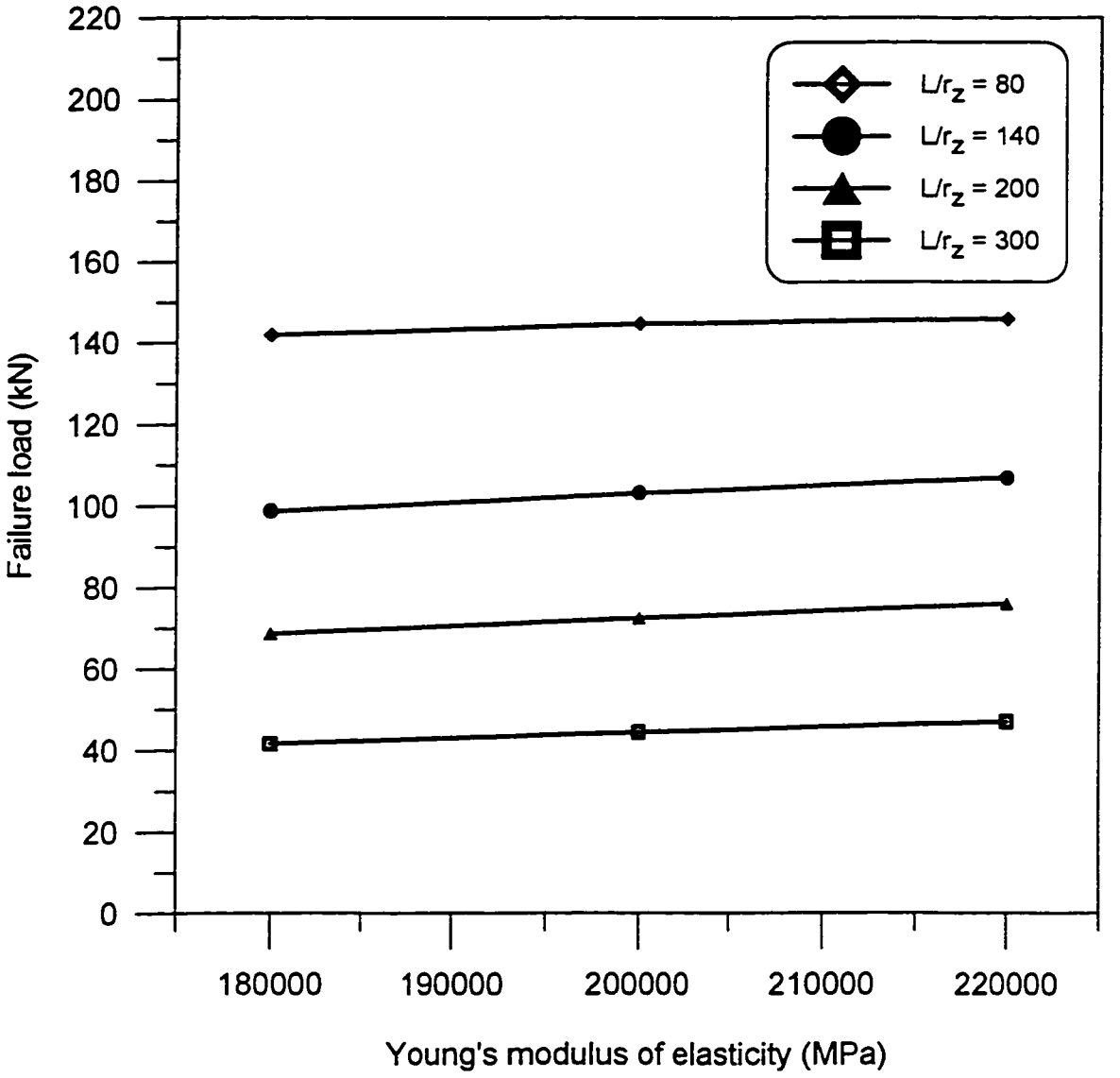

Figure 7-3. Effect of varying Young's modulus of elasticity on the failure load

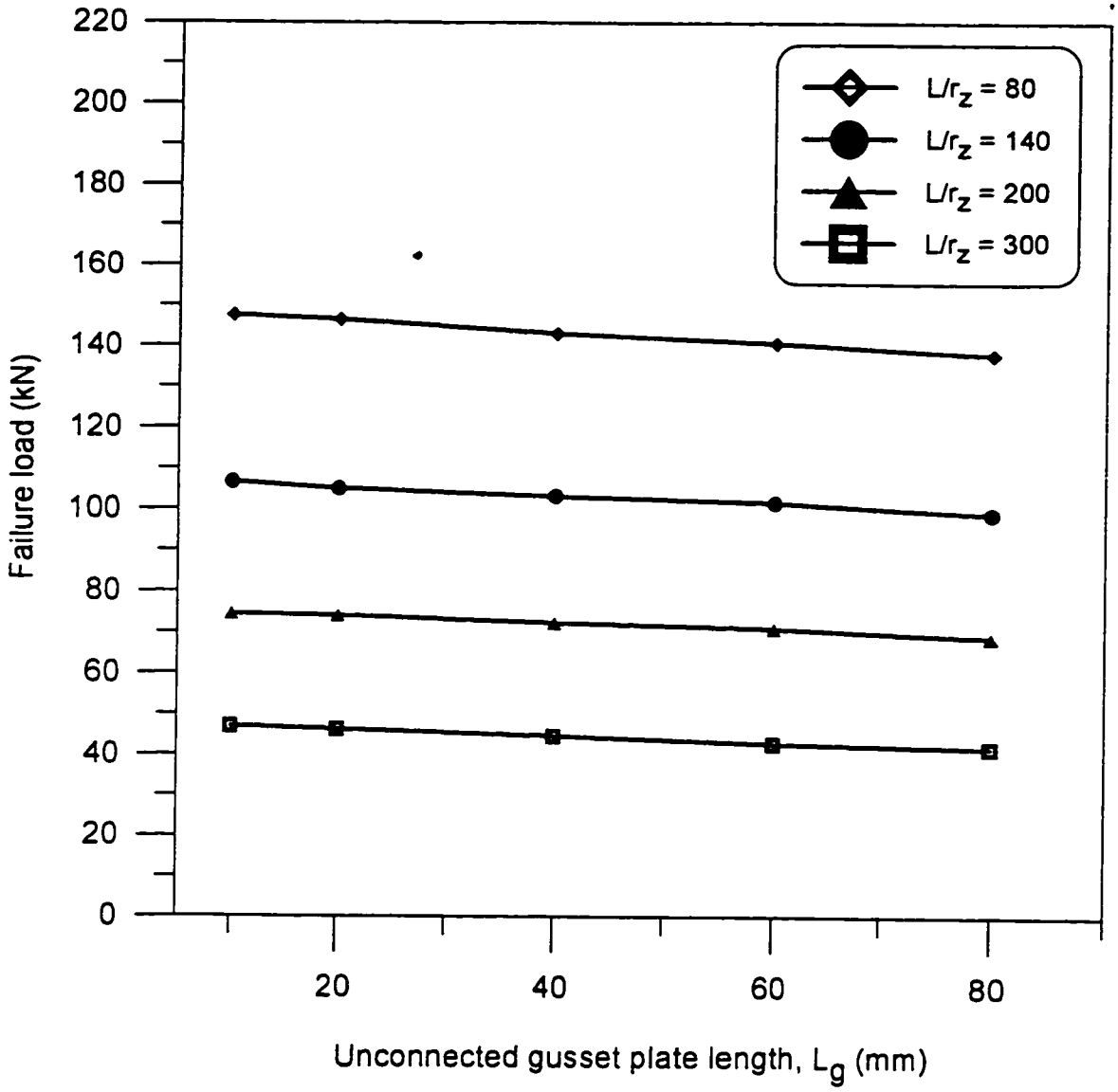

Figure 7-4. Effect of varying the unconnected length of the gusset plate on the failure load

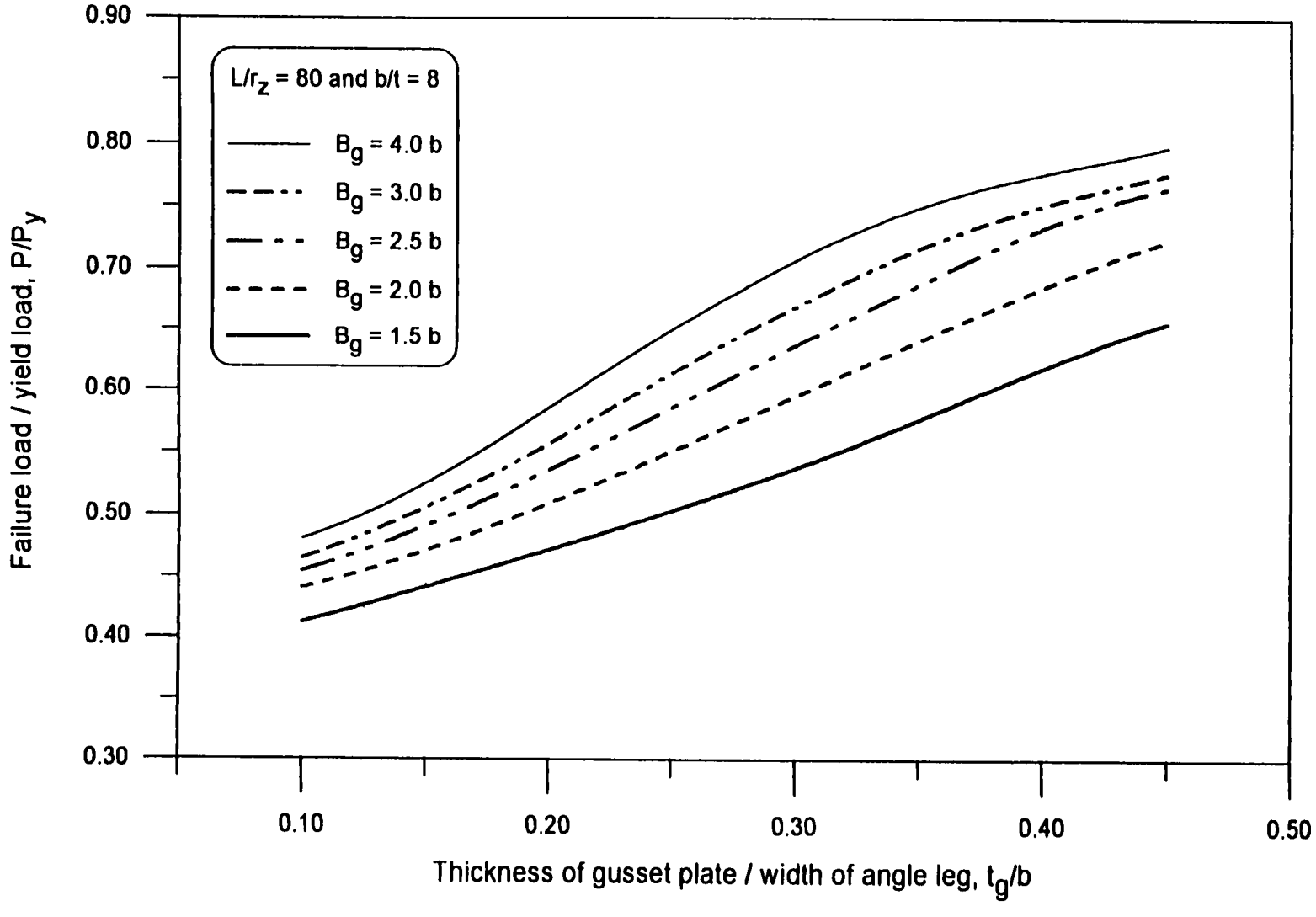

Figure 7-5. Effect of varying the gusset plate thickness on the failure load, $L/r_z = 80$

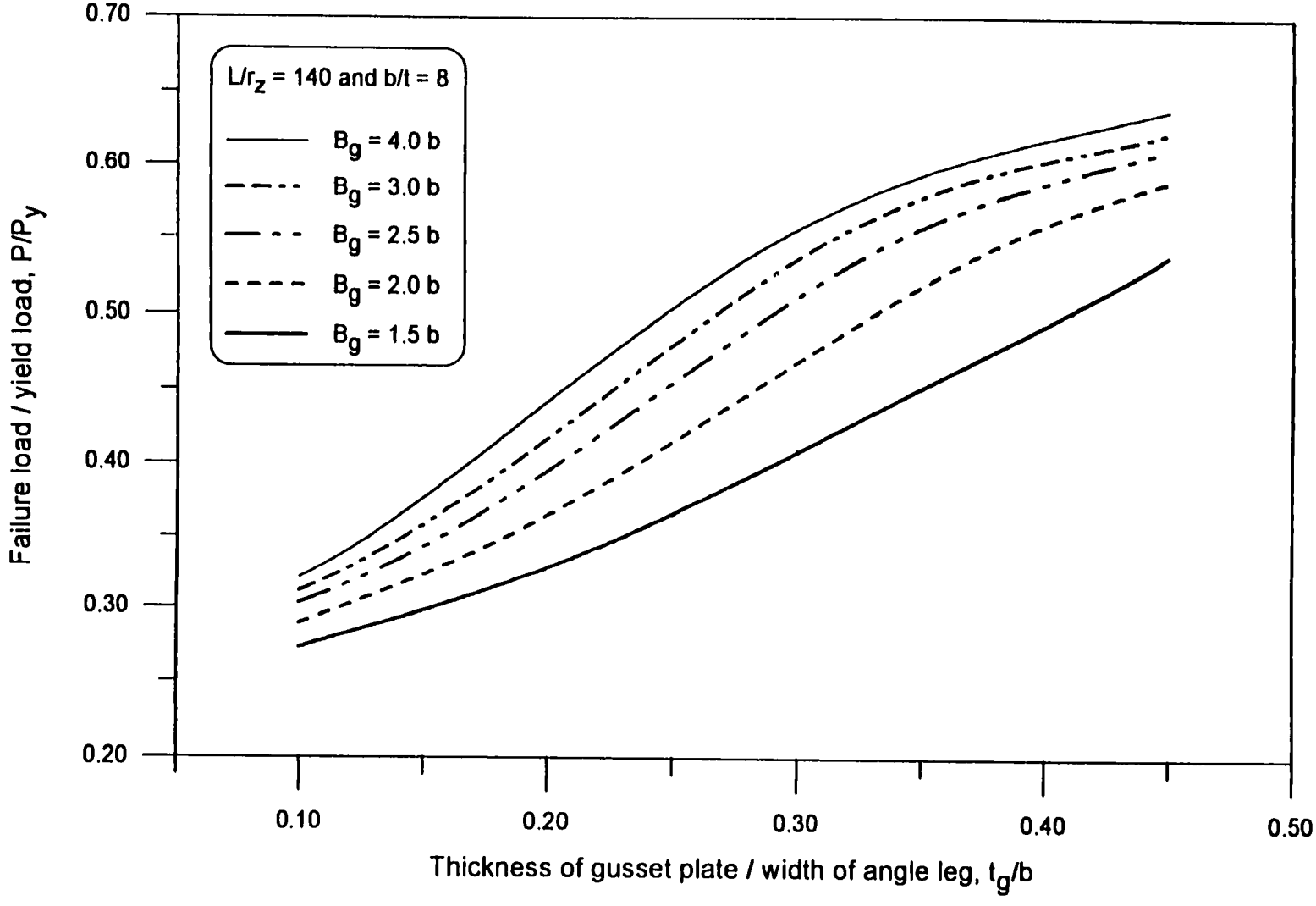

Figure 7-6. Effect of varying the gusset plate thickness on the failure load, $L/r_z = 140$

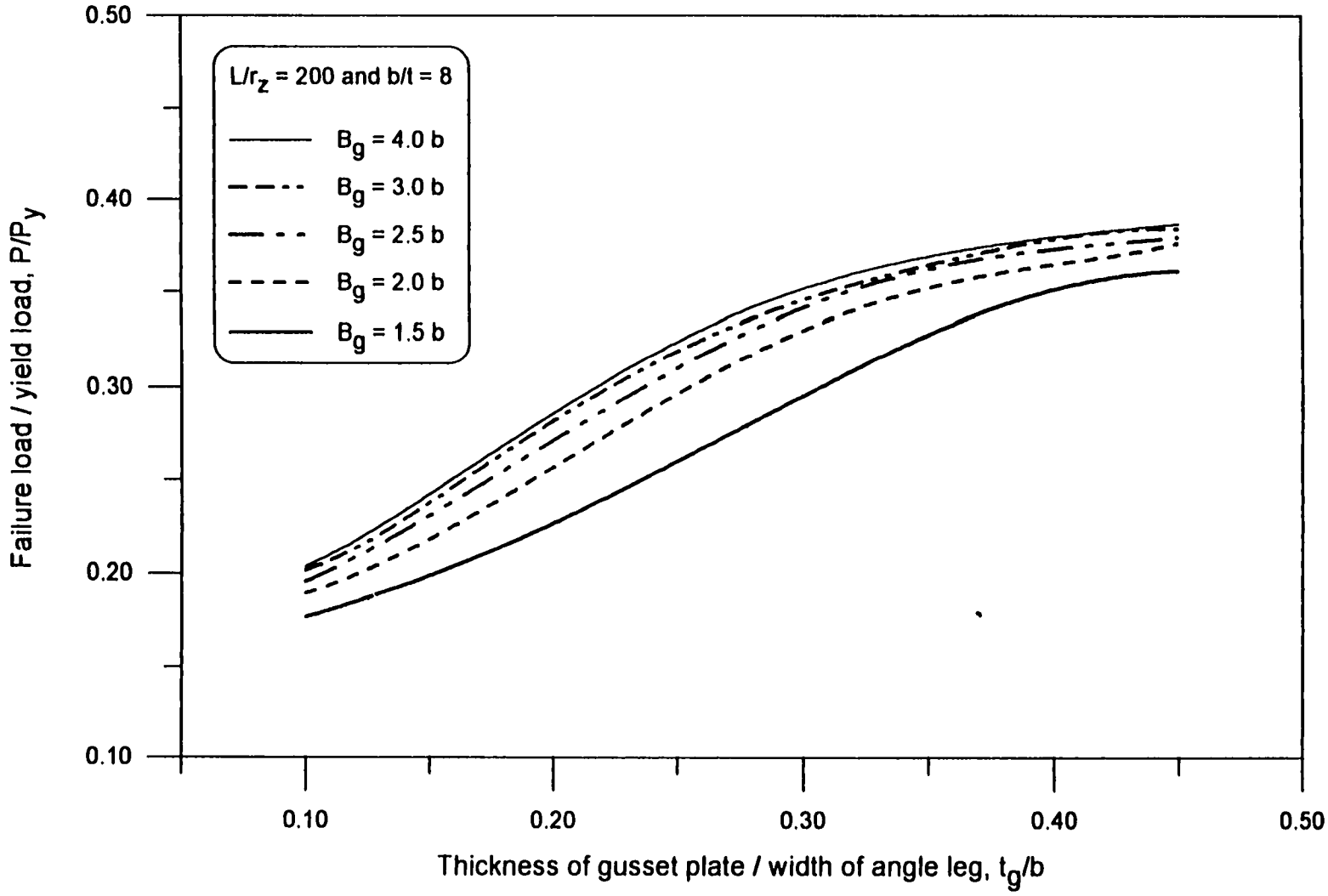

Figure 7-7. Effect of varying the gusset plate thickness on the failure load, $L/r_z = 200$

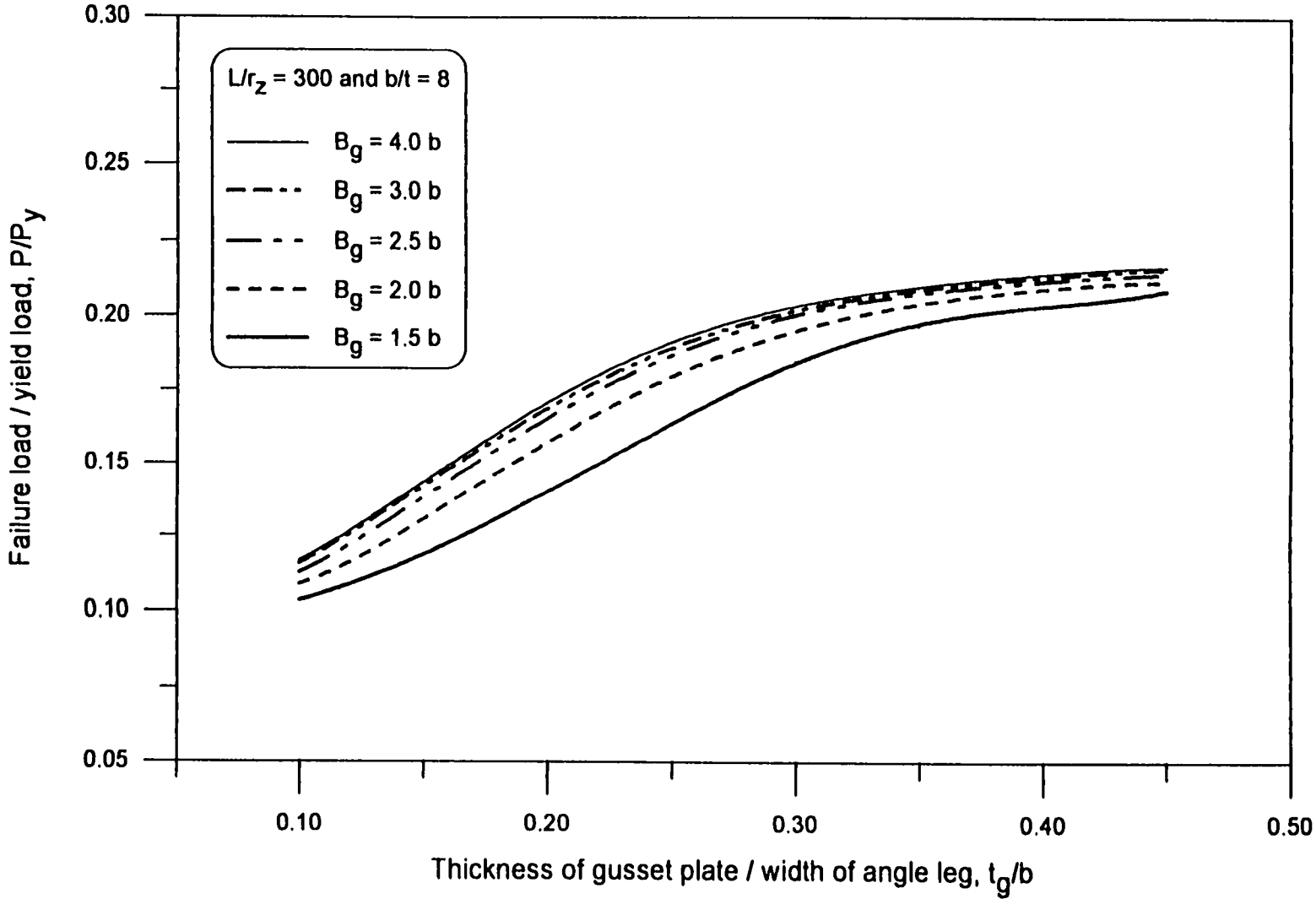

Figure 7-8. Effect of varying the gusset plate thickness on the failure load, $L/r_z = 300$

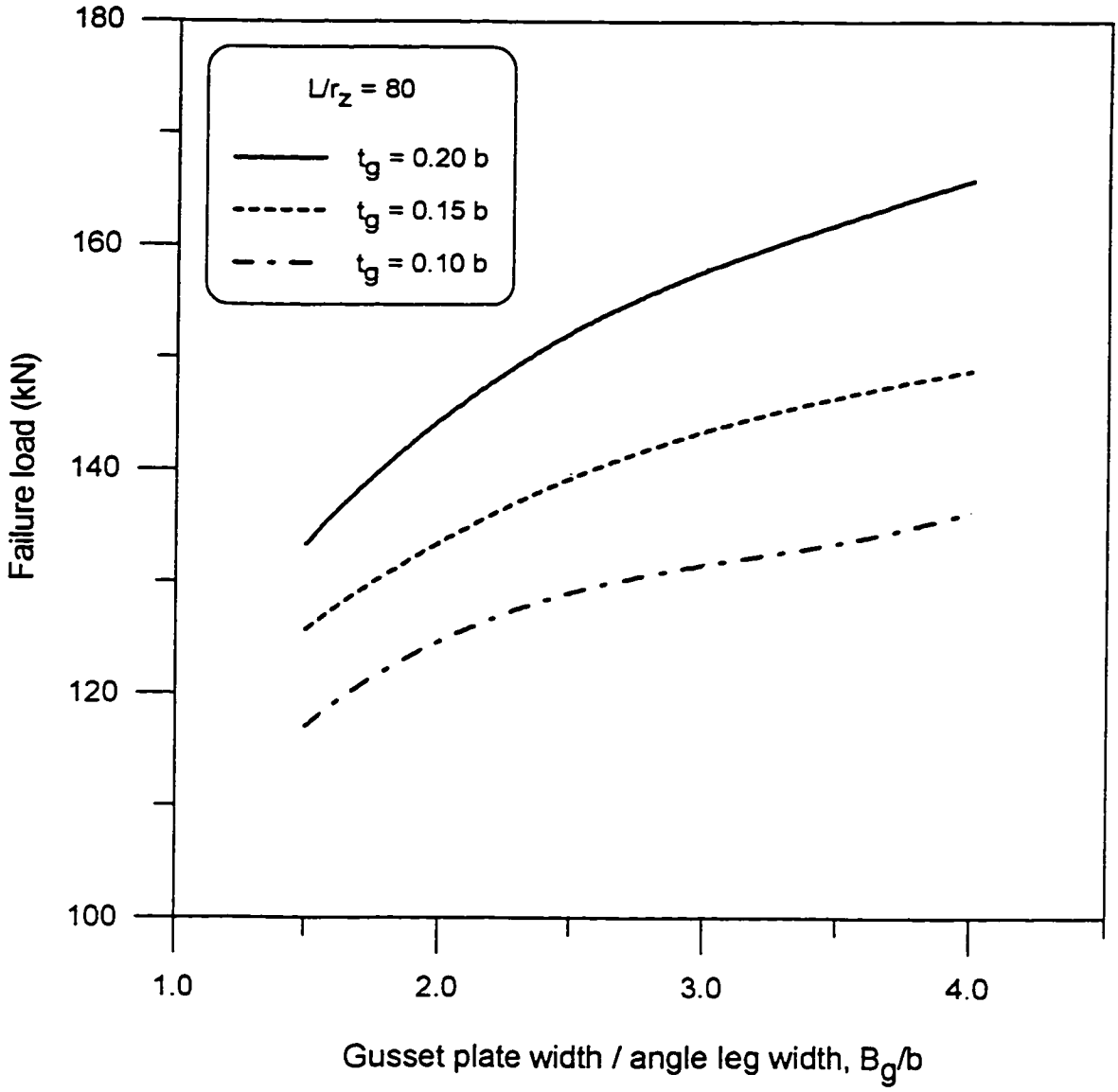

Figure 7-9. Effect of varying the gusset plate width on the failure load, $L/r_z = 80$

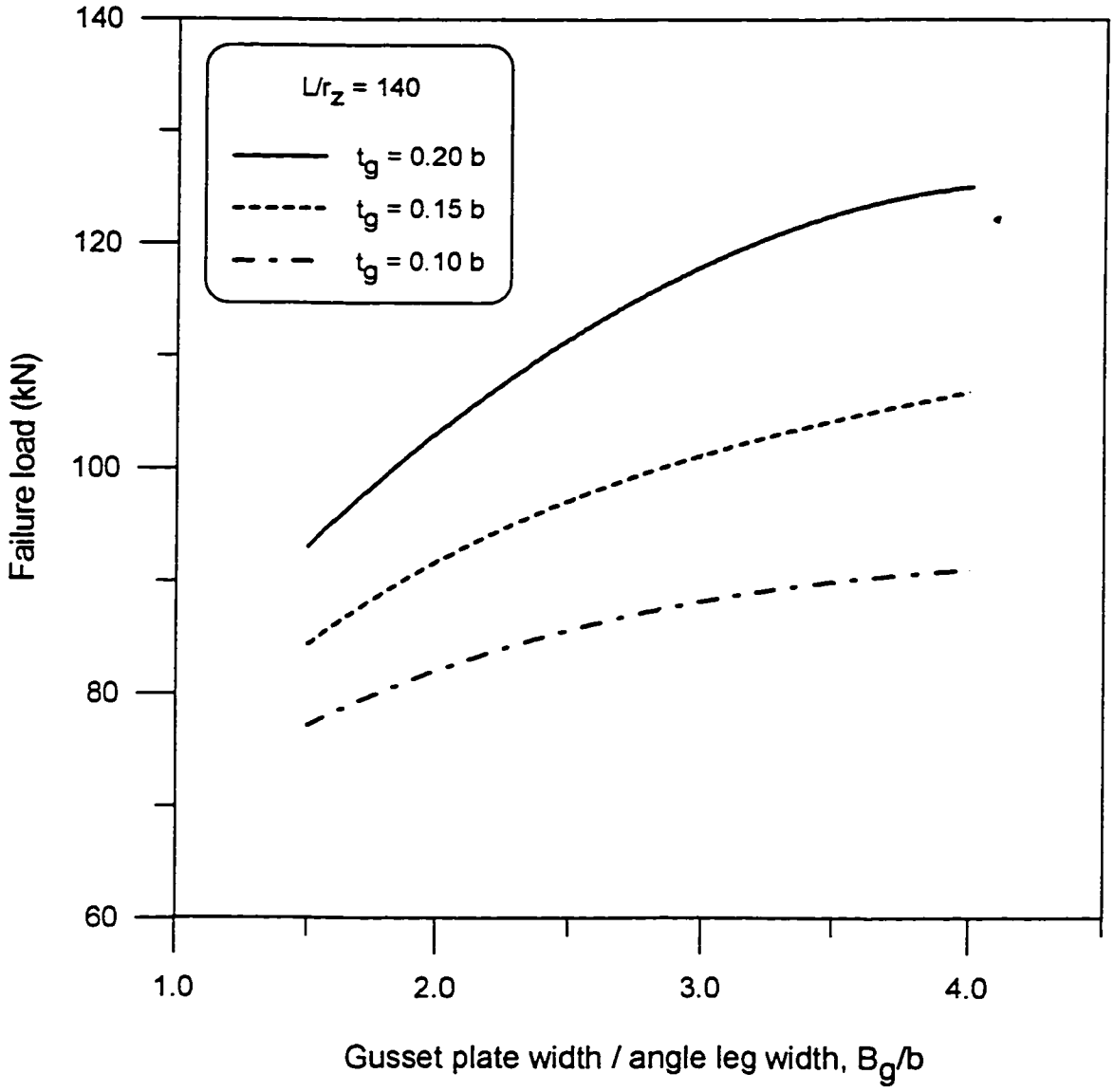

Figure 7-10. Effect of varying the gusset plate width on the failure load, $L/r_z = 140$

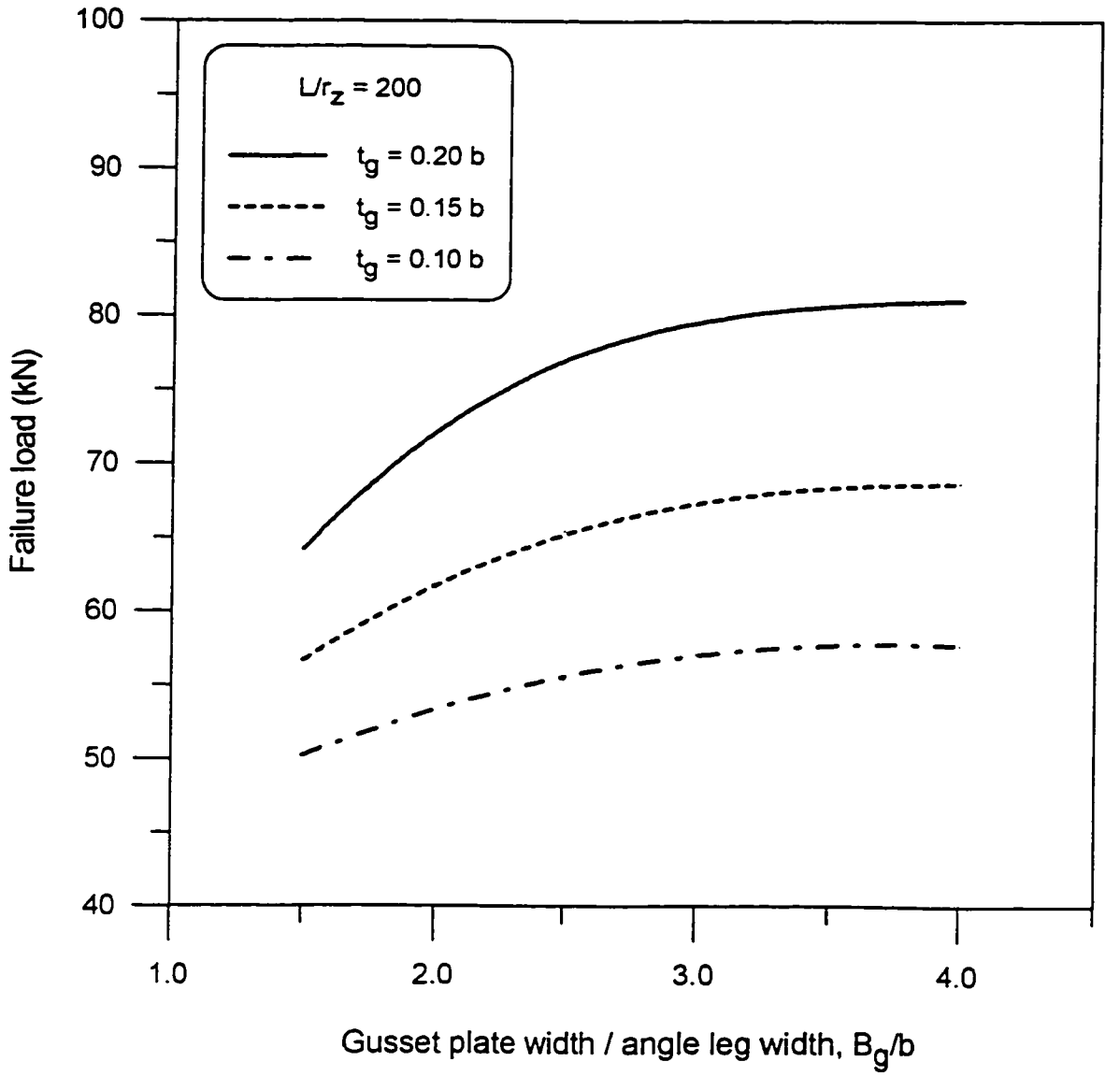

Figure 7-11. Effect of varying the gusset plate width on the failure load, $L/r_z = 200$

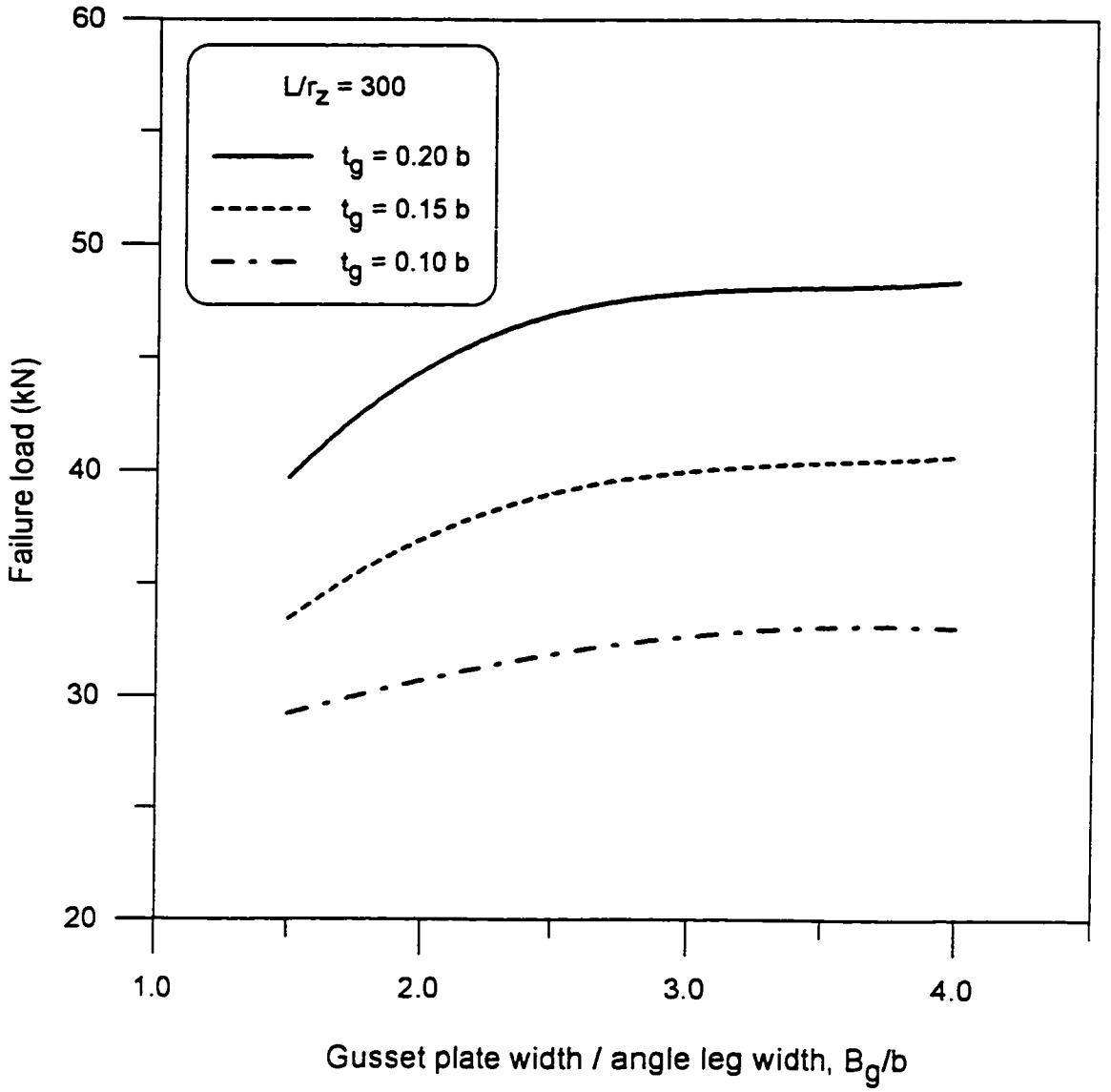

Figure 7-12. Effect of varying the gusset plate width on the failure load, $L/r_z = 300$

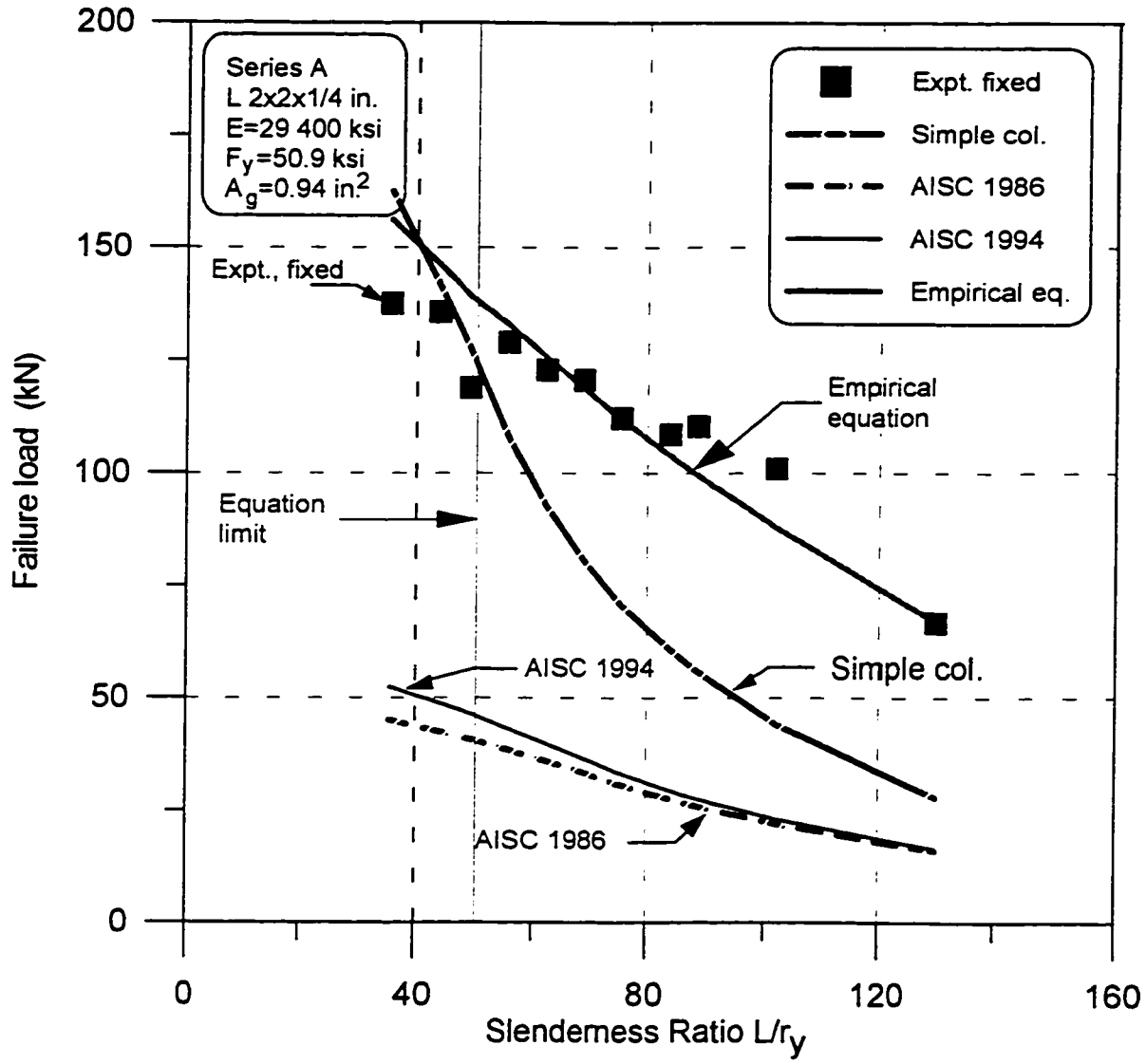

Figure 7-13. Comparison of Trahair et al. experimental results and predicted failure loads

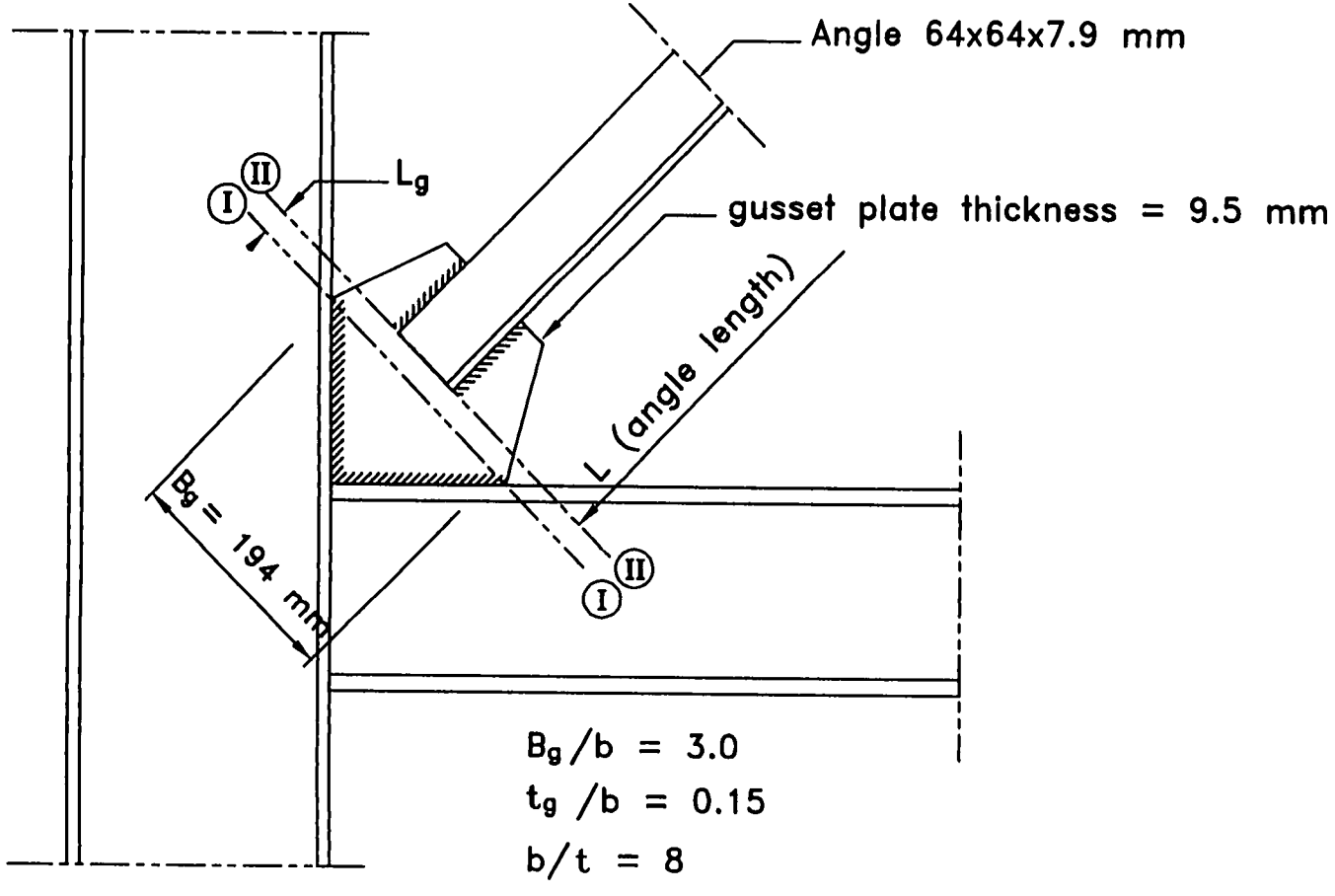

Figure 7-14. Gusset plate, Example II

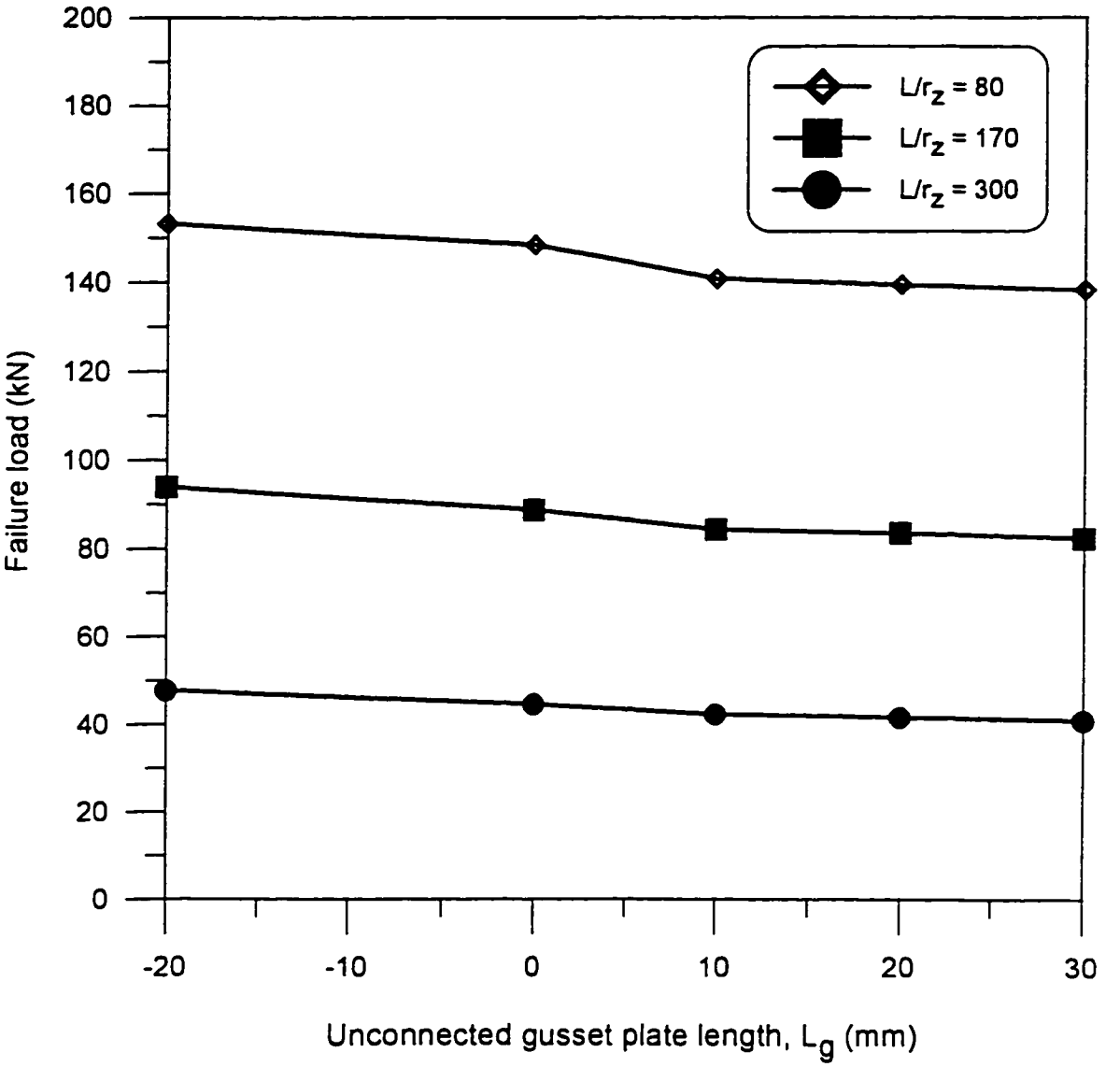

Figure 7-17. Effect of varying the unconnected gusset plate length on the failure load in Example II

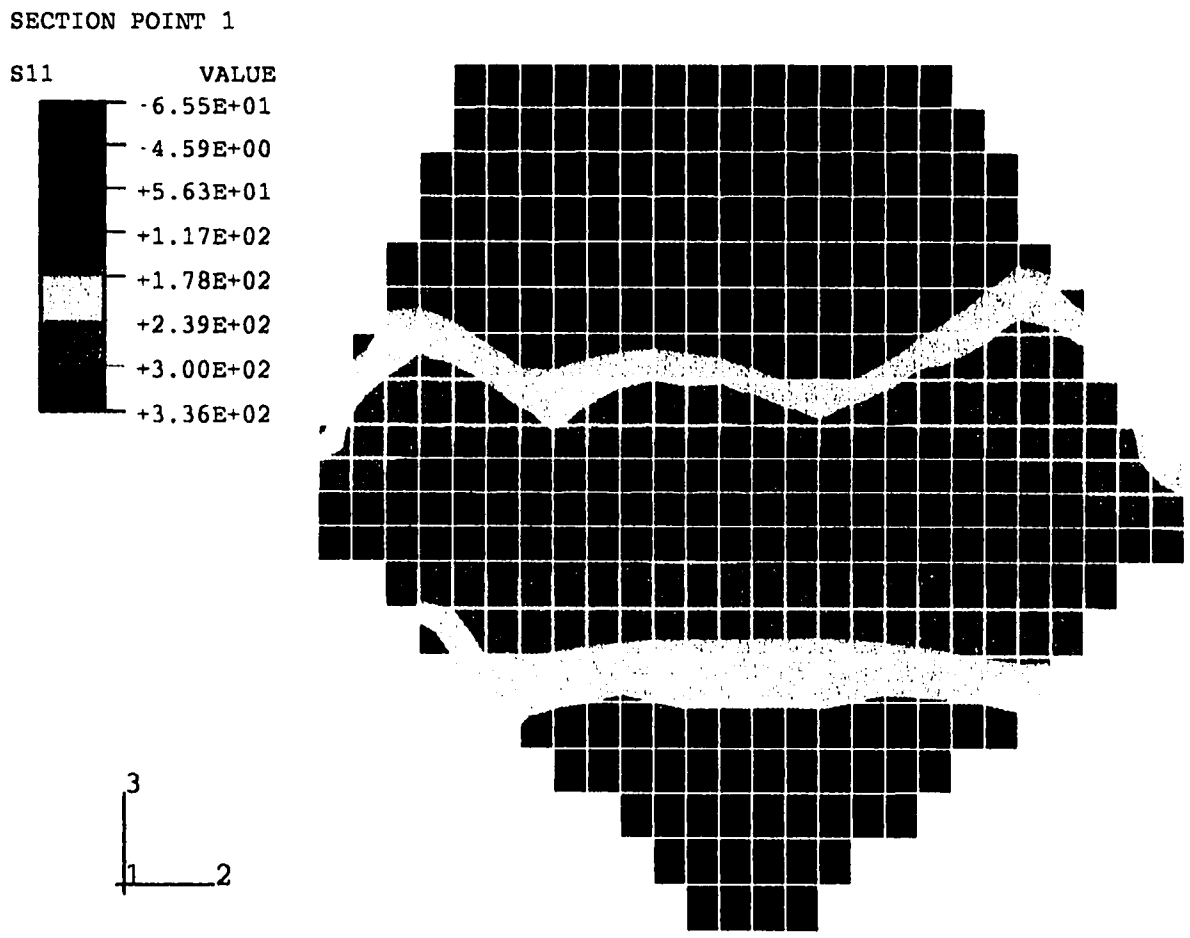

Figure 7-16. Stress distribution in the tension side of the gusset plate at ultimate load (Example II, $L/r_z = 170$)

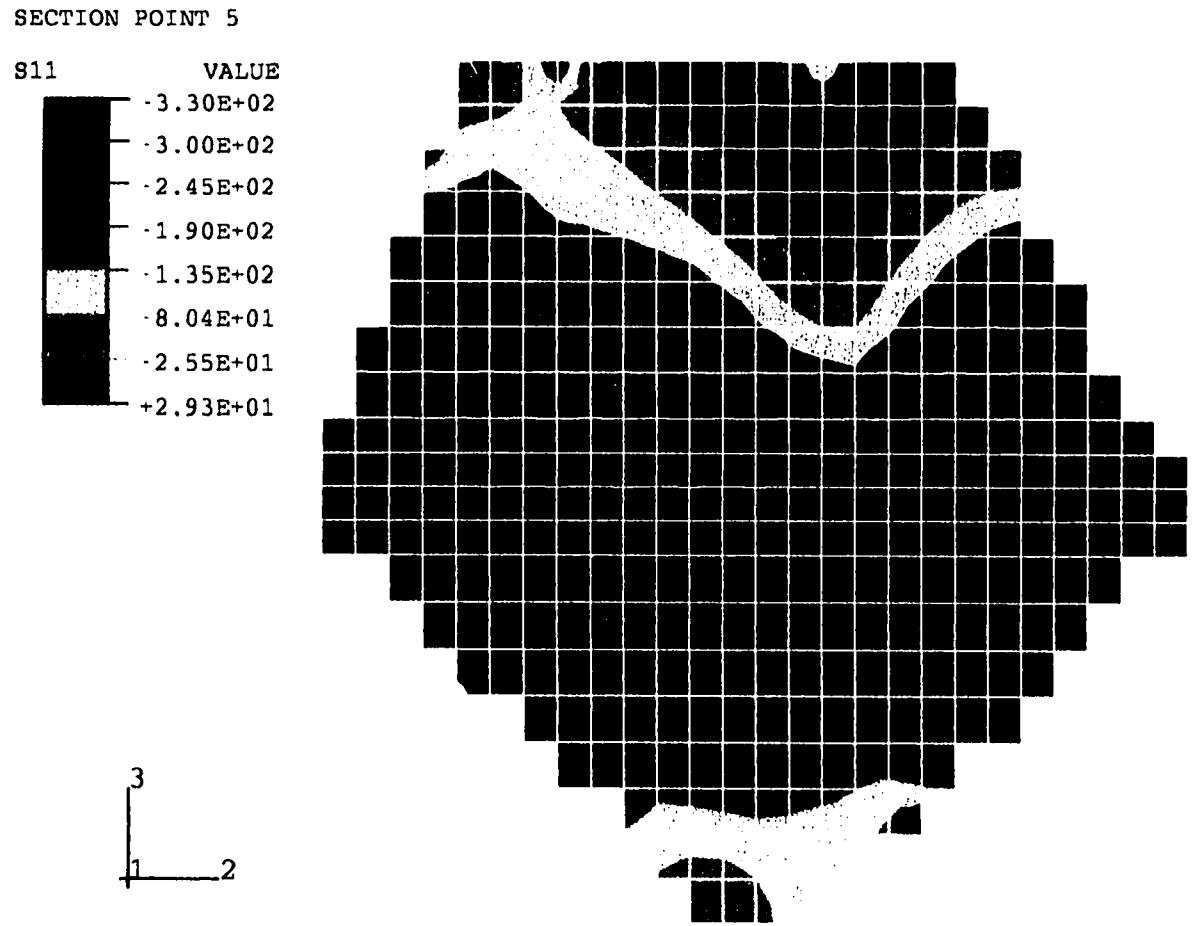

Figure 7-17. Stress distribution in the compression side of the gusset plate at ultimate load (Example II, $L/r_z = 170$)

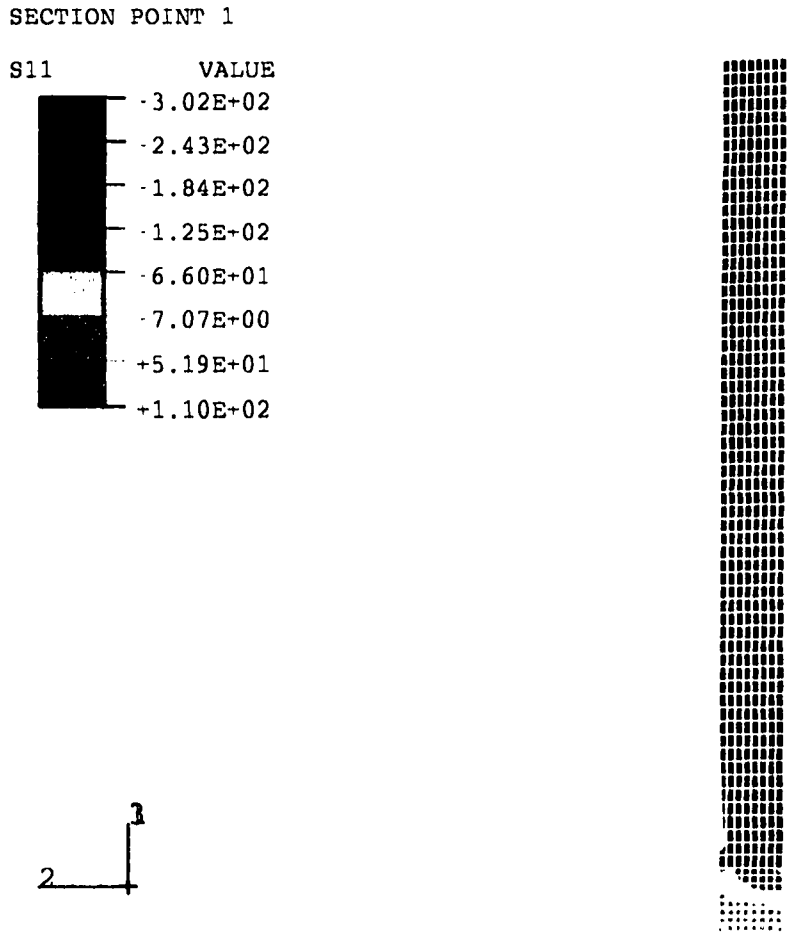

Figure 7-18. Stress distribution in the connected leg of the angle at ultimate load (Example II, $L/r_z = 170$)

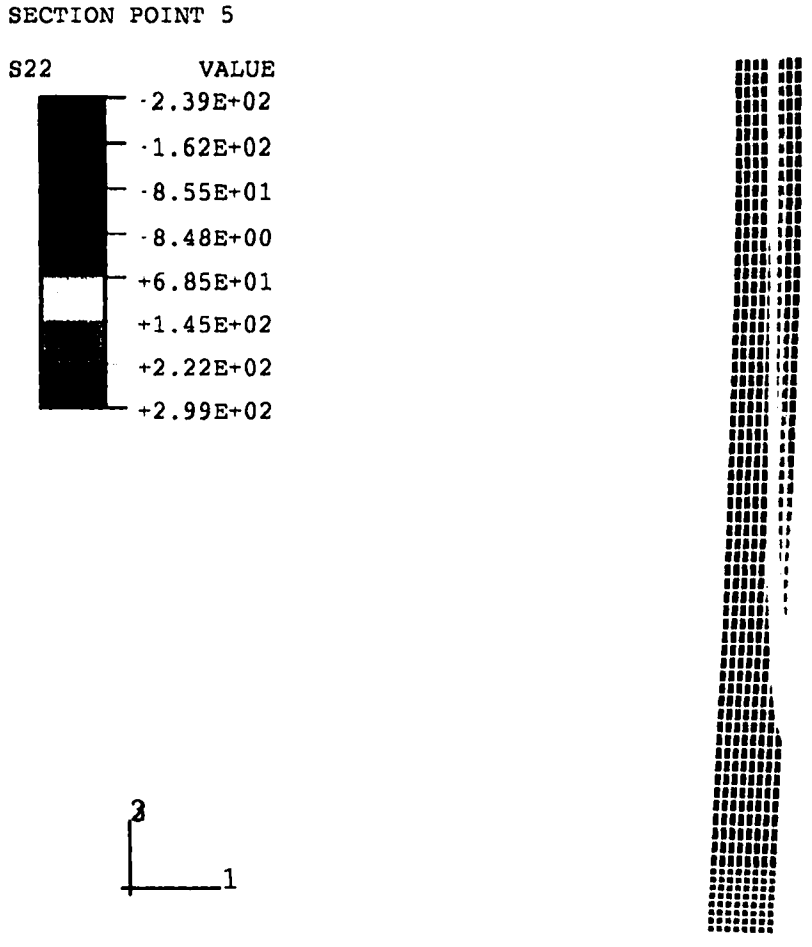

Figure 7-19. Stress distribution in the outstanding leg of the angle at ultimate load (Example II, $L/r_z = 170$)

APPENDIX A

LOAD-DEFORMATION CURVES OF TEST SPECIMENS

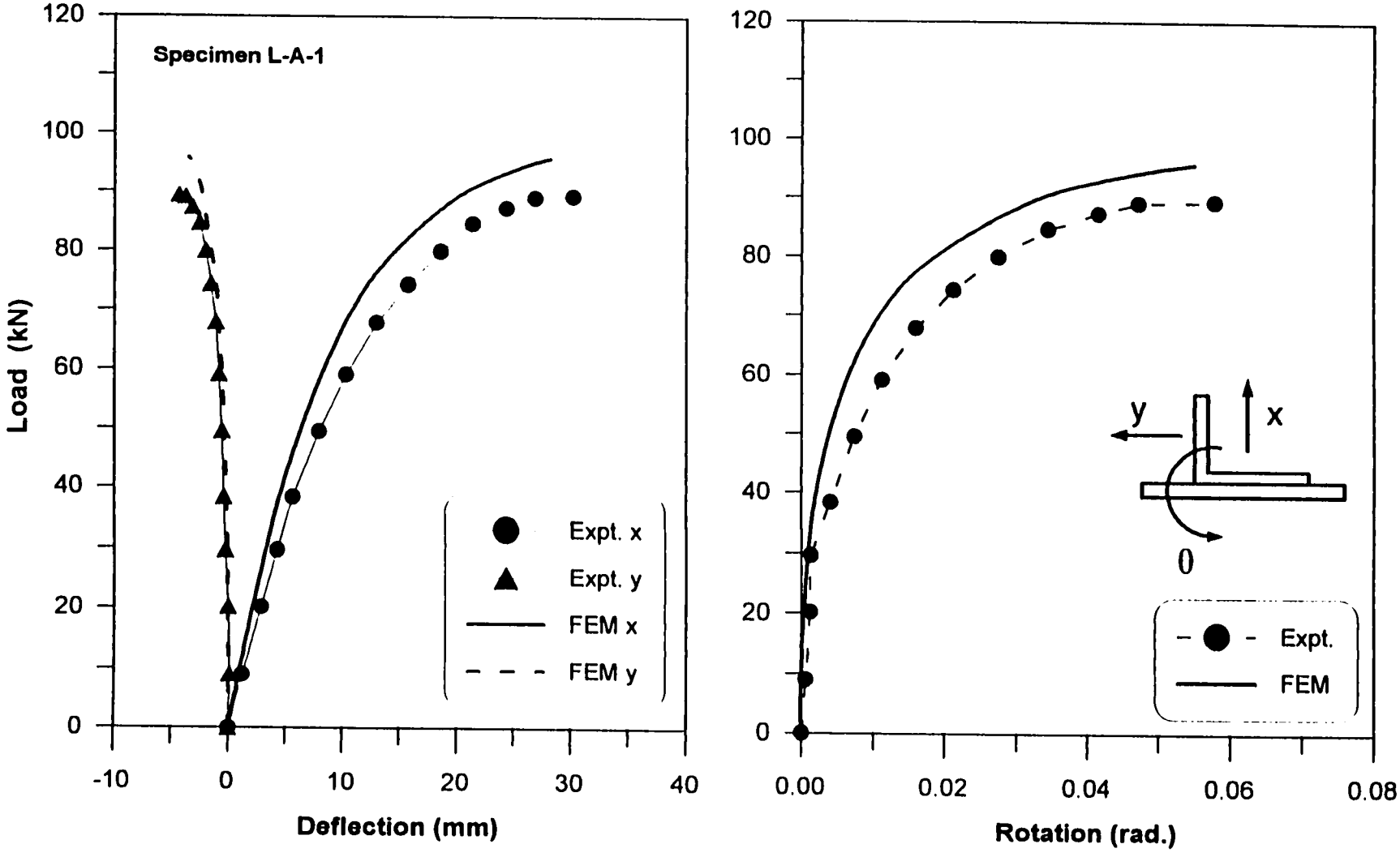

Figure A-1. Load versus deflection and rotation for Specimen L-A-1

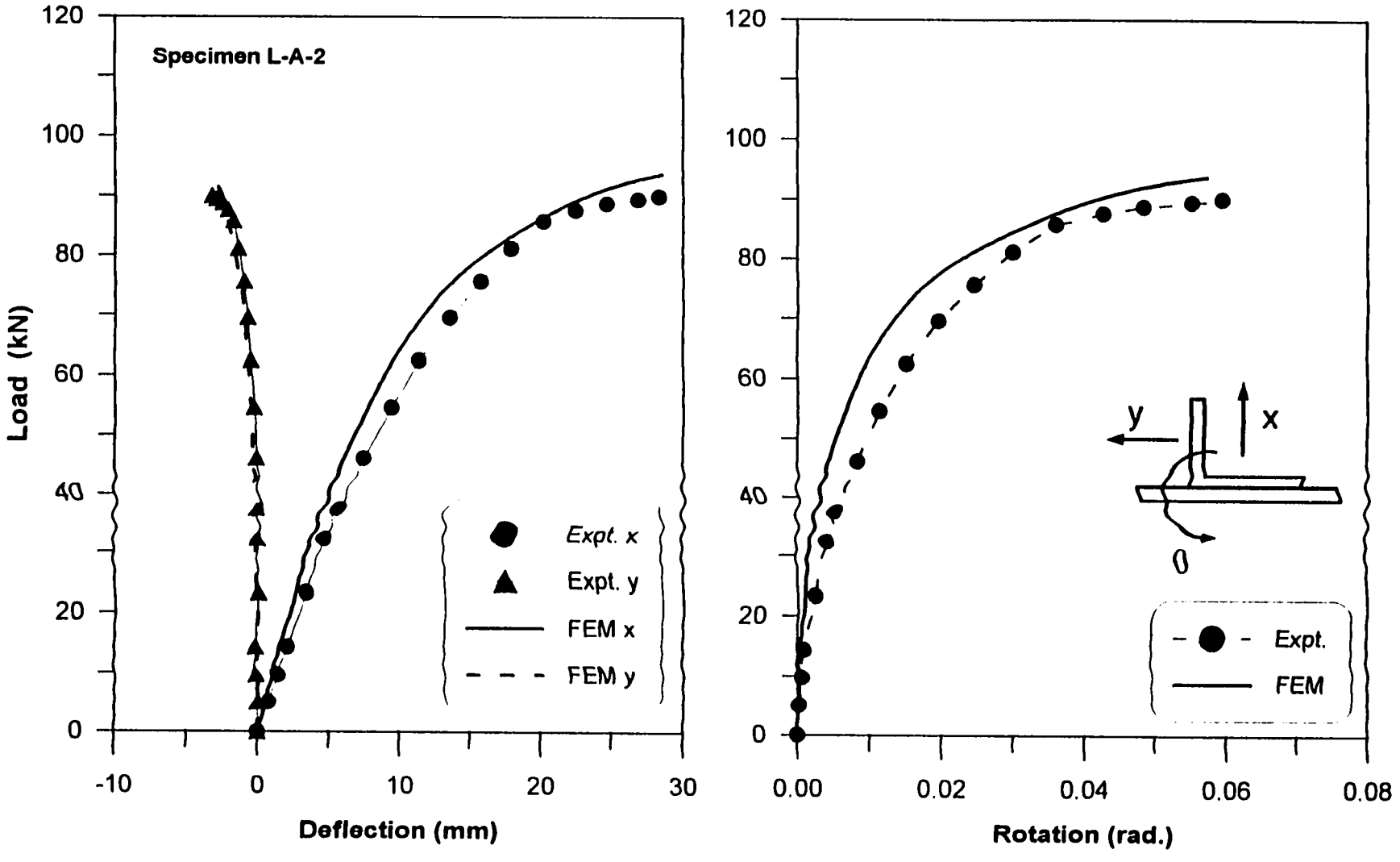

Figure A-2. Load versus deflection and rotation for Specimen L-A-2

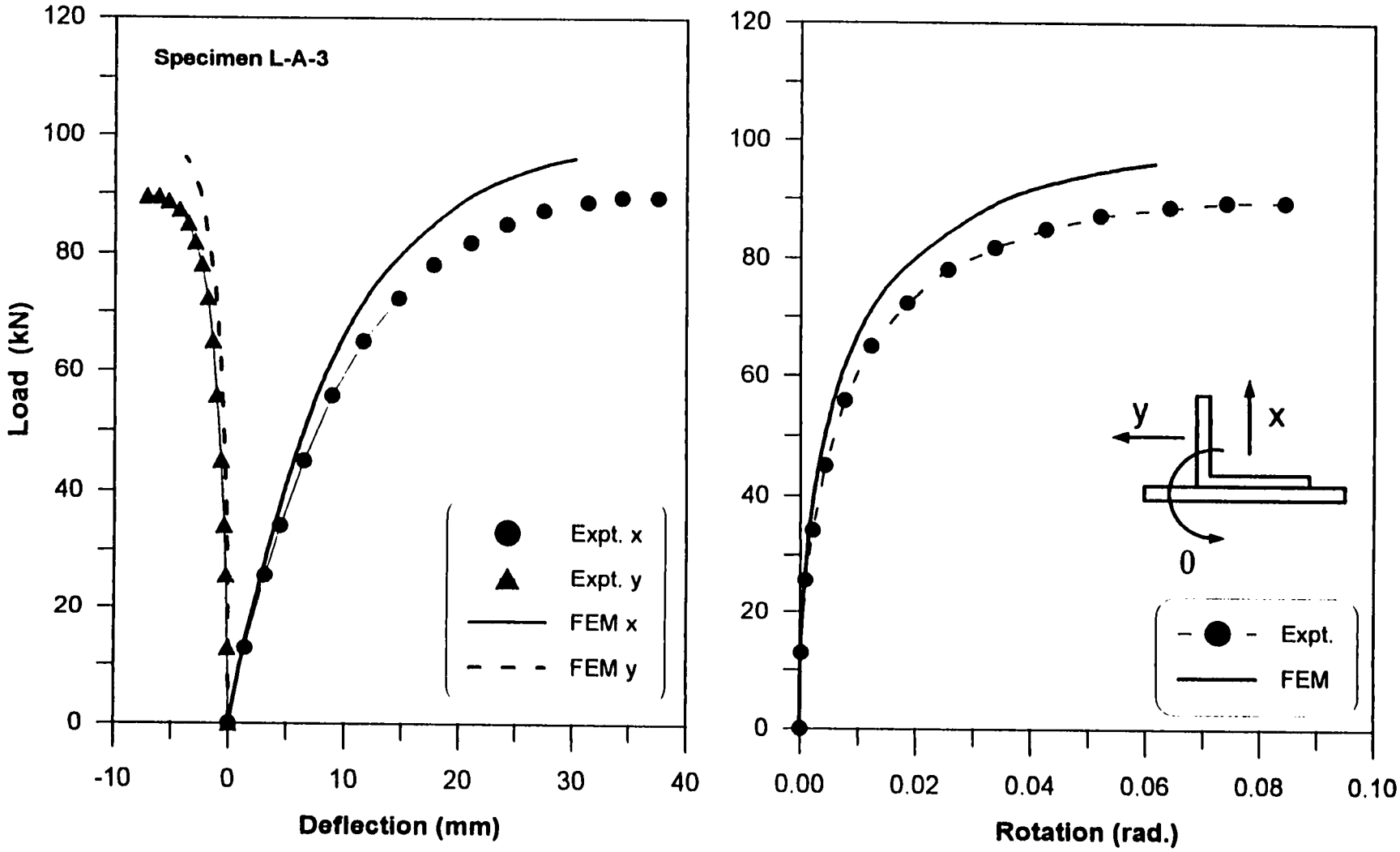

Figure A-3. Load versus deflection and rotation for Specimen L-A-3

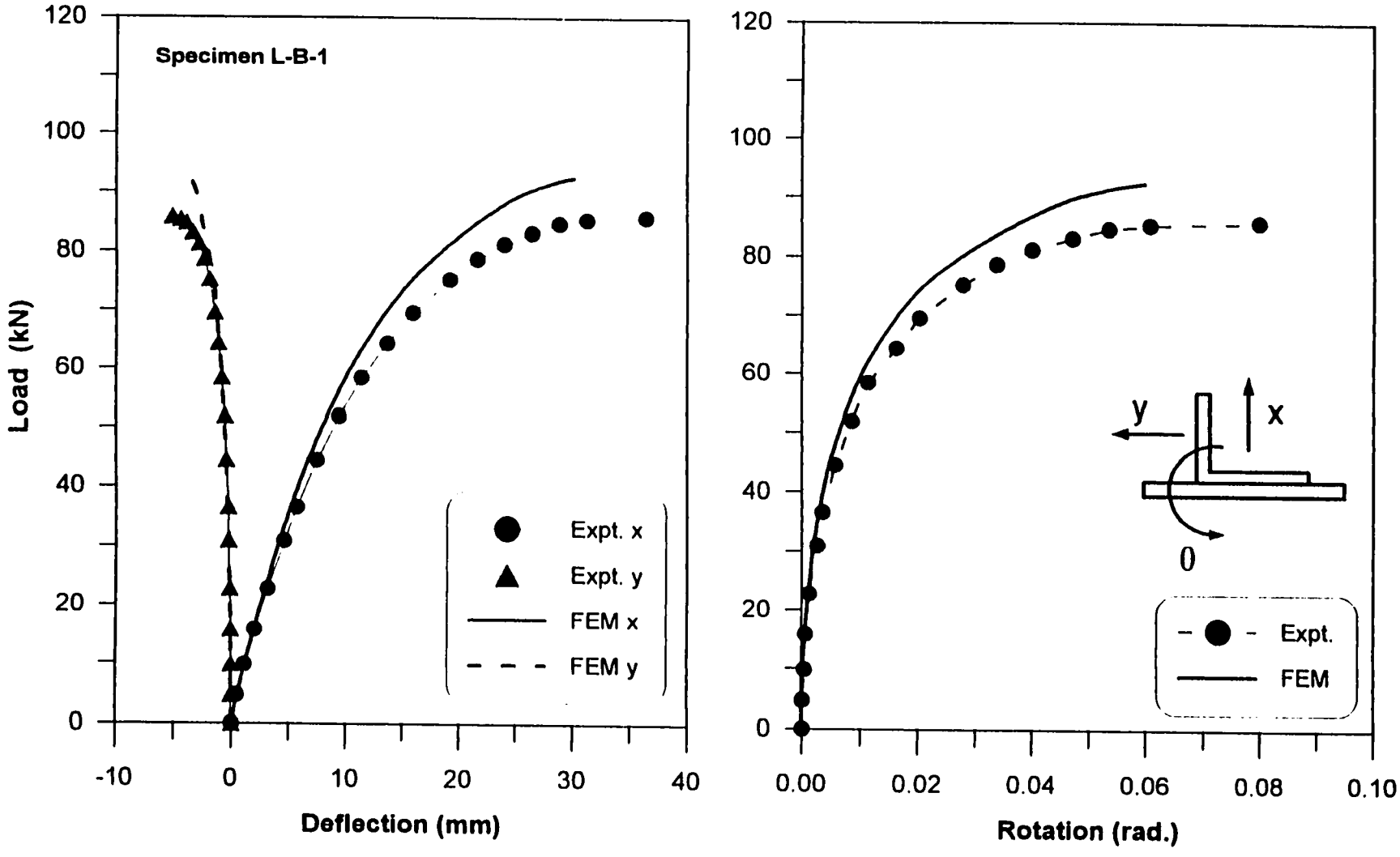

Figure A-4. Load versus deflection and rotation for Specimen L-B-1

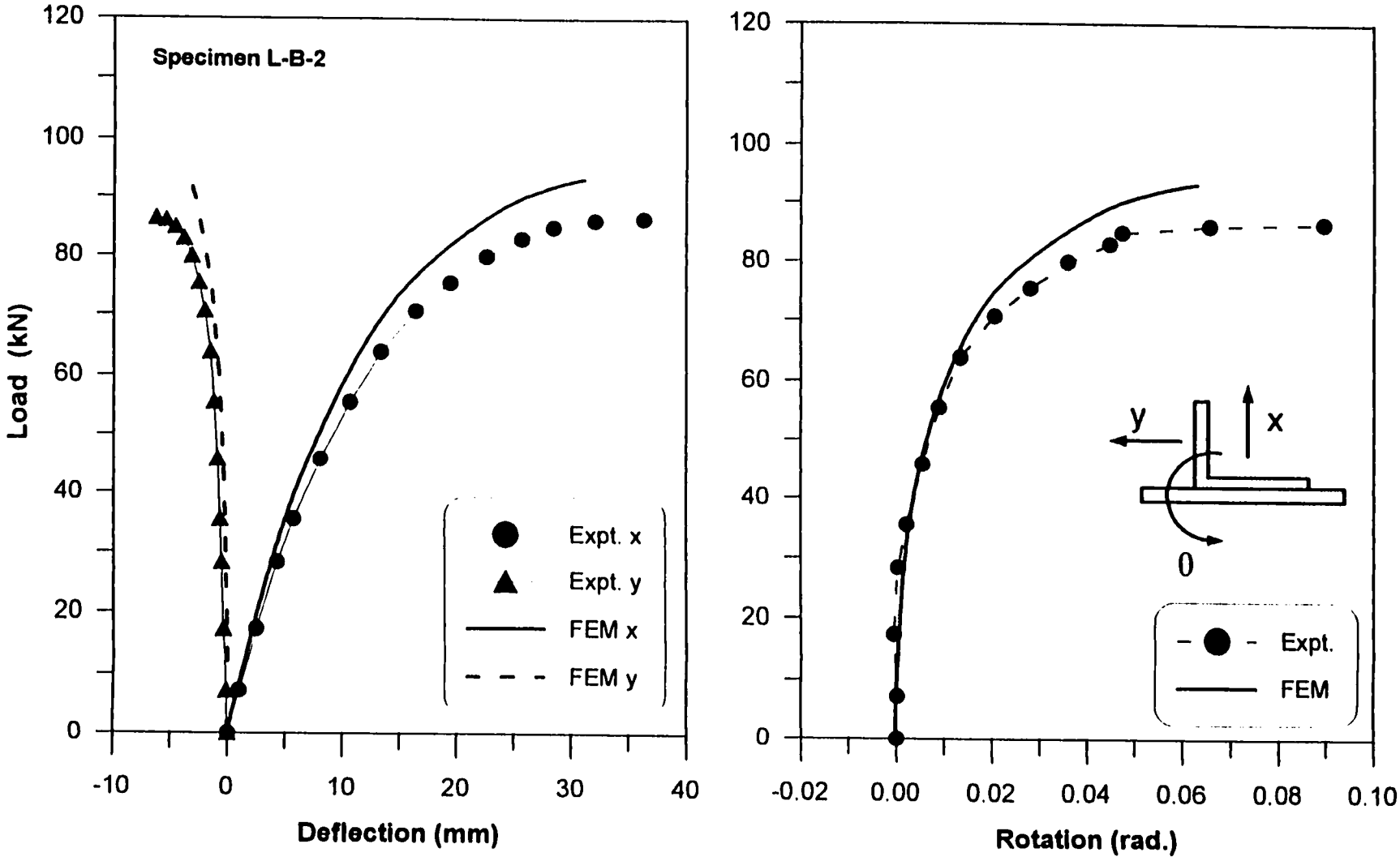

Figure A-5. Load versus deflection and rotation for Specimen L-B-2

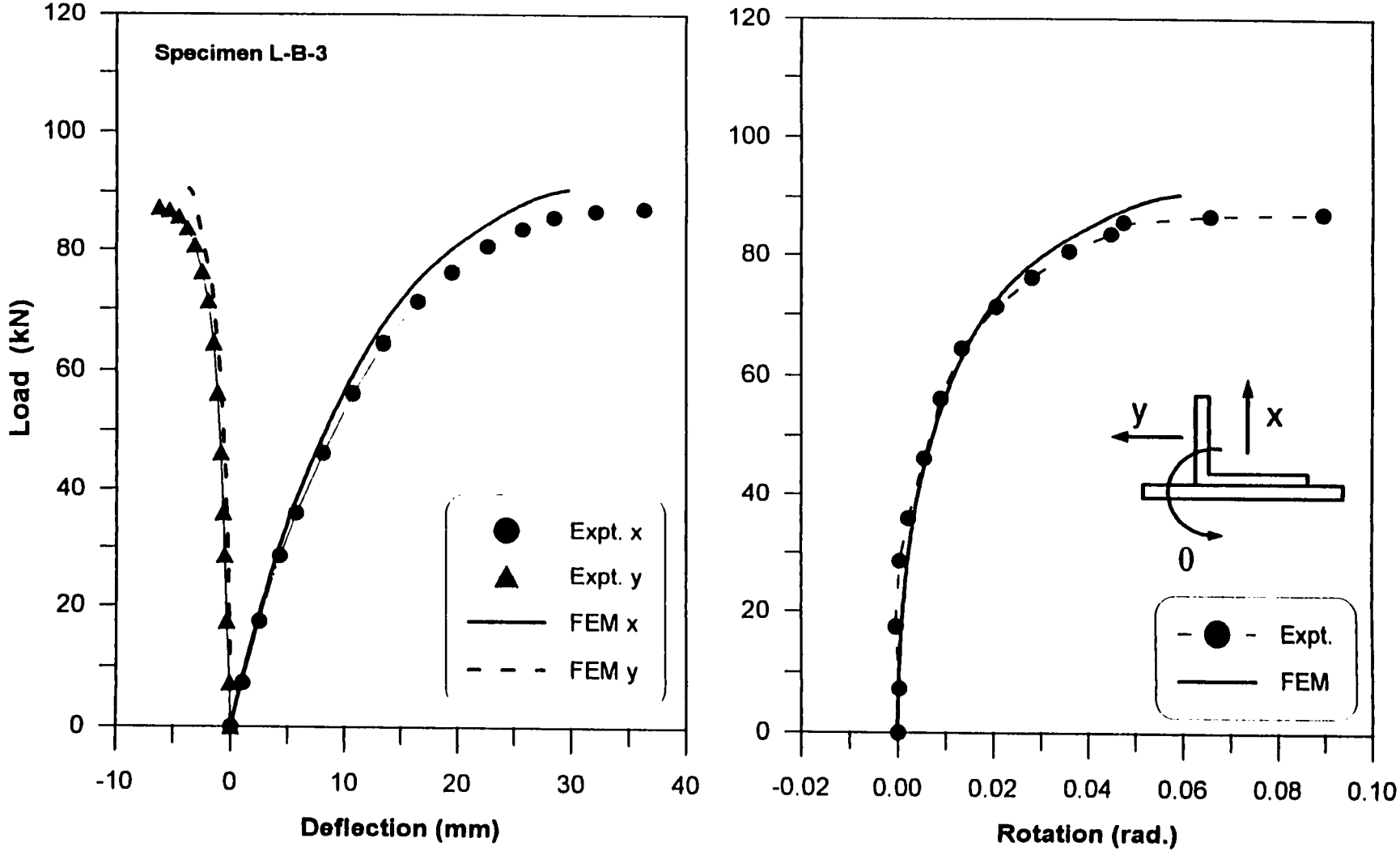

Figure A-6. Load versus deflection and rotation for Specimen L-B-3

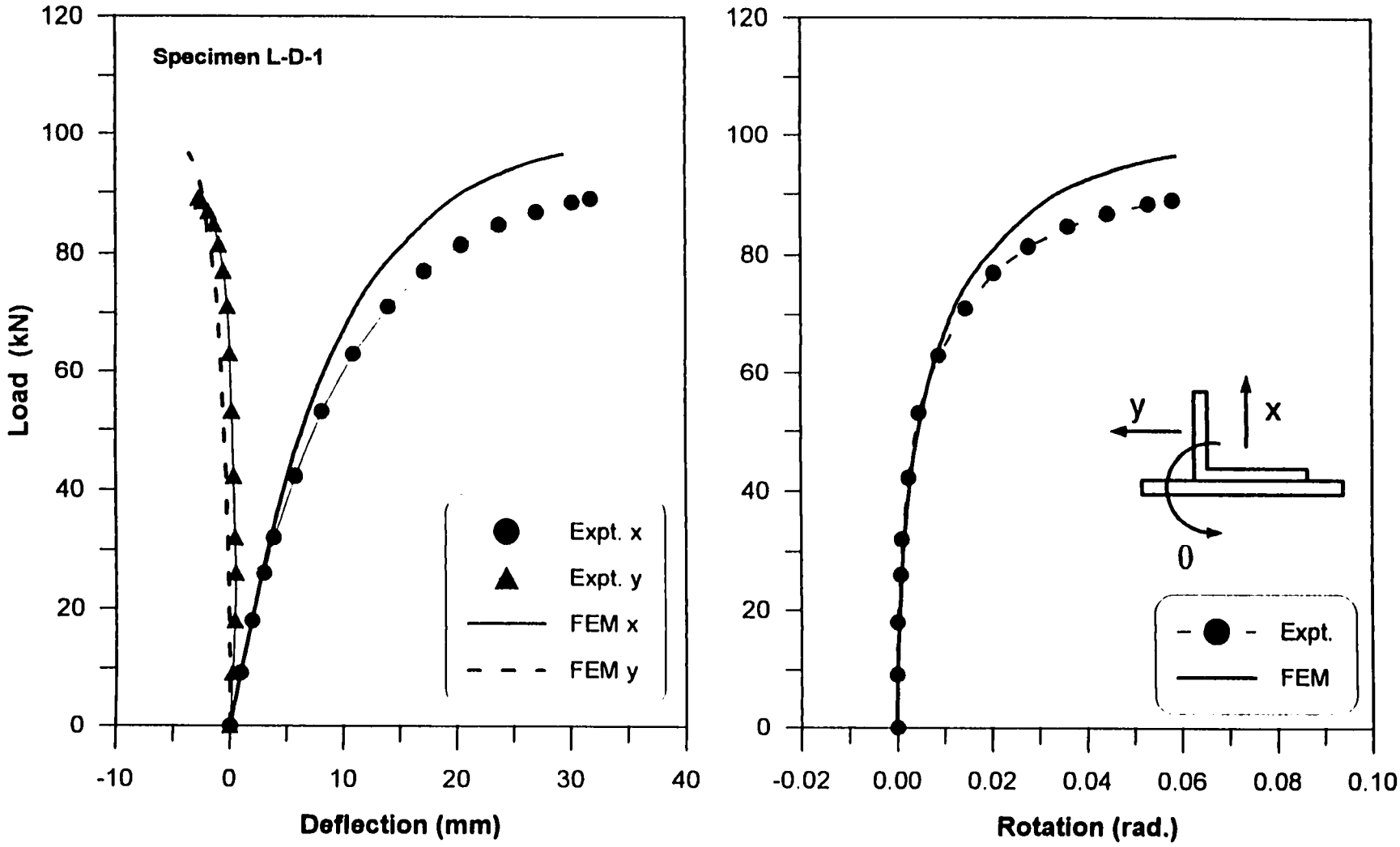

Figure A-7. Load versus deflection and rotation for Specimen L-D-1

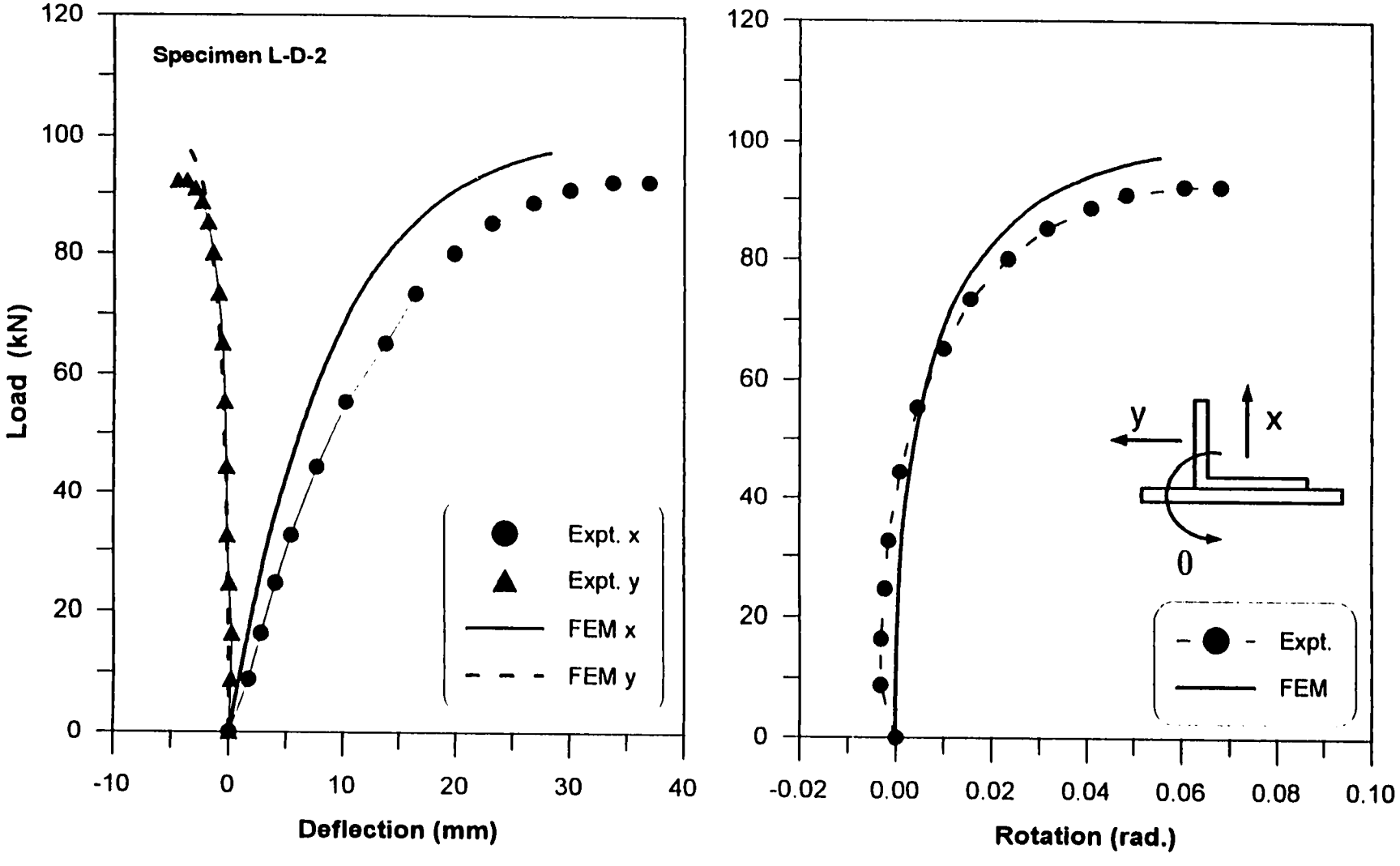

Figure A-8. Load versus deflection and rotation for Specimen L-D-2

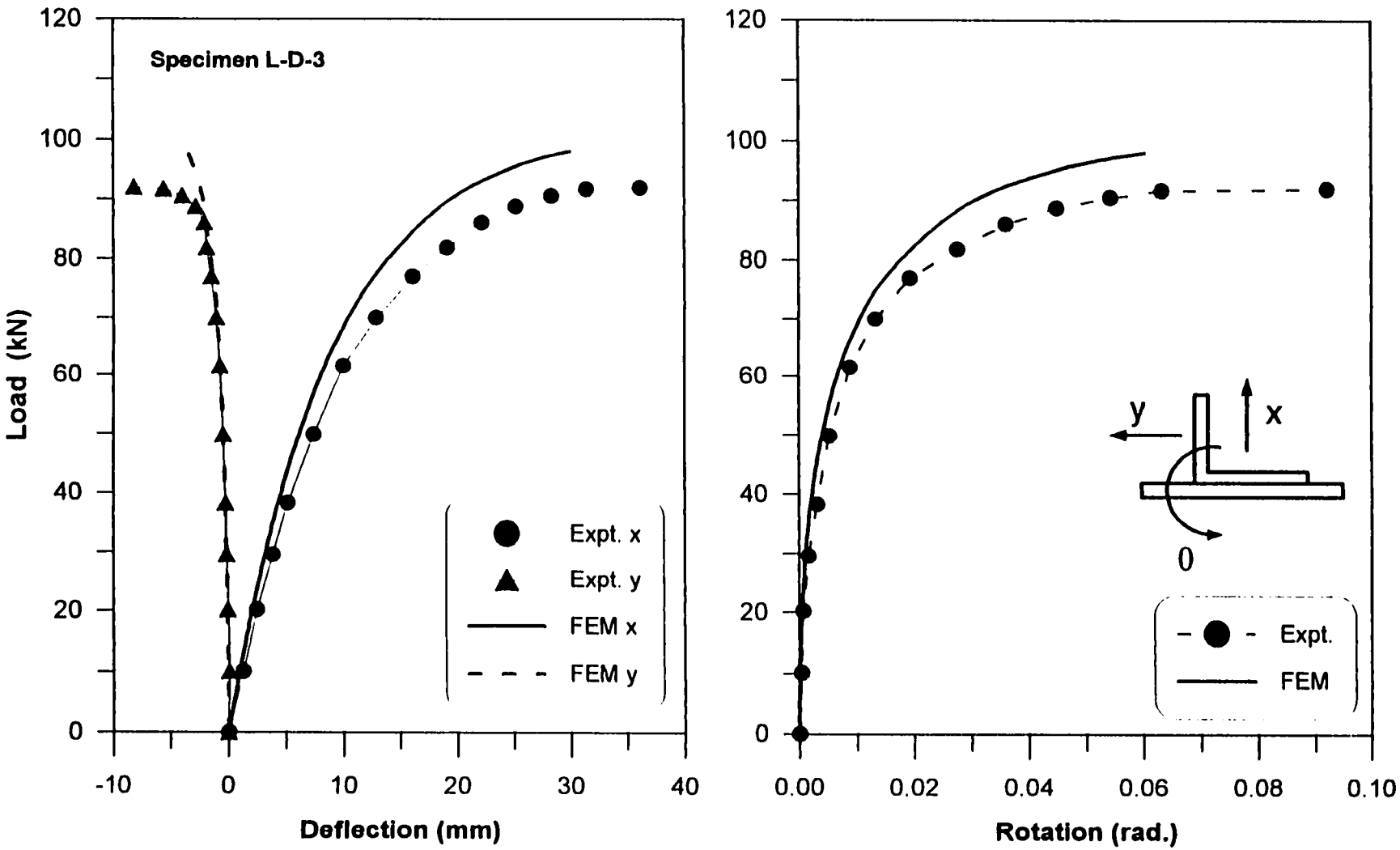

Figure A-9. Load versus deflection and rotation for Specimen L-D-3

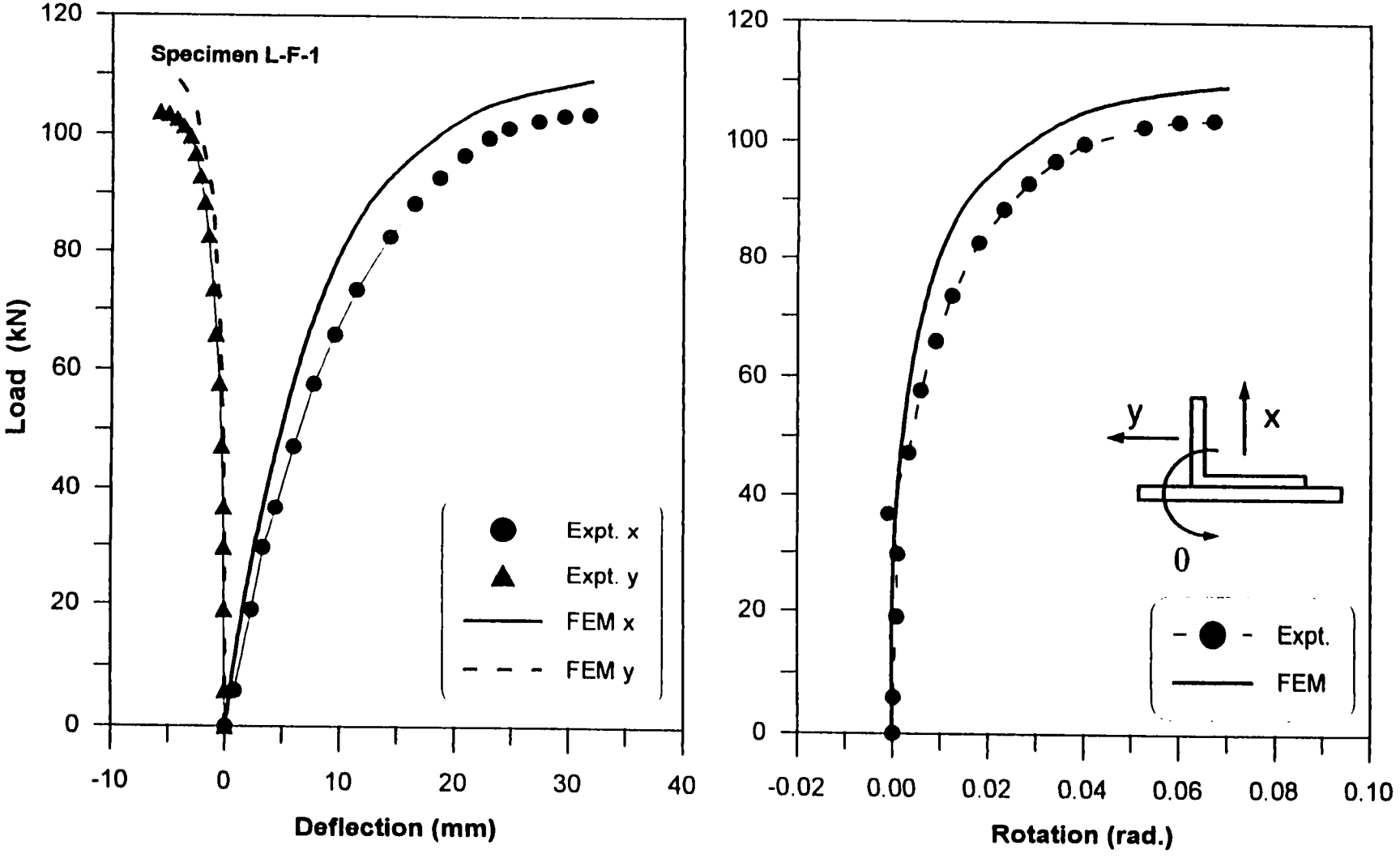

Figure A-10. Load versus deflection and rotation for Specimen L-F-1

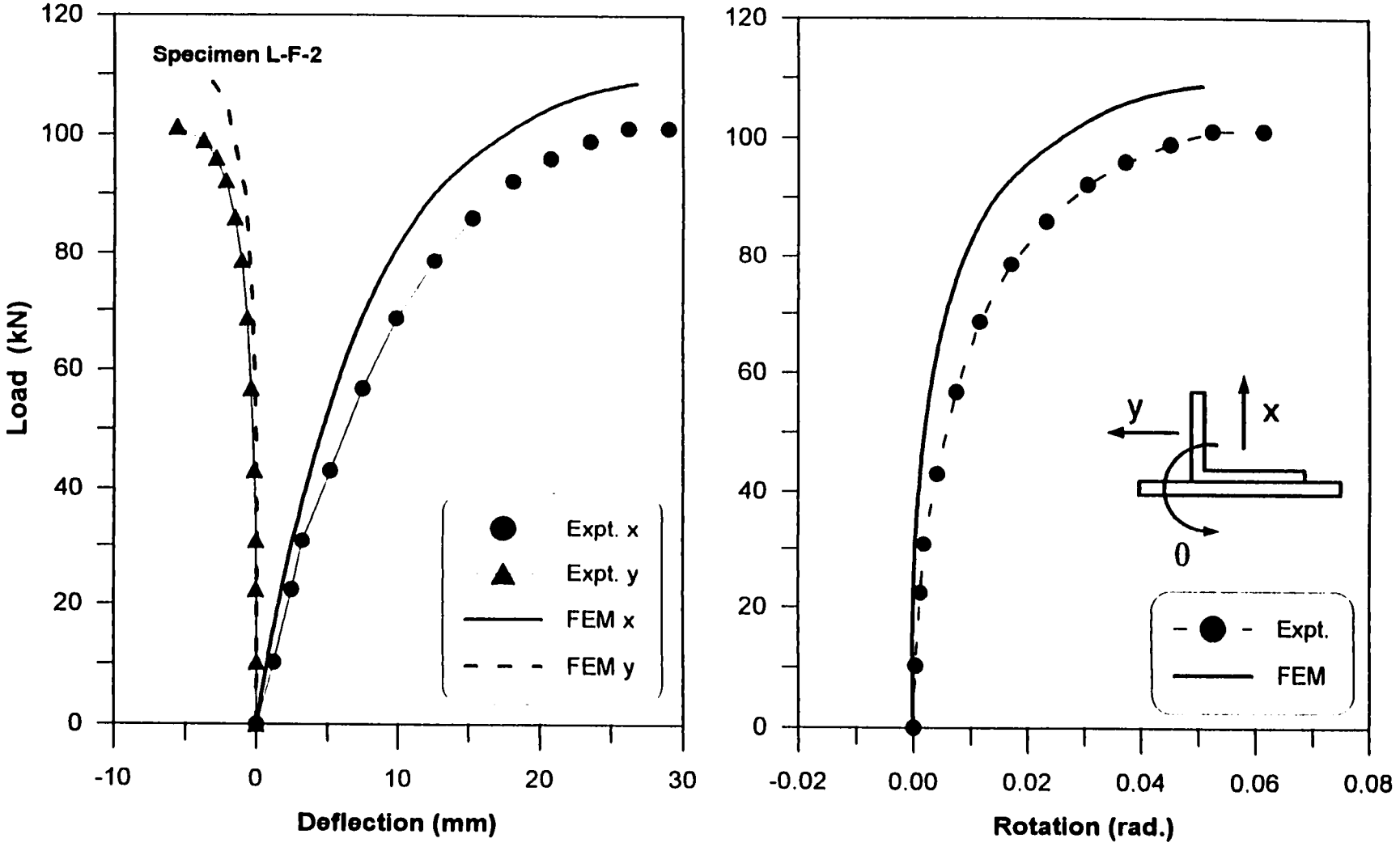

Figure A-11. Load versus deflection and rotation for Specimen L-F-2

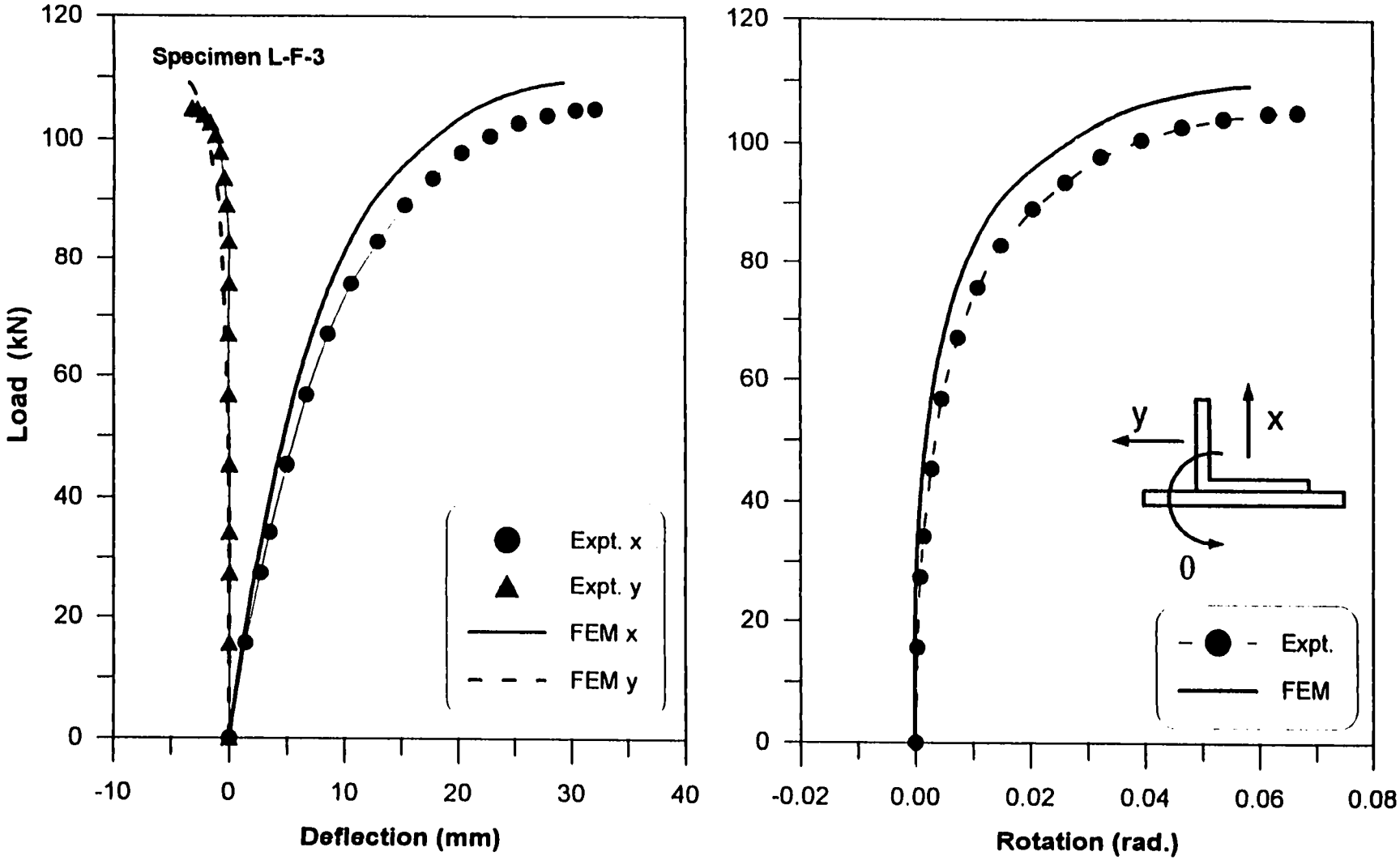

Figure A-12. Load versus deflection and rotation for Specimen L-F-3

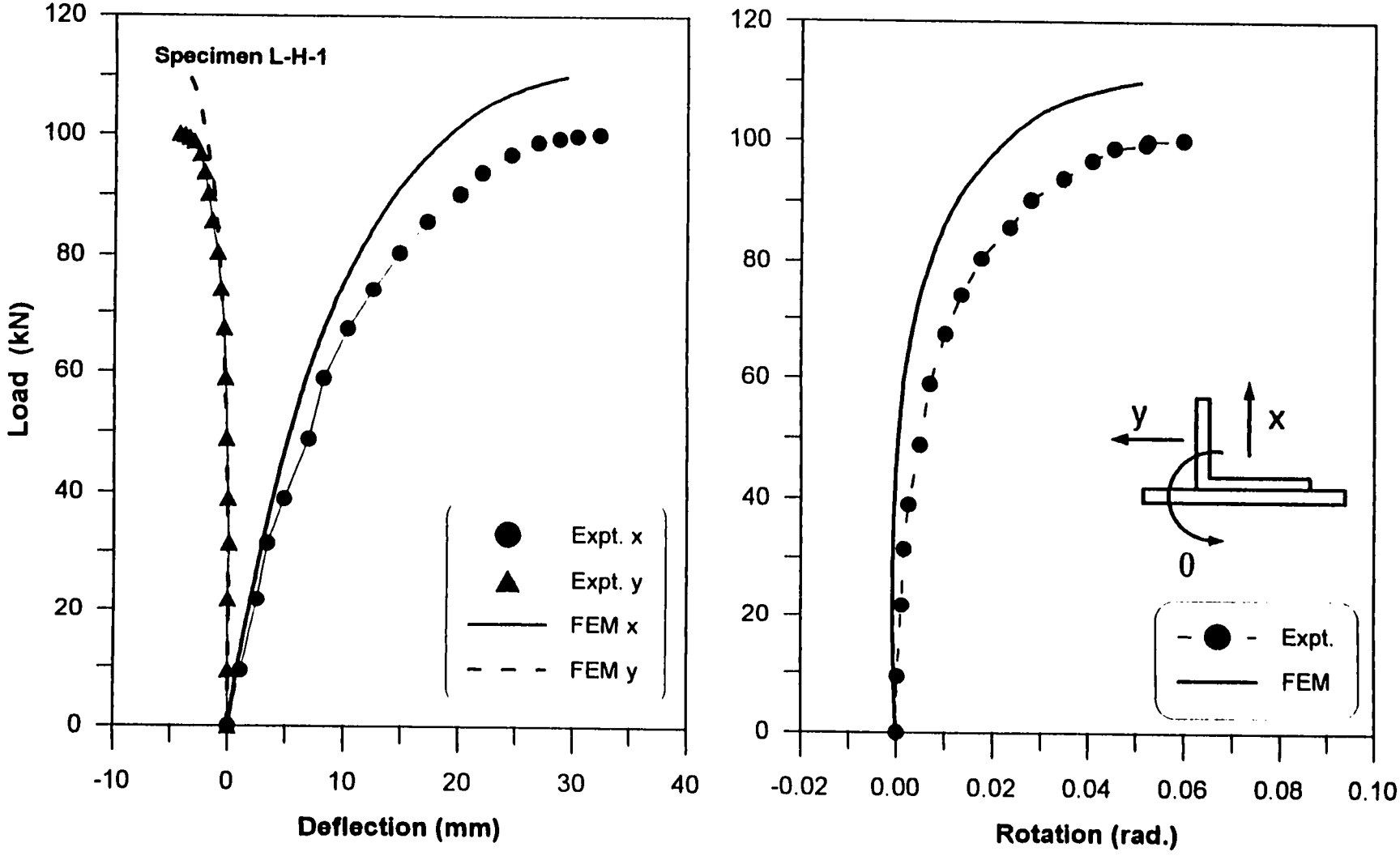

Figure A-13. Load versus deflection and rotation for Specimen L-H-1

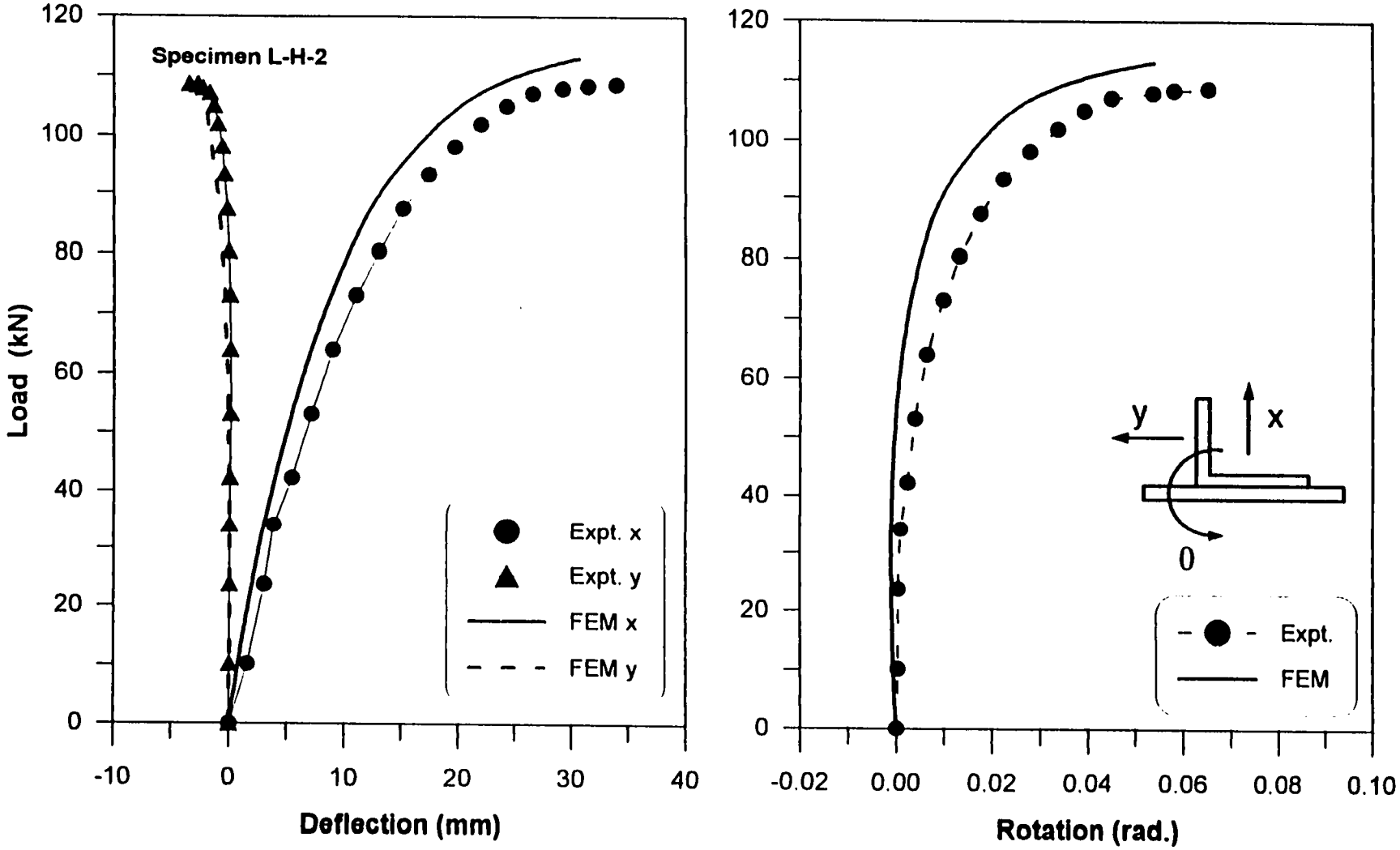

Figure A-14. Load versus deflection and rotation for Specimen L-H-2

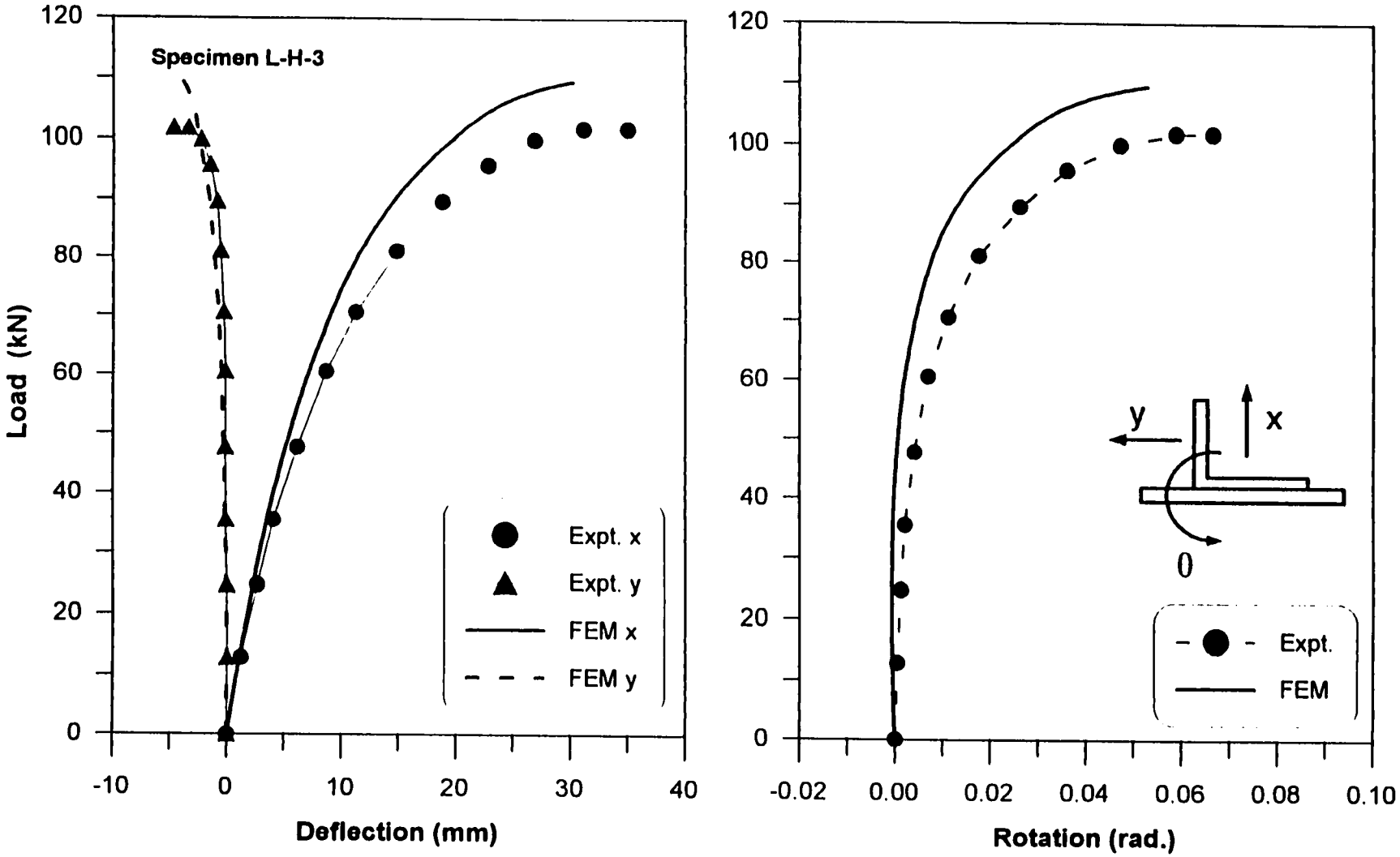

Figure A-15. Load versus deflection and rotation for Specimen L-H-3

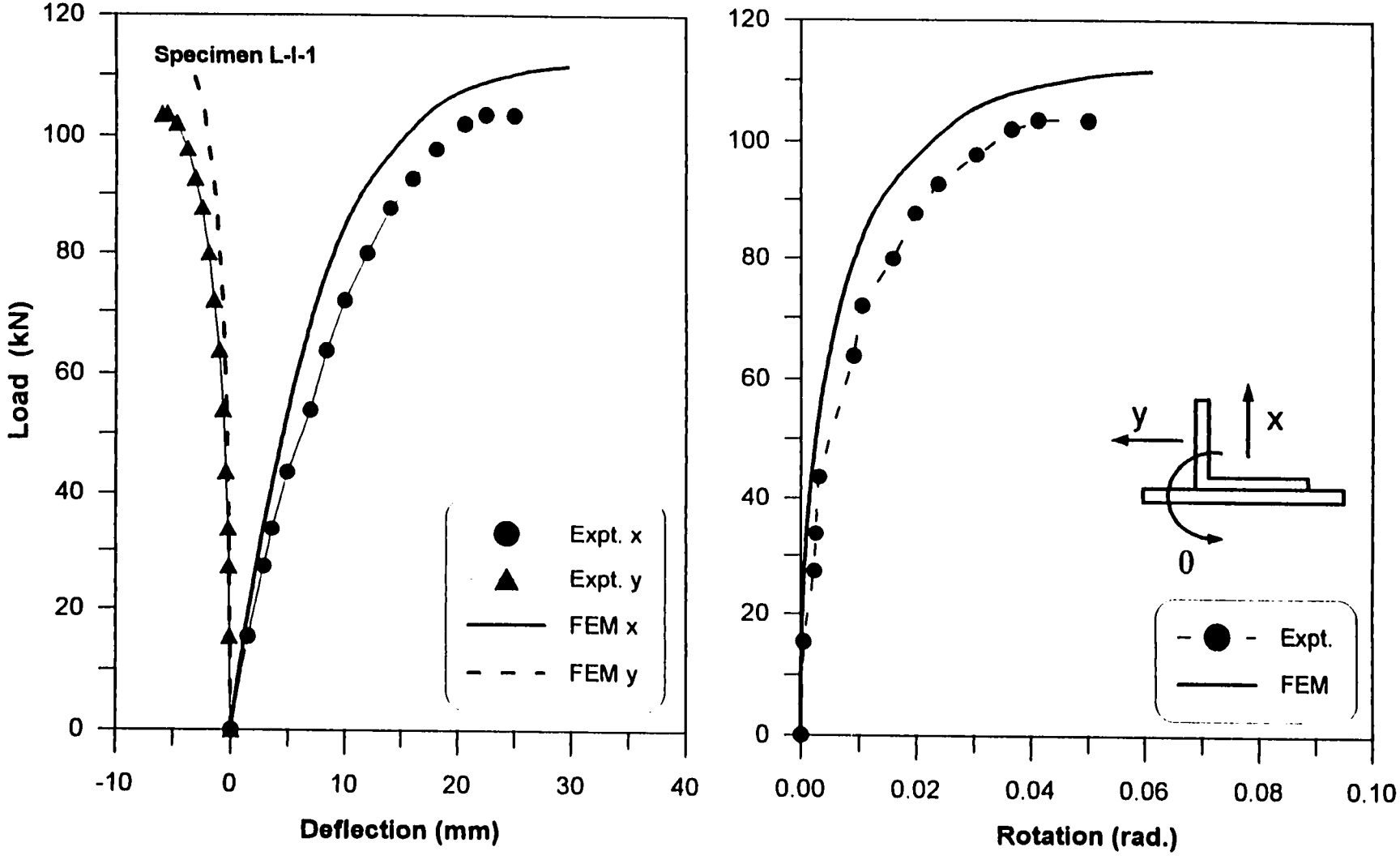

Figure A-16. Load versus deflection and rotation for Specimen L-I-1

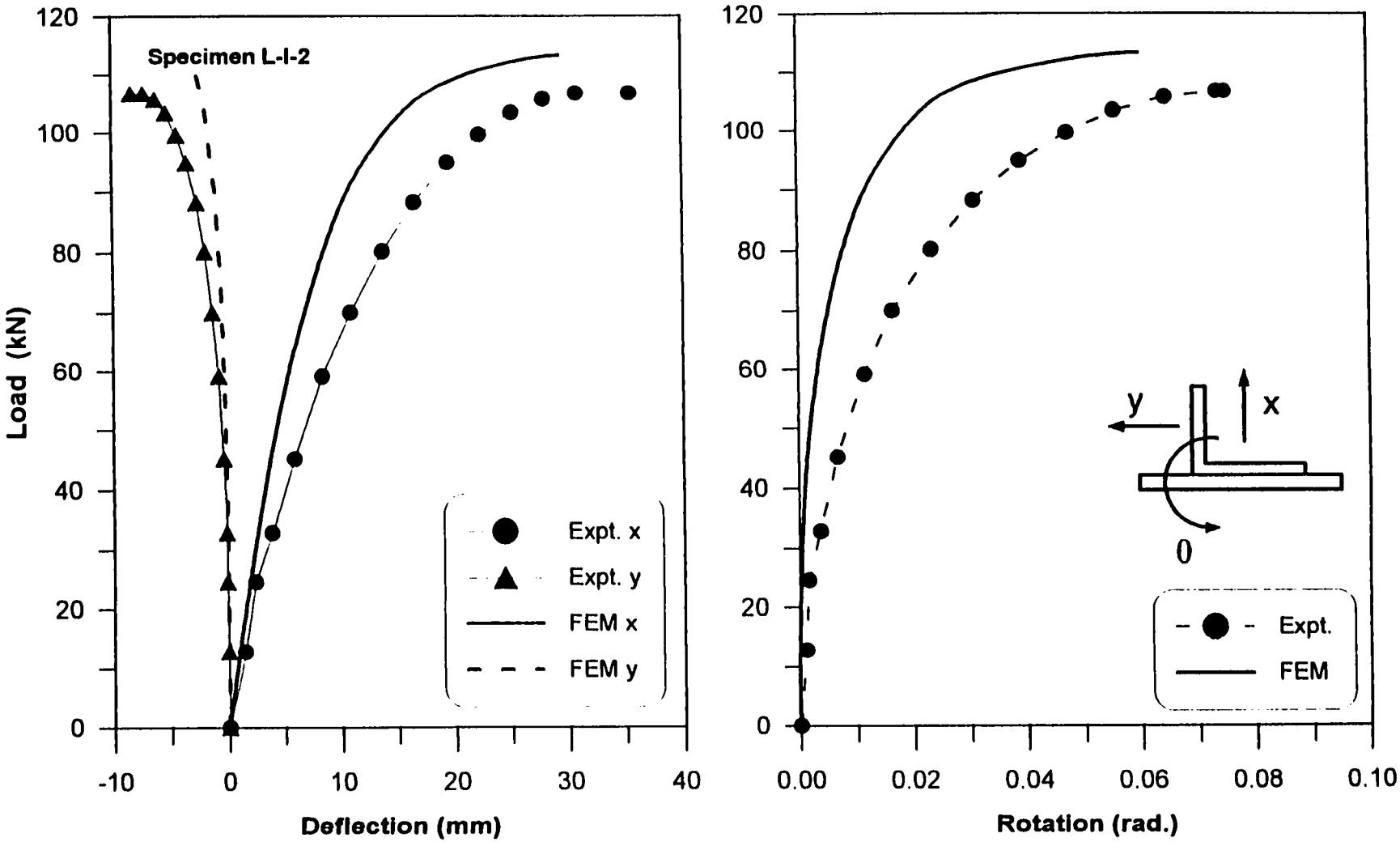

Figure A-17. Load versus deflection and rotation for Specimen L-I-2

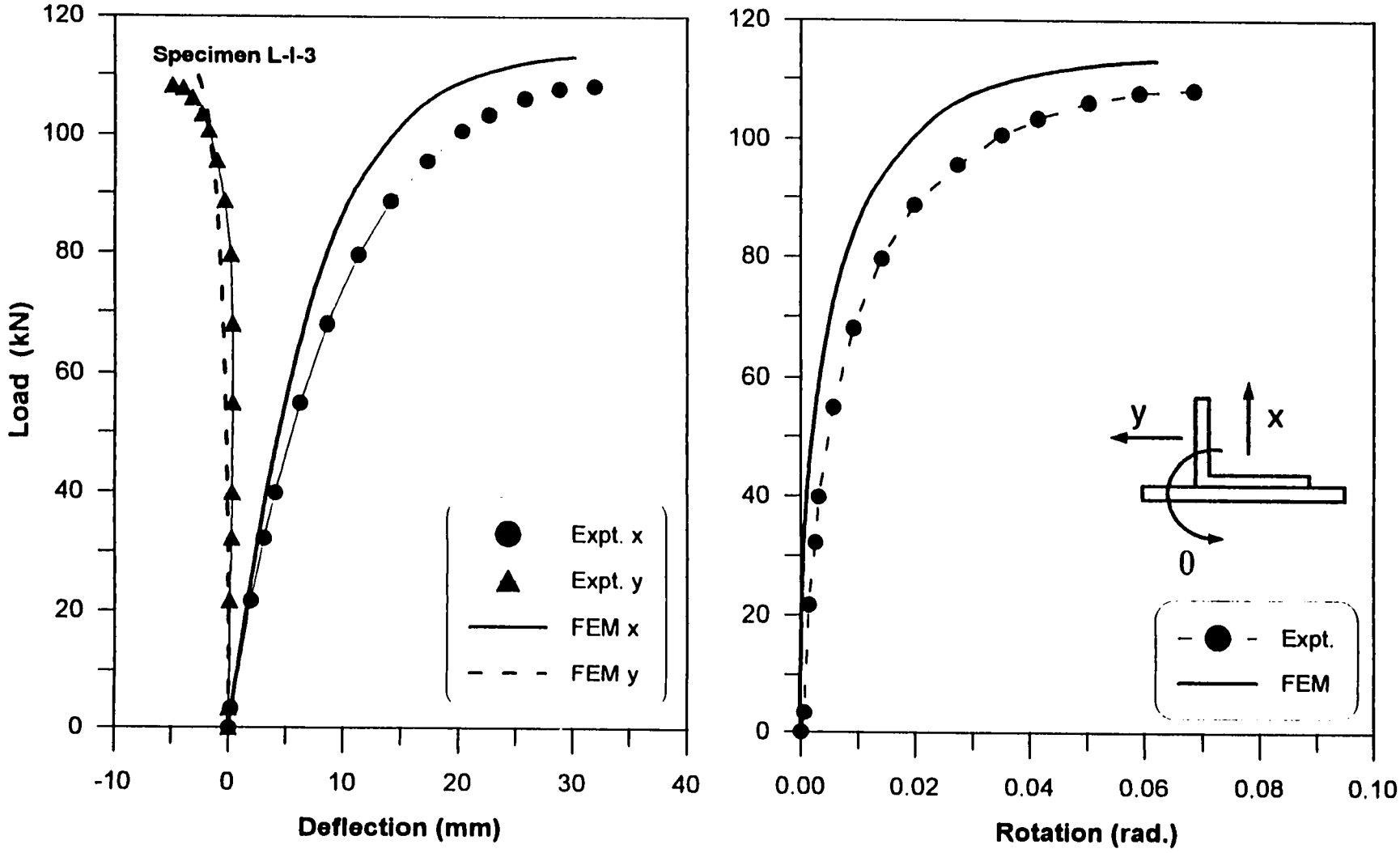

Figure A-18. Load versus deflection and rotation for Specimen L-I-3

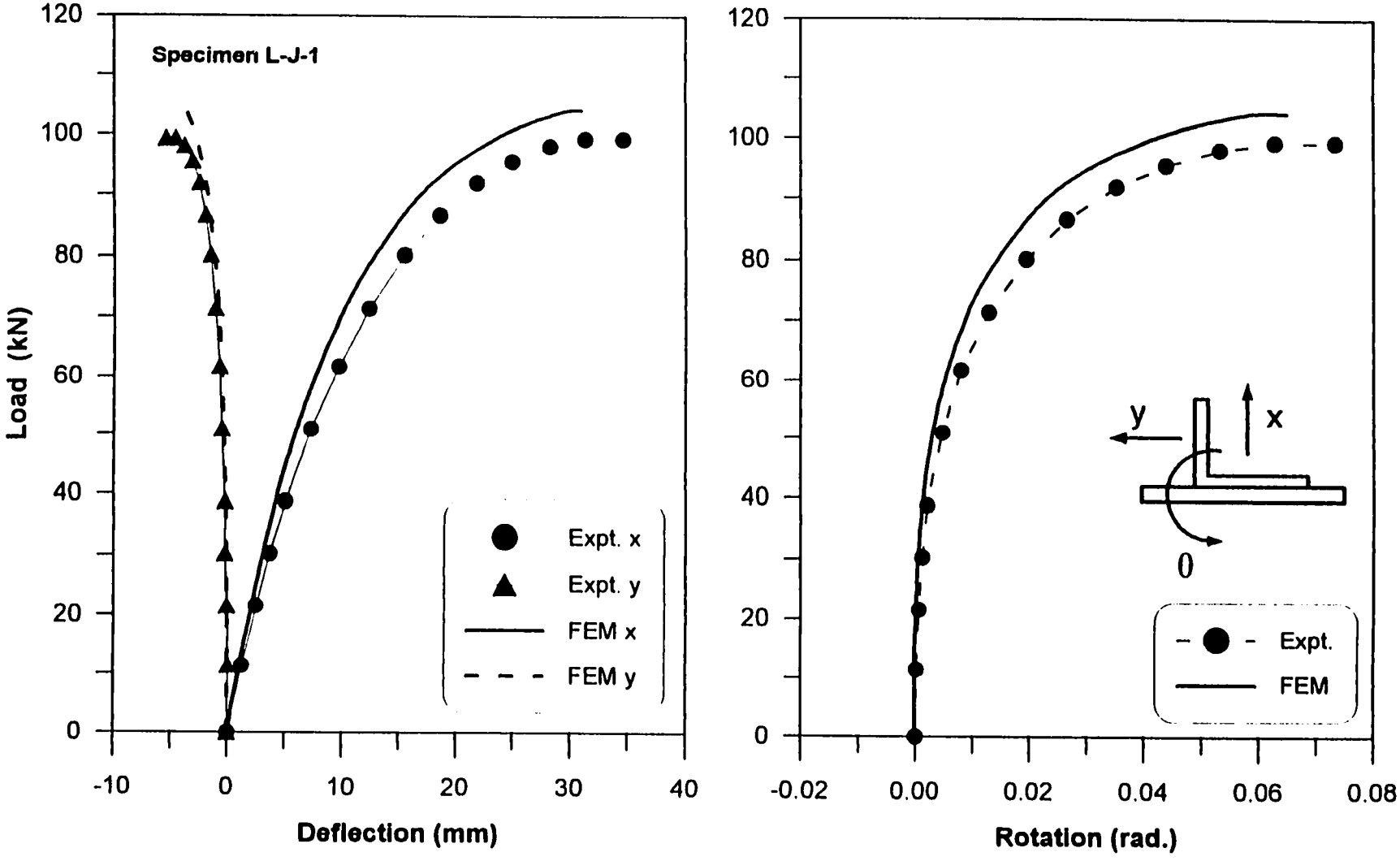

Figure A-19. Load versus deflection and rotation for Specimen L-J-1

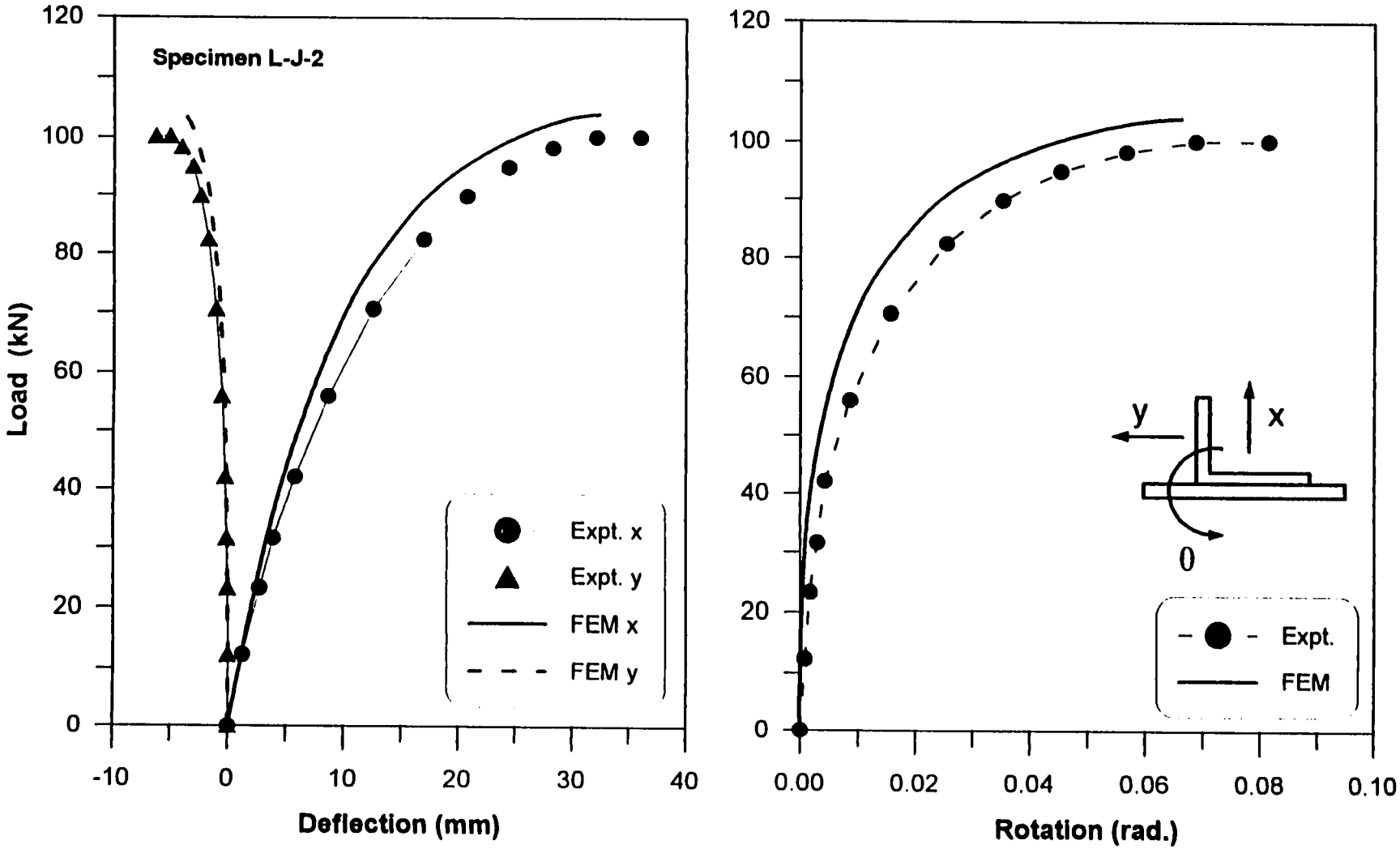

Figure A-20. Load versus deflection and rotation for Specimen L-J-2

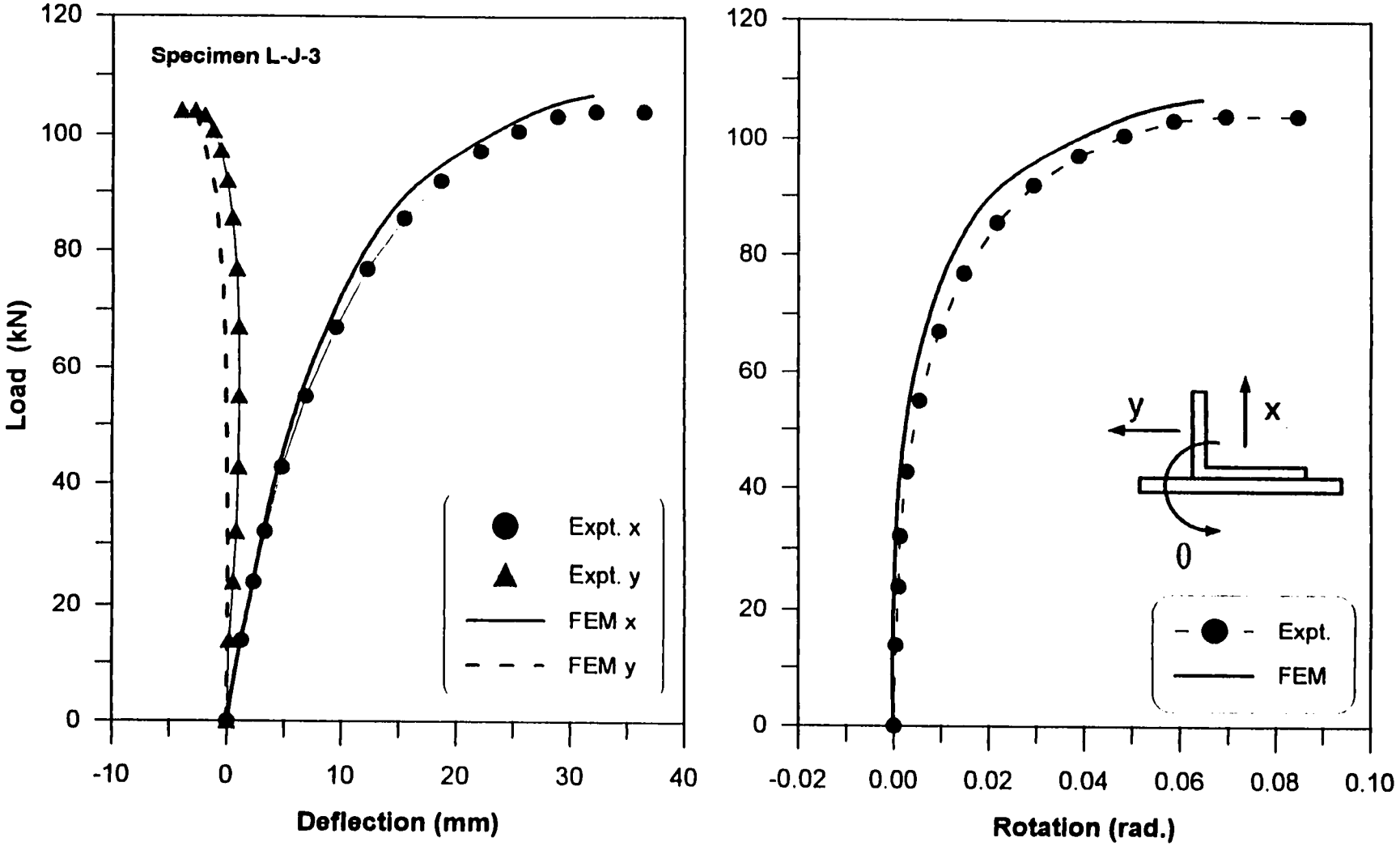

Figure A-21. Load versus deflection and rotation for Specimen L-J-3

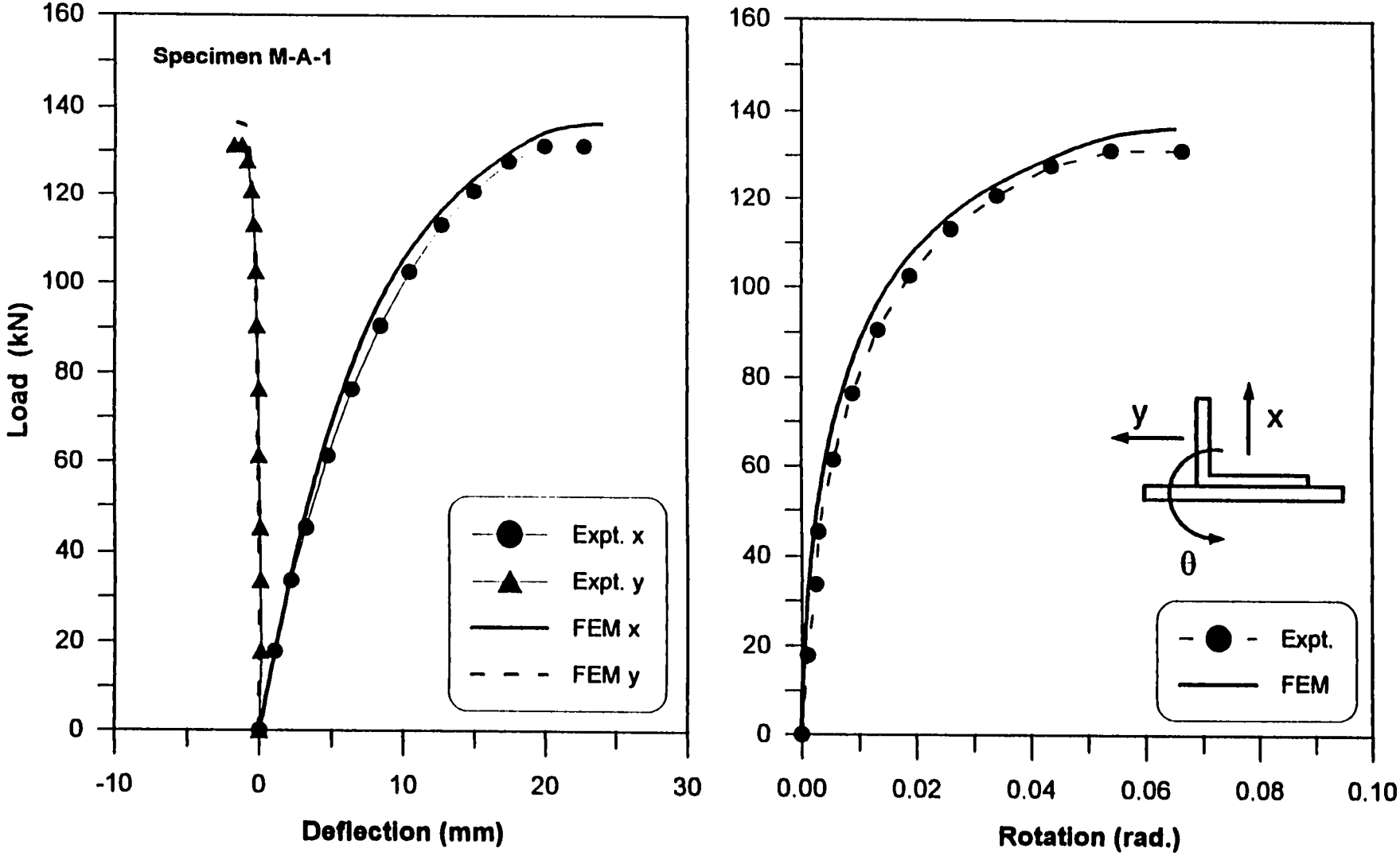

Figure A-22. Load versus deflection and rotation for Specimen M-A-1

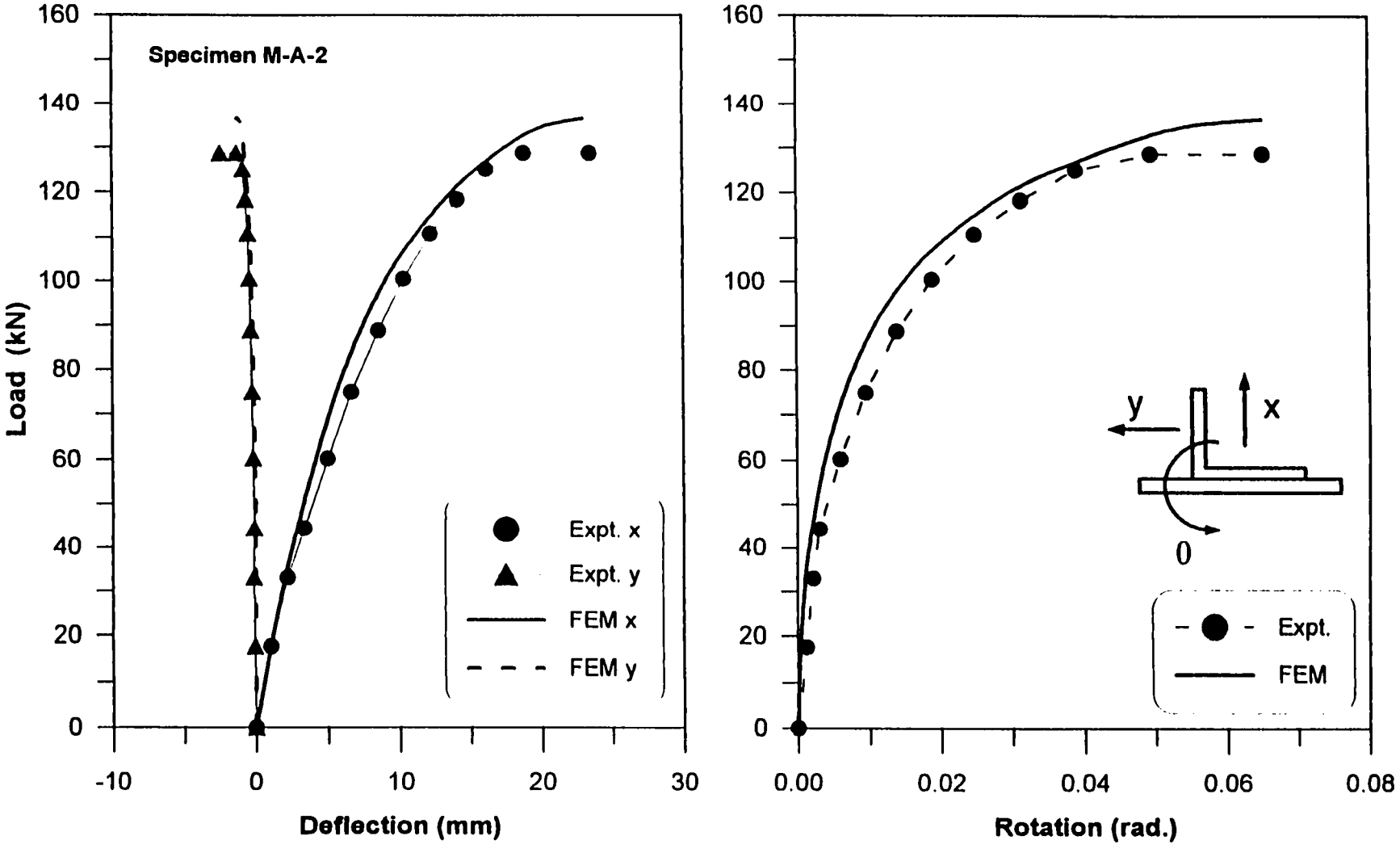

Figure A-23. Load versus deflection and rotation for Specimen M-A-2

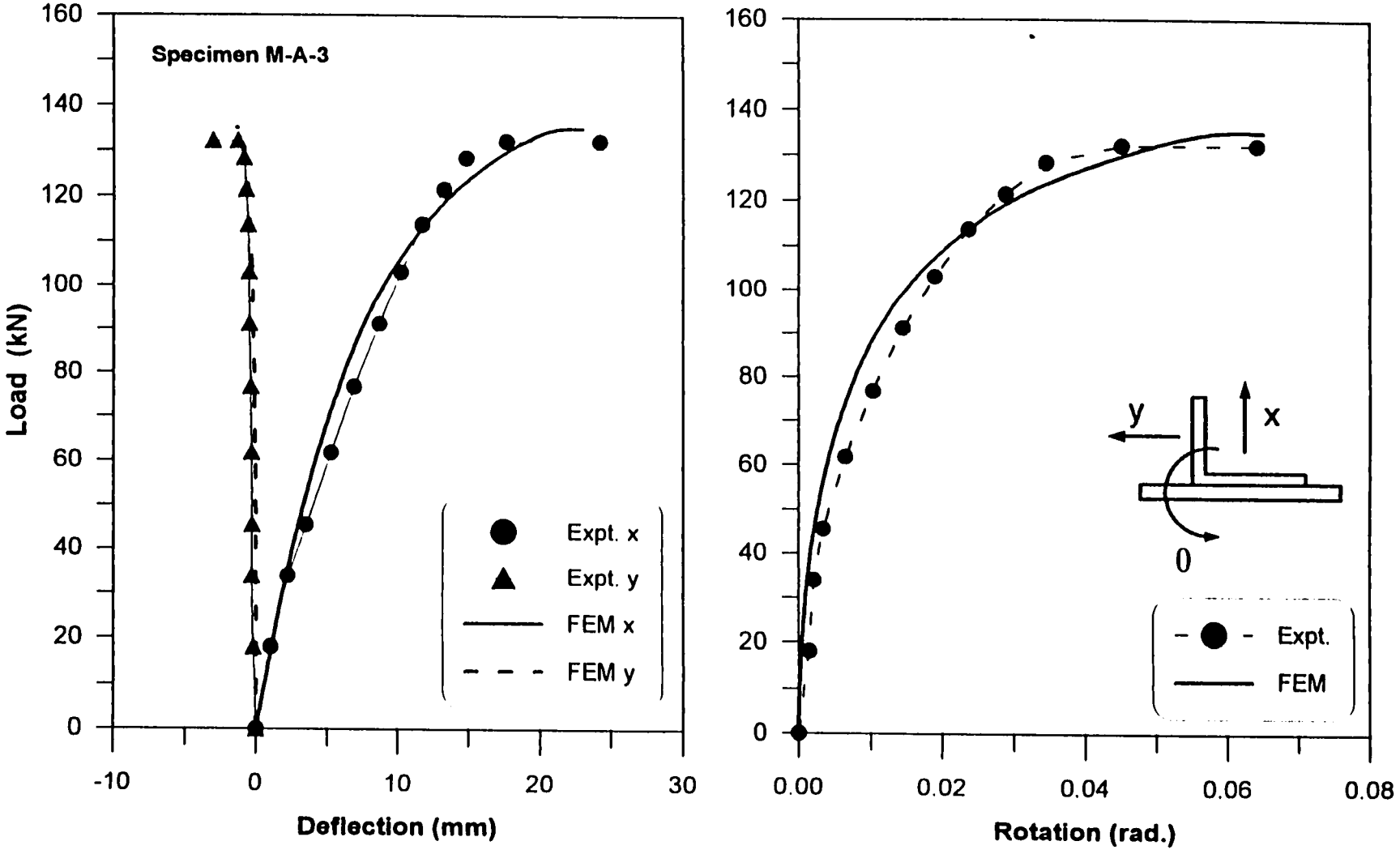

Figure A-24. Load versus deflection and rotation for Specimen M-A-3

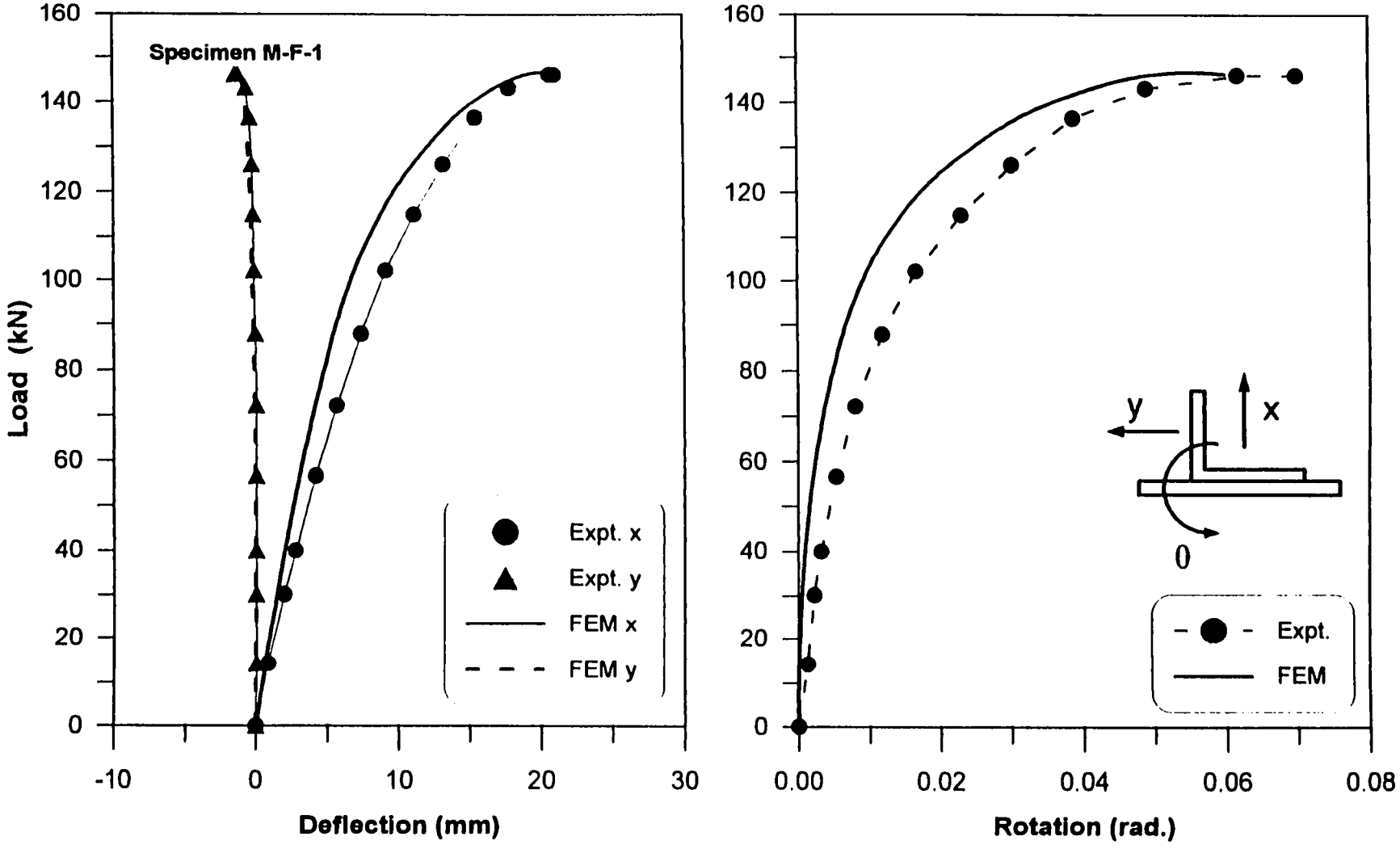

Figure A-25. Load versus deflection and rotation for Specimen M-F-1

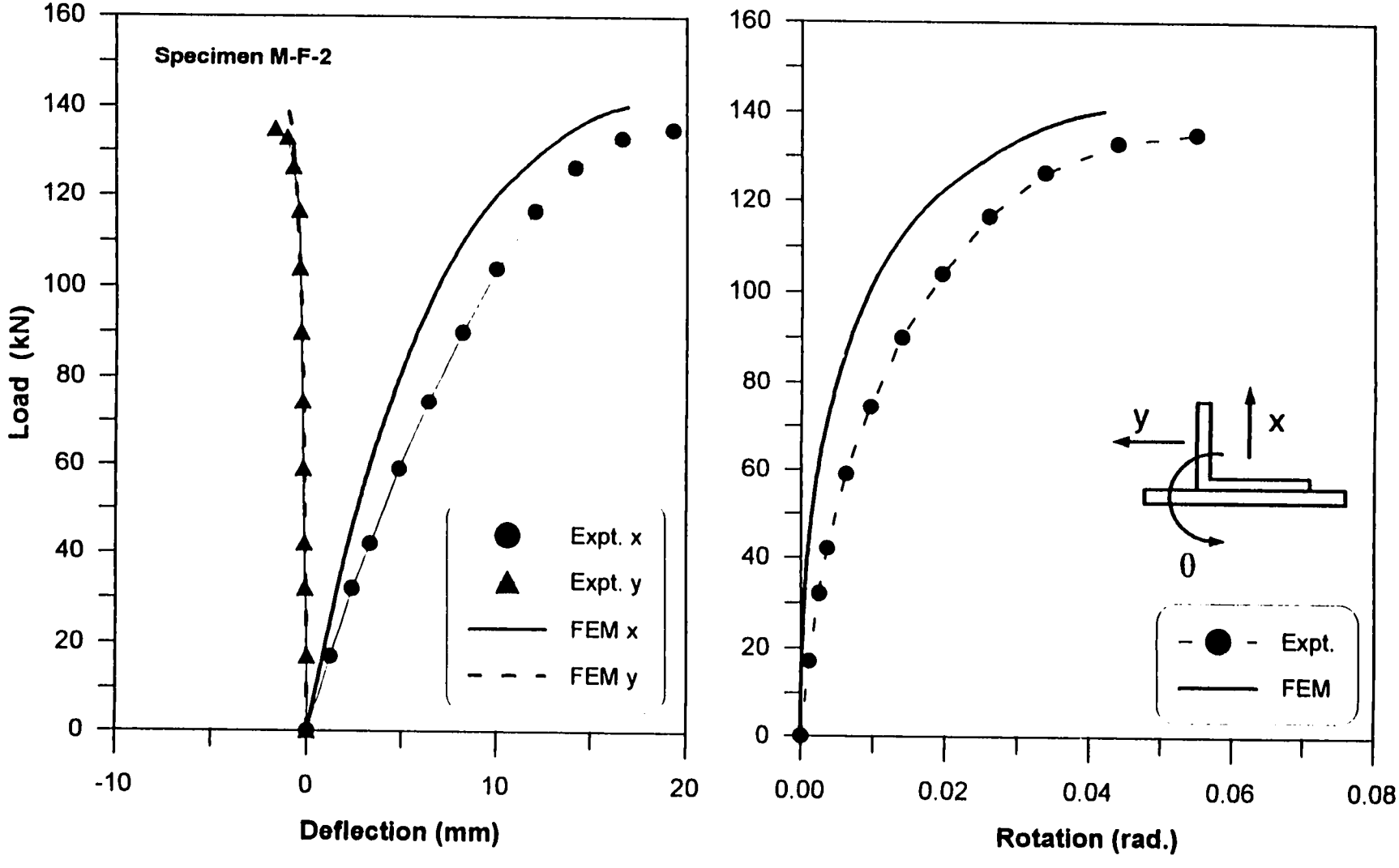

Figure A-26. Load versus deflection and rotation for Specimen M-F-2

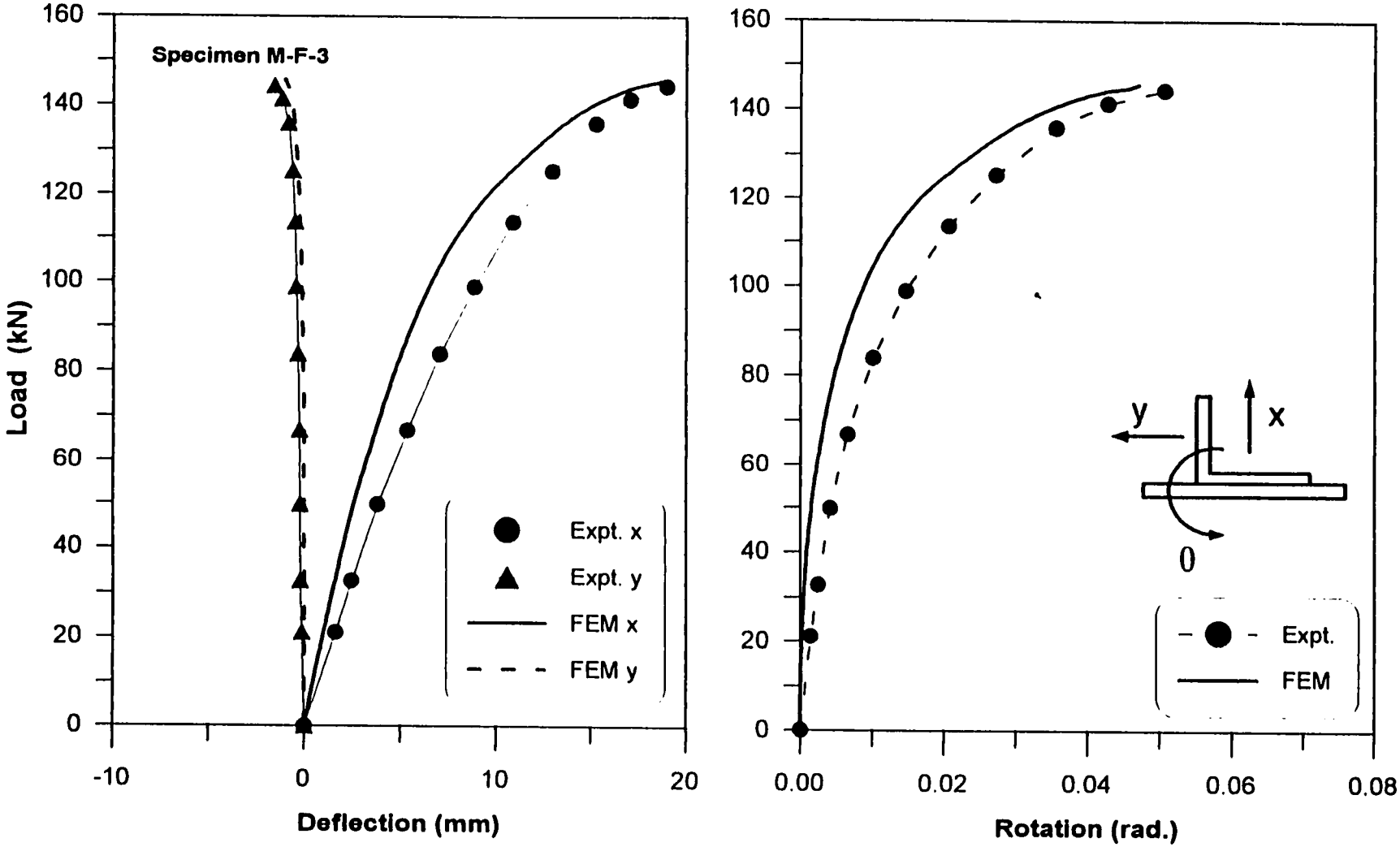

Figure A-27. Load versus deflection and rotation for Specimen M-F-3

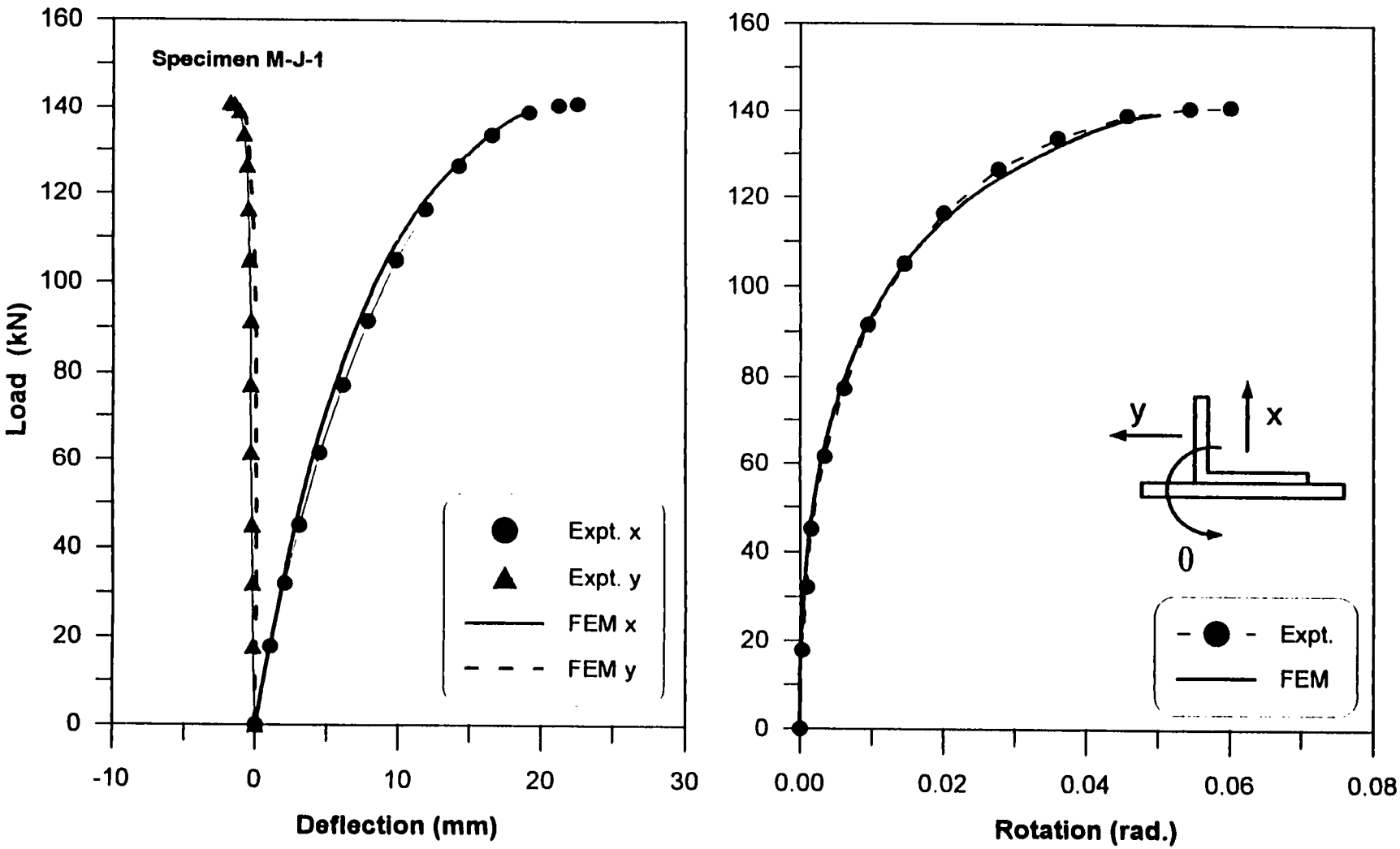

Figure A-28. Load versus deflection and rotation for Specimen M-J-1

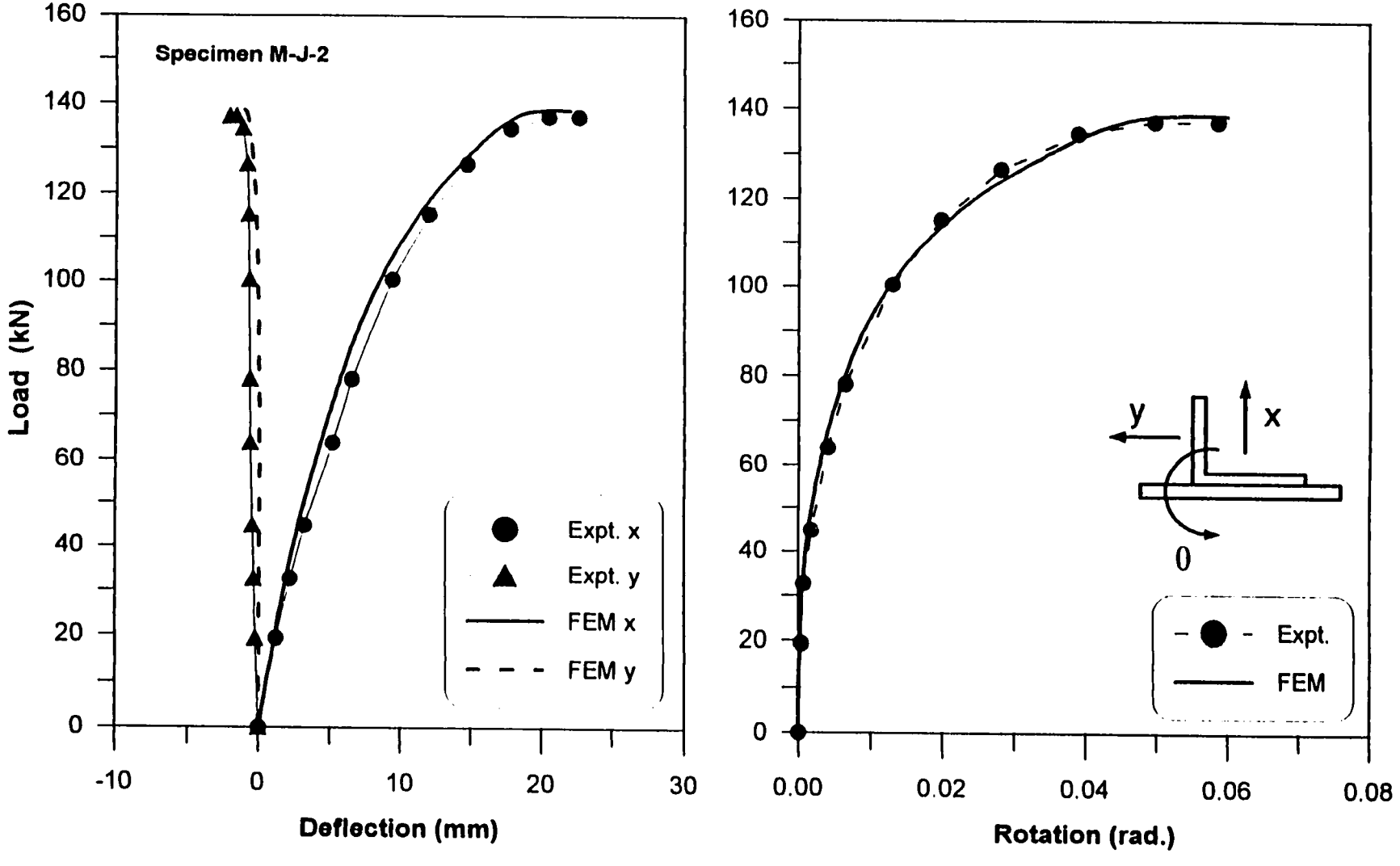

Figure A-29. Load versus deflection and rotation for Specimen M-J-2

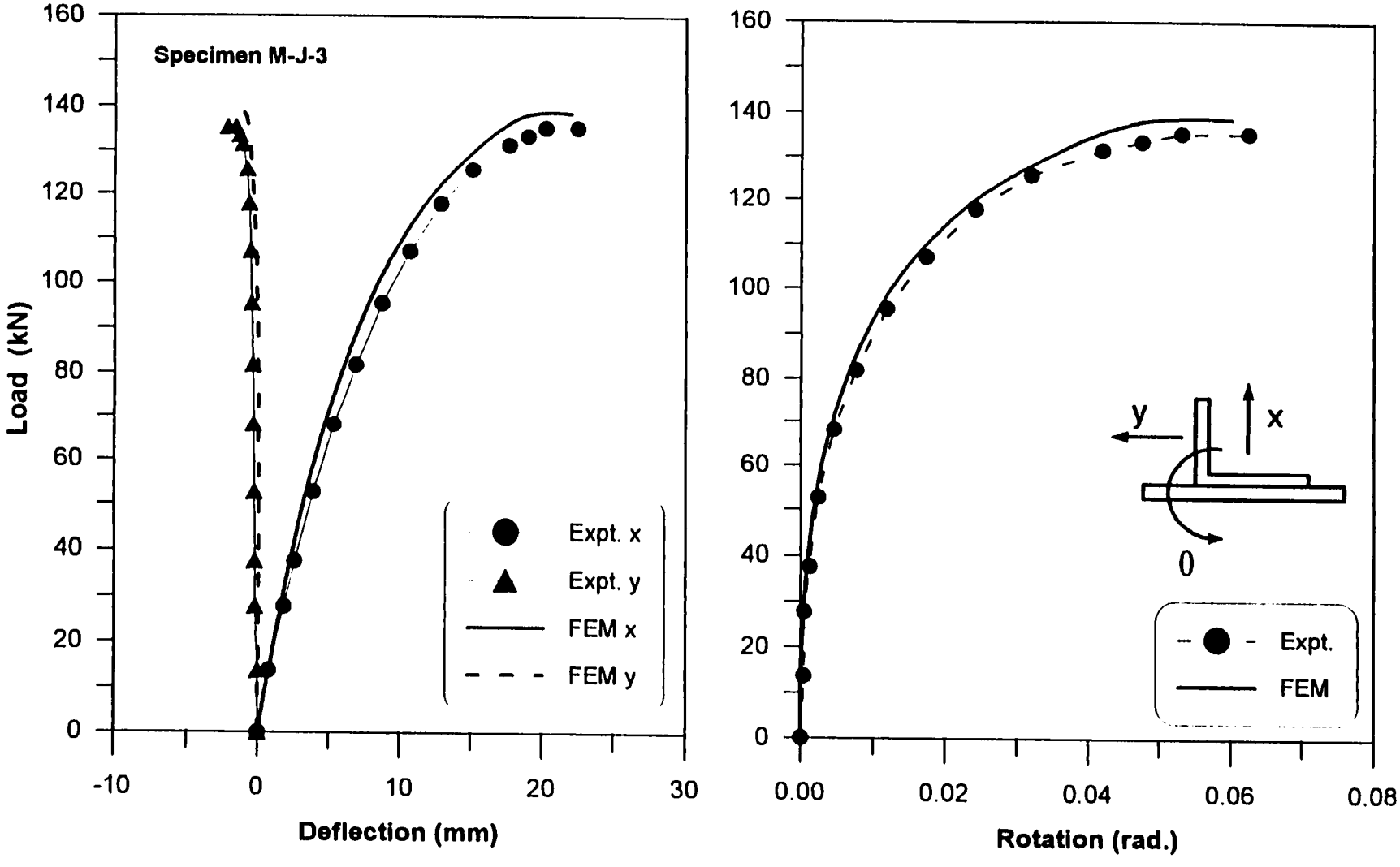

Figure A-30. Load versus deflection and rotation for Specimen M-J-3

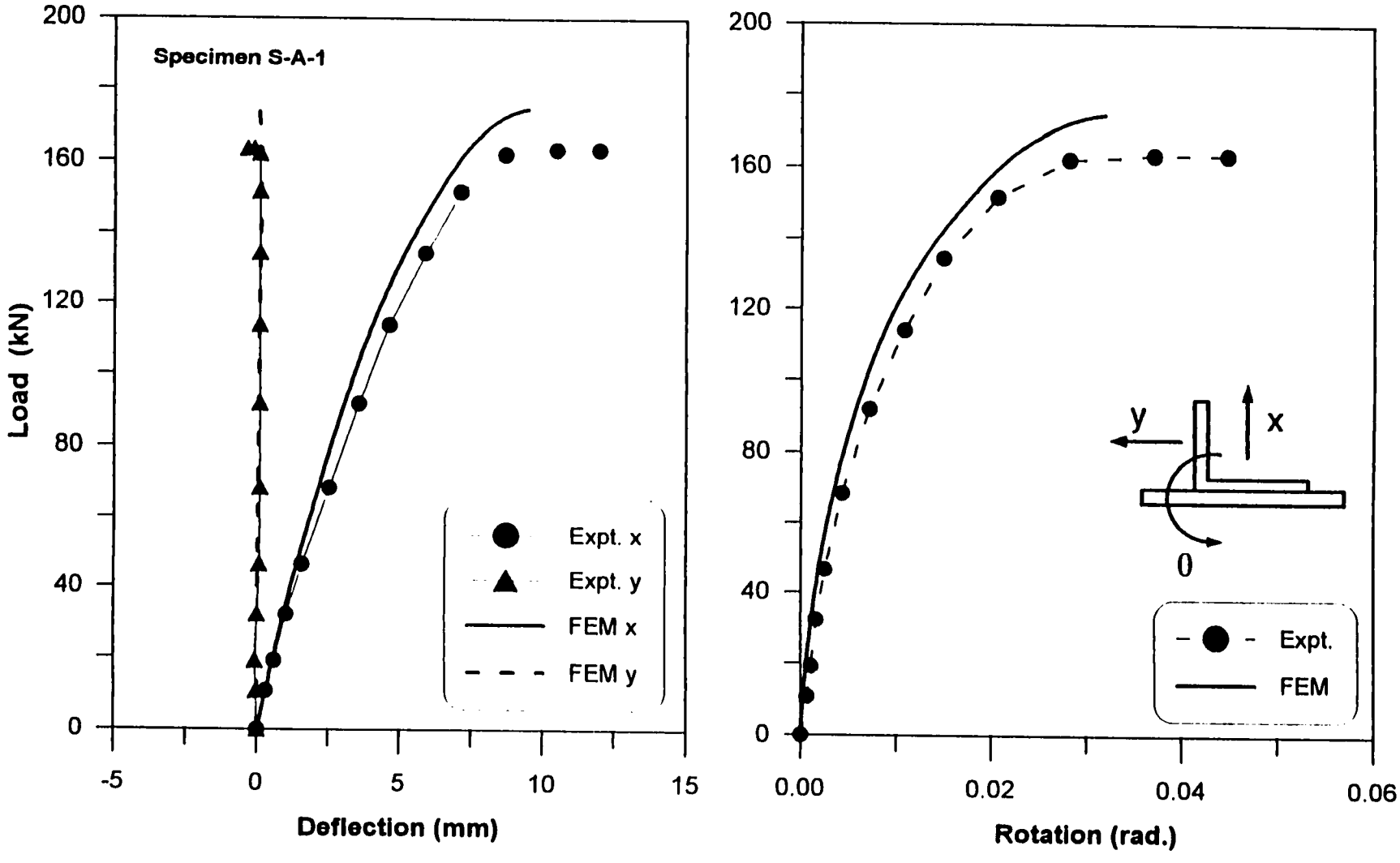

Figure A-31. Load versus deflection and rotation for Specimen S-A-1

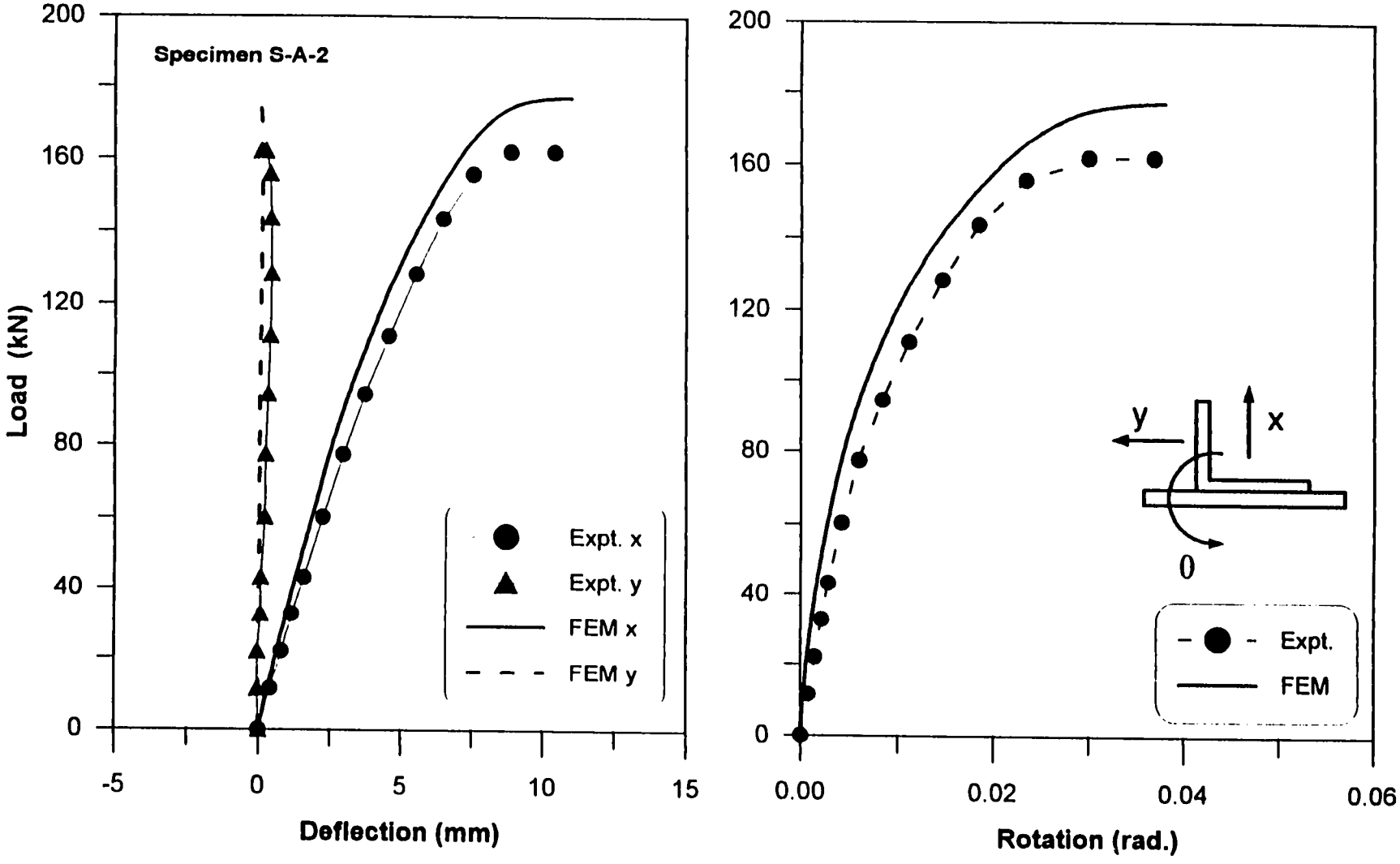

Figure A-32. Load versus deflection and rotation for Specimen S-A-2

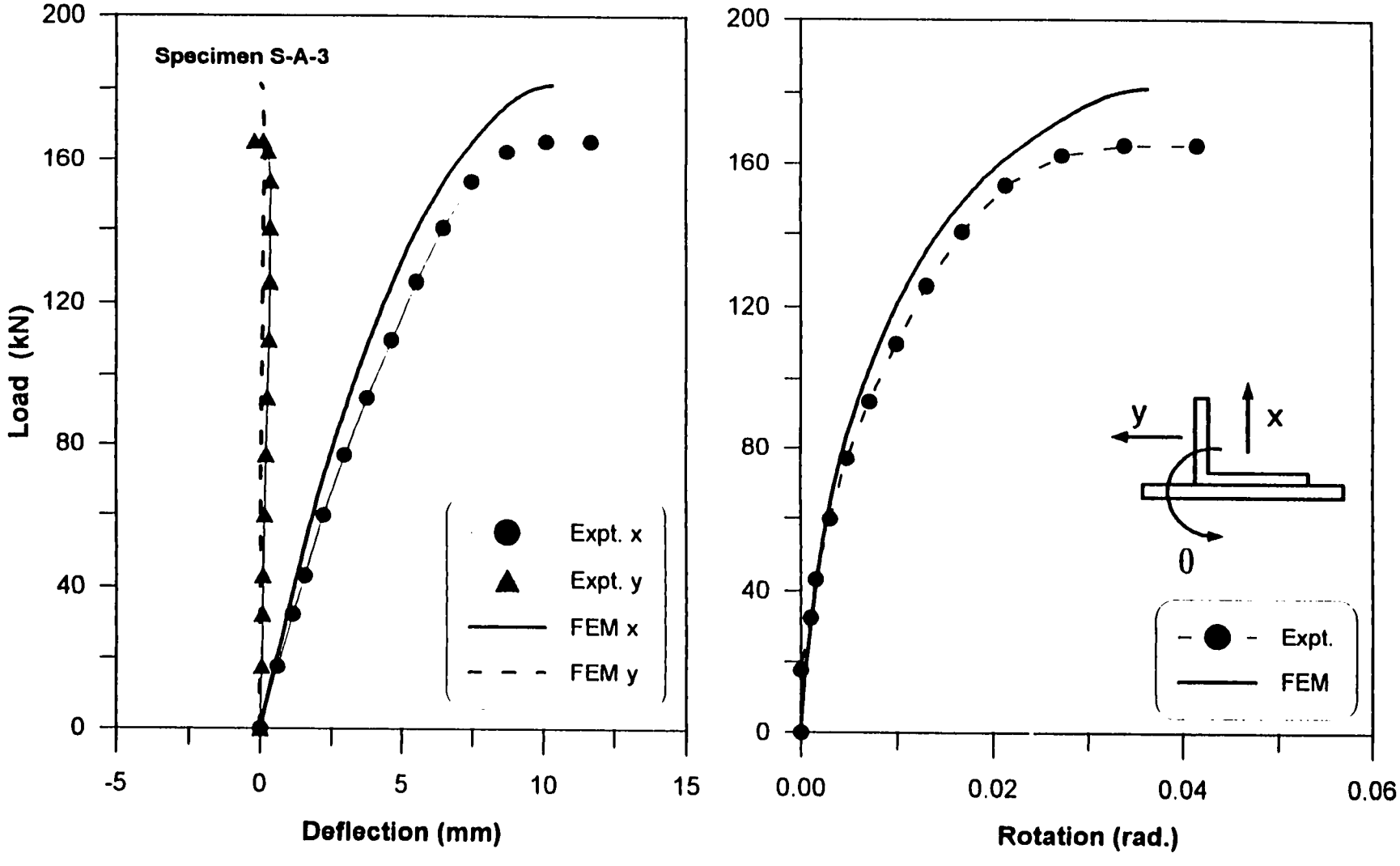

Figure A-33. Load versus deflection and rotation for Specimen S-A-3

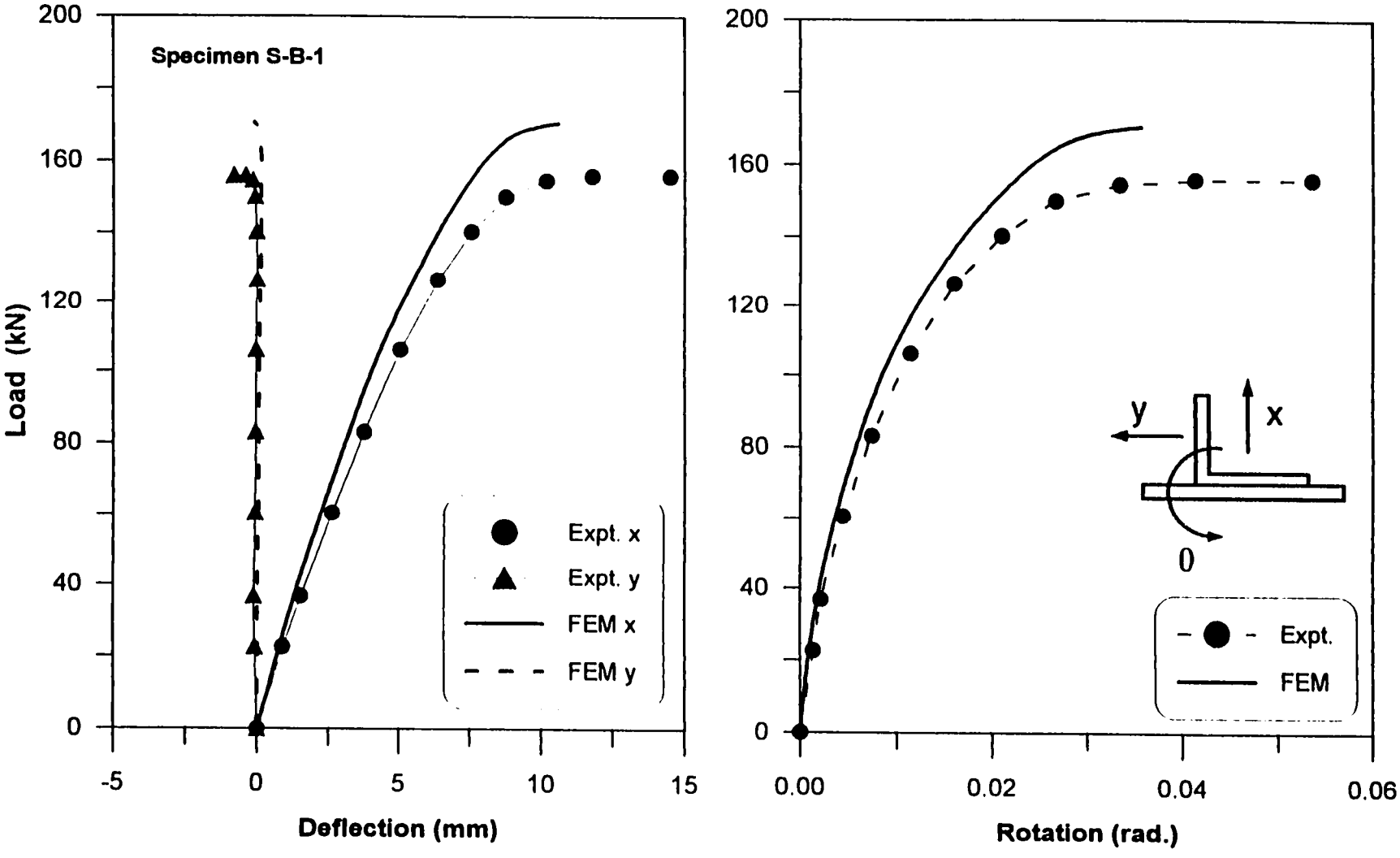

Figure A-34. Load versus deflection and rotation for Specimen S-B-1

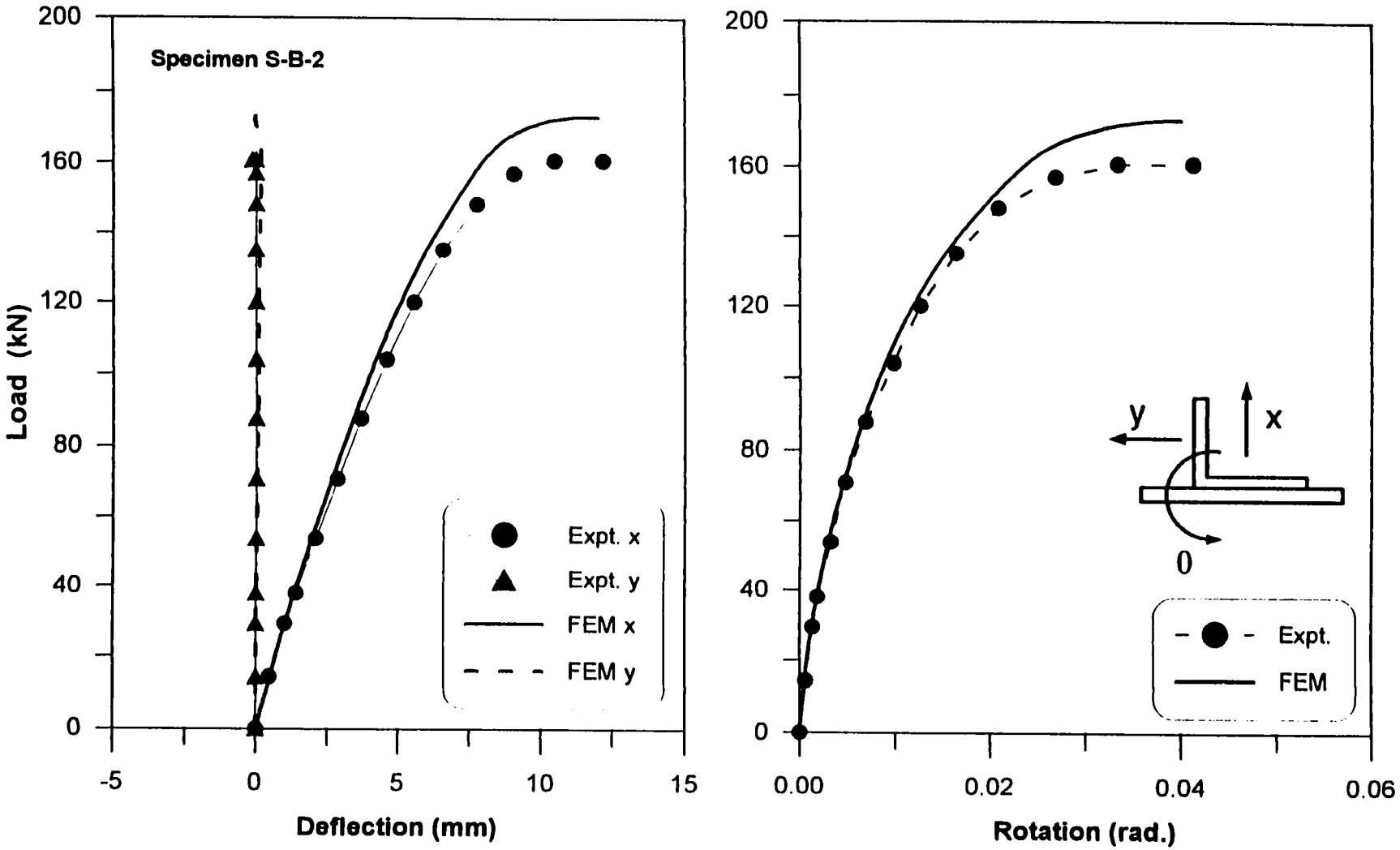

Figure A-35. Load versus deflection and rotation for Specimen S-B-2

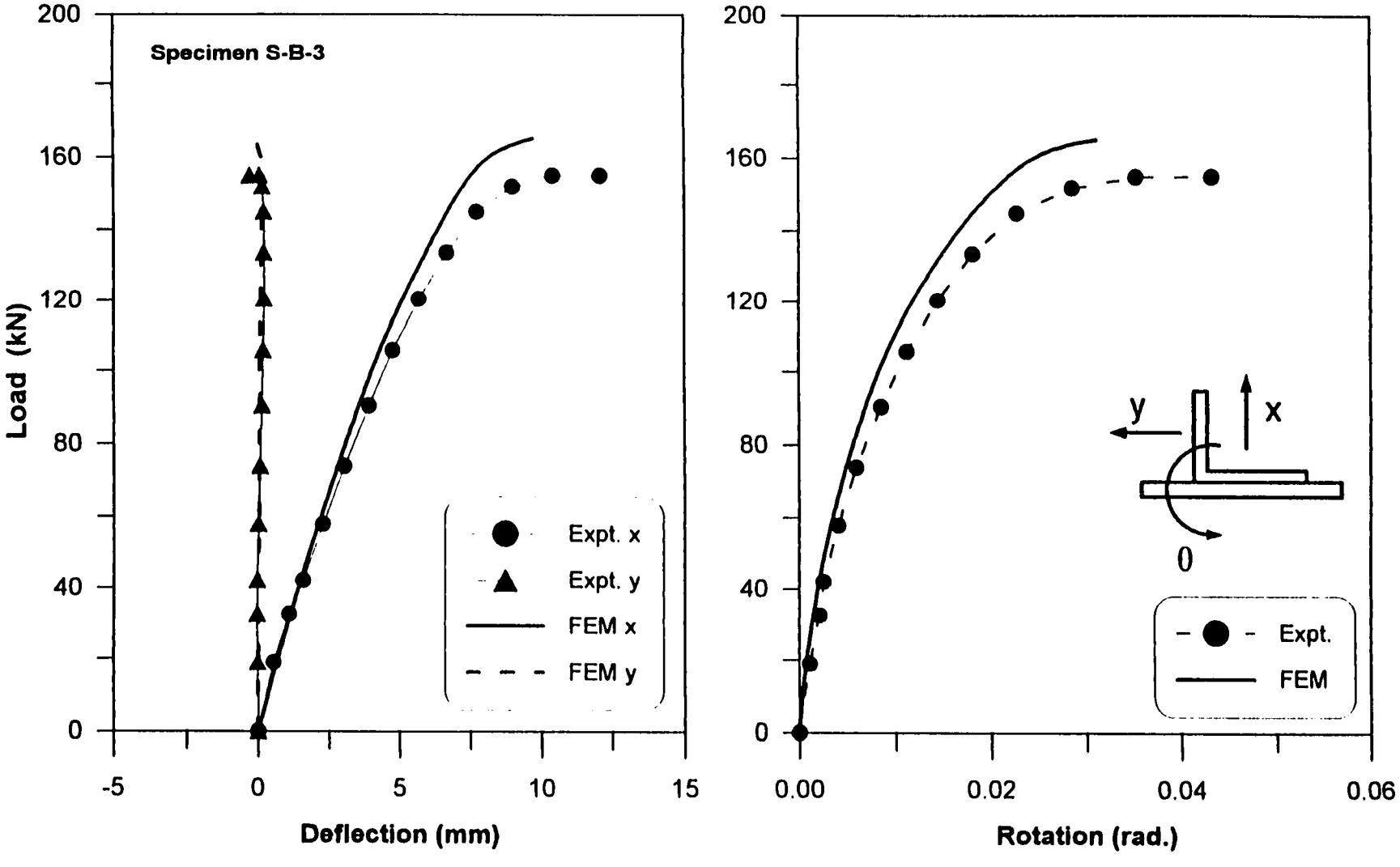

Figure A-36. Load versus deflection and rotation for Specimen S-B-3

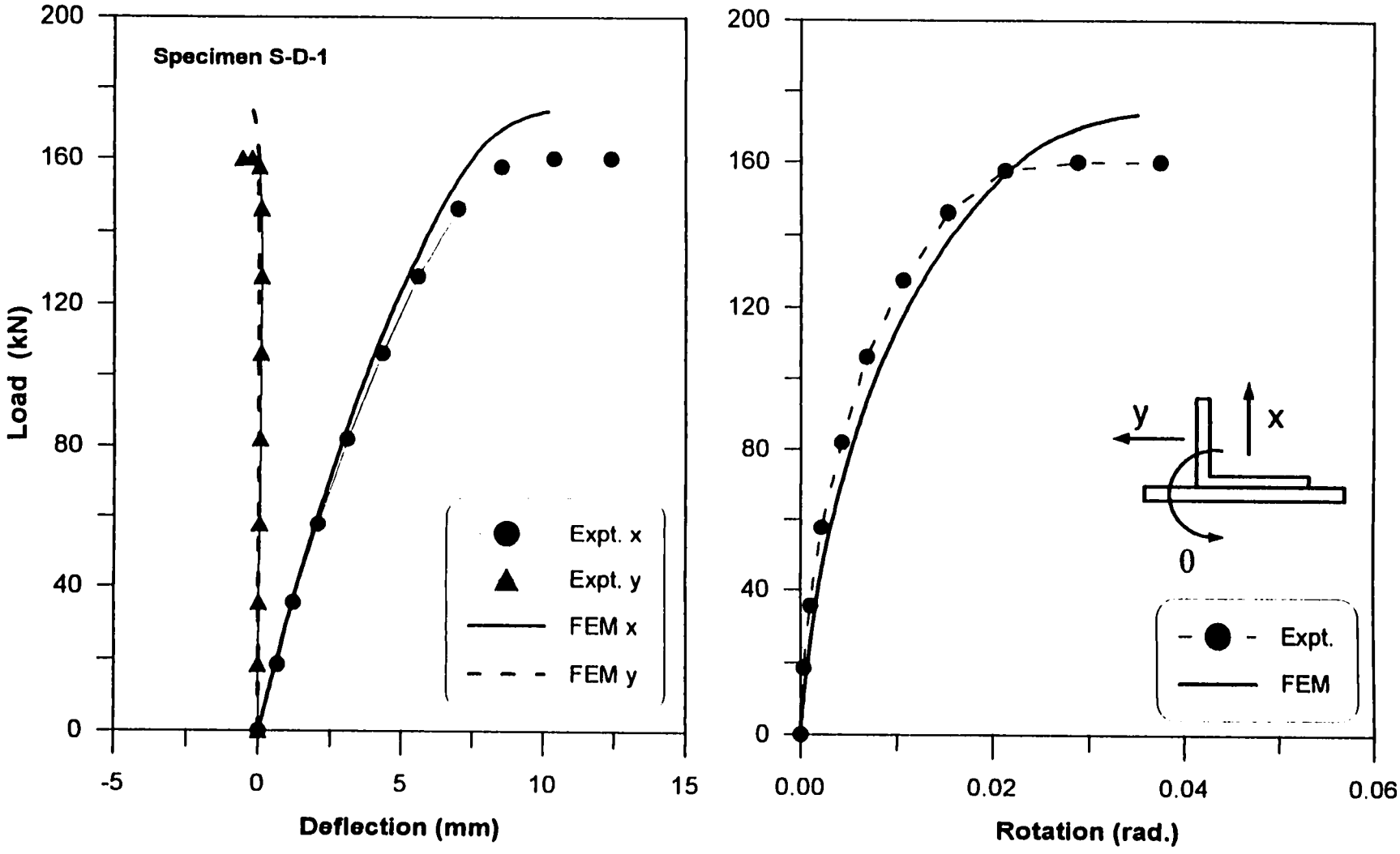

Figure A-37. Load versus deflection and rotation for Specimen S-D-1

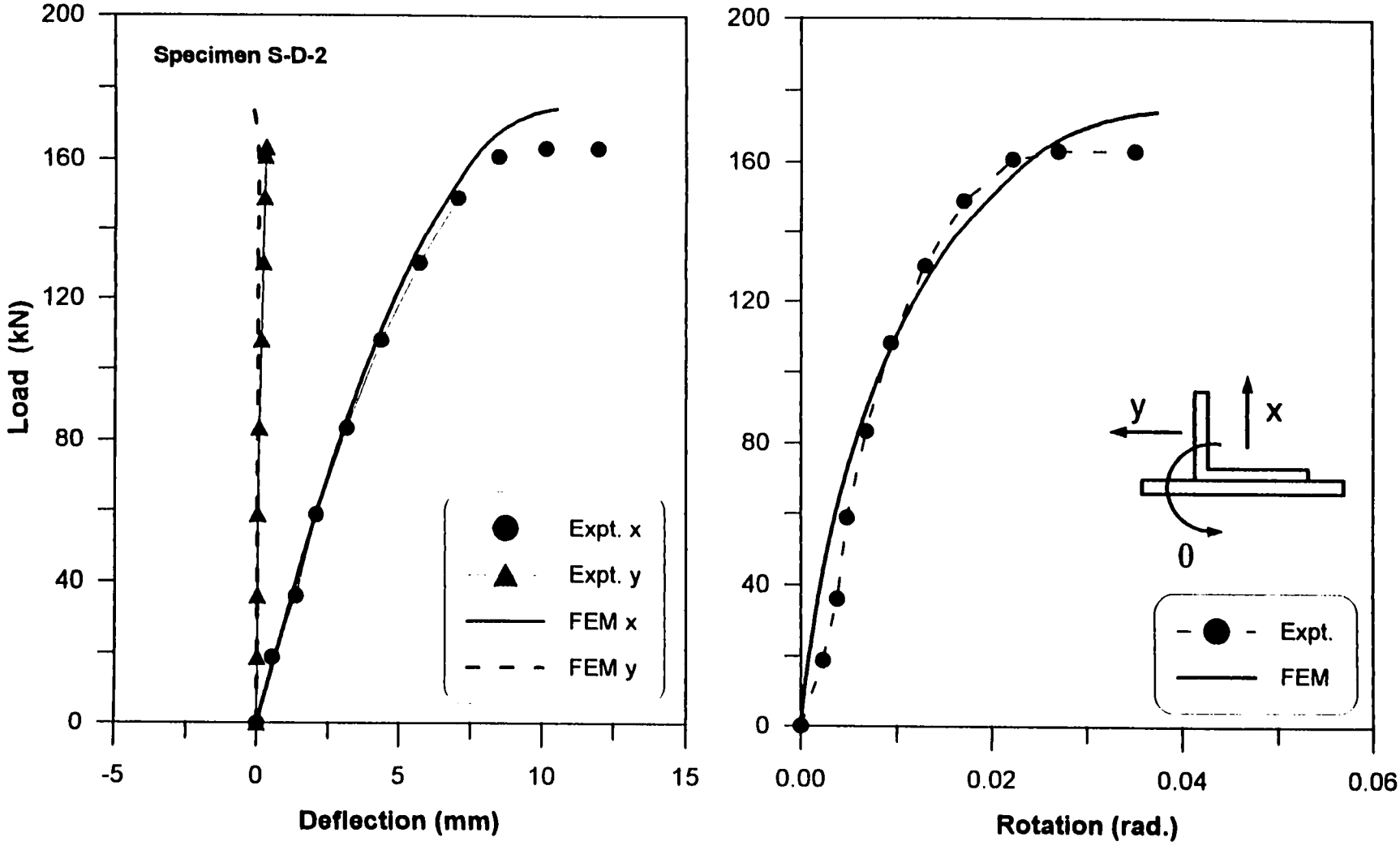

Figure A-38. Load versus deflection and rotation for Specimen S-D-2

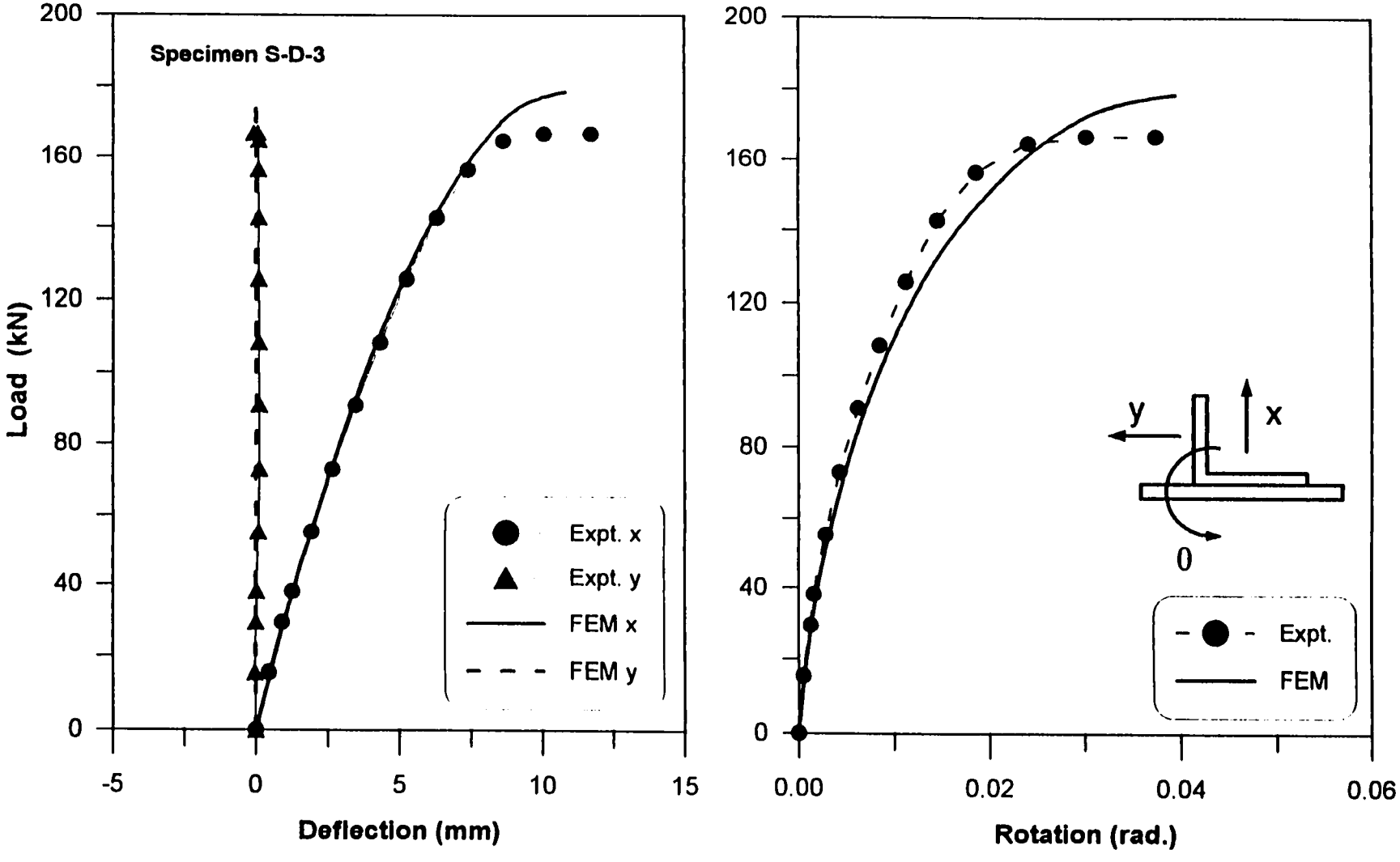

Figure A-39. Load versus deflection and rotation for Specimen S-D-3

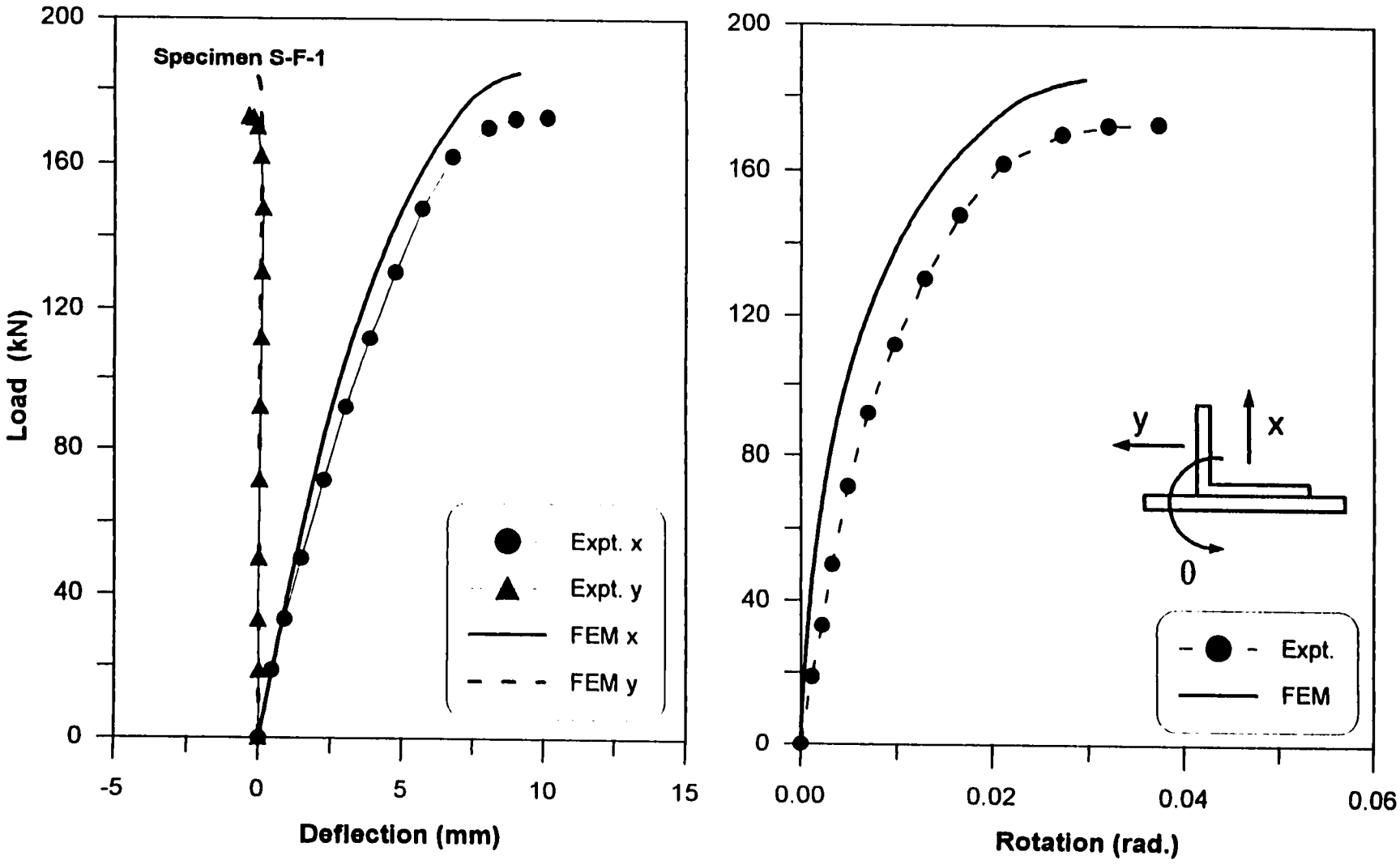

Figure A-40. Load versus deflection and rotation for Specimen S-F-1

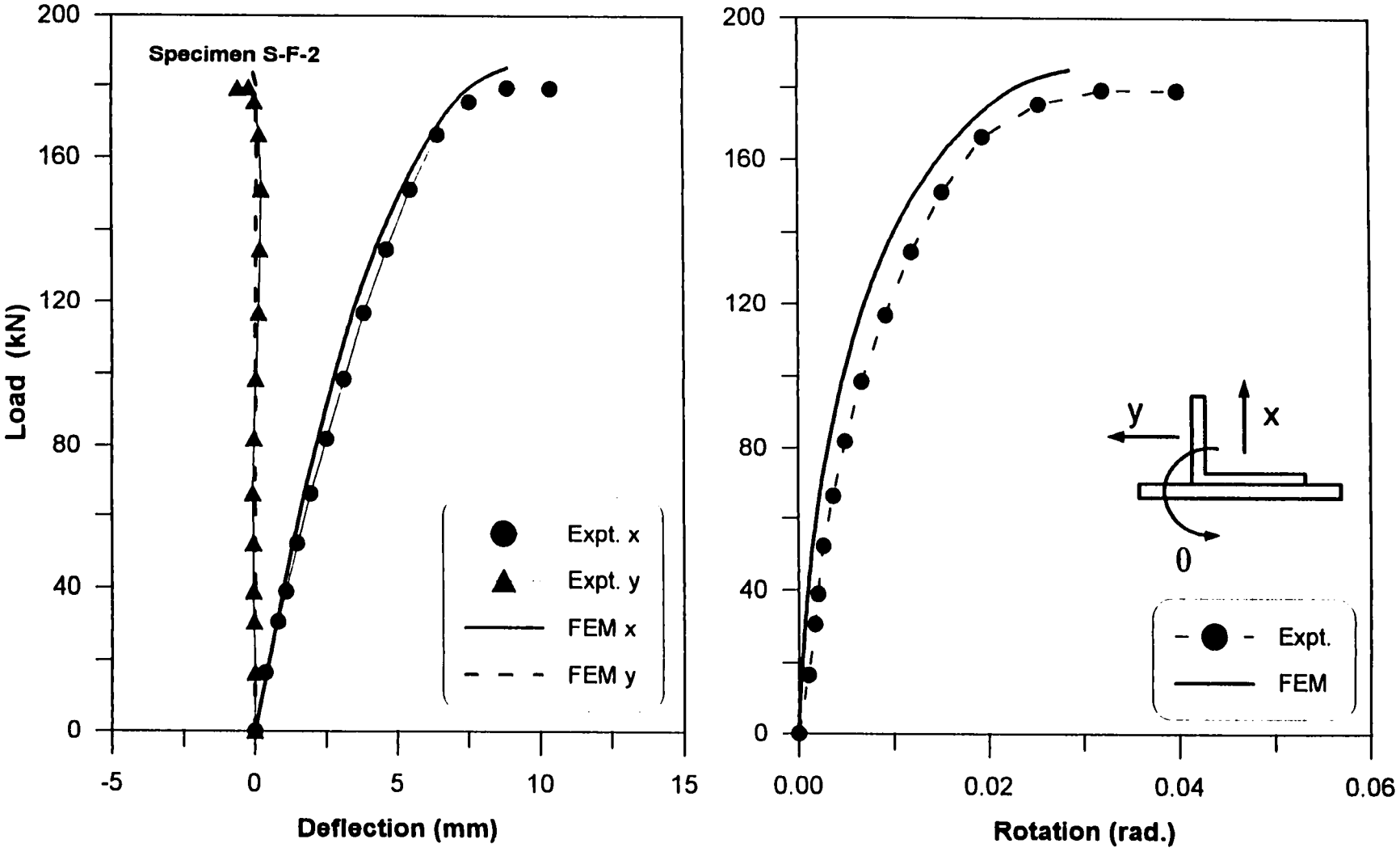

Figure A-41. Load versus deflection and rotation for Specimen S-F-2

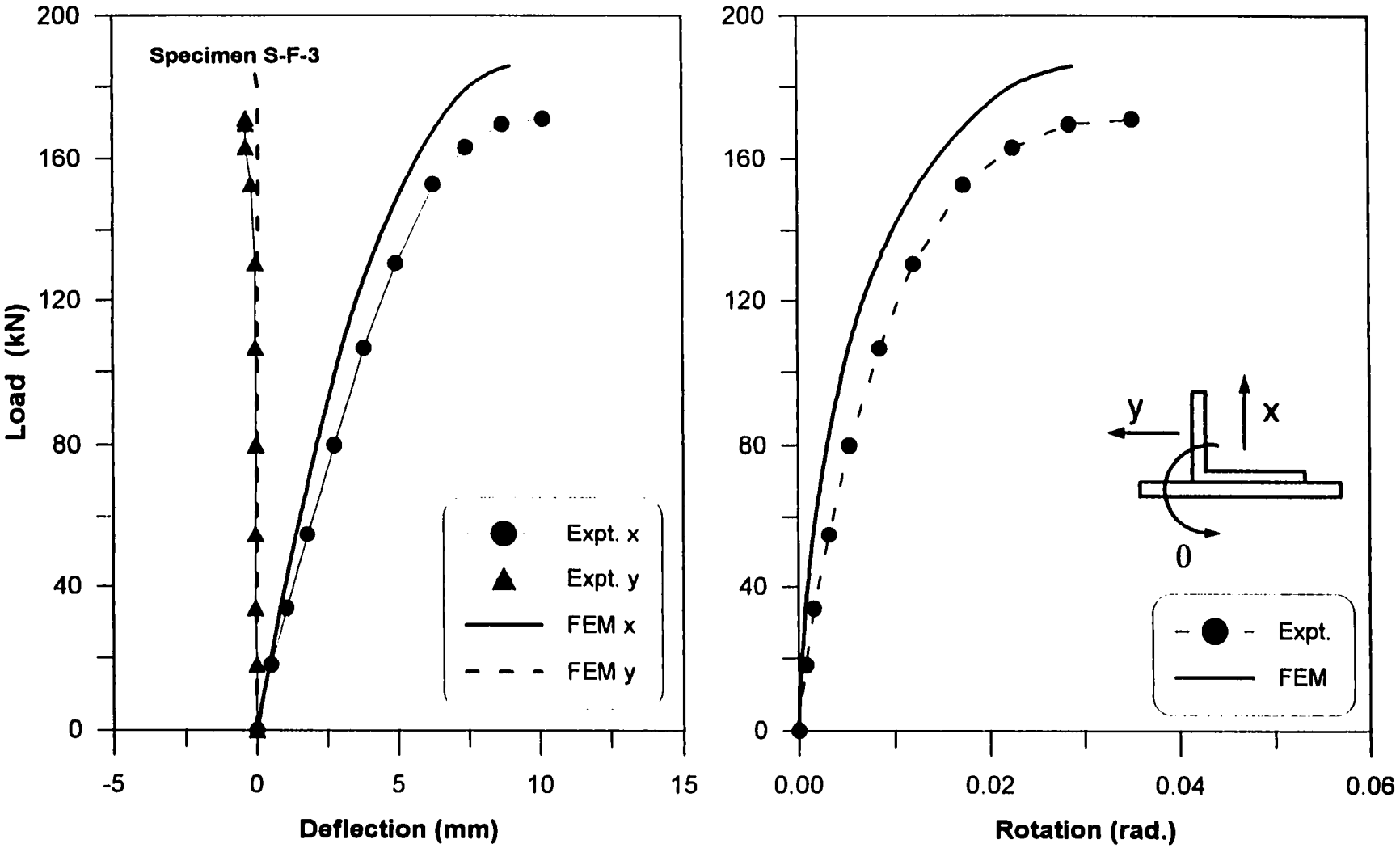

Figure A-42. Load versus deflection and rotation for Specimen S-F-3

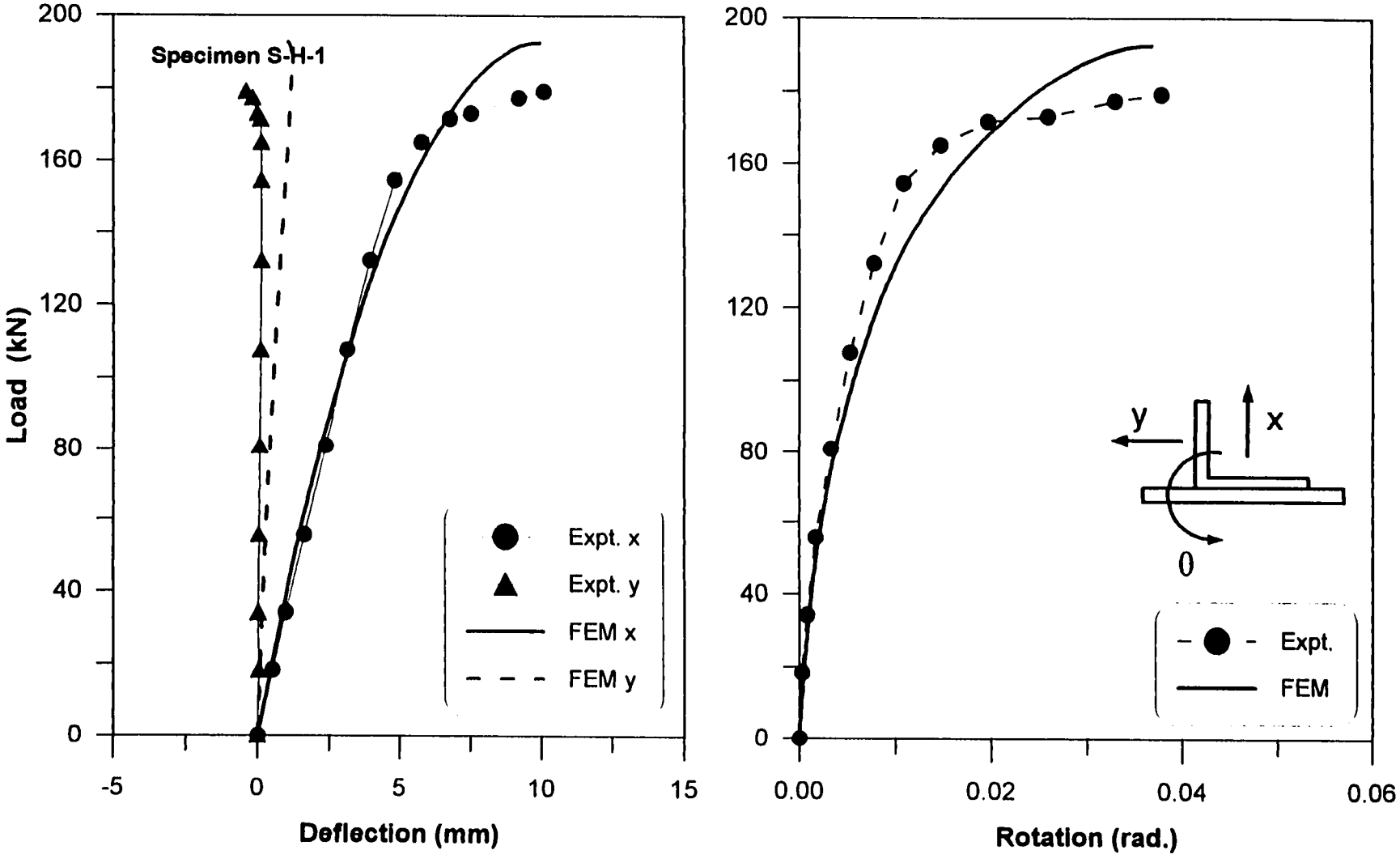

Figure A-43. Load versus deflection and rotation for Specimen S-H-1

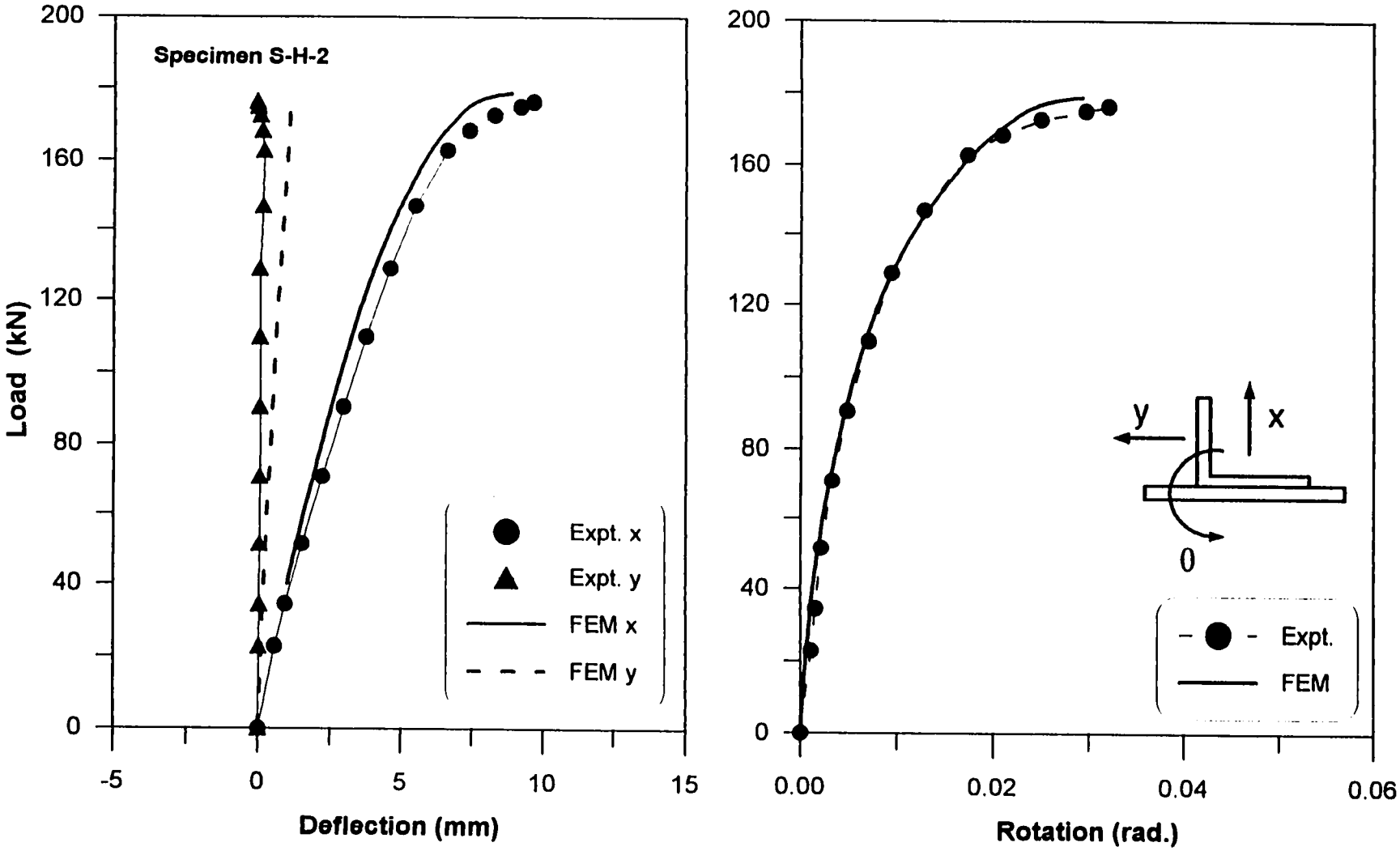

Figure A-44. Load versus deflection and rotation for Specimen S-H-2

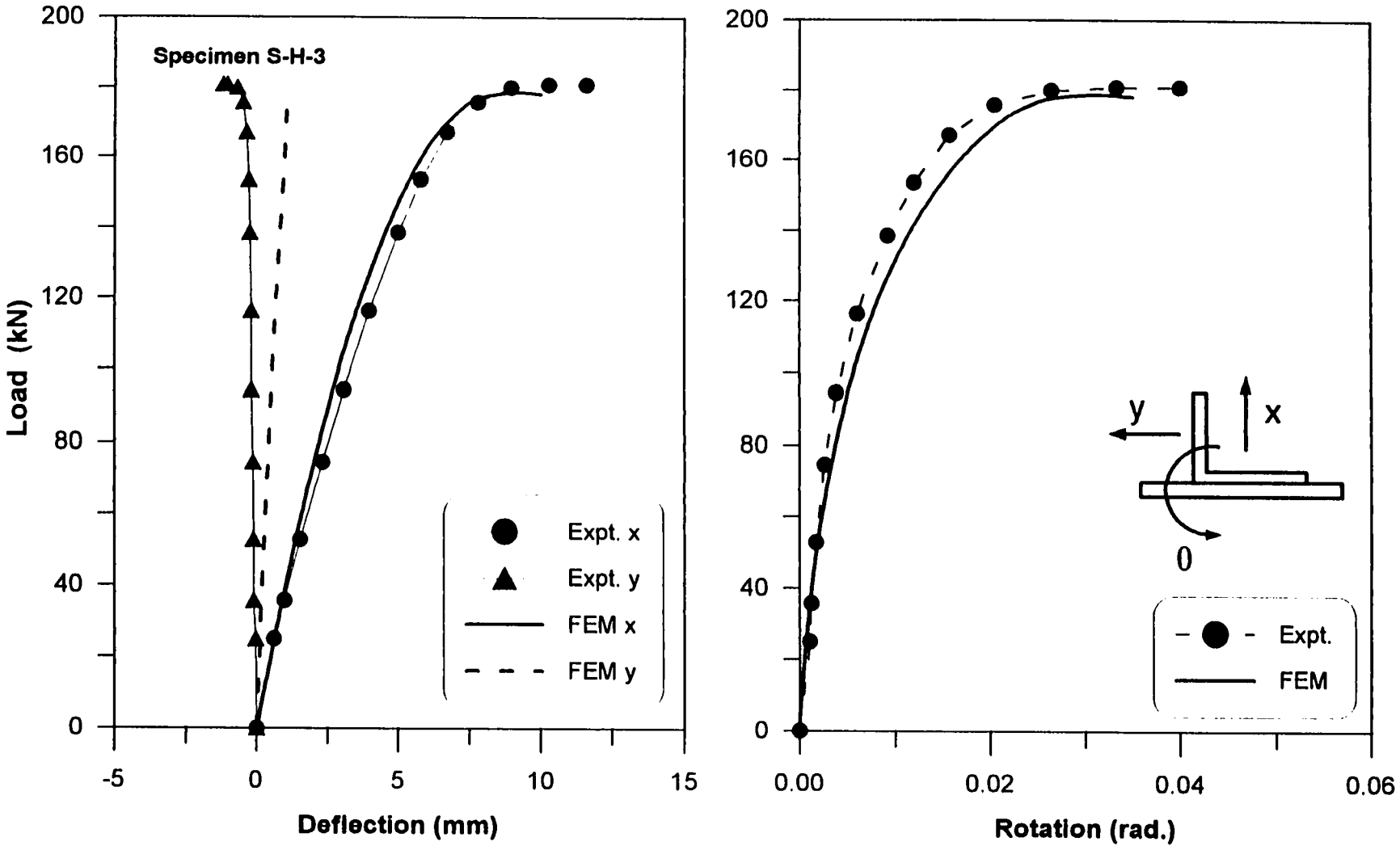

Figure A-45. Load versus deflection and rotation for Specimen S-H-3

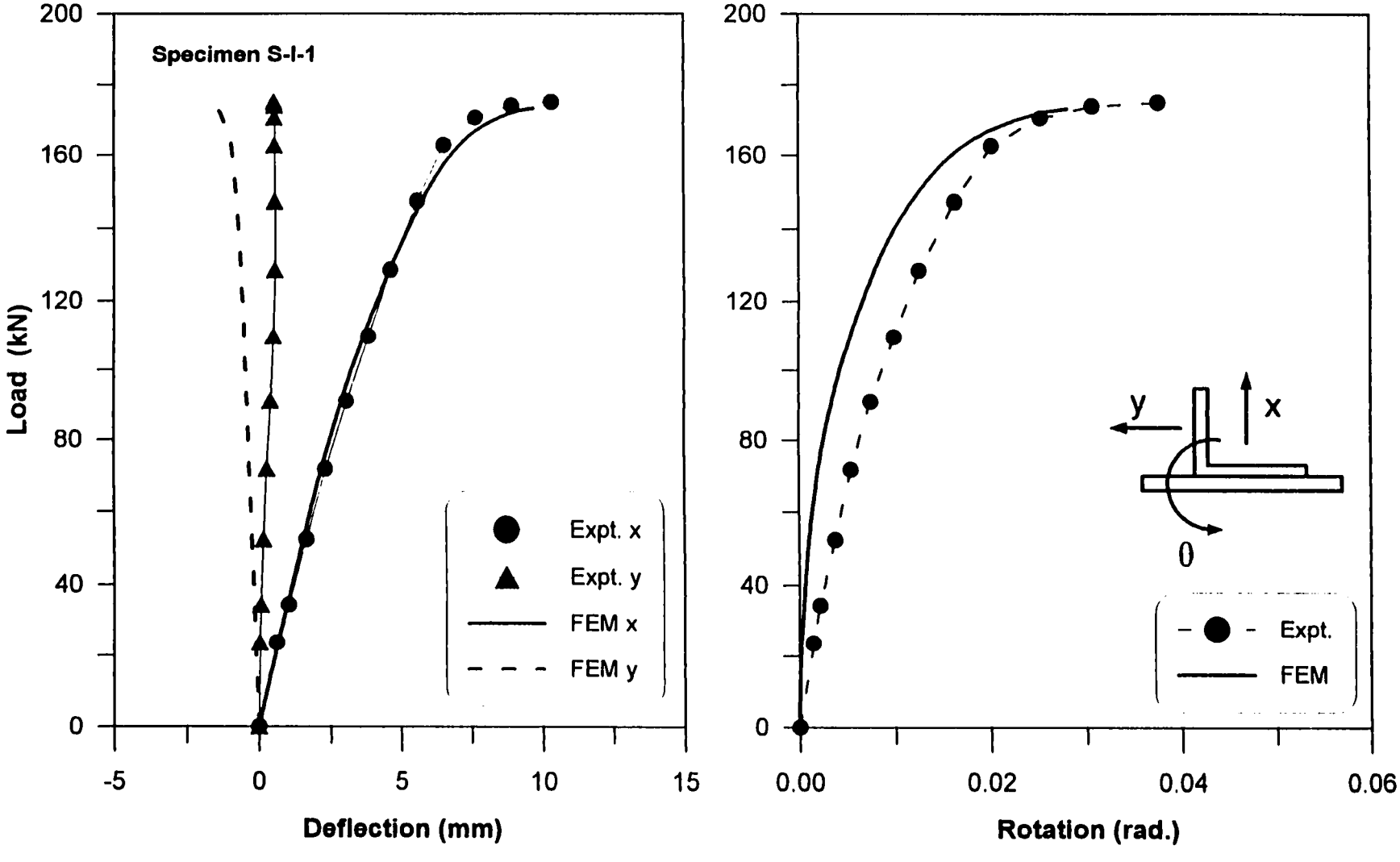

Figure A-46. Load versus deflection and rotation for Specimen S-I-1

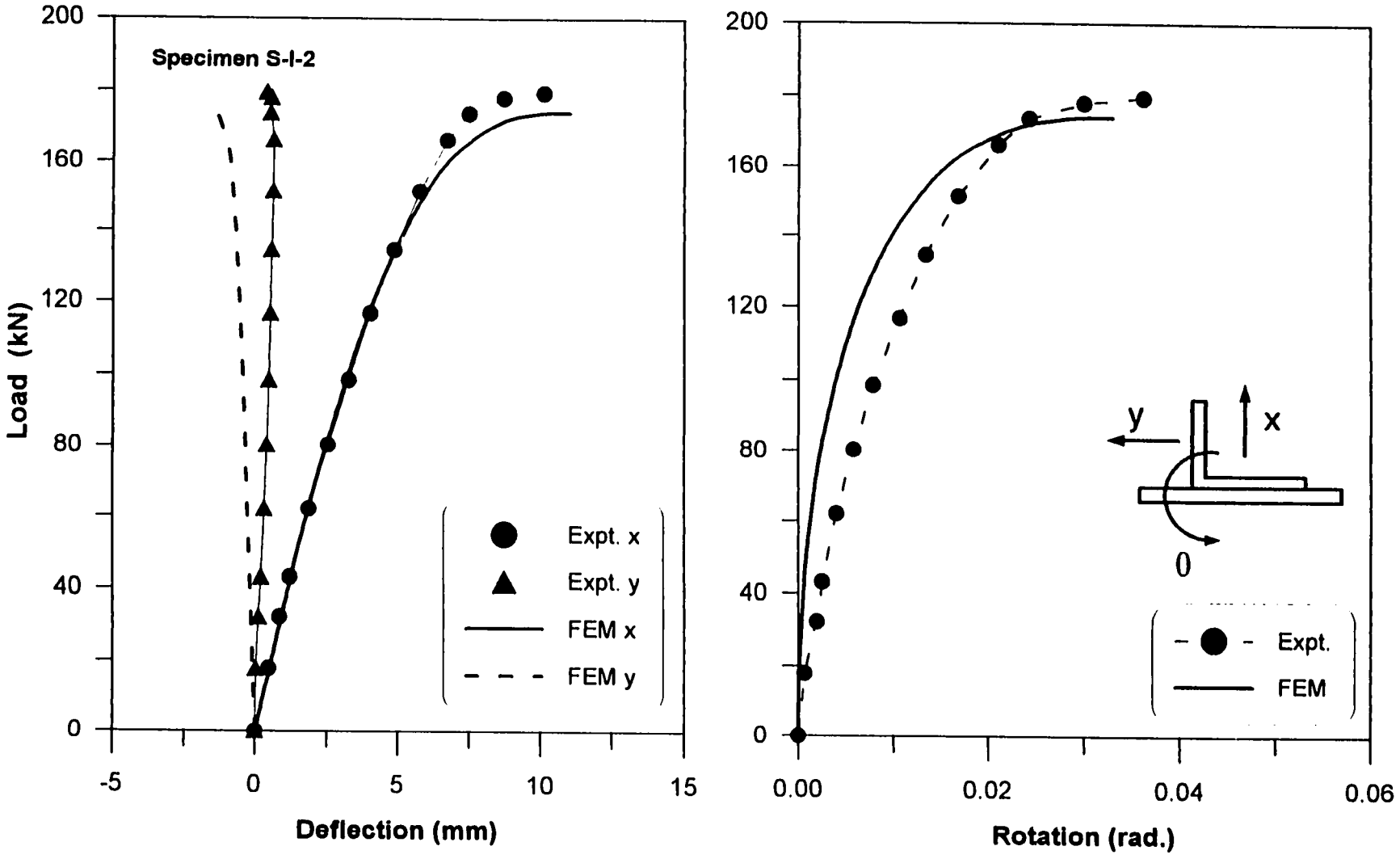

Figure A-47. Load versus deflection and rotation for Specimen S-I-2

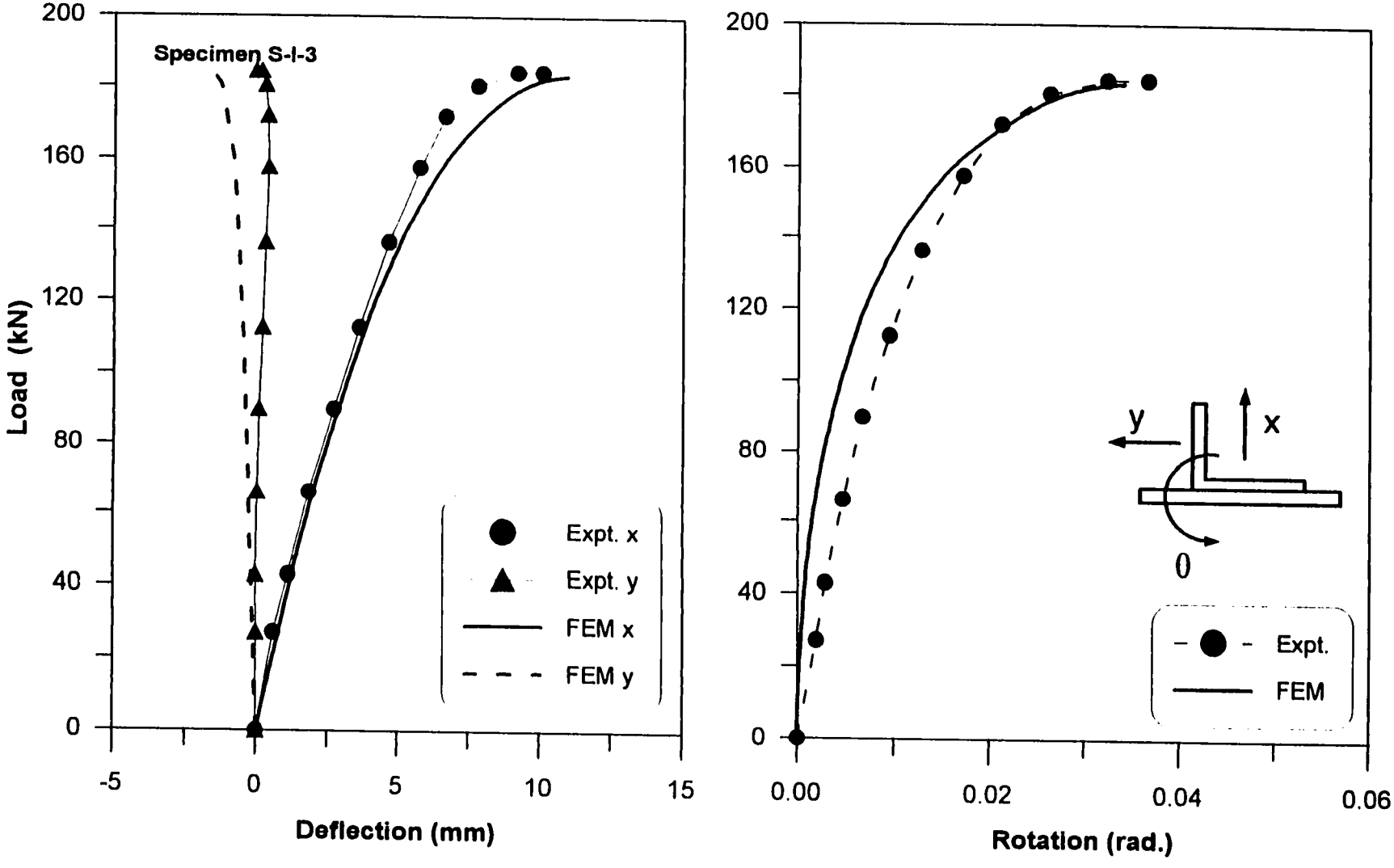

Figure A-48. Load versus deflection and rotation for Specimen S-I-3

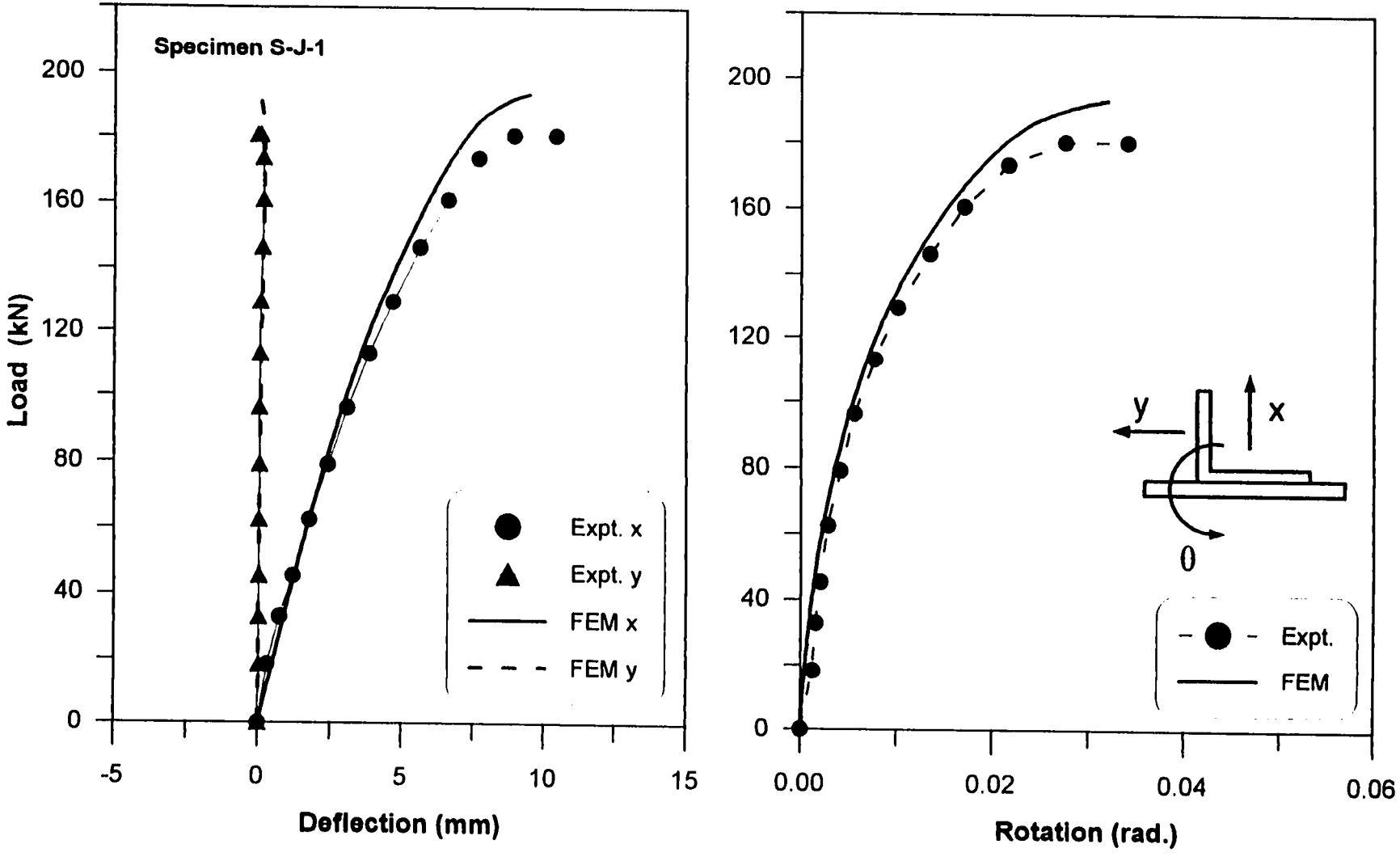

Figure A-49. Load versus deflection and rotation for Specimen S-J-1

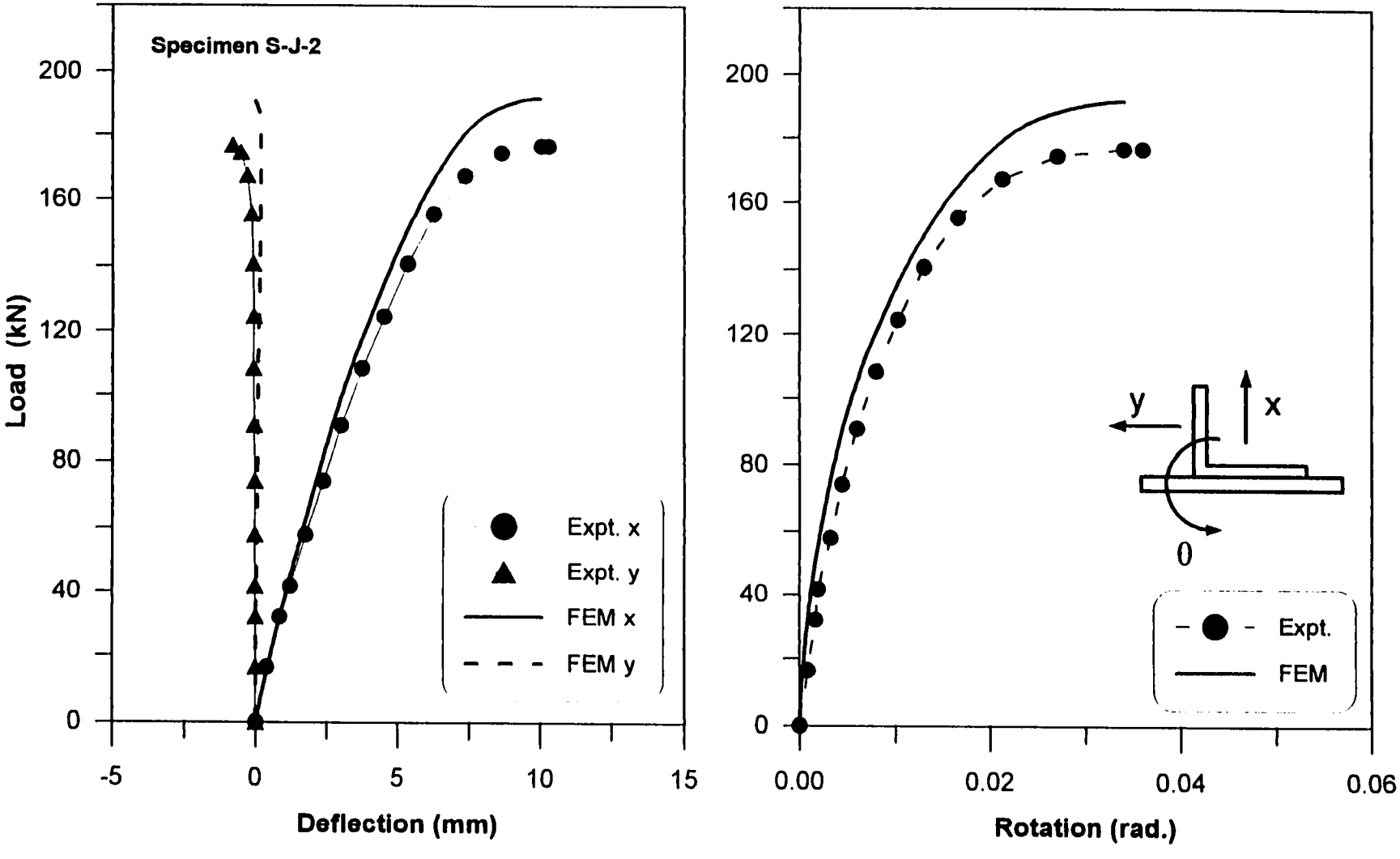

Figure A-50. Load versus deflection and rotation for Specimen S-J-2

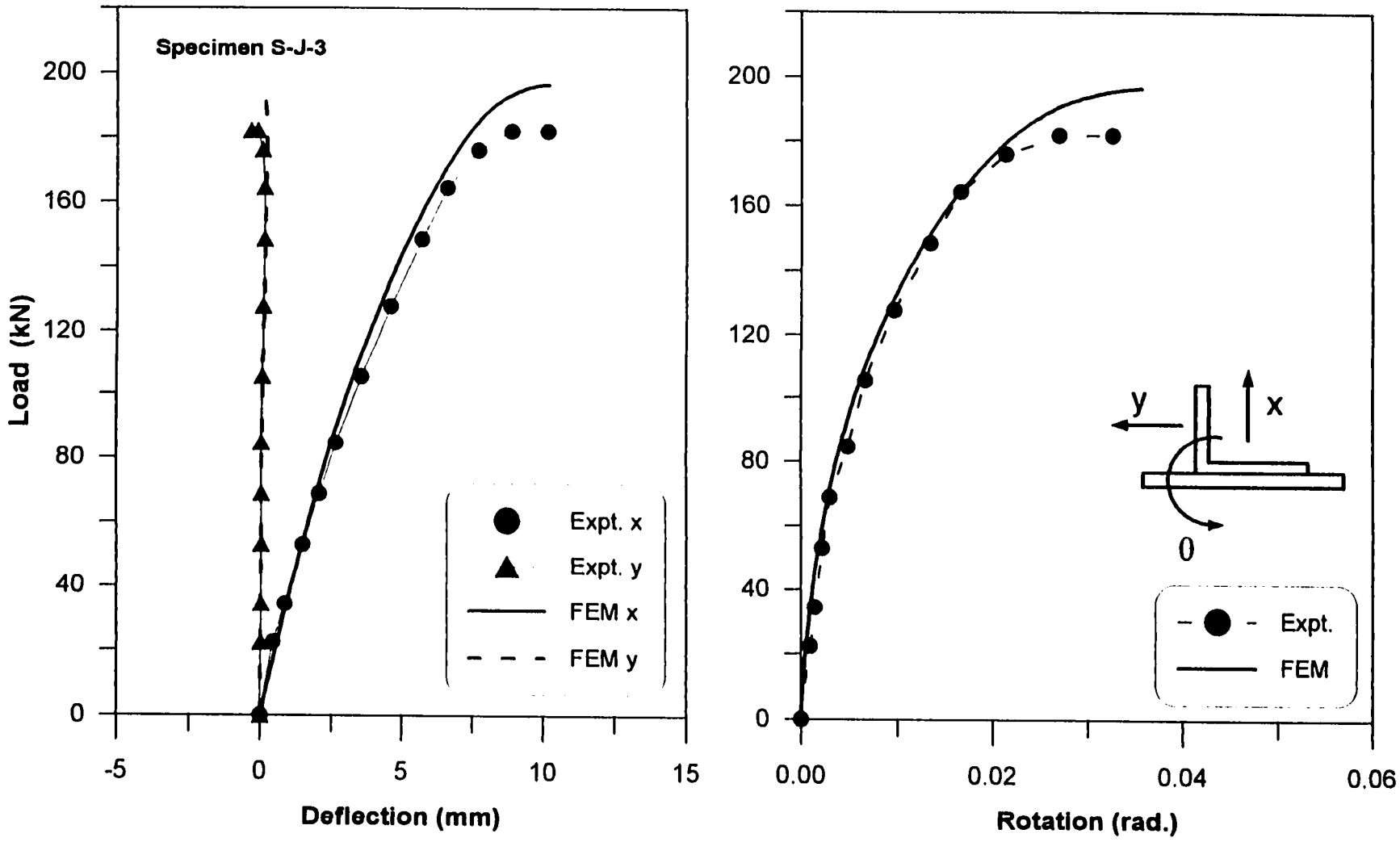

Figure A-51. Load versus deflection and rotation for Specimen S-J-3

APPENDIX B

DESIGN CURVES

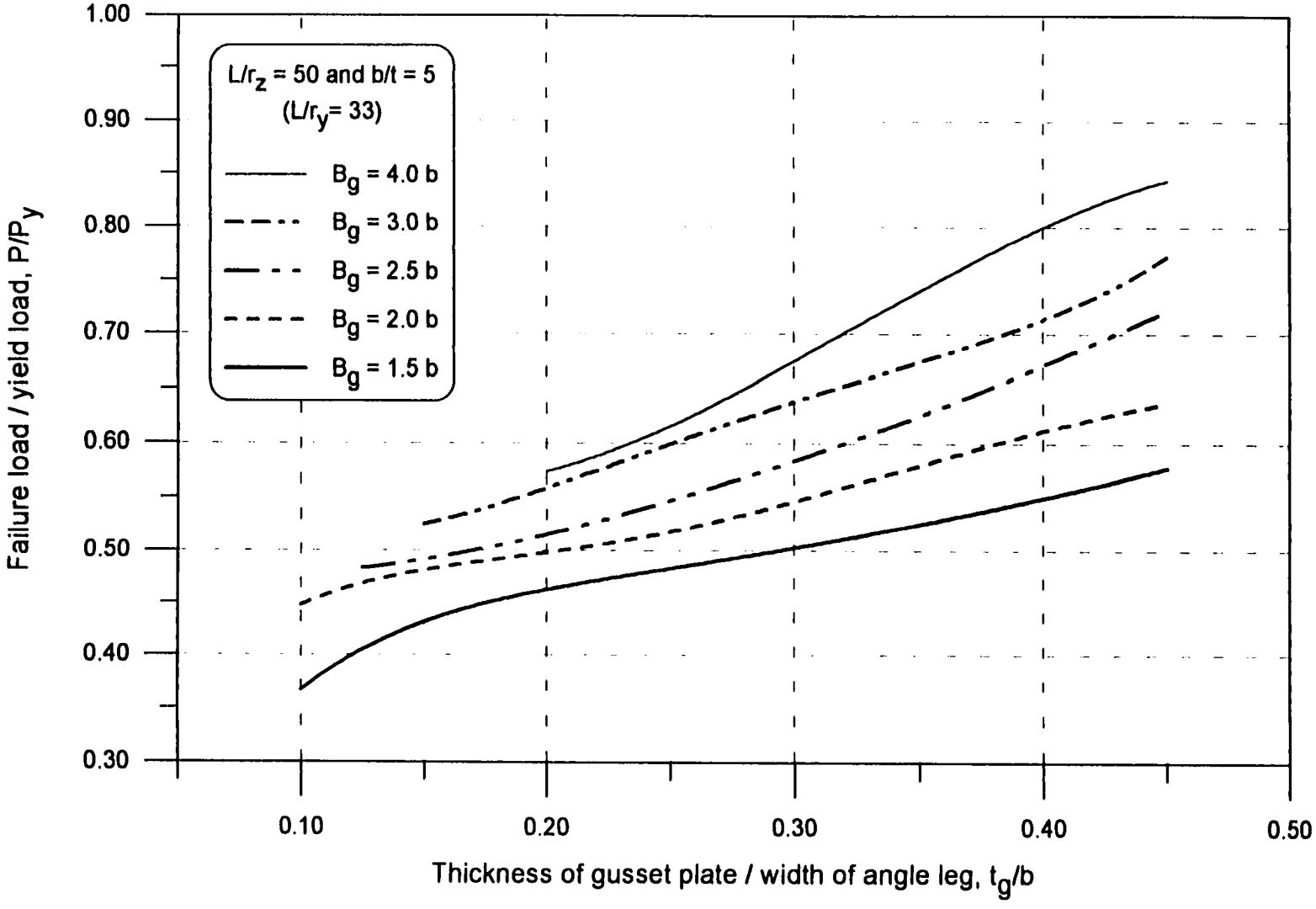

Figure B-1. Failure load predicted by finite element analysis when b/t = 5 and L/r_z = 50

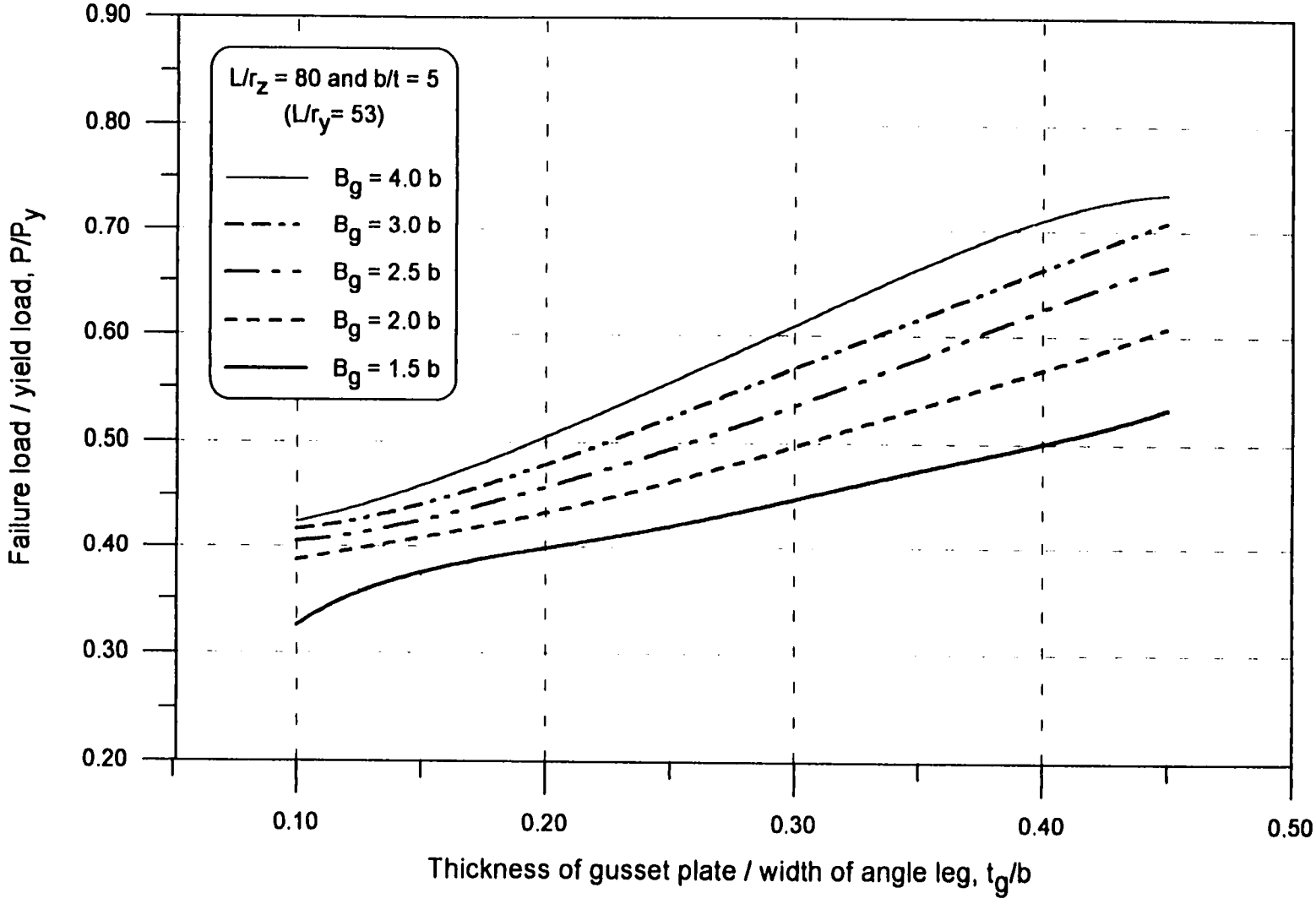

Figure B-2. Failure load predicted by finite element analysis when b/t = 5 and L/r_z = 80

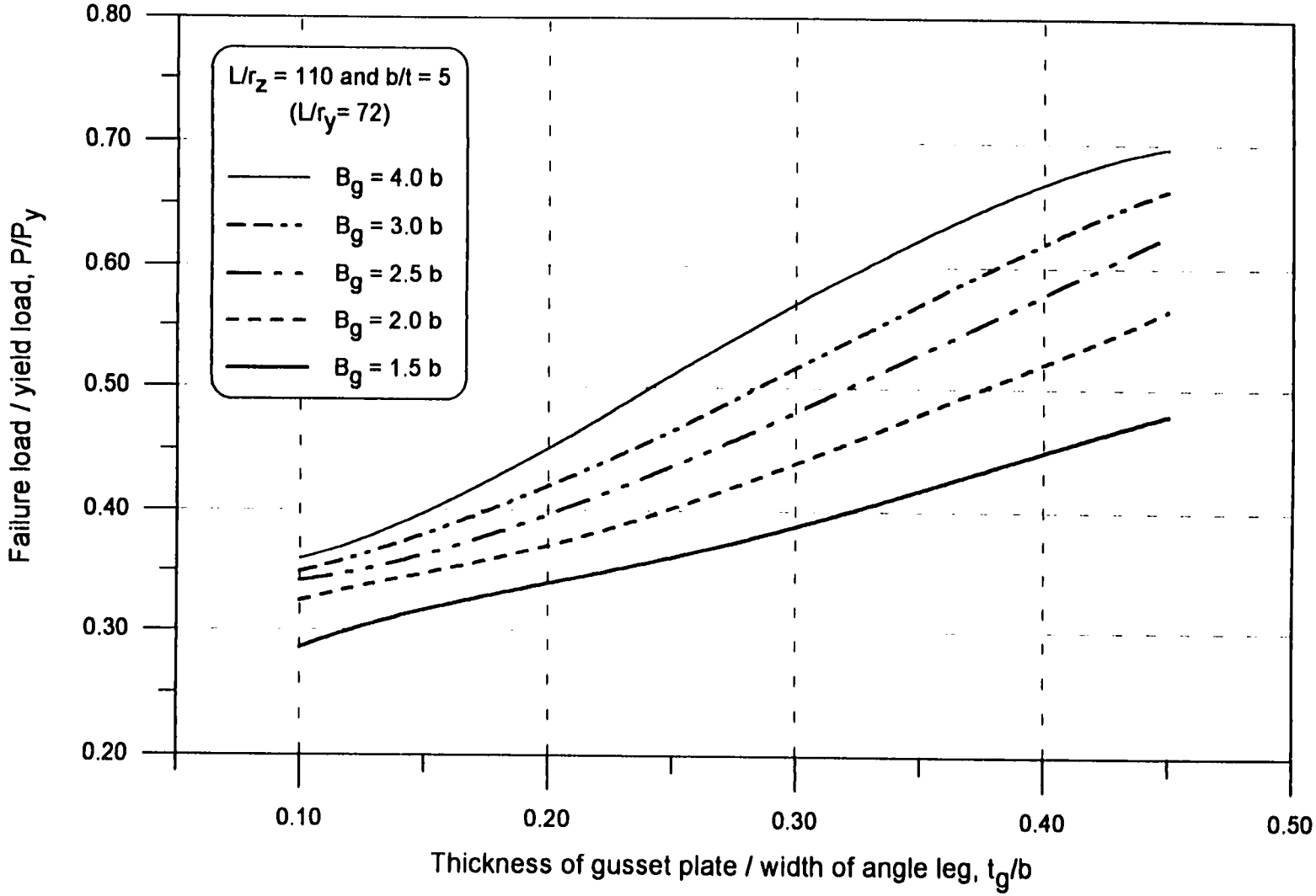

Figure B-3. Failure load predicted by finite element analysis when b/t = 5 and L/r_z = 110

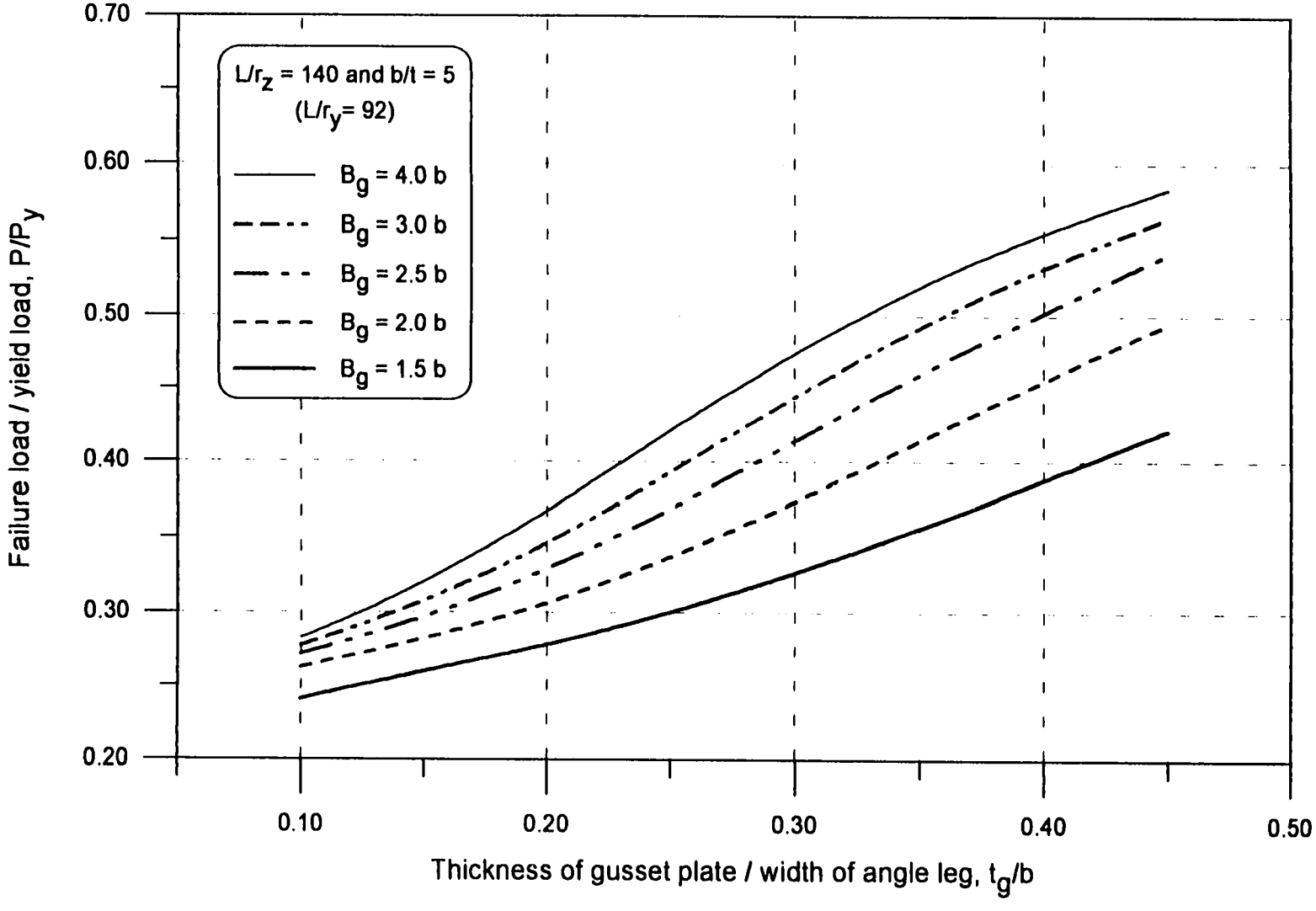

Figure B-4. Failure load predicted by finite element analysis when b/t = 5 and L/r_z = 140

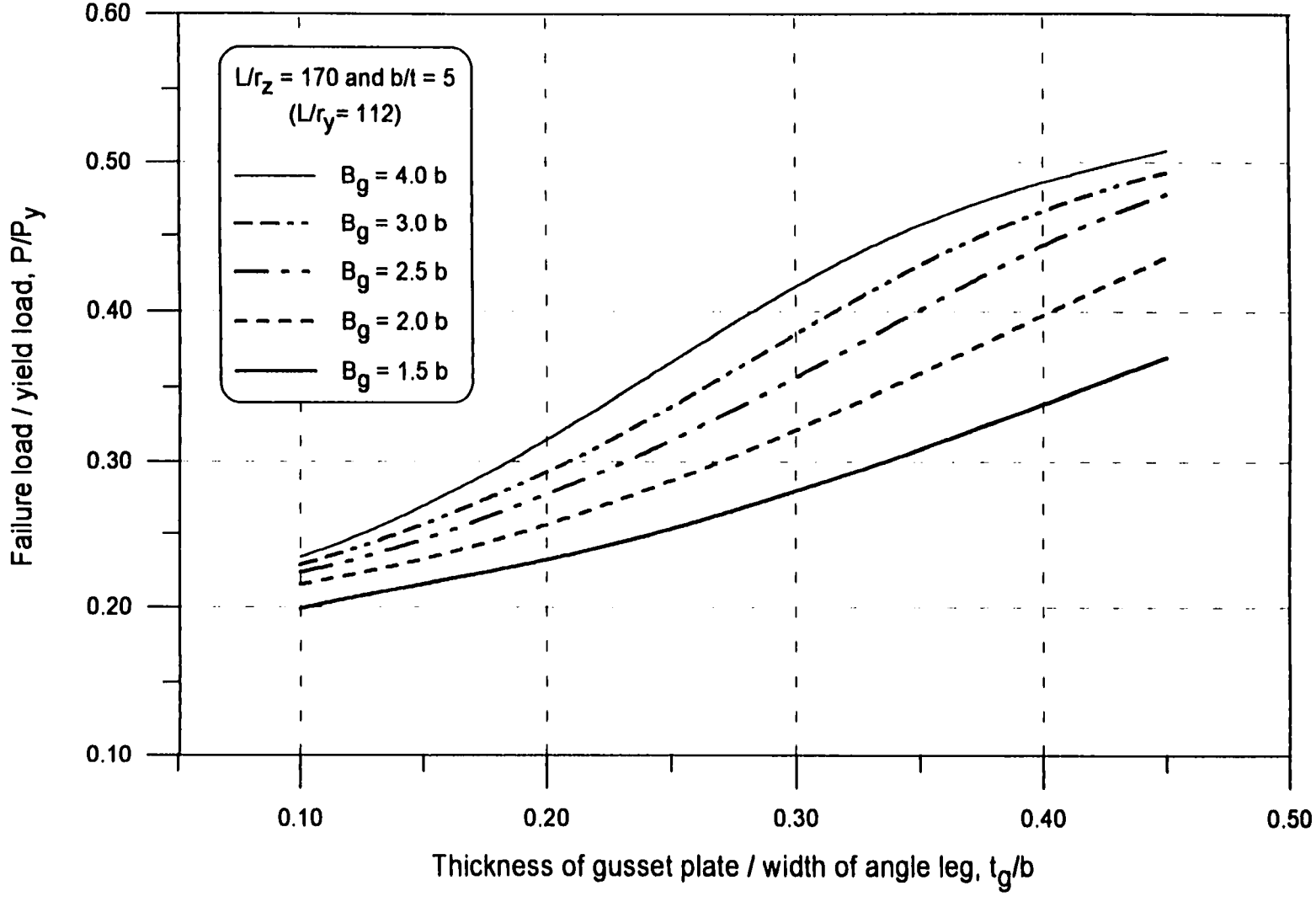

Figure B-5. Failure load predicted by finite element analysis when b/t = 5 and L/r_z = 170

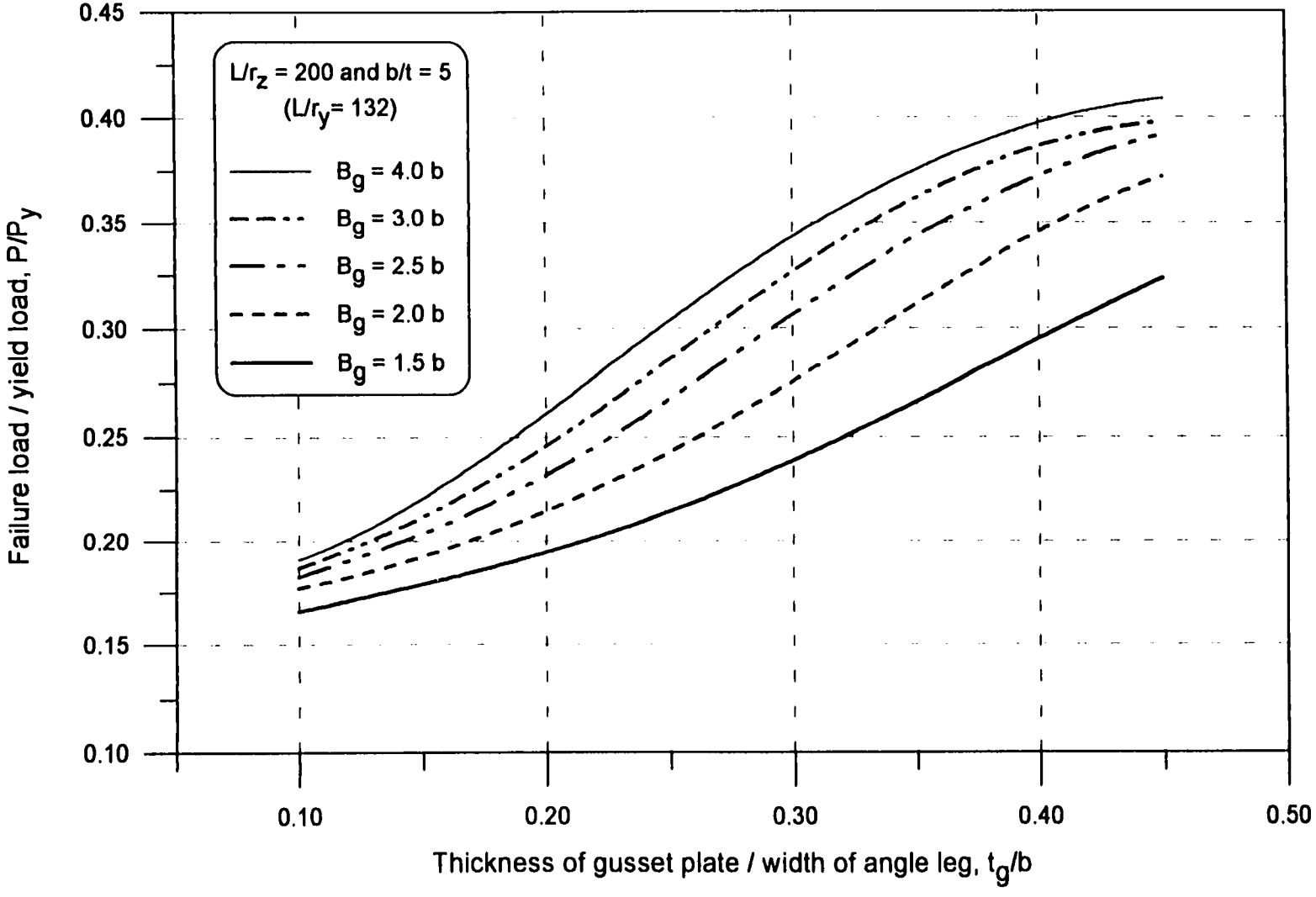

Figure B-6. Failure load predicted by finite element analysis when b/t = 5 and L/r_z = 200

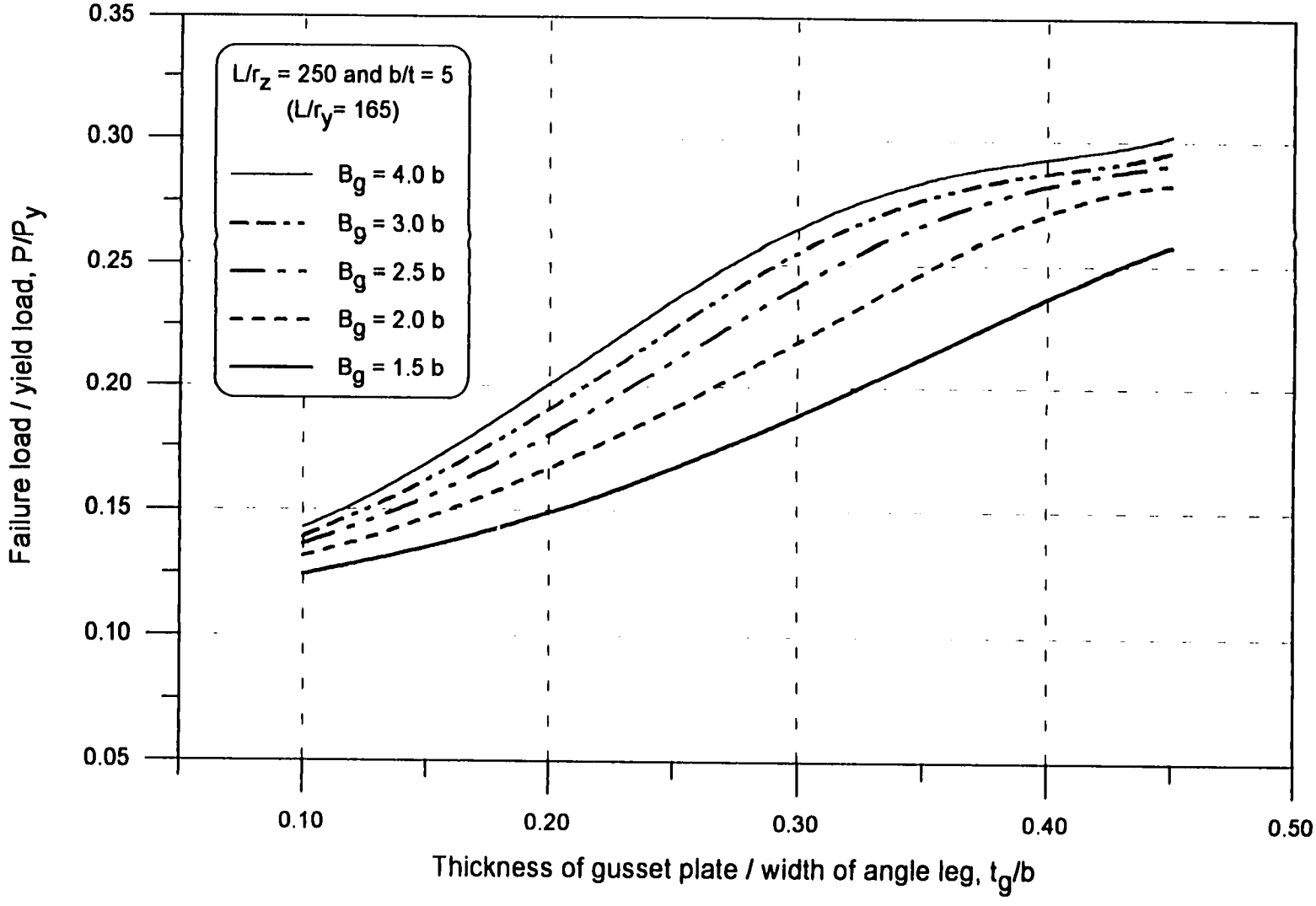

Figure B-7. Failure load predicted by finite element analysis when b/t = 5 and L/r_z = 250

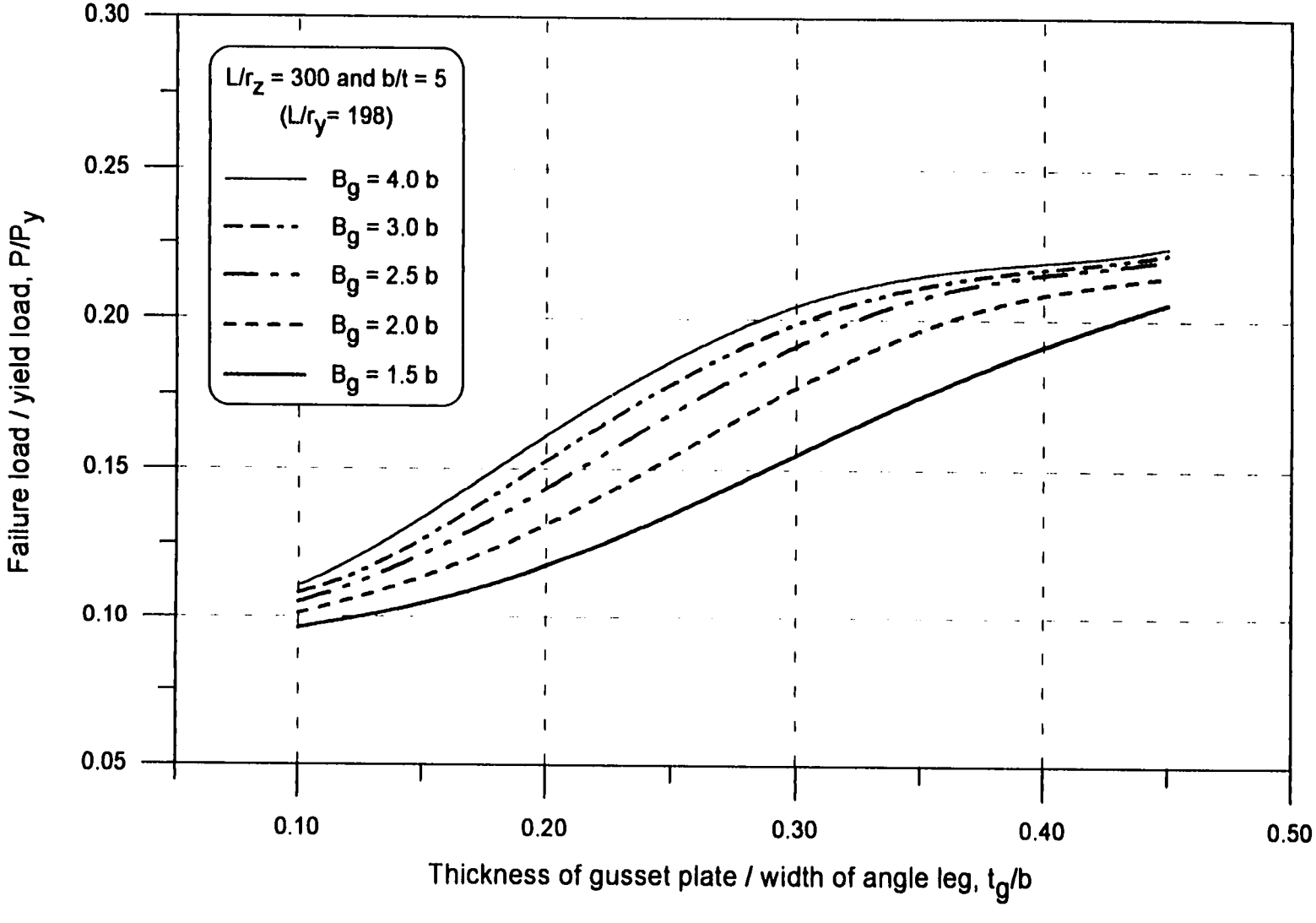

Figure B-8. Failure load predicted by finite element analysis when b/t = 5 and L/r_z = 300

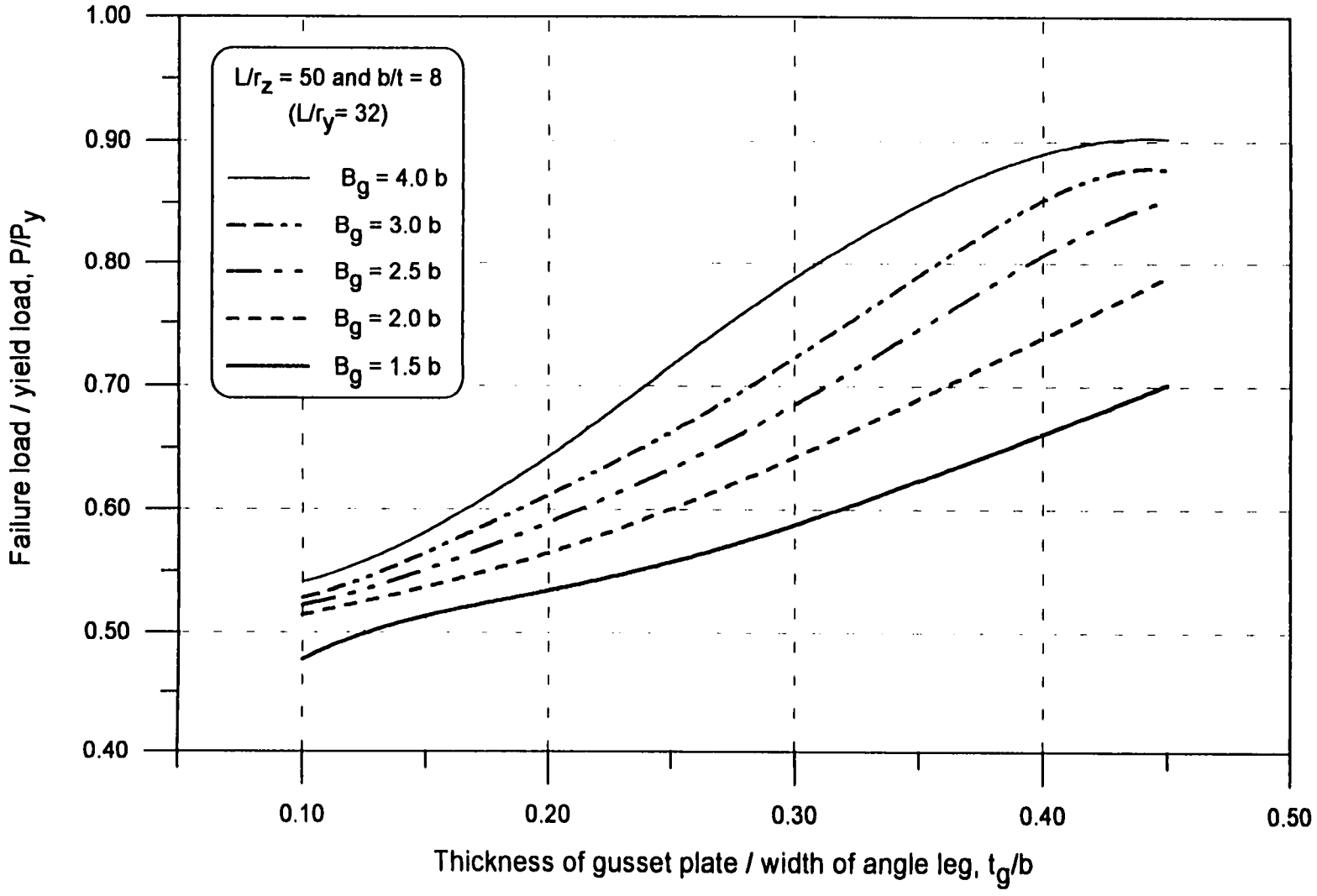

Figure B-9. Failure load predicted by finite element analysis when b/t = 8 and $L/r_z = 50$

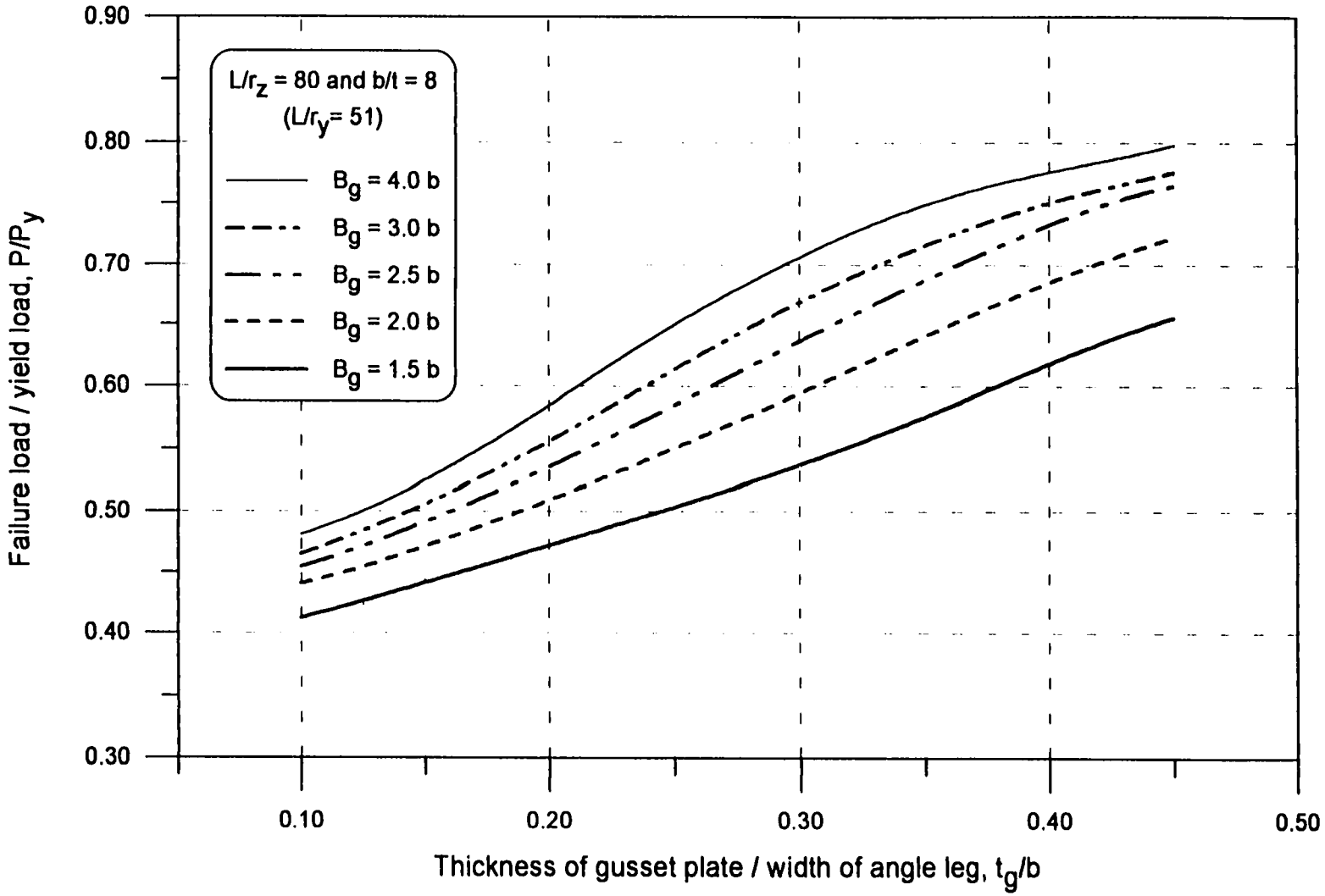

Figure B-10. Failure load predicted by finite element analysis when b/t = 8 and L/r_z = 80

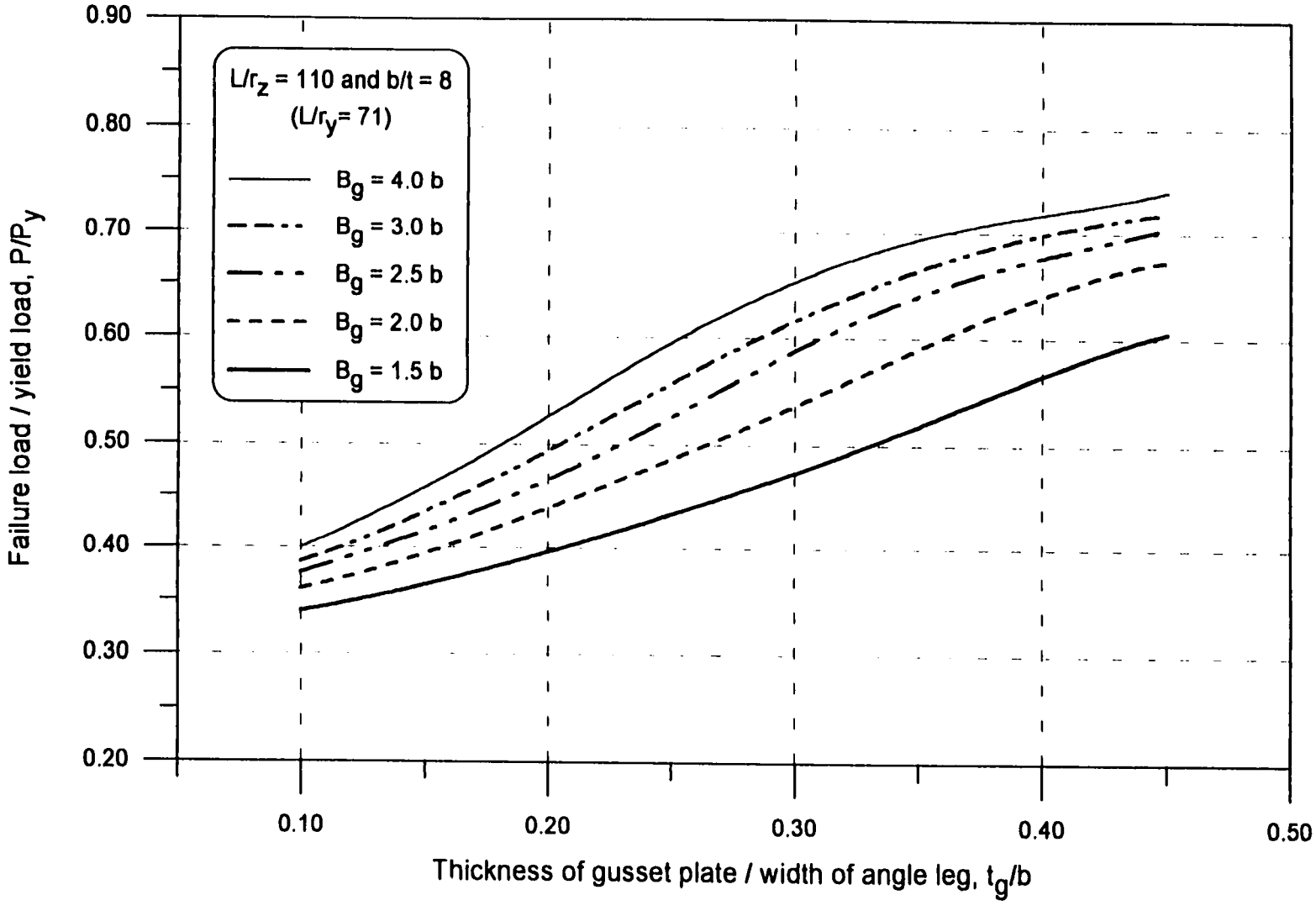

Figure B-11. Failure load predicted by finite element analysis when b/t = 8 and L/r_z = 110

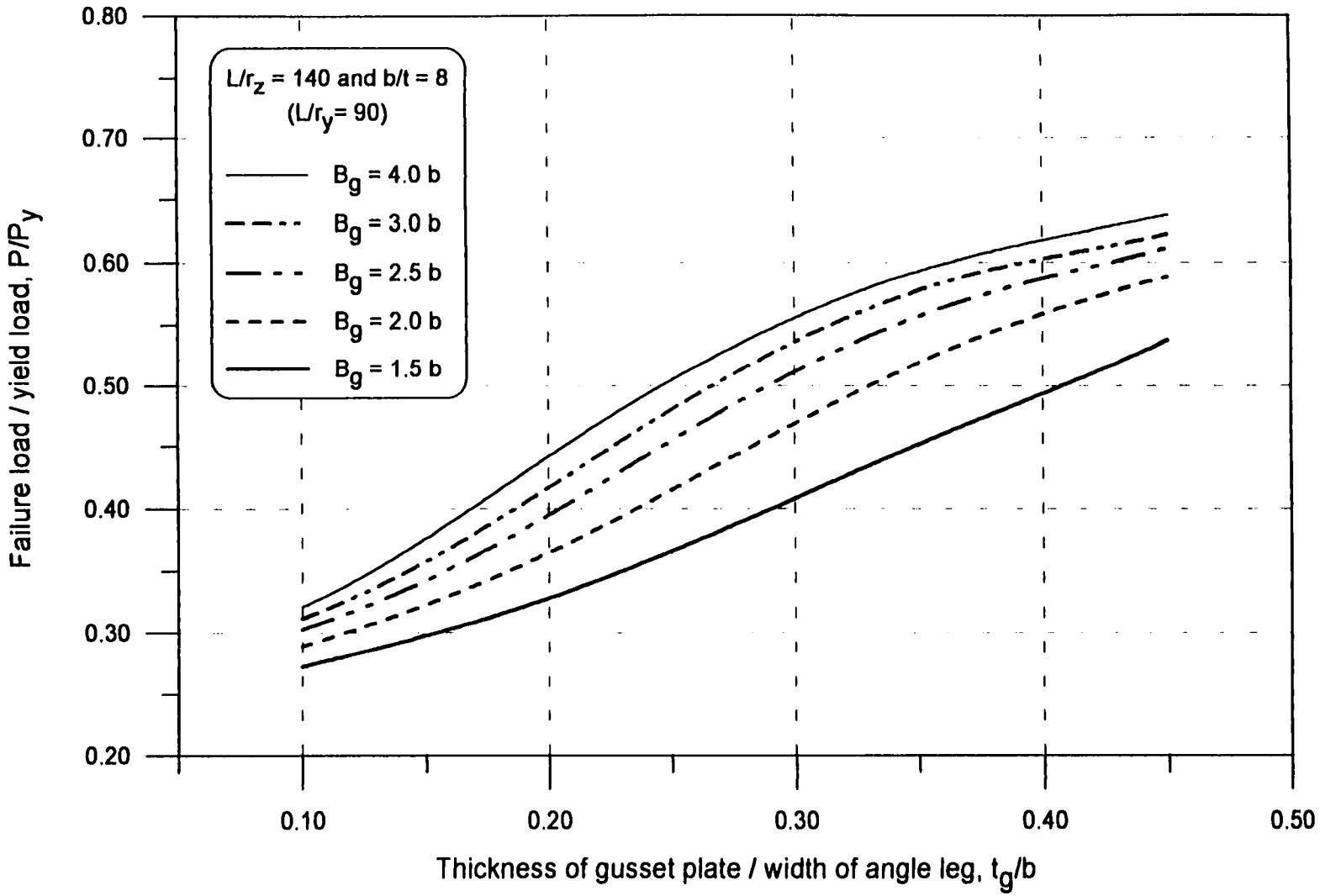

Figure B-12. Failure load predicted by finite element analysis when b/t = 8 and L/r_z = 140

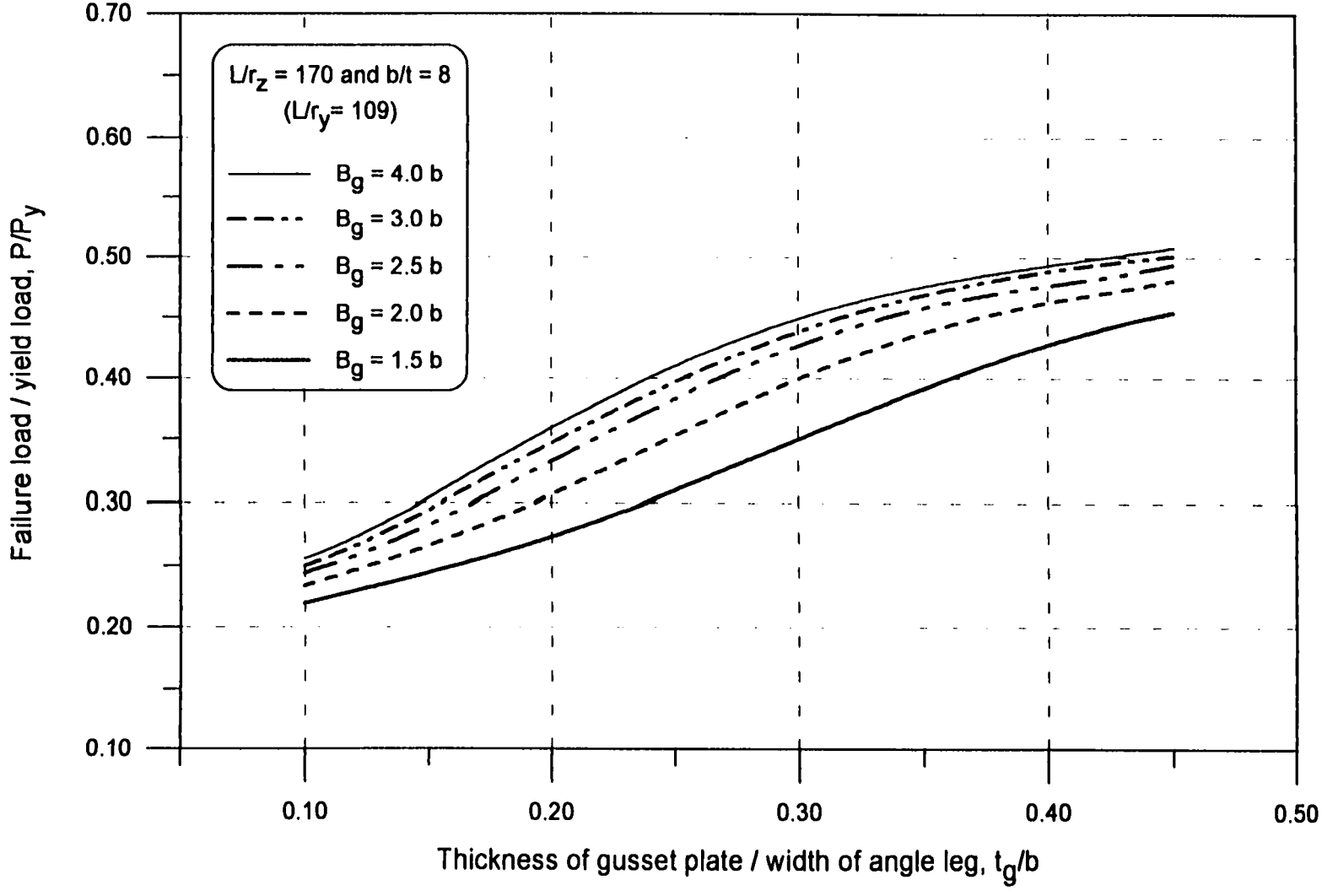

Figure B-13. Failure load predicted by finite element analysis when b/t = 8 and L/r_z = 170

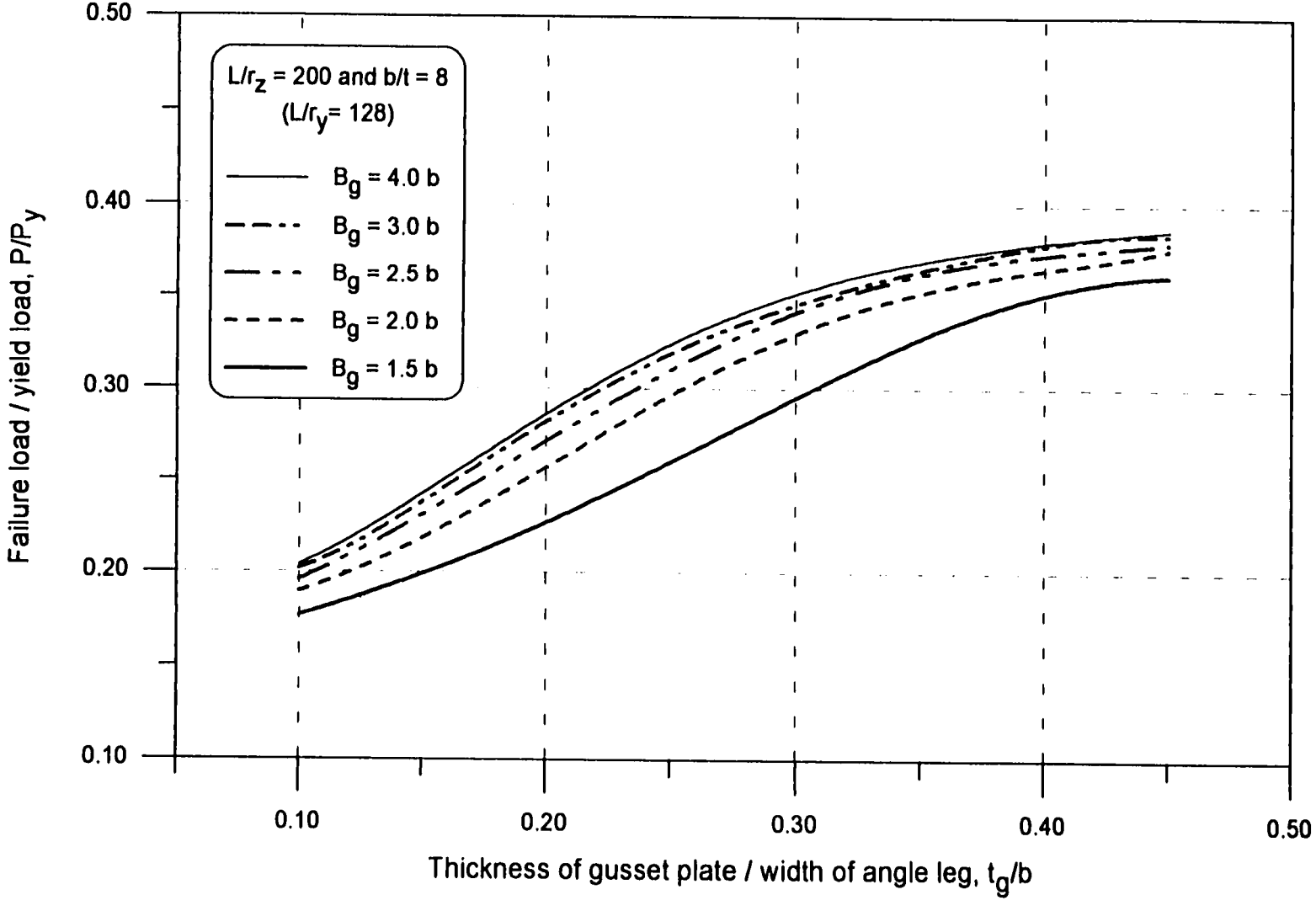

Figure B-14. Failure load predicted by finite element analysis when b/t = 8 and L/r_z = 200

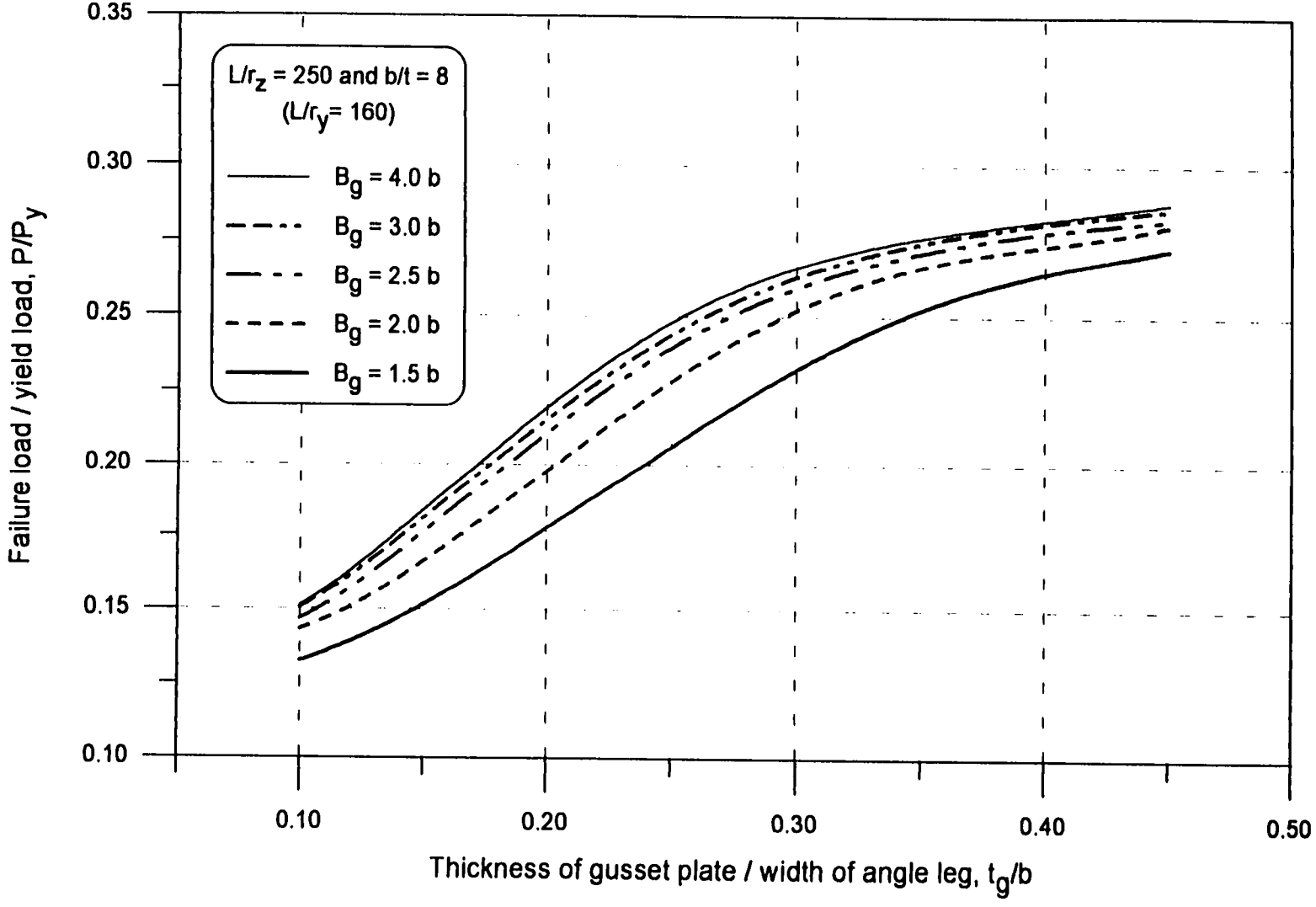

Figure B-15. Failure load predicted by finite element analysis when b/t = 8 and L/r_z = 250

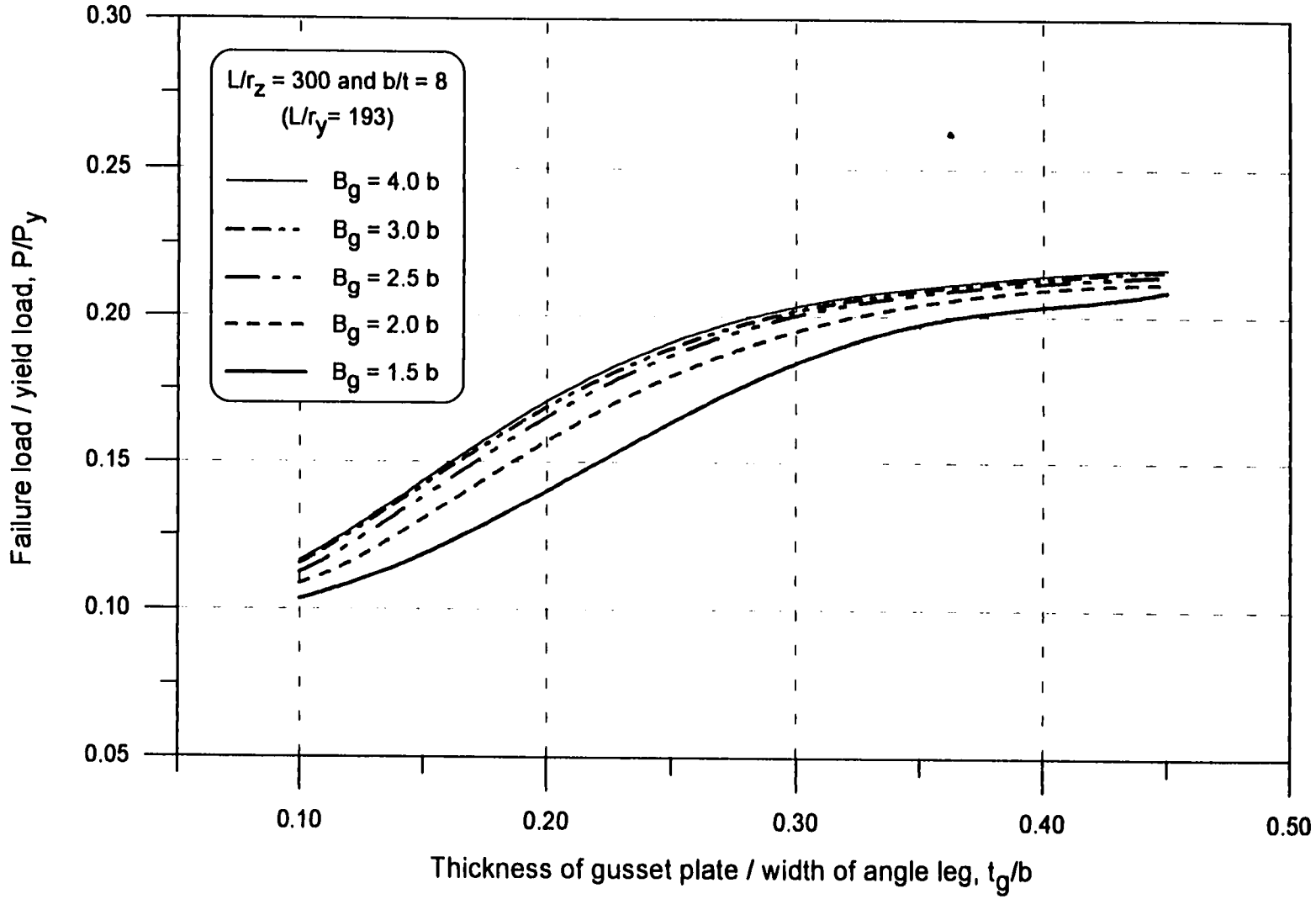

Figure B-16. Failure load predicted by finite element analysis when b/t = 8 and L/r_z = 300

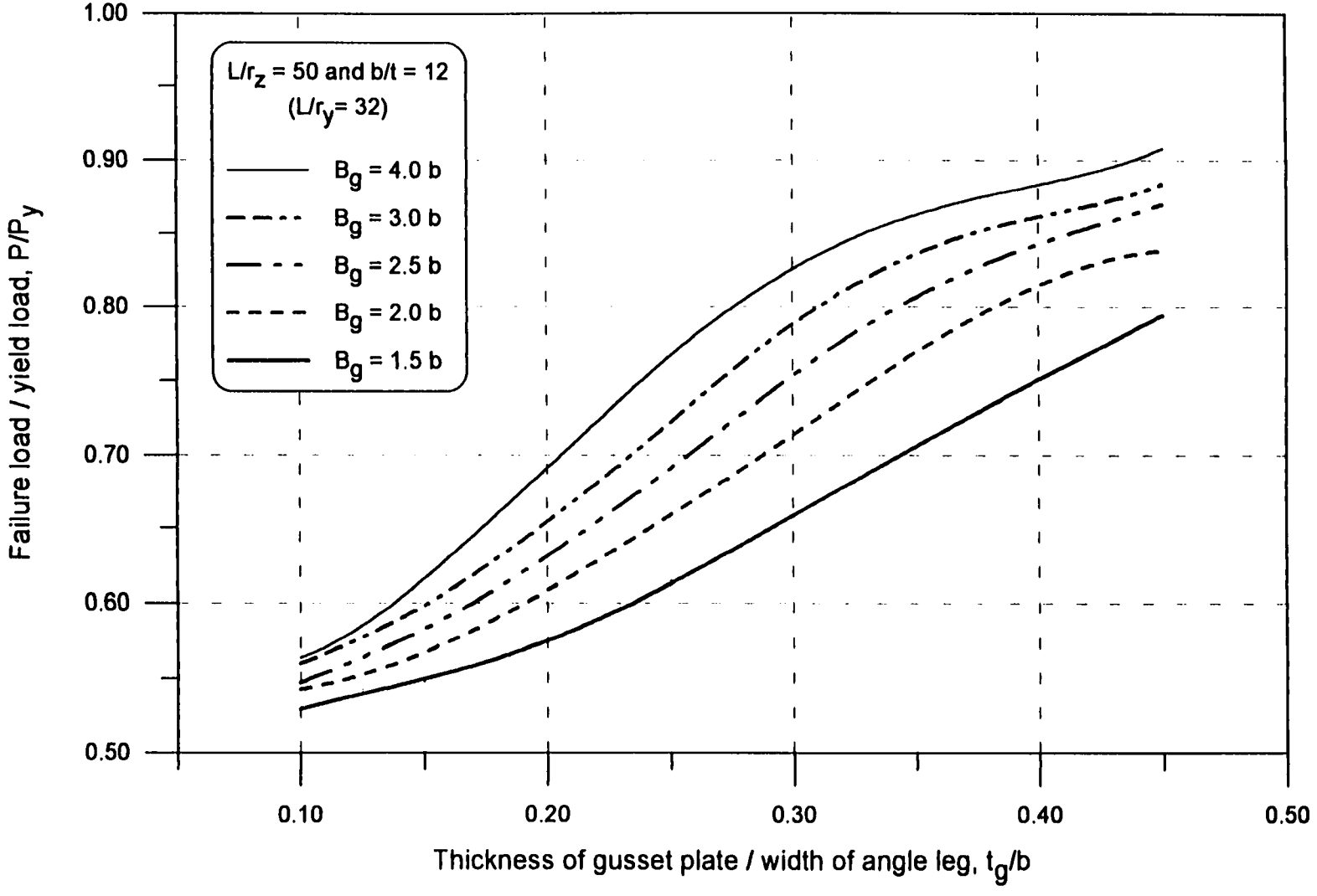

Figure B-17. Failure load predicted by finite element analysis when b/t = 12 and $L/r_z = 50$

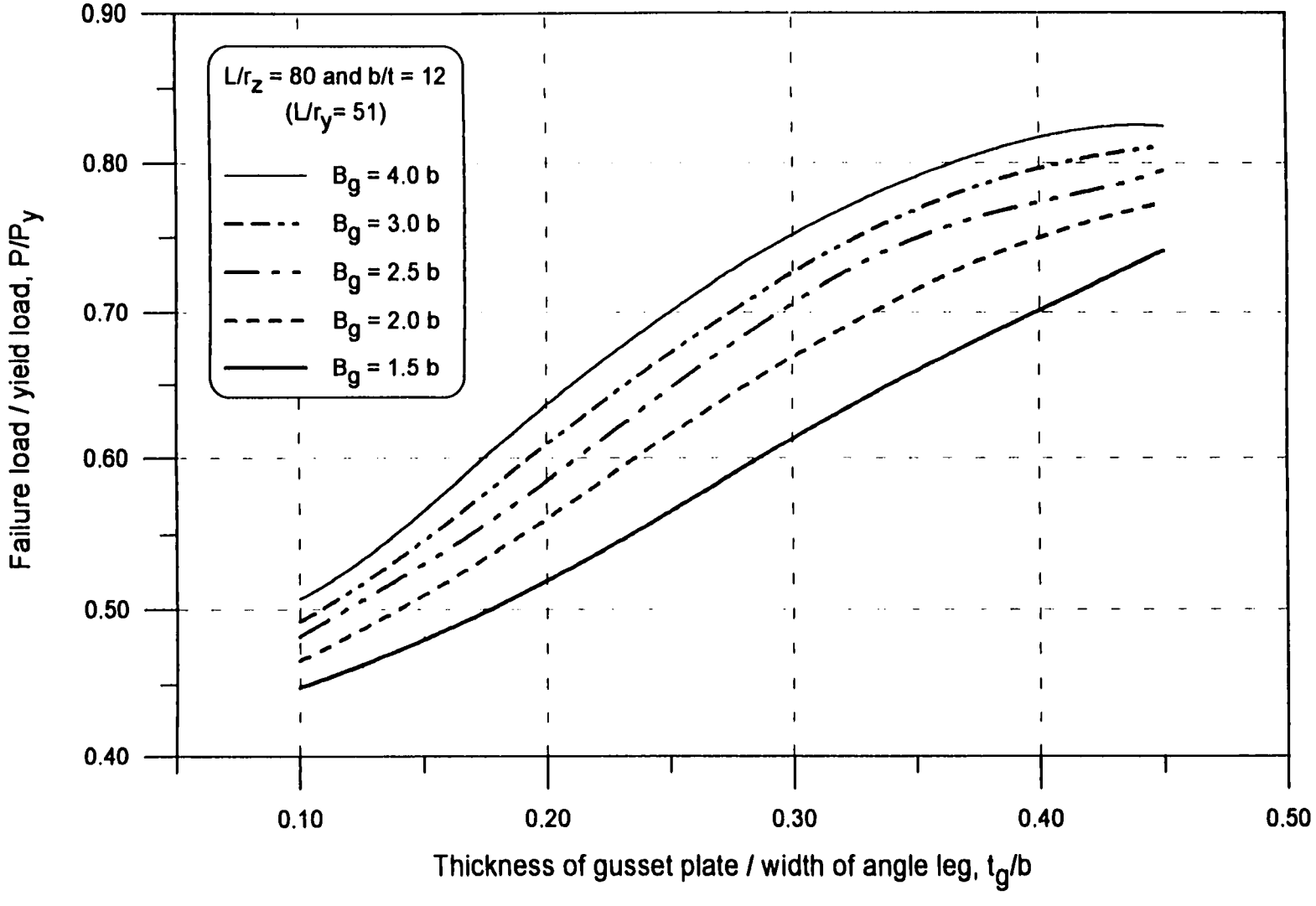

Figure B-18. Failure load predicted by finite element analysis when b/t = 12 and L/r_z = 80

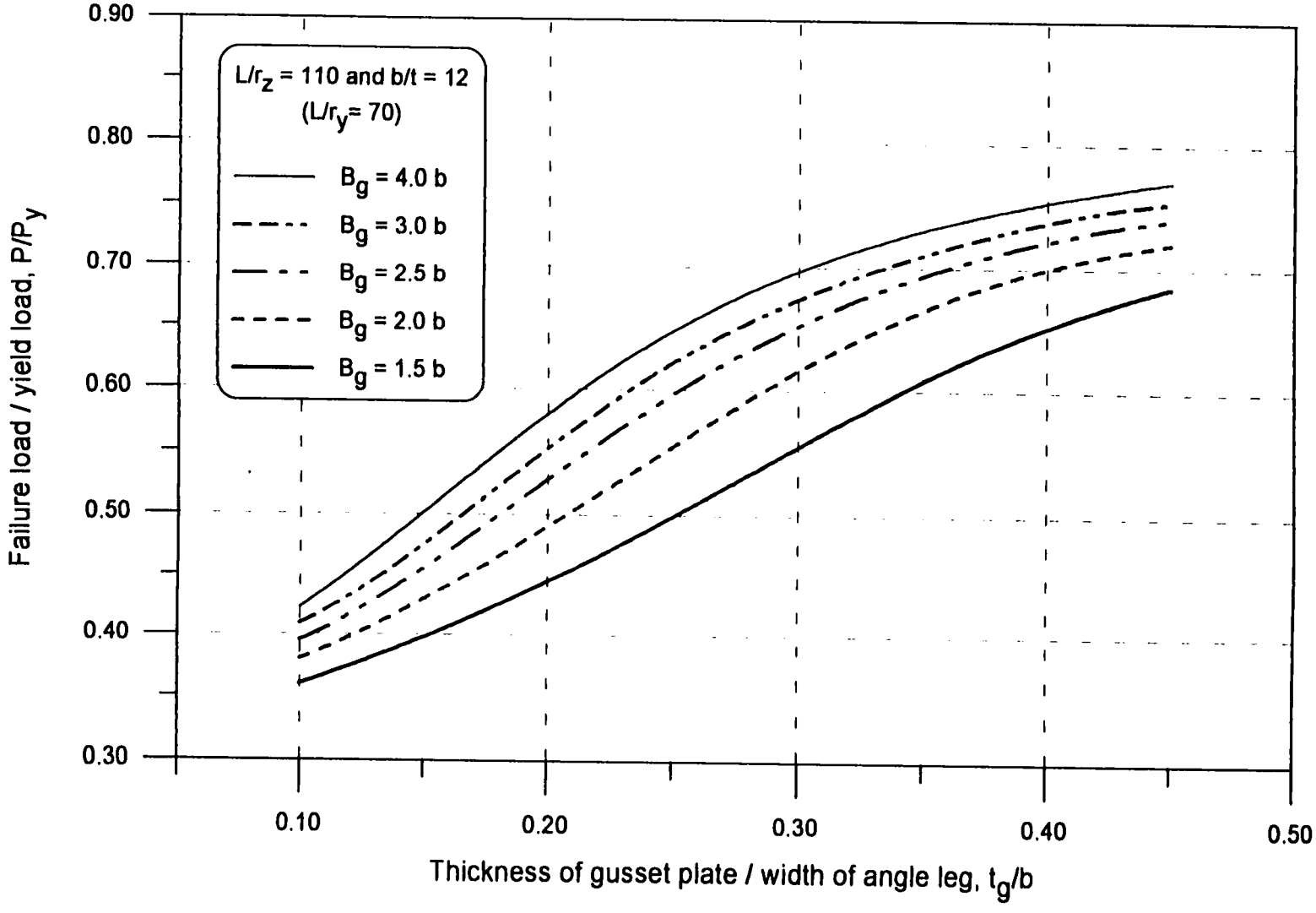

Figure B-19. Failure load predicted by finite element analysis when b/t = 12 and L/r_z = 110

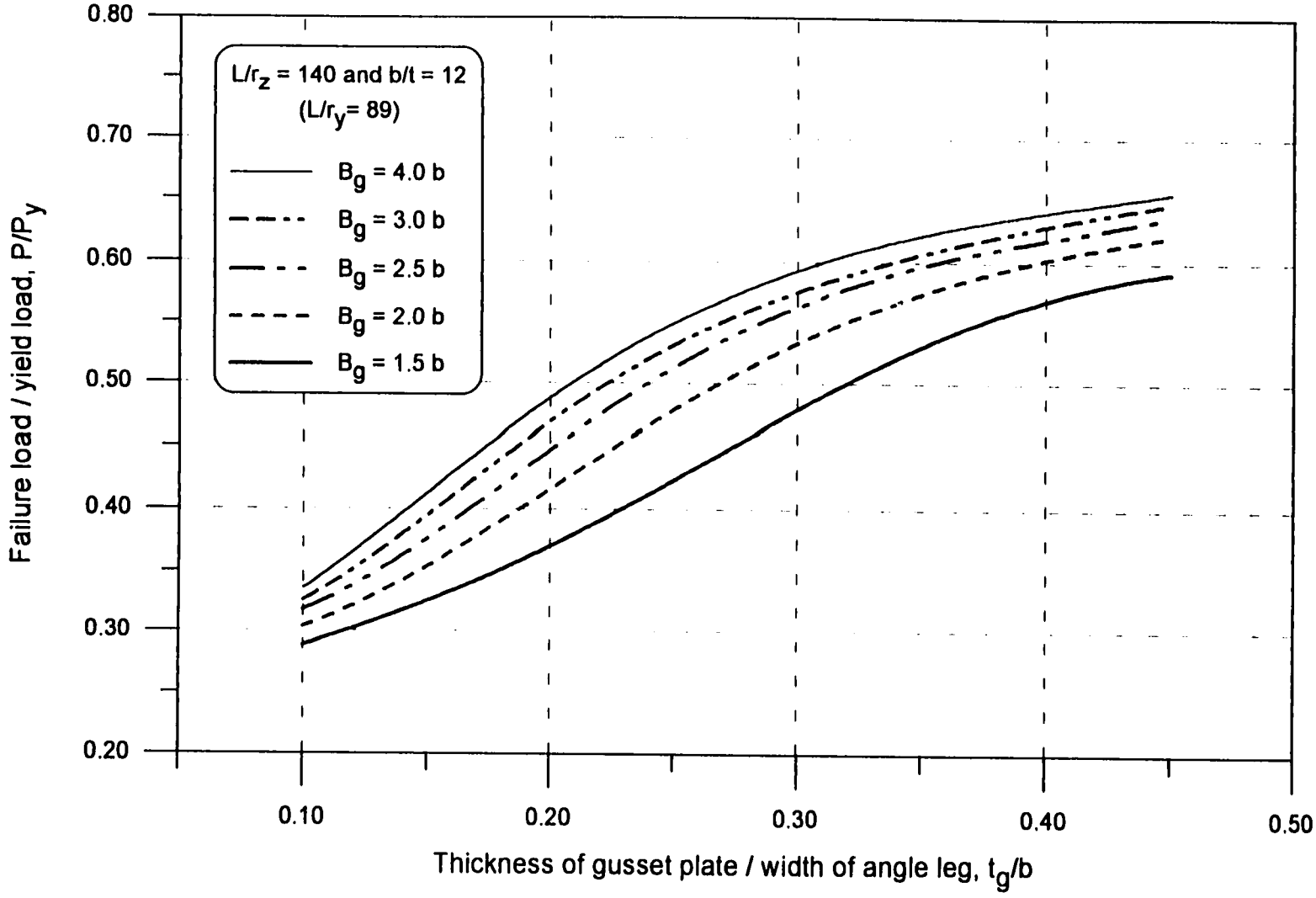

Figure B-20. Failure load predicted by finite element analysis when b/t = 12 and L/r_z = 140

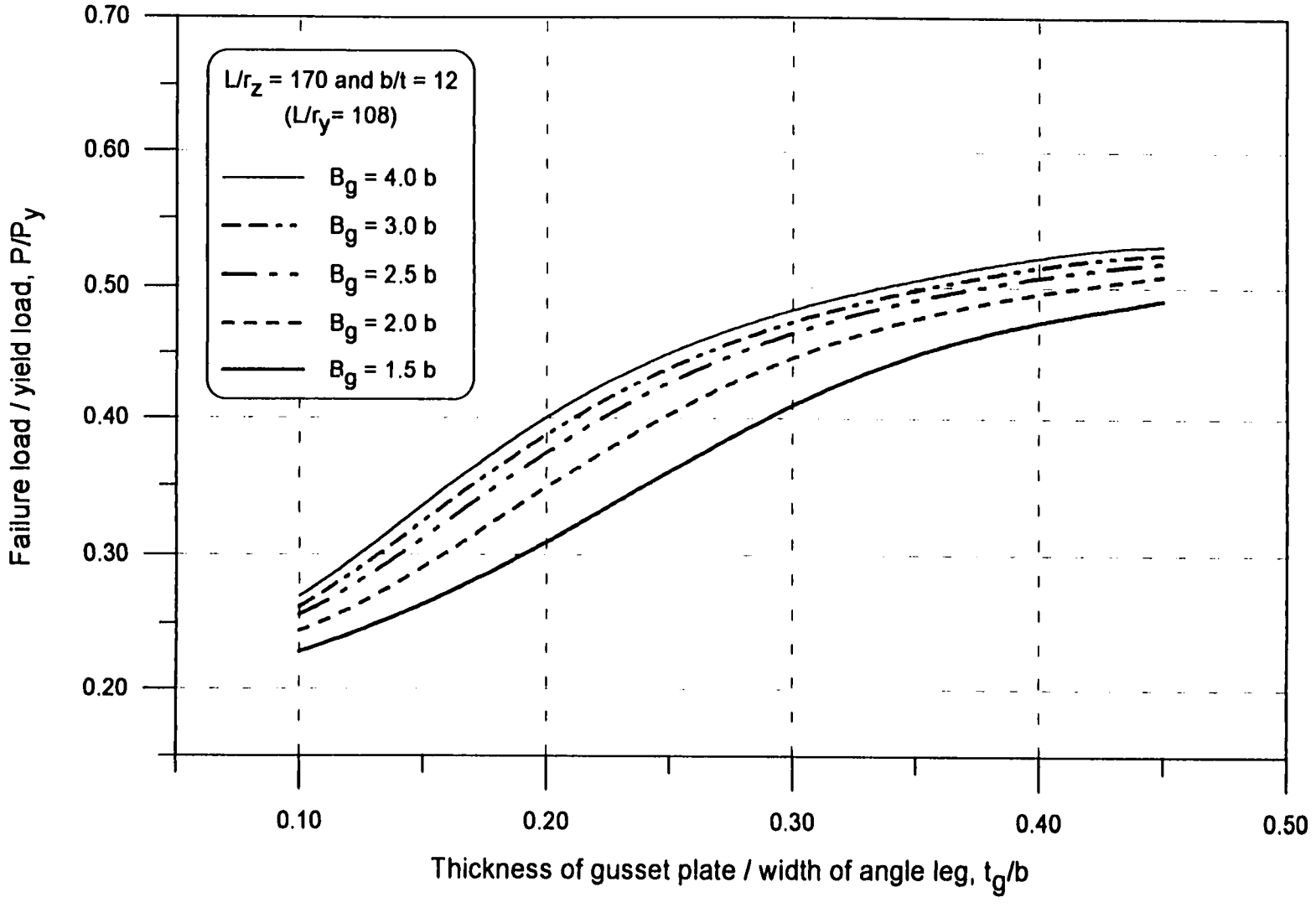

Figure B-21. Failure load predicted by finite element analysis when b/t = 12 and L/r_z = 170

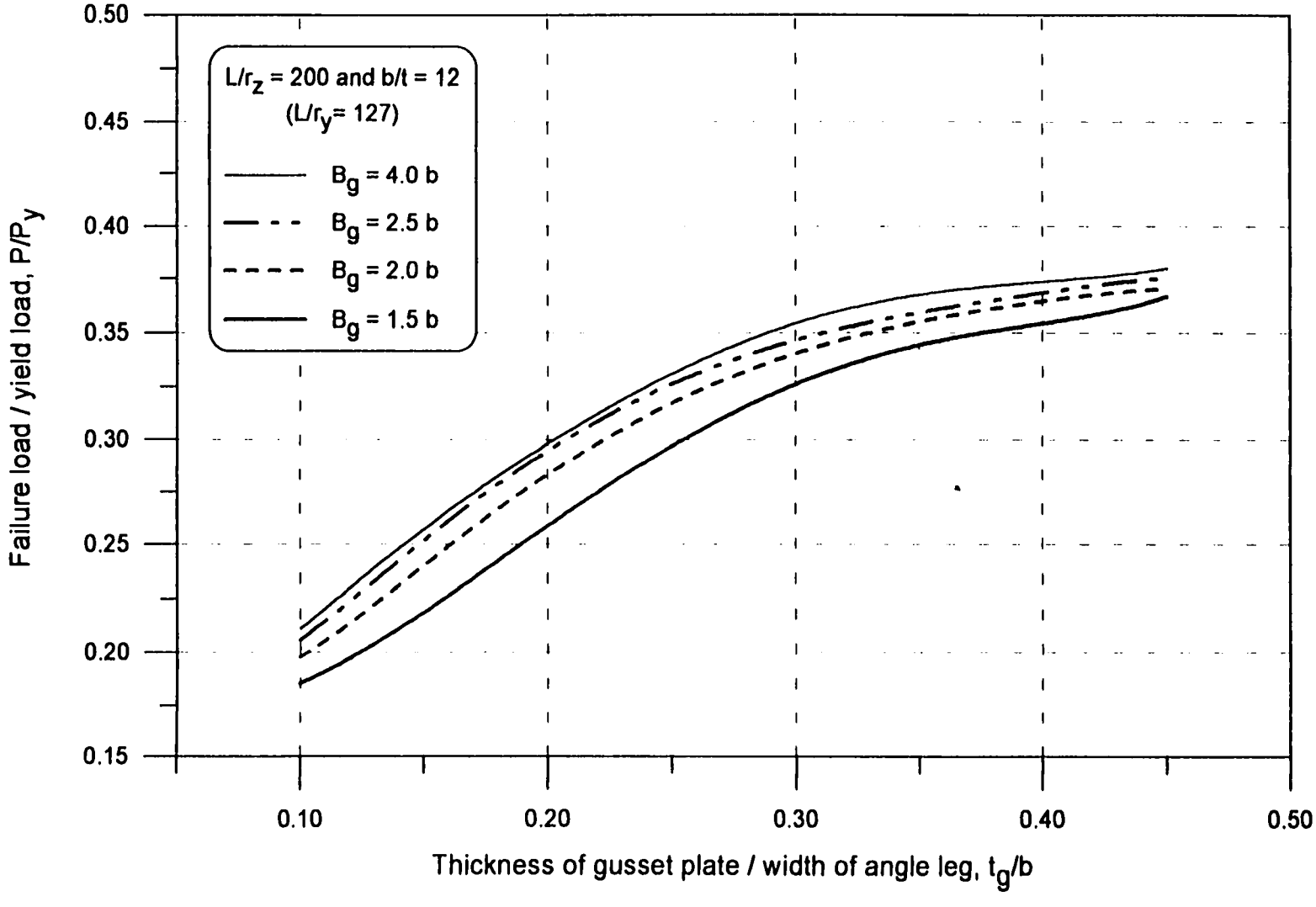

Figure B-22. Failure load predicted by finite element analysis when b/t = 12 and L/r_z = 200

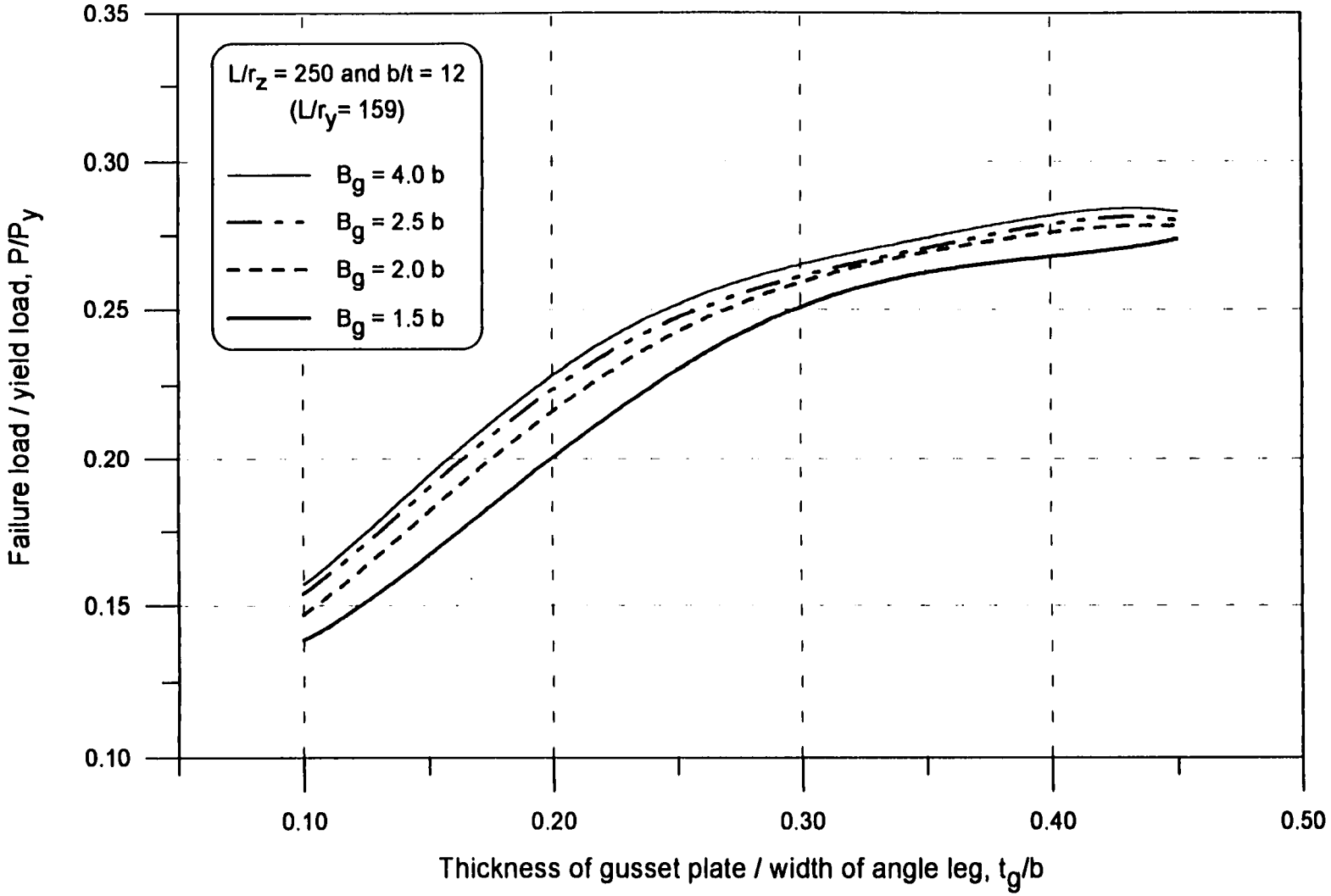

Figure B-23. Failure load predicted by finite element analysis when b/t = 12 and L/r_z = 250

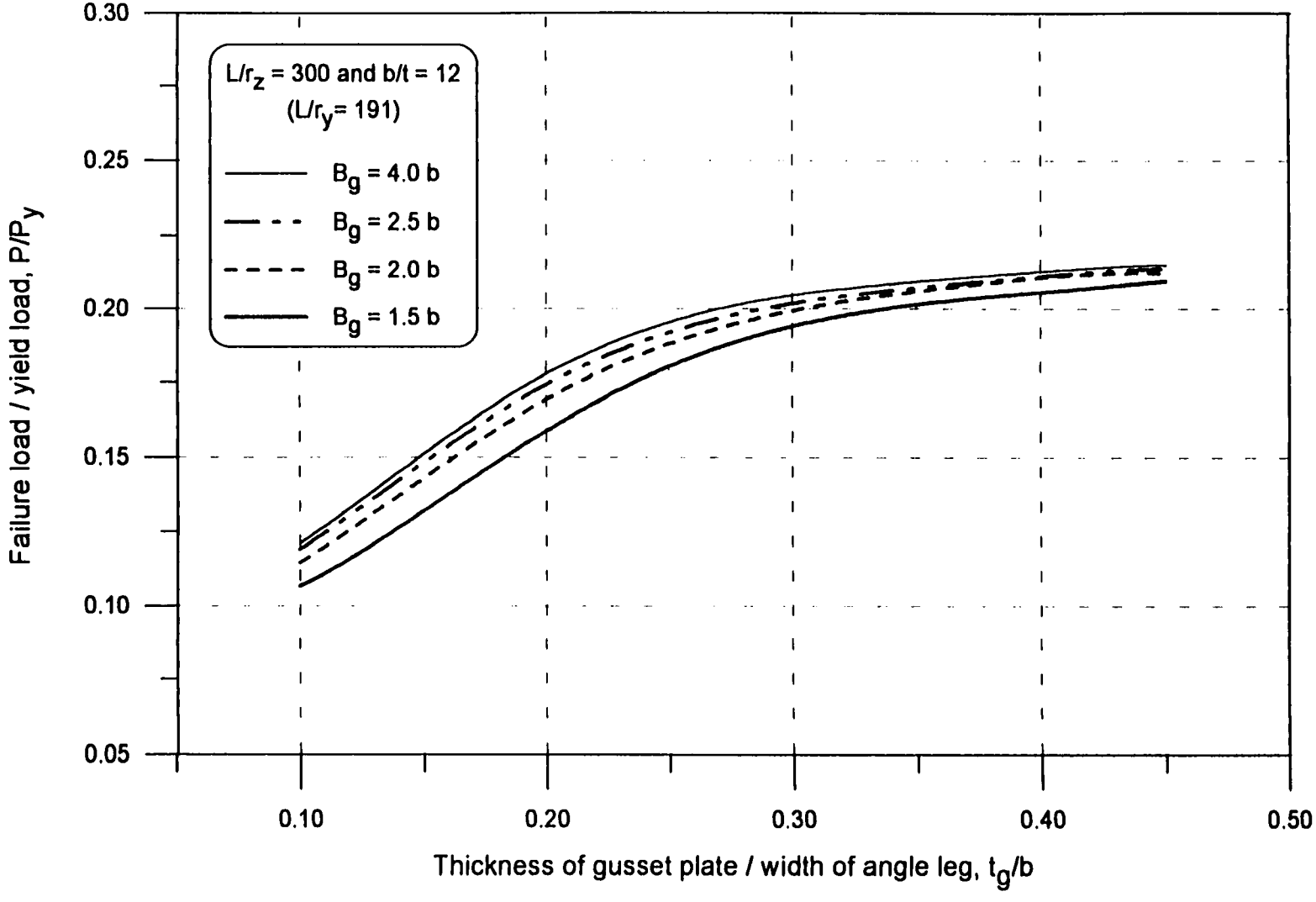

Figure B-24. Failure load predicted by finite element analysis when b/t = 12 and L/r_z = 300

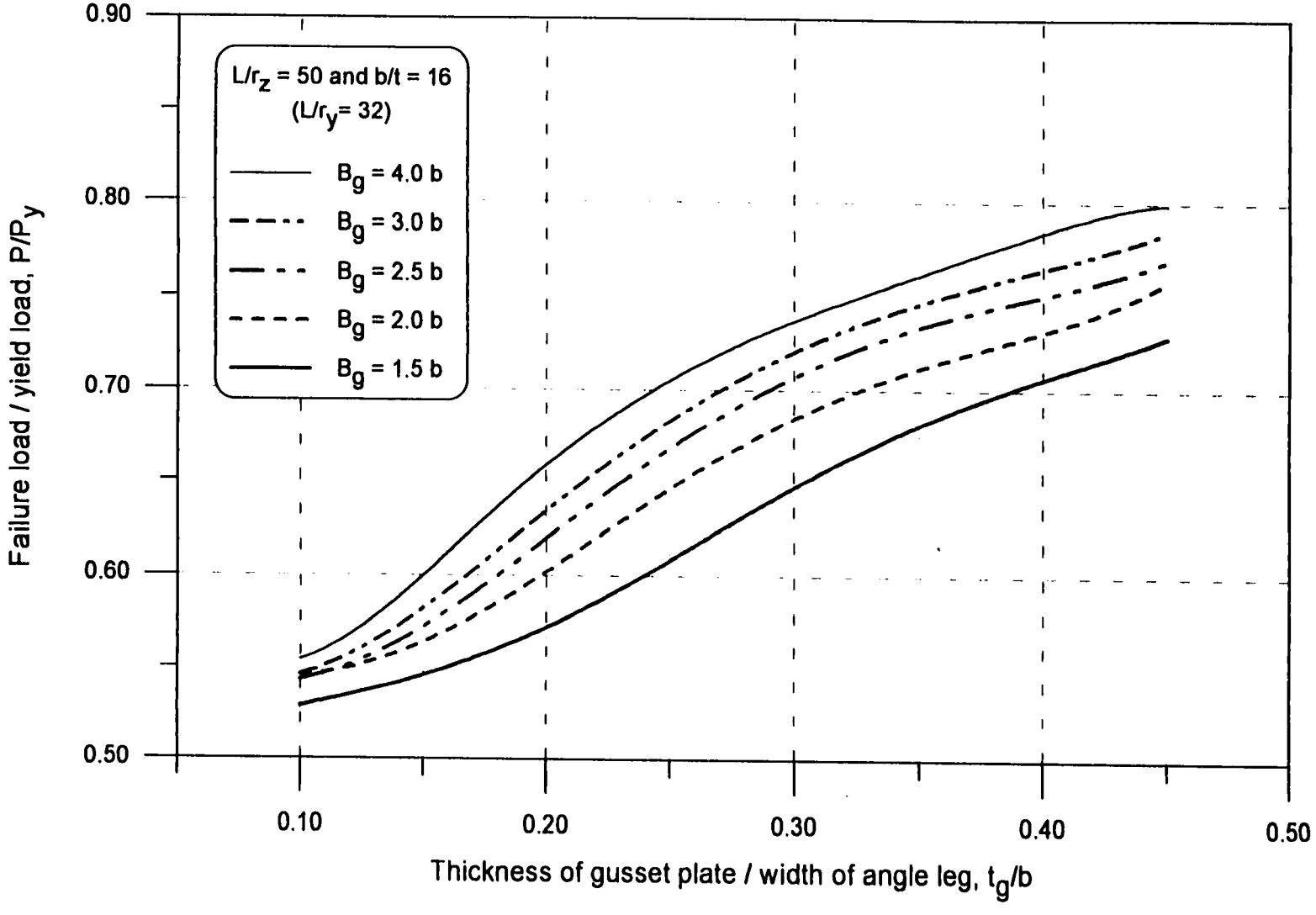

Figure B-25. Failure load predicted by finite element analysis when b/t = 16 and L/r_z = 50

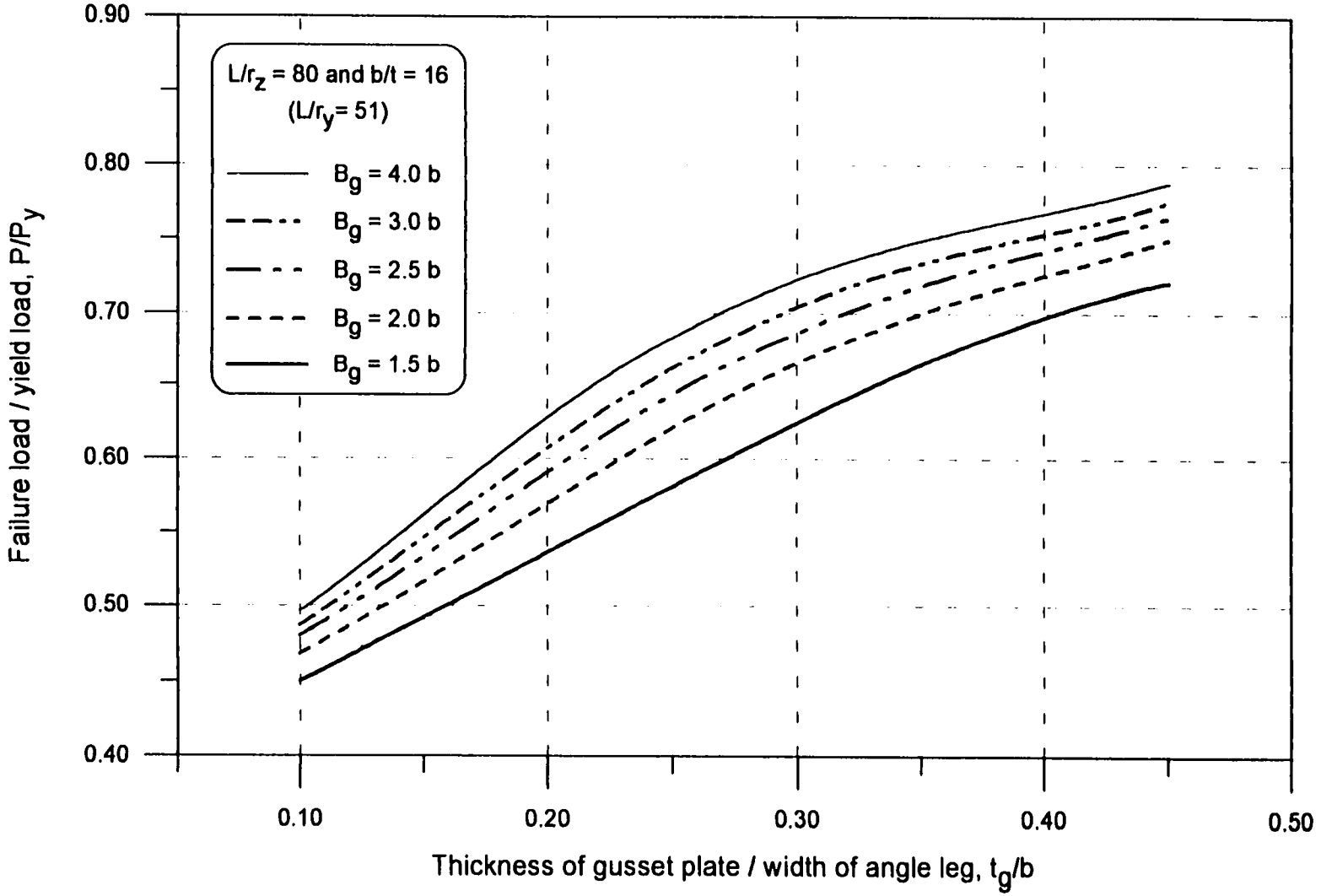

Figure B-26. Failure load predicted by finite element analysis when b/t = 16 and L/r_z = 80

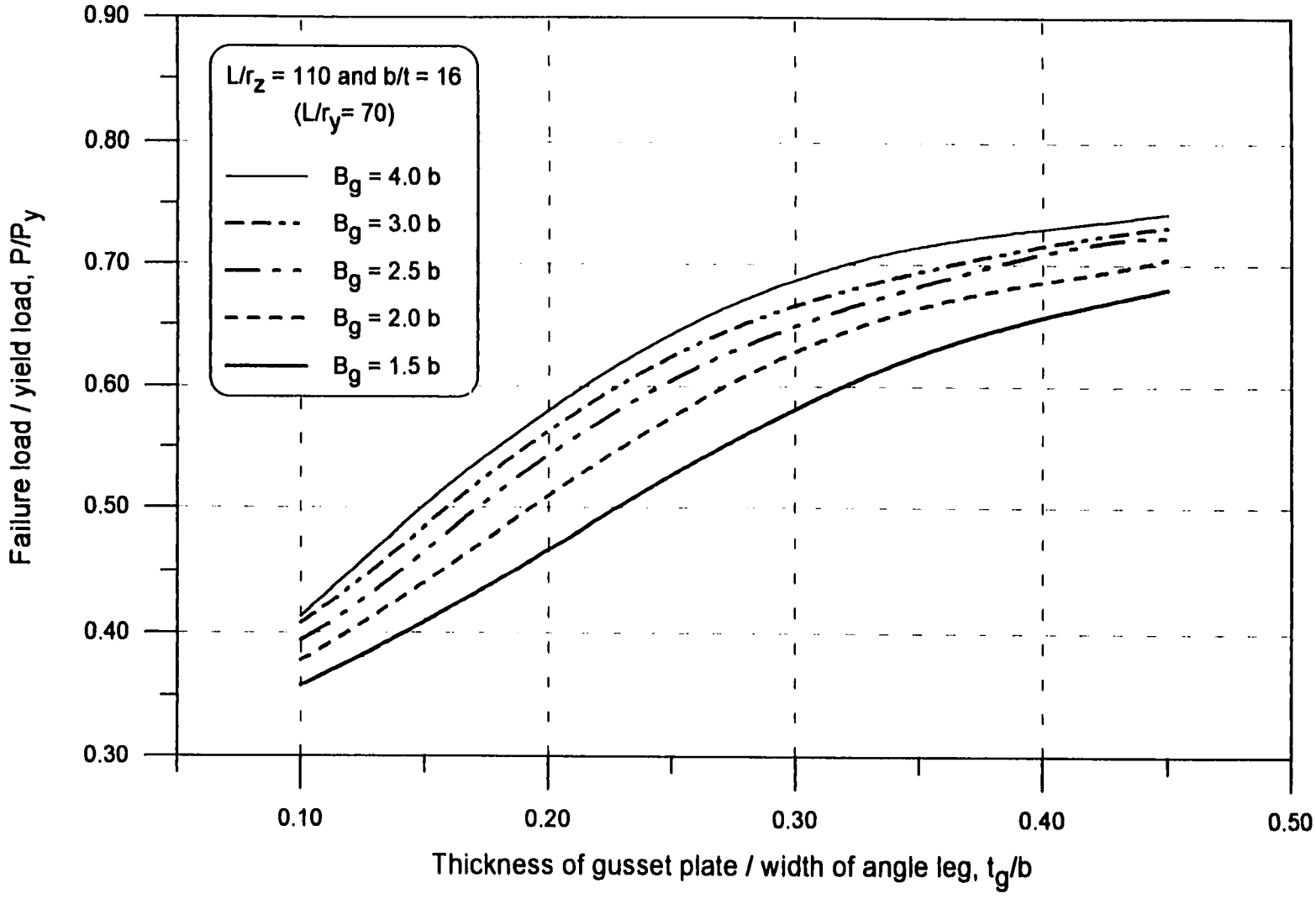

Figure B-27. Failure load predicted by finite element analysis when b/t = 16 and L/r_z = 110

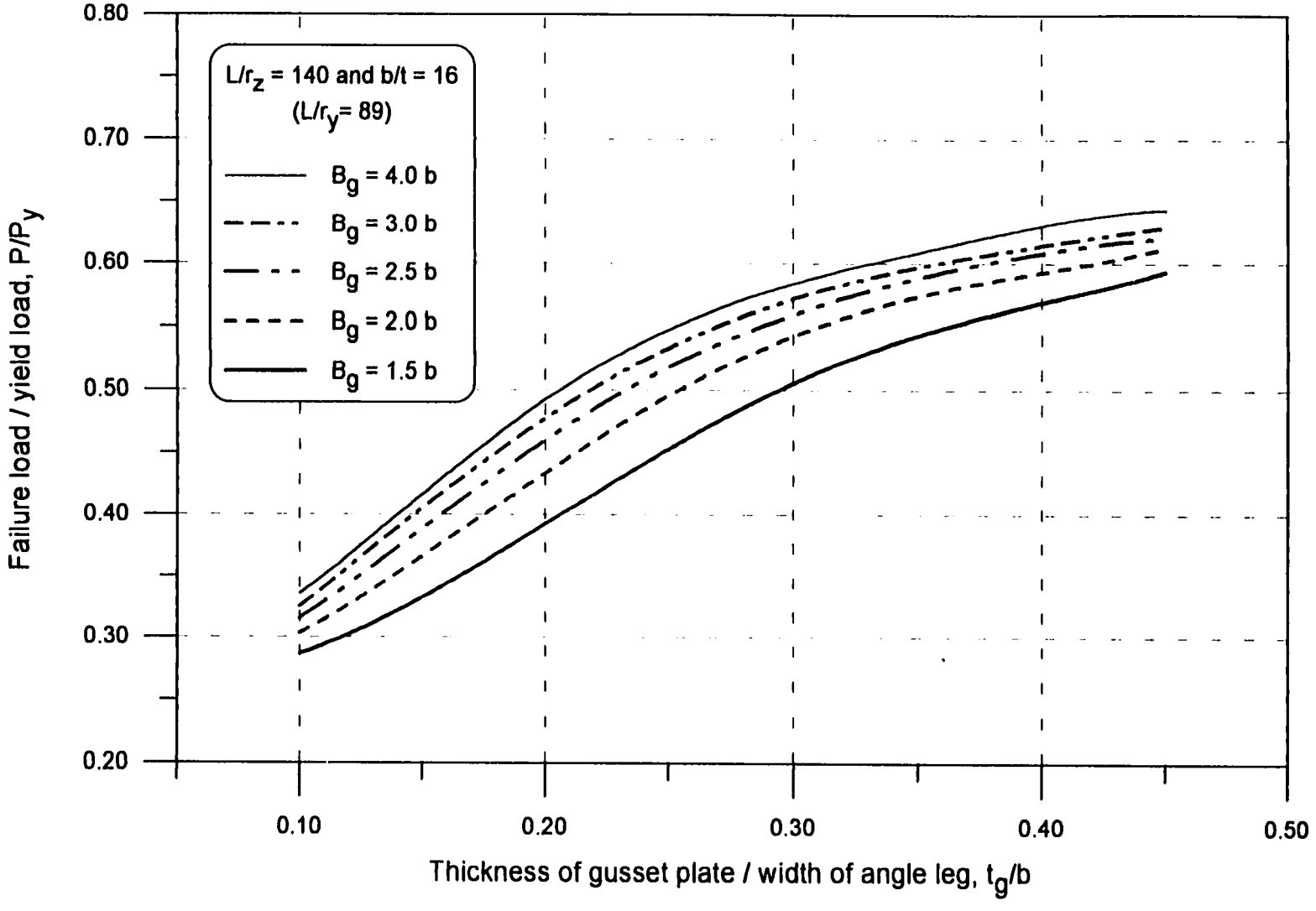

Figure B-28. Failure load predicted by finite element analysis when b/t = 16 and L/r_z = 140

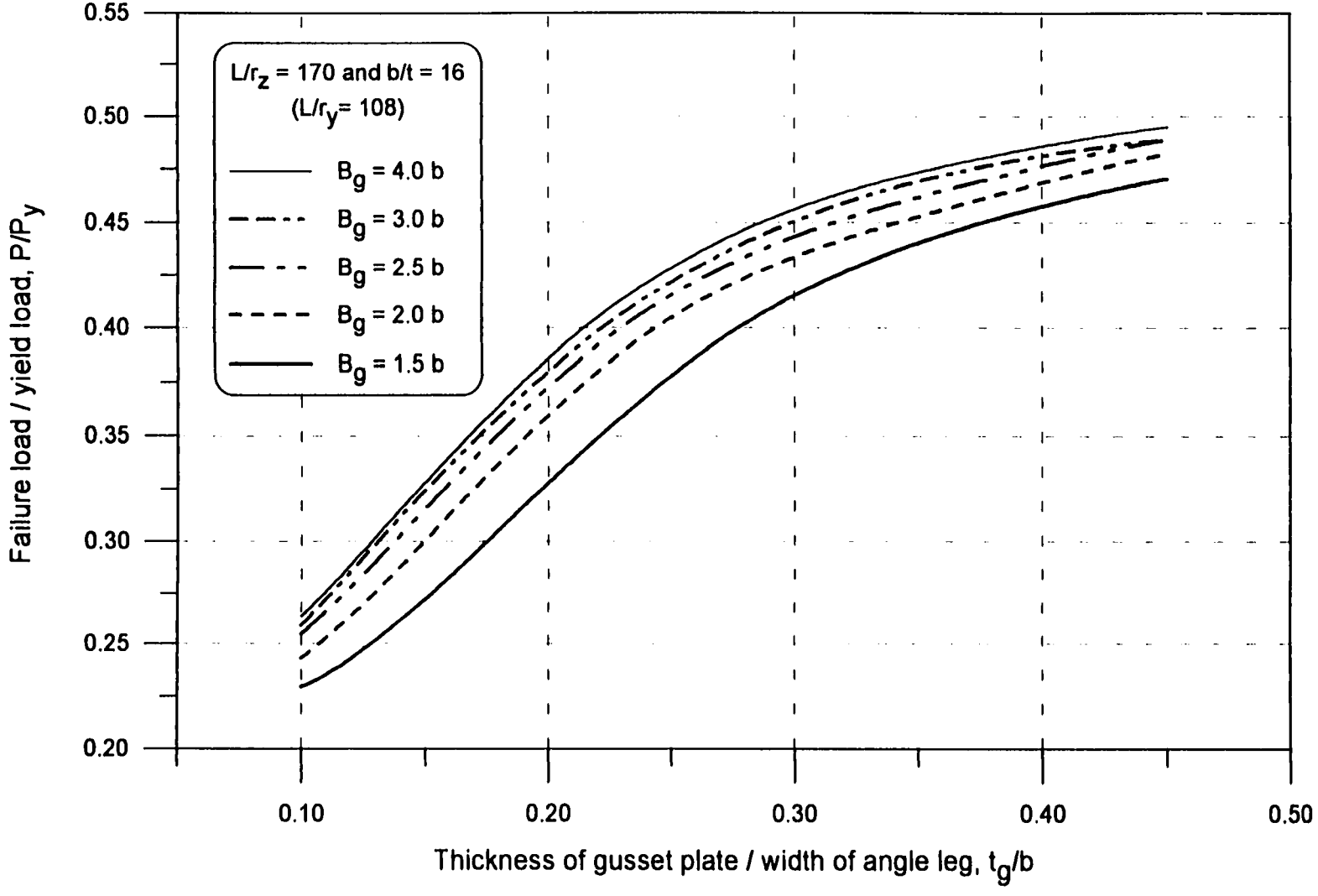

Figure B-29. Failure load predicted by finite element analysis when b/t = 16 and L/r_z = 170

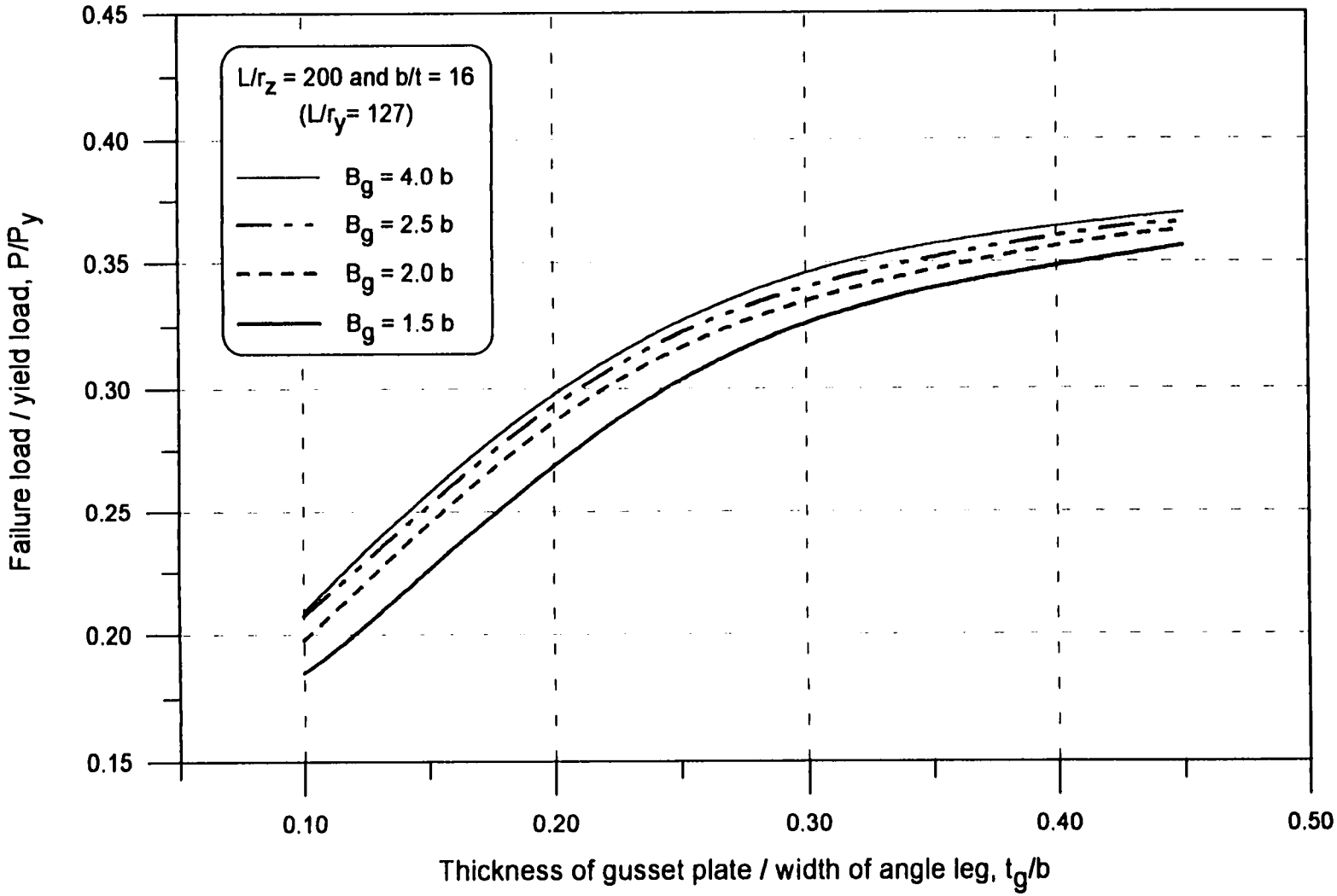

Figure B-30. Failure load predicted by finite element analysis when b/t = 16 and L/r_z = 200

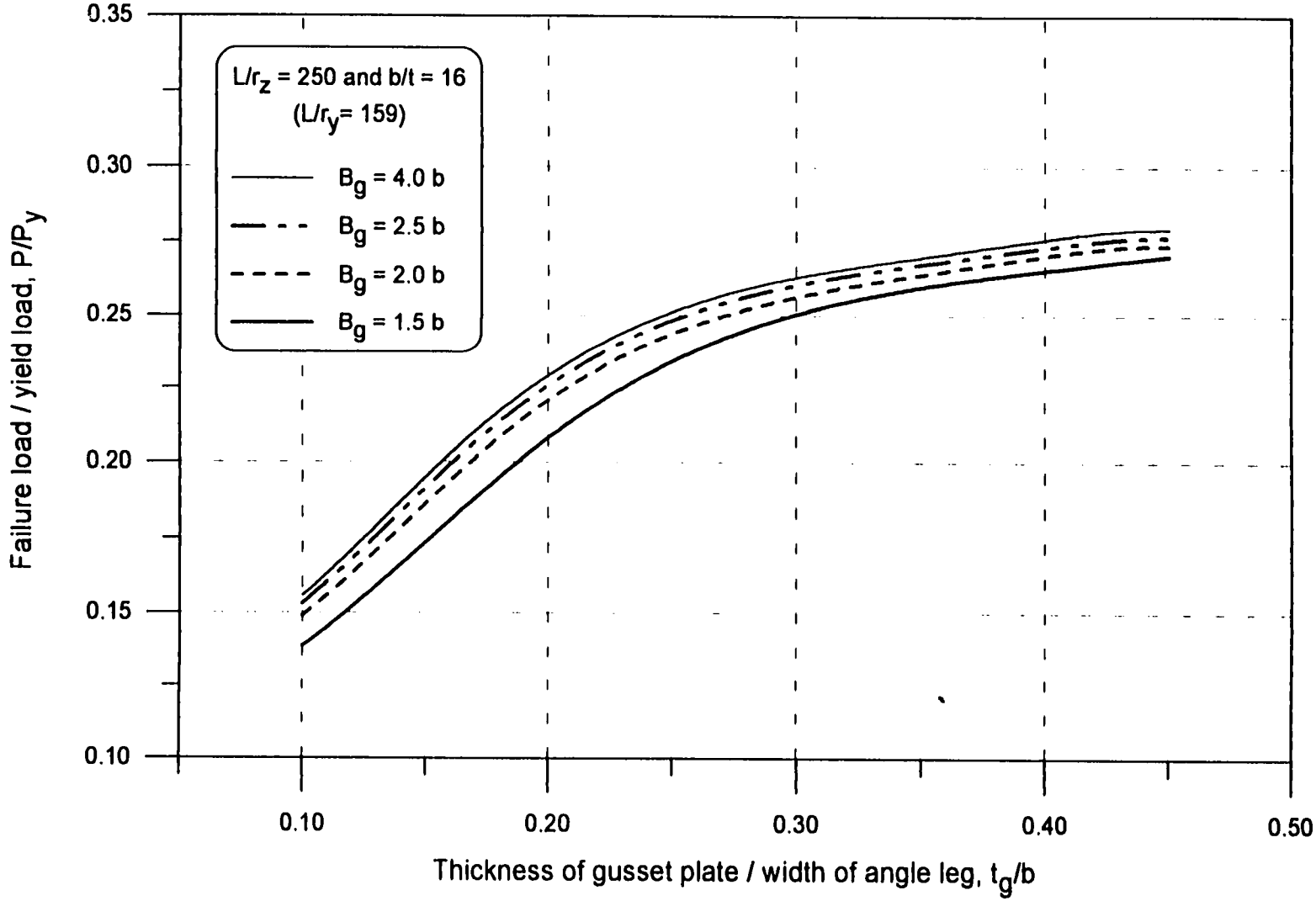

Figure B-31. Failure load predicted by finite element analysis when b/t = 16 and L/r_z = 250

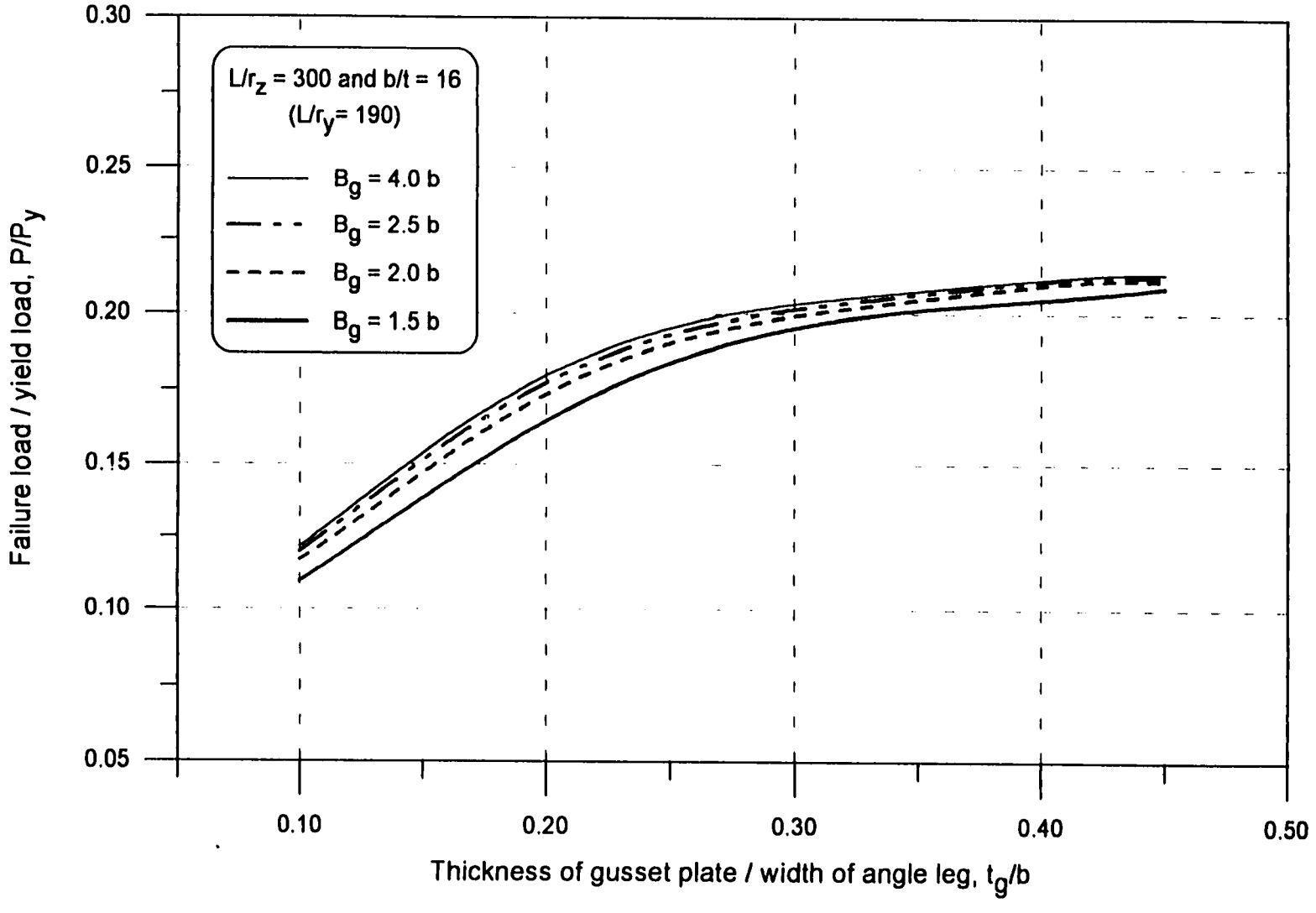

Figure B-32. Failure load predicted by finite element analysis when b/t = 16 and L/r_z = 300

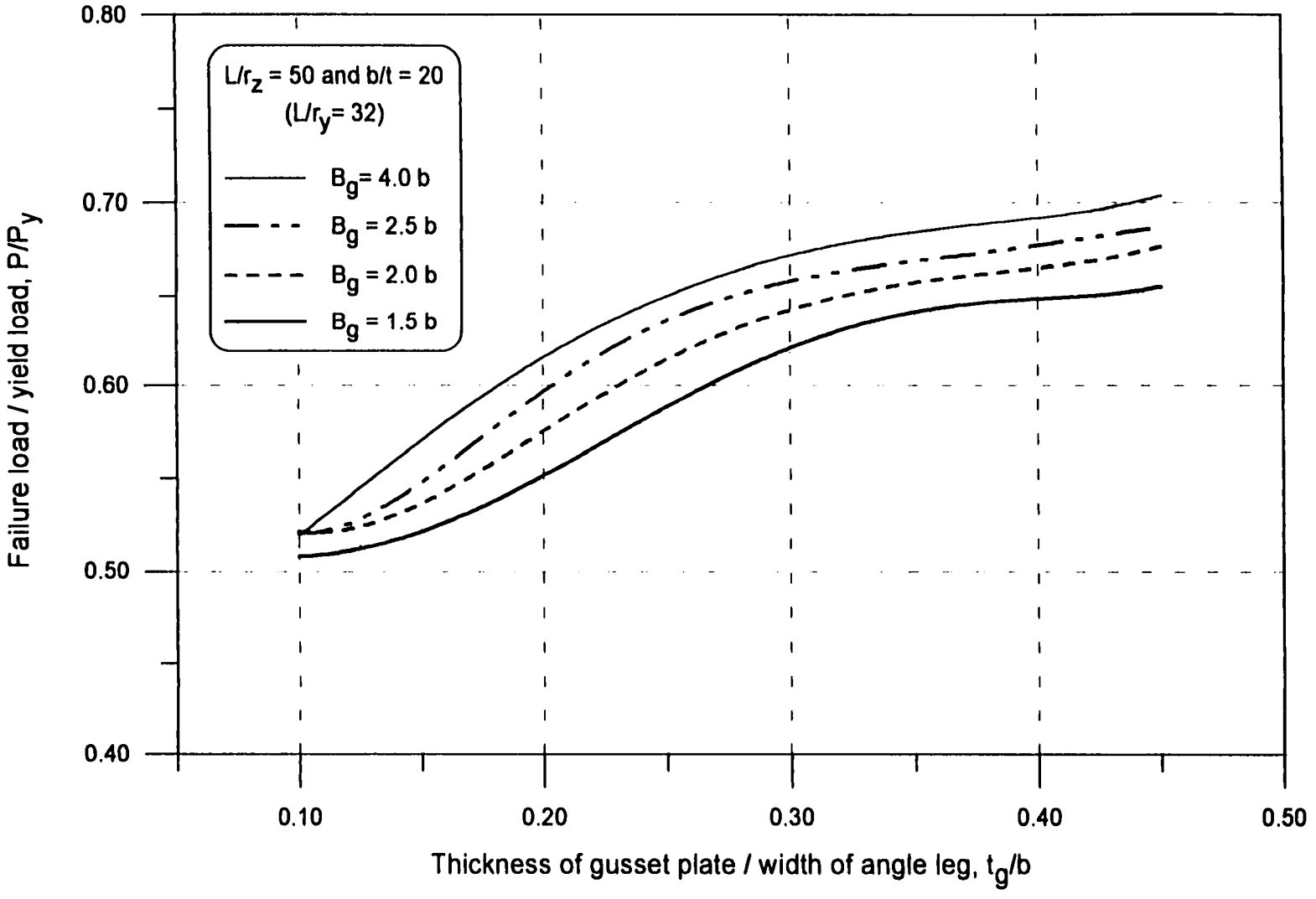

Figure B-33. Failure load predicted by finite element analysis when b/t = 20 and L/r_z = 50

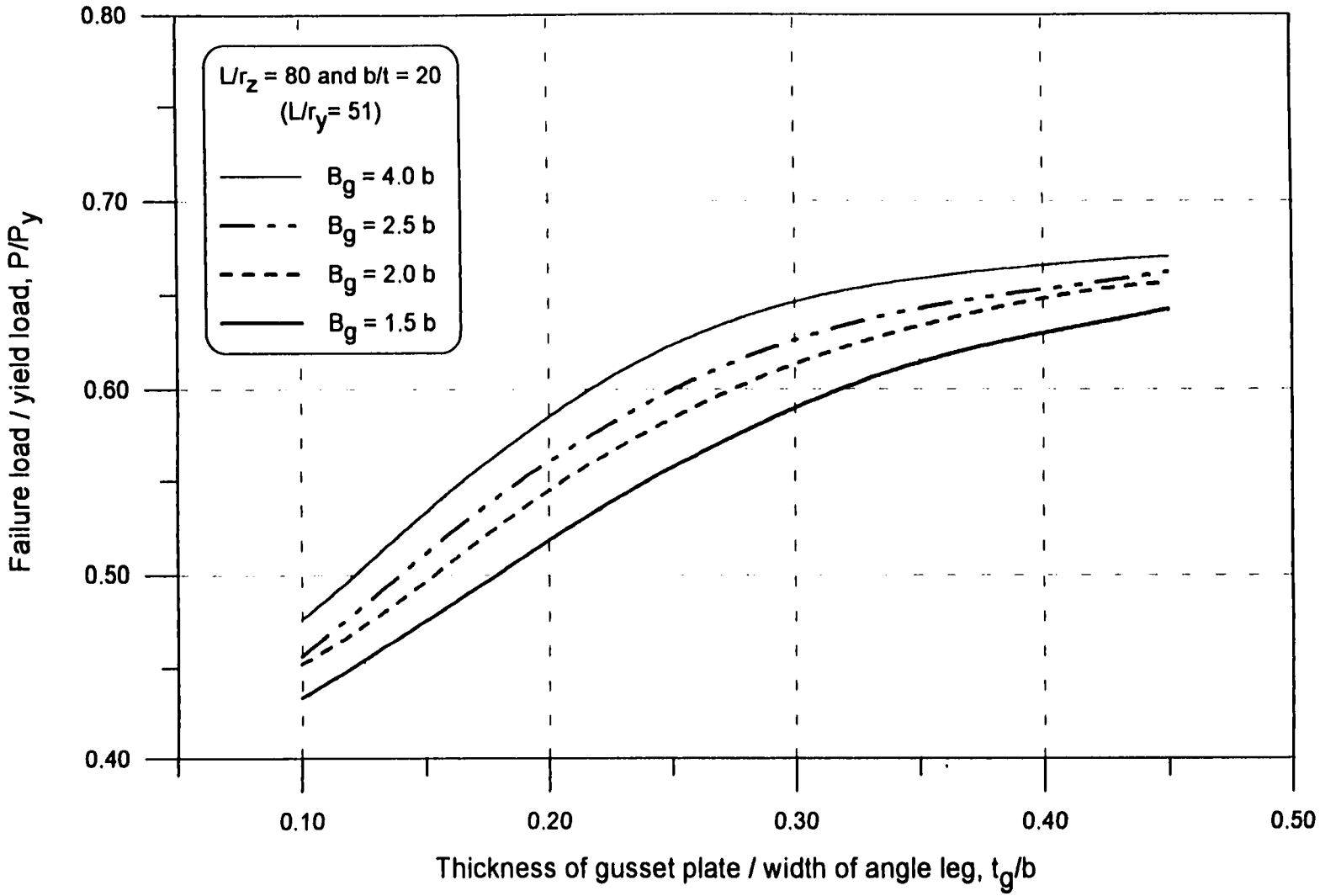

Figure B-34. Failure load predicted by finite element analysis when b/t = 20 and $L/r_z = 80$

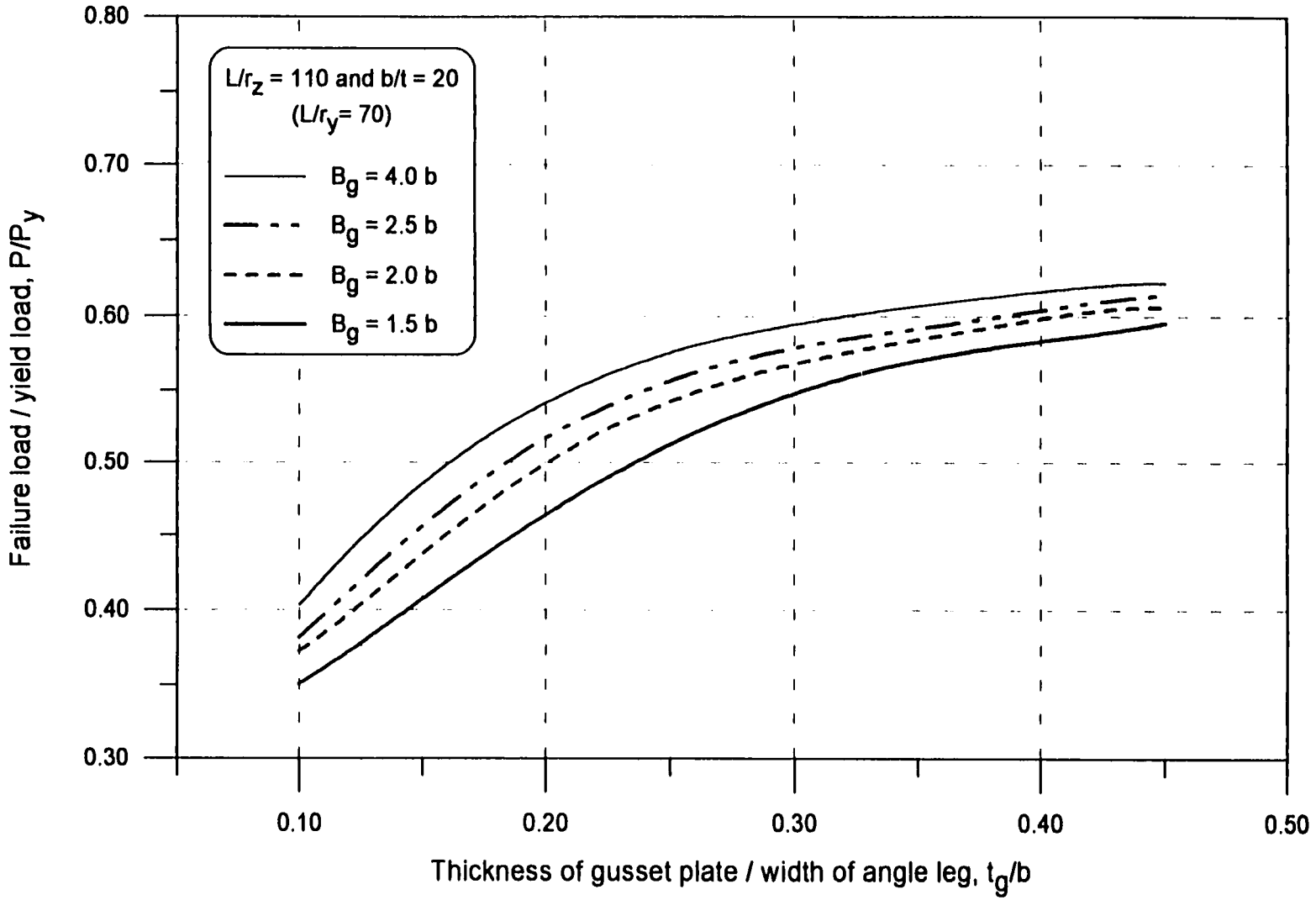

Figure B-35. Failure load predicted by finite element analysis when b/t = 20 and L/r_z = 110

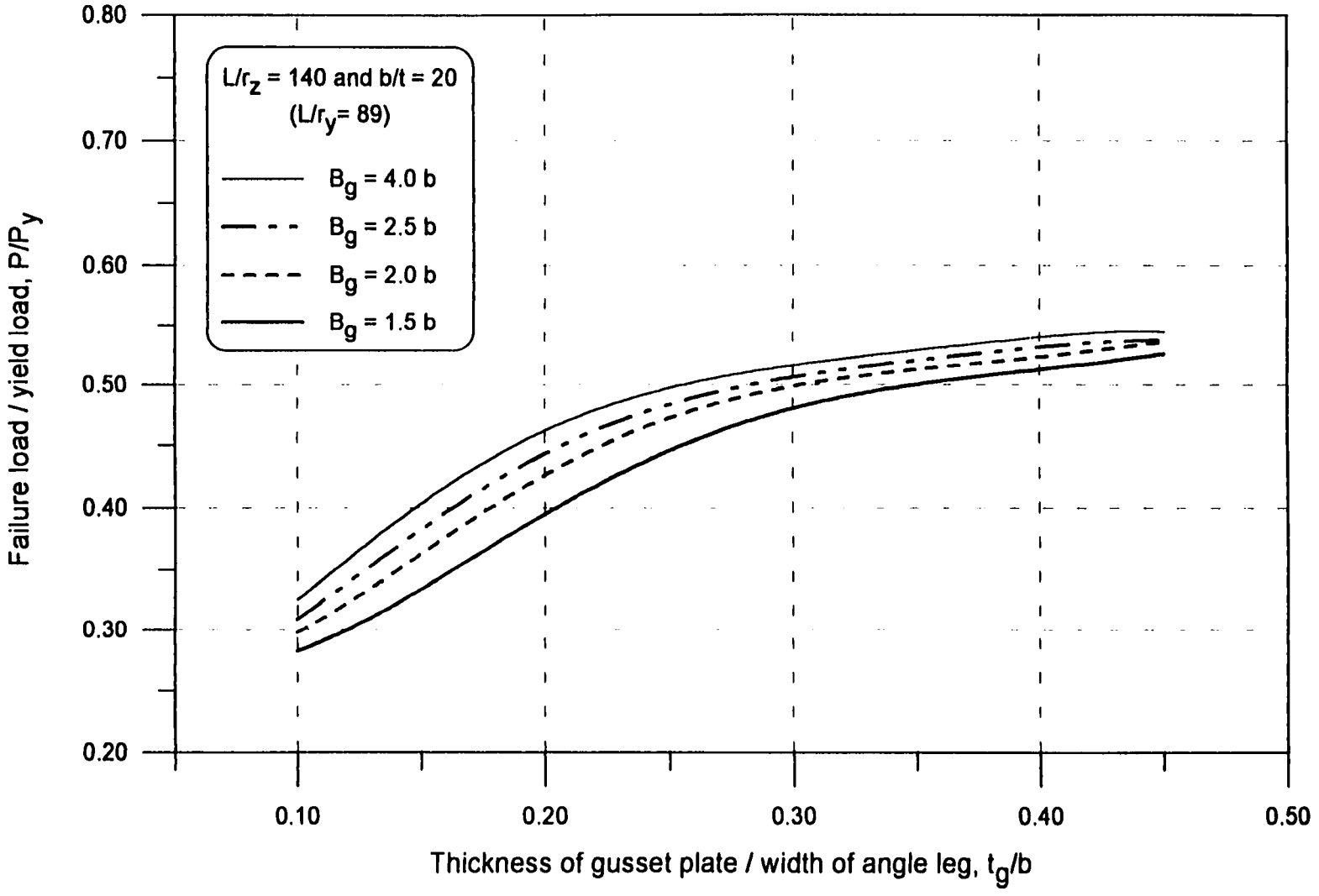

Figure B-36. Failure load predicted by finite element analysis when b/t = 20 and L/r_z = 140

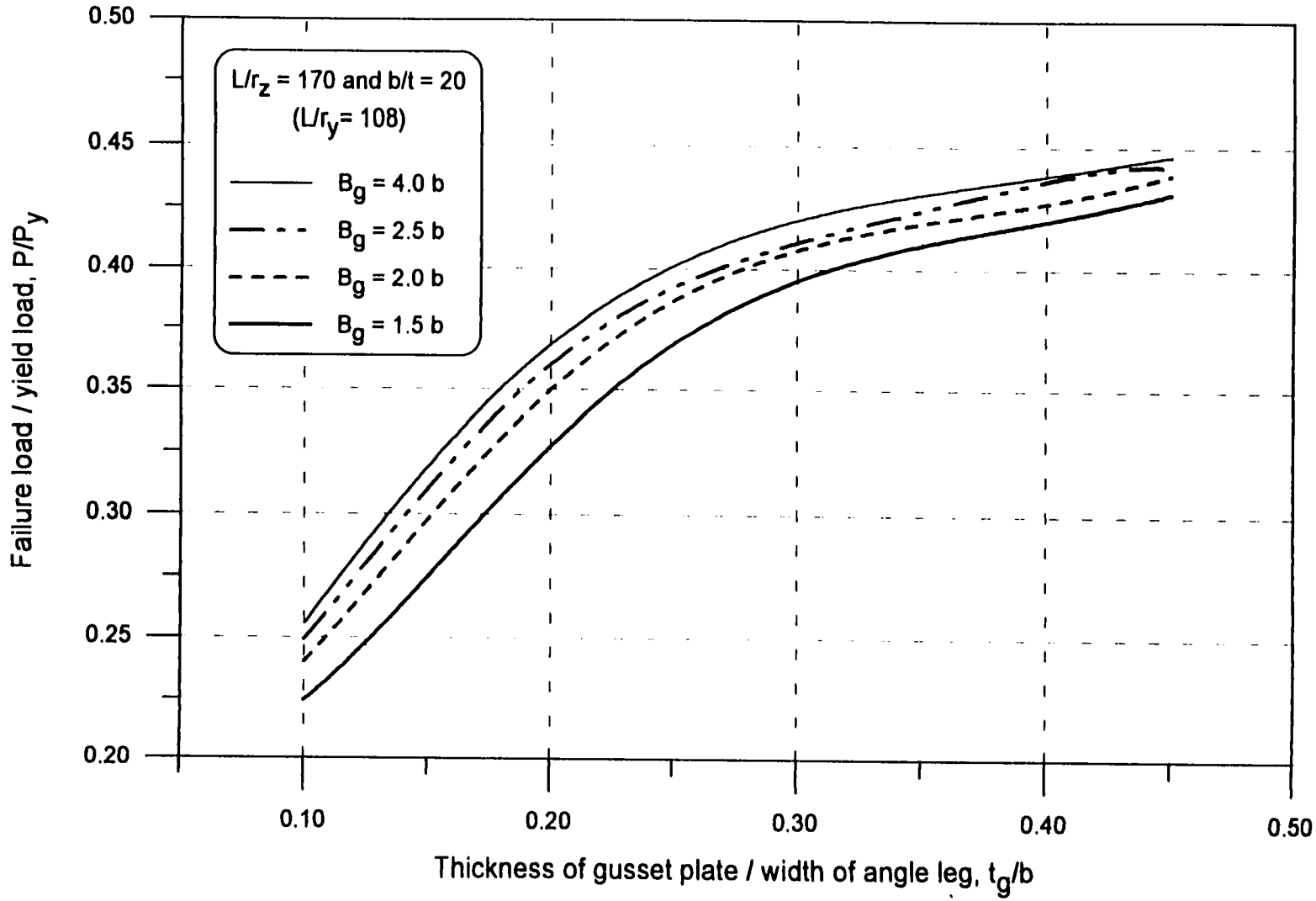

Figure B-37. Failure load predicted by finite element analysis when b/t = 20 and L/r_z = 170

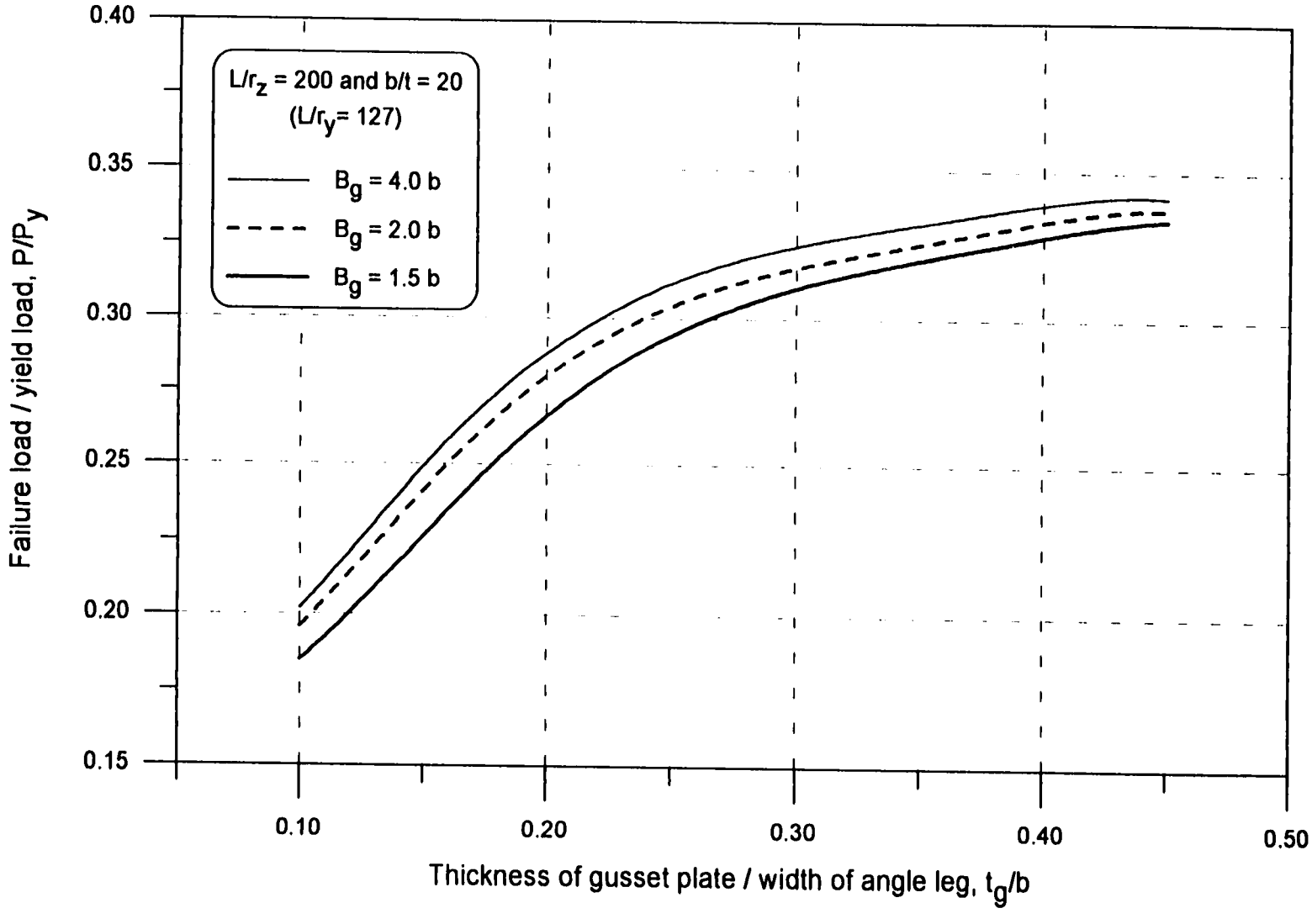

Figure B-38. Failure load predicted by finite element analysis when b/t = 20 and L/r_z = 200

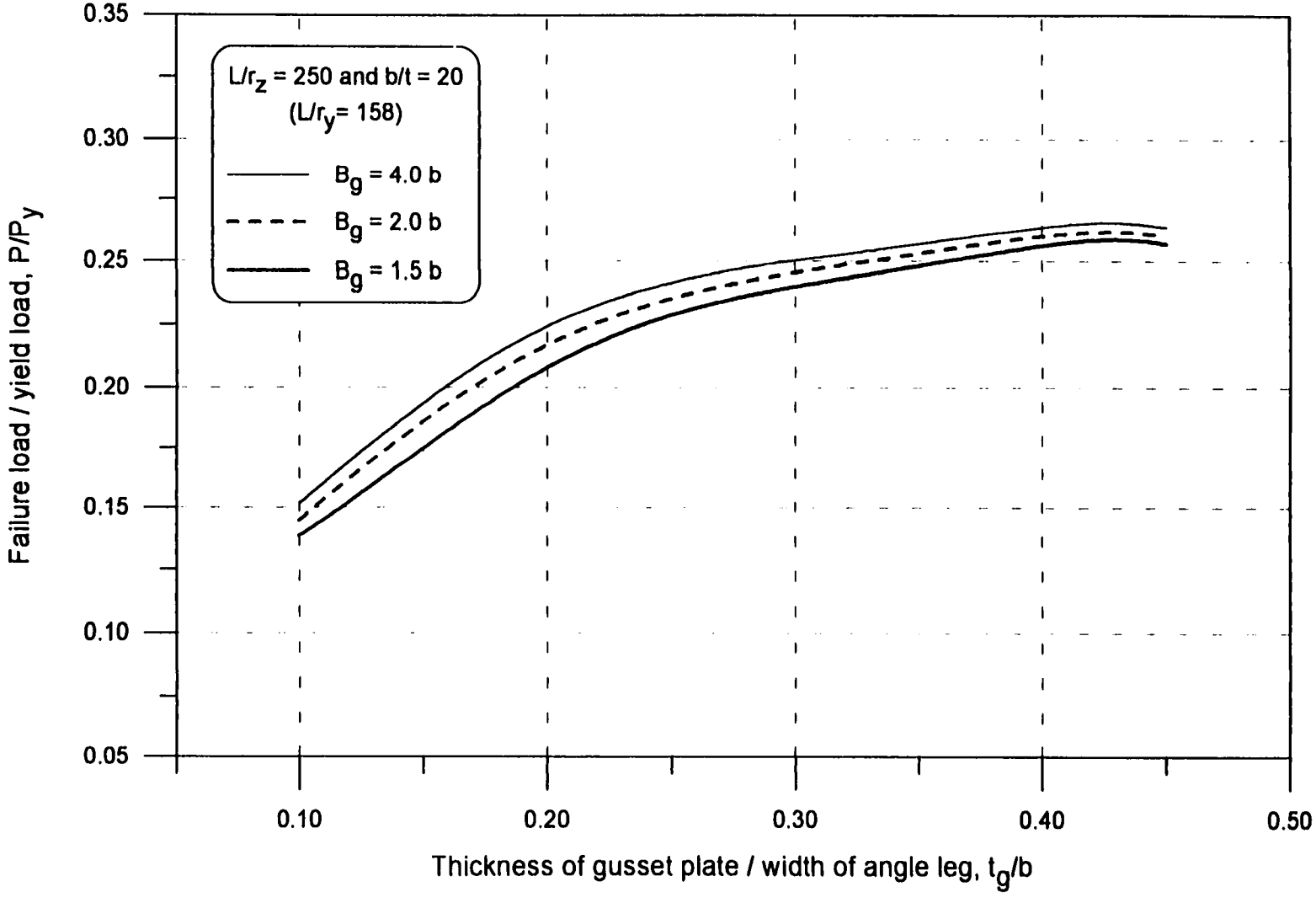

Figure B-39. Failure load predicted by finite element analysis when b/t = 20 and L/r_z = 250

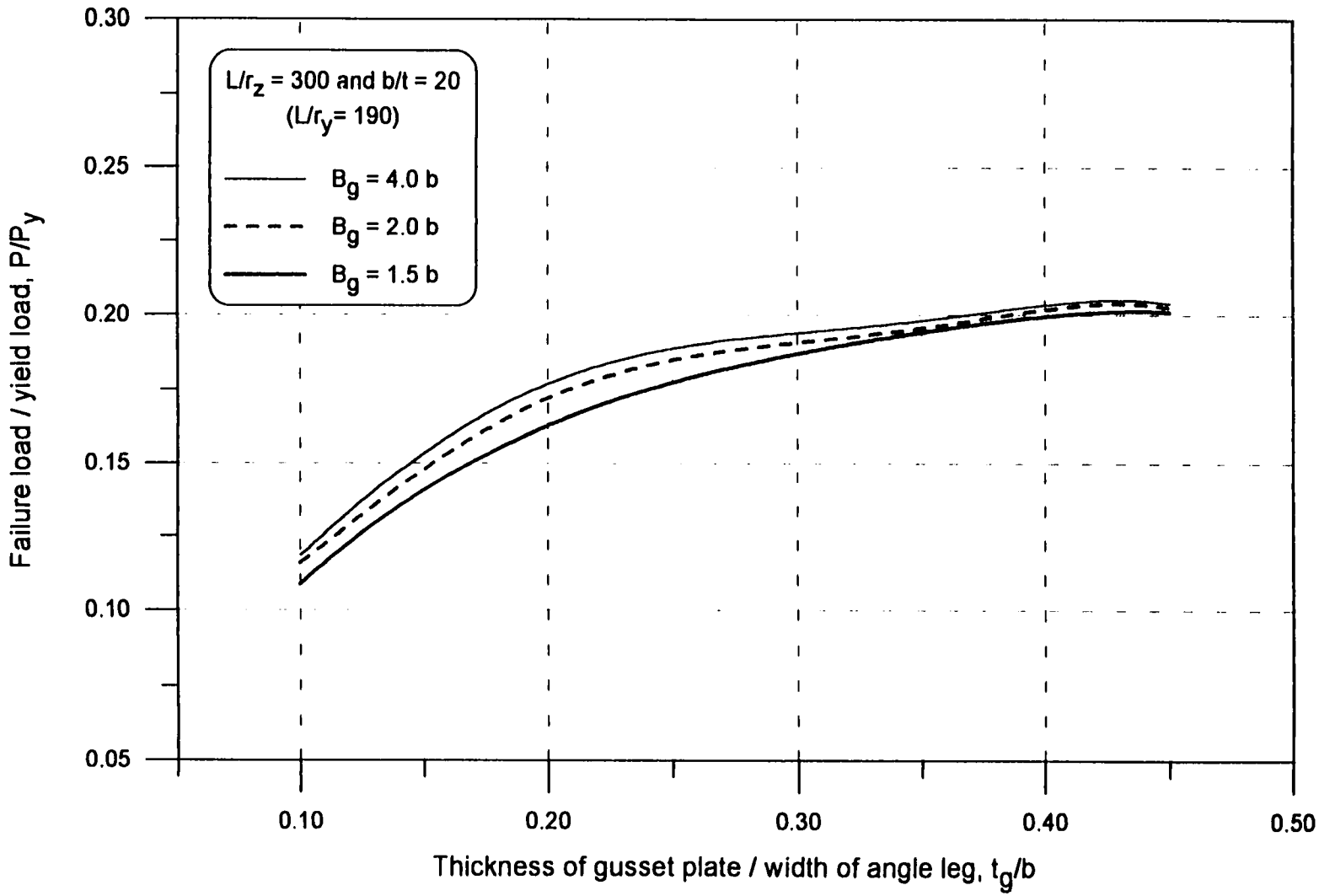

Figure B-40. Failure load predicted by finite element analysis when b/t = 20 and L/r_z = 300

VITA AUCTORIS

SHERIEF SHARL SHUKRY SAKLA

1967 Born on the 20th of November in Assiout, Egypt.

1989 Graduated with B.Sc. (Honour) degree in Civil Engineering fro El-Mansourah University, Egypt. Top of a 240 students class.

1993 Graduated with M.A.Sc. Degree in Civil Engineering from the University of Windsor, Ontario.

1993 Enrolled in the Faculty of Graduate Studies, University of Windsor, in a program leading to the degree of Doctor of Philosophy in Civil Engineering.

1997 Licensed Professional Engineer in the Province of Ontario, Canada.

1997 Licensed Professional Engineer in the State of Michigan, U. S. A.

IMAGE EVALUATION
TEST TARGET (QA-3)

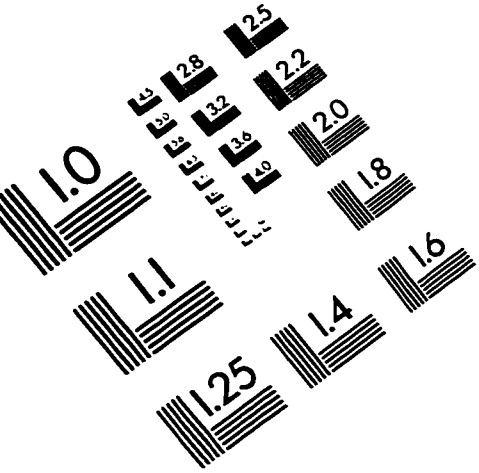

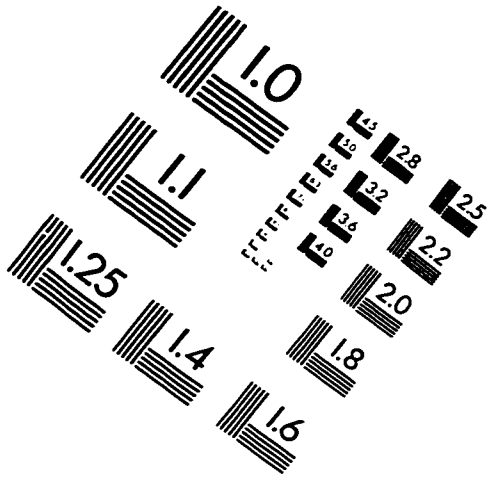

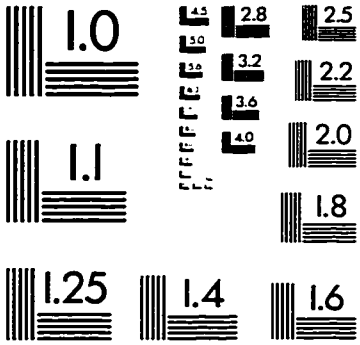

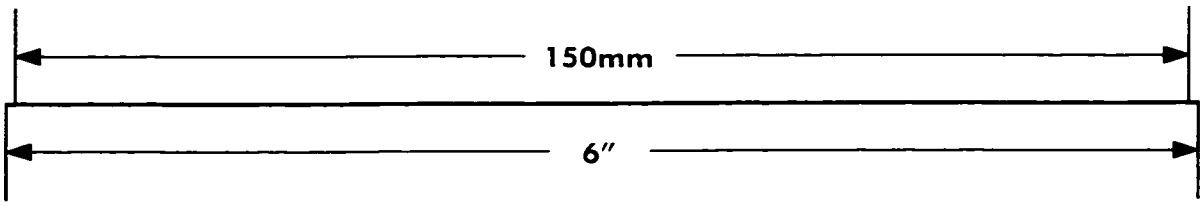

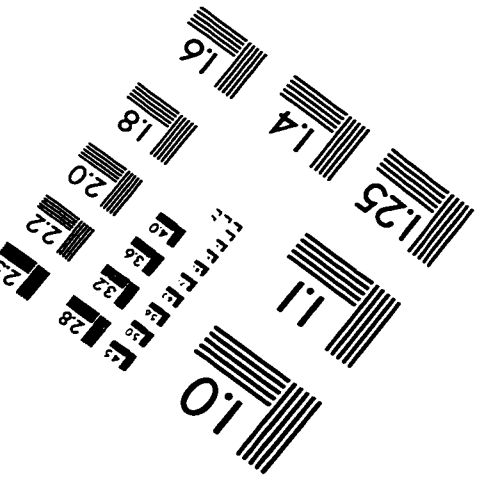

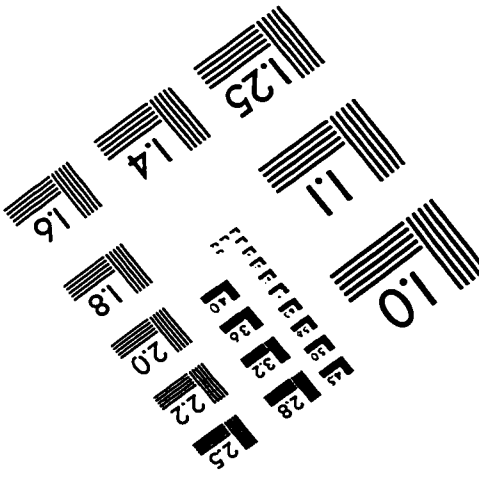

APPLIED IMAGE . Inc
1653 East Main Street
Rochester, NY 14609 USA
Phone: 716/482-0300
Fax: 716/288-5989